THE UNIVERSITY
OF MICHIGAN
FEB 3 1959
ENGINEERING

JOURNAL OF FLUID MECHANICS

VOLUME 5 PART 1

JANUARY 1959

PUBLISHED BY

CAMBRIDGE UNIVERSITY PRESS

BENTLEY HOUSE, 200 EUSTON ROAD, LONDON, N.W.1

AMERICAN BRANCH: 32 EAST 57TH STREET, NEW YORK 22, N.Y.

Price 30*s.* (*U.S.A.* $5.00)

The JOURNAL OF FLUID MECHANICS exists for the publication of theoretical and experimental investigations of all aspects of the mechanics of fluids, and is issued in four parts per volume.

EDITOR

DR G. K. BATCHELOR

Cavendish Laboratory, University of Cambridge, Cambridge, England

ASSISTANT EDITORS

DR T. B. BENJAMIN, DR I. PROUDMAN, DR P. G. SAFFMAN

Cavendish Laboratory, University of Cambridge, Cambridge, England

ASSOCIATE EDITORS

PROF. G. F. CARRIER

Pierce Hall, Harvard University, Cambridge 38, *Massachusetts, U.S.A.*

DR W. C. GRIFFITH

Research and Development Laboratory, Missile Systems Division, Lockheed Aircraft Corporation, Palo Alto, California, U.S.A.

PROF. M. J. LIGHTHILL

Department of Mathematics, The University, Manchester, England

PROF. R. R. LONG

School of Engineering, The Johns Hopkins University, Baltimore 18, *Maryland, U.S.A.*

Authors wishing to have papers published in the JOURNAL should communicate them to any one of the persons named above, choosing one in their own country where possible.

Authors are urged to ensure that their papers are written clearly and attractively, in order that their work will be readily accessible to readers.

Manuscripts should be typed in double spacing on one side of the paper only, with references listed at the end in alphabetical order of authors. Drawings should be done on a large scale in Indian ink on tracing cloth or drawing paper, the lettering being shown clearly in pencil for reproduction by the printer; the list of captions should be typed at the end of the manuscript. Proofs of papers from overseas will usually be despatched to authors by airmail. There is no charge for publication. Authors are entitled to receive 50 offprints of a paper in the JOURNAL free of charge, and additional offprints can be purchased if ordered in advance.

SUBSCRIPTIONS

The subscription price for a volume of four parts is £5. 10*s*. net, post free, payable in advance; separate parts 30*s*. net, plus postage. Subscriptions may be sent to any bookseller, or to the Cambridge University Press, Bentley House, 200 Euston Road, London, N.W.1.

Subscribers in the United States should send their orders to the Cambridge University Press, American Branch, 32 East 57th Street, New York 22. The subscription price per volume is $18.50, post free, payable in advance; separate parts $5.00, plus postage.

The prediction of separation of the turbulent boundary layer

By B. S. STRATFORD
National Gas Turbine Establishment, Farnborough

(Received 17 July 1958)

A rapid method for the prediction of flow separation results from an approximate solution of the equations of motion; a single empirical factor is required. The equations are integrated by a modified 'inner and outer solutions' technique developed recently for laminar boundary layers, the criterion for separation being obtained as a simple formula applying directly to the separation position. At Reynolds numbers of the order of 10^6, the criterion is

$$C_p(x\,dC_p/dx)^{\frac{1}{2}} = 0{\cdot}39(10^{-6}R)^{\frac{1}{10}},$$

when $d^2p/dx^2 \geqslant 0$ and $C_p \leqslant \frac{4}{7}$; the coefficient 0·39 is replaced by 0·35 when $d^2p/dx^2 < 0$.

The prediction of the pressure rise to separation is likely to be from 0 to 10% too low, which puts it second in accuracy to those methods, such as Maskell's (1951), which utilize the Ludweig–Tillmann skin friction law. However, the convenience of the method makes the present error acceptable for many applications, while a greater accuracy should be attainable from an improved allowance for the quantity d^2p/dx^2.

The main derivation is for arbitrary pressure distributions, while an extension leads to the pressure distribution which just maintains zero skin friction throughout the region of pressure rise.

The concept of a turbulent inner layer with zero wall stress is put forward, and it is deduced that in the neighbourhood of the wall the velocity is proportional to the square root of the distance from the wall.

1. Introduction

Previous methods for calculating the position of separation for the turbulent boundary layer—i.e. the position at which the flow 'stalls' or separates from the wall—have solved the momentum or energy equations in conjunction with empirical expressions representing the shape and behaviour of the velocity profile (see von Doenhoff & Tetervin 1943; Goldstein 1938; Kalikhmann 1943; Rotta 1953; Spence 1956*a*, *b*; Squire & Young 1937; and Maskell 1951). These methods are reasonably accurate, but provide only a limited understanding of the flow.

The present method is based upon the equations of motion (Goldstein 1938), the analysis of the turbulence utilizing either dimensional analysis or mixing length theory (Durand 1943, §25). Moreover, a closer physical picture than

hitherto is attempted for the flow. The method postulates that, as for the laminar layer (Stratford 1954), the turbulent layer in a pressure rise may be divided into two distinct regions. The outer is an historical region in which the pressure rise just causes a lowering of the dynamic head profile, the losses due to the shear

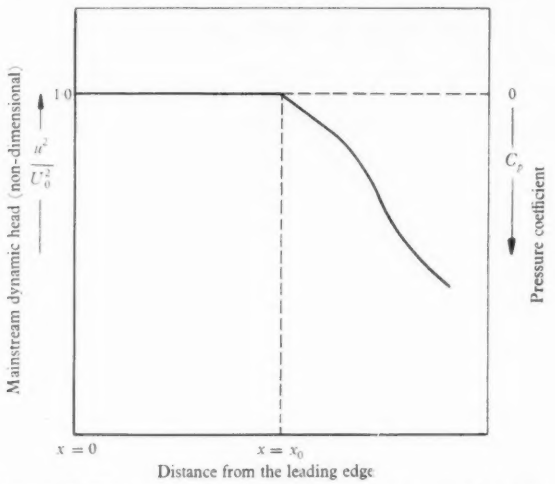

FIGURE 1. The type of pressure distribution treated initially.

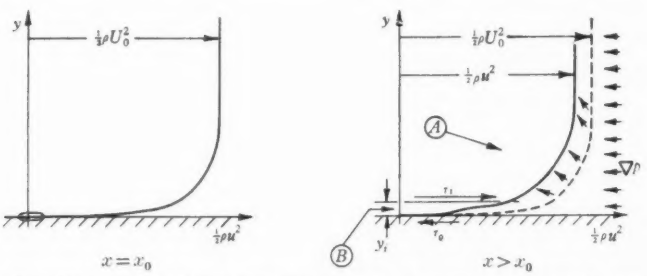

FIGURE 2. Development of a boundary layer in a sudden pressure gradient. At $x = x_0$ the profile is unchanged except at $y = 0$. Just downstream of x_0 there is a general lowering of velocity in the outer layer (A) and a change of shape in the inner layer (B).

stresses being almost the same as for the flow on a flat plate. The general solution is obtained in terms of the flow on a flat plate, the relationship to the flat plate flow being identical with the corresponding relationship for the laminar boundary layer. In the inner layer, on the other hand, the inertia forces are small so that the velocity profile is distorted by the pressure gradient until the latter is largely balanced by the transverse gradient of shear stress. The solution found for the inner layer at the separation position is such that close to the wall the velocity is proportional to the square root of the distance from the wall. This velocity profile is in contrast to that for the laminar boundary layer at separation, where the velocity is proportional to the square of the distance from the wall. A summary of the treatment and a picture of the flow is sketched in figures 1 to 3. It will be seen

from figure 1 that the pressure distribution considered initially has a simplified form in which a sharp pressure rise starts abruptly at the position $x = x_0$ after constant pressure for a distance x_0.

The final solution is given by equations (19*a*), (19*c*) and (23). These relate x, C_p and dC_p/dx at the separation position, and may be applied very rapidly to any given pressure distribution.

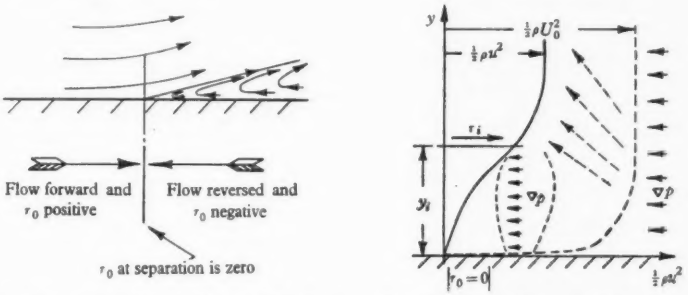

FIGURE 3. The separation position. The flow reaches the separation condition of zero skin friction when the backward force $y_i \nabla p$ can only be adequately balanced by the shear stress difference $(\tau_i - \tau_0)$ if τ_0 is zero.

2. The outer layer

Where there is a rapid pressure rise the shear forces in the outer part of the boundary layer are small compared with either the inertia forces or the pressure gradient. As a preliminary it will be found helpful to consider the solution for a flow in which, downstream of x_0, the shear forces are supposed zero, even though vorticity is present.

In such a flow the total pressure, P, will remain constant along a streamline and Bernoulli's equation holds:

$$\frac{\partial P}{\partial s} = 0 \quad \text{(zero shear stress)},$$

where s is the distance along a streamline. Thus

$$P(x, \psi) = P(x_0, \psi) \quad \text{(zero shear stress)}.$$

The solution is therefore that the dynamic head at any point is equal to the dynamic head on the same streamline at x_0 minus the rise in static pressure. Since the flow at x_0 is known, the flow in the outer region of the boundary layer downstream of x_0 is solved.

For the real flow the shear forces cause a decrease in total pressure along a streamline, Bernoulli's equation being replaced by

$$\frac{\partial P}{\partial s} = \frac{\partial \tau}{\partial y}, \tag{1}$$

as may be deduced from the equations of motion and continuity; τ is the shear stress and y is the distance from the wall. Thus

$$P(x, \psi) = P(x_0, \psi) + \int_{x_0}^{x} \frac{\partial \tau}{\partial y} ds. \tag{2}$$

Let the flow under consideration now be compared with a second flow which has identical conditions as far as $x = x_0$, but which continues at constant static pressure thereafter. The distributions of $\partial\tau/\partial y$ for the two flows will be identical for points away from the wall at $x = x_0$; also the distributions will remain closely the same for a short distance downstream of x_0, because the effect of the pressure rise in the outer part of the boundary layer in this region is to cause a general lowering of the velocity profile rather than a change in shape. It follows, using equation (2), that the total pressure loss caused by the shear forces will be approximately the same for the two flows. Thus the total pressures, which were equal at x_0, may as an approximation still be supposed equal at points just downstream of x_0, i.e.

$$P(x,\psi) = P'(x,\psi) \quad (\psi \geqslant \psi_i), \tag{3}$$

where the dash denotes the comparison profile,

$$\psi = \int_0^y u\,dy,$$

and where the condition $\psi \geqslant \psi_i$ denotes an application limited to the outer region of the profile (ψ_i is the value of ψ at the edge of the inner layer).

Since p' = constant = p_0, where p is the static pressure, equation (3) gives

$$\tfrac{1}{2}\rho u^2(x,\psi) = \tfrac{1}{2}\rho u'^2(x,\psi) - (p - p_0) \quad (\psi \geqslant \psi_i). \tag{4}$$

The dynamic head at any point is therefore equal to the dynamic head at the corresponding point in the comparison flow minus the rise in static pressure.

Equation (4) represents for the outer part of the boundary layer a solution which is almost exact at positions a short distance downstream of x_0 (since the values of both $\frac{1}{2}\rho u^2$ and $(\partial/\partial s)\,\frac{1}{2}\rho u^2$ are exact at x_0), and which would be expected to indicate at least the main behaviour for large distances downstream of x_0. (For an alternative assessment, the reduction in the value of the local dynamic head $\frac{1}{2}\rho u^2$ from its initial value $\frac{1}{2}\rho U_0^2$ may be divided into three parts, these being due respectively to the rise in static pressure, to the viscosity between $x = 0$ and $x = x_0$, and to the viscosity downstream of x_0. Of these three effects, the first two have been included exactly in equation (4). The third effect, which is likely to be relatively small for the outer part of a boundary layer at separation, has been allowed for approximately.)

The standard solution required for u', the velocity in the boundary layer without pressure rise, may for the turbulent boundary layer be taken as the following semi-empirical form. (The usual derivation is that given by Goldstein (1938), while Schlichting (1941) obtains the result by approximate solution of the equations of motion.)

$$\frac{u'}{U_0} = \left(\frac{y'}{\delta'}\right)^{1/n}, \tag{5a}$$

where

$$\delta' = \frac{(n+1)(n+2)}{n}\,\theta', \tag{5b}$$

$$\theta' = 0{\cdot}036 x R^{-\frac{1}{4}}, \tag{5c}$$

and where the value of n varies slightly with the Reynolds number but is usually close to 7.

Equations (4) and (5) provide a general solution for the outer region of the boundary layer.

Differentiation of equation (4) with respect to ψ, and replacing $u(\partial/\partial\psi)$ by $\partial/\partial y$, gives

$$\left[\frac{\partial u}{\partial y}\right]_{(x,\psi)} = \left[\frac{\partial u'}{\partial y'}\right]_{(x,\psi)} \quad (\psi \geqslant \psi_i). \tag{6}$$

3. The inner layer

The action of the pressure rise in the outer layer has been interpreted as a direct reduction in the dynamic head along each streamline, the only effect of the shear forces being to cause a superposed, and almost independent, loss. It can therefore be said that in the outer layer the back pressure force is balanced by the fluid inertia forces.

In the inner layer the effect of the fluid inertia is too small for the above mechanism to be possible. In particular the inertial forces at the wall are zero, so that the pressure forces must be balanced entirely by the gradient of the shear force, i.e.

$$\frac{\partial p}{\partial x} = \frac{\partial \tau}{\partial y} \quad (y = 0), \tag{7}$$

as follows from the equations of motion, or from equation (1), by putting $\partial u/\partial s = 0$. Now this balance at the wall can occur only after there has been a change in the profile shape. When the sudden pressure gradient is reached at $x = x_0$, the dynamic head and hence the general level of velocity would start to fall everywhere, were it not for the no slip condition at the wall. This, as it were, anchors the velocity profile, which distorts instantaneously at $x = x_0$, $y = 0$, until, just at the wall, the required balance is attained. The inner layer commences its growth at the discontinuity at $x = x_0$, $y = 0$ and is the region in which the slope of the velocity profile has changed. In the inner layer there is a transition between fluid at the wall, for which the pressure force is balanced entirely by the shear force gradient, and fluid in the outer layer, where the pressure force causes simply a direct reduction of dynamic head.

The analysis may proceed either on dimensional arguments* or by mixing length theory. Using dimensional arguments, suppose we have a layer within which the motion is determined by energy transport due to working by shear stresses, there being relatively little effect from energy advection by the mean flow. The motion then depends on

$$\tau_0, \quad (\partial\tau/\partial y)_0, \quad (\partial^2\tau/\partial y^2)_0,$$

and the kinematic viscosity. If the wall stress, τ_0, is zero, dimensional similarity requires that

$$u = \left(\frac{\nu}{\rho}\frac{\partial\tau}{\partial y}\right)^{\frac{1}{3}} F\left(\frac{1}{\rho}\left(\frac{\partial\tau}{\partial y}\right)_0 \frac{y^3}{\nu^2}\right) \tag{8}$$

sufficiently close to the wall to satisfy $y(\partial^2\tau/\partial y^2)_0 \ll (\partial\tau/\partial y)_0$. In the fully turbulent part of the flow, the relative motion is independent of the viscosity and so

$$u = A\left(\frac{y}{\rho}\frac{\partial\tau}{\partial y}\right)^{\frac{1}{2}} + B\left(\frac{\nu}{\rho}\frac{\partial\tau}{\partial y}\right)^{\frac{1}{3}}, \tag{9}$$

* These were suggested by the referee.

where A, B are absolute constants. For large values of $\left(\frac{1}{\rho}\frac{\partial\tau}{\partial y}\frac{y^3}{\nu^2}\right)$, (9) is nearly

$$\tfrac{1}{2}\rho u^2 = \tfrac{1}{2}A^2 y(\partial\tau/\partial y)_0 = \tfrac{1}{2}A^2 y\,\partial p/\partial x. \tag{10}$$

The alternative analysis by mixing length theory is able to indicate the order of magnitude of the constant of proportionality. The momentum transfer hypothesis will be adopted and, as is conventionally assumed for the flow on a flat plate, the mixing length will as a first approximation be assumed proportional to the distance from the wall. Now by the standard theory (e.g. Durand 1943, § 25) the shear stress when $\partial u/\partial y$ is positive is

$$\tau = \rho K^2 y^2 (\partial u/\partial y)^2 \quad (y \text{ small}), \tag{11}$$

where K is the Karman constant. The boundary layer at separation has zero skin friction, so that the integration of equation (7), regarding this equation as holding over a small region close to the wall, gives

$$\tau = y\,\partial p/\partial x \quad (\tau_0 = 0,\ y \text{ small}). \tag{12}$$

Elimination of τ between equations (11) and (12) yields

$$\left(\frac{\partial u}{\partial y}\right) = \left(\frac{1}{\rho K^2}\frac{\partial p}{\partial x}\right)^{\frac{1}{2}} y^{-\frac{1}{2}} \quad (\tau_0 = 0, y \text{ small}), \tag{13}$$

while for no slip at the wall, $u = 0$ at $y = 0$, and equation (13) integrates to

$$u = \left(\frac{4}{\rho K^2}\frac{\partial p}{\partial x}\right)^{\frac{1}{2}} y^{\frac{1}{2}} \quad (\tau_0 = 0, y \text{ small}), \tag{14}$$

which is in agreement with equation (10).

Thus close to the wall the asymptotic form of the separation profile is that the velocity is proportional to $y^{\frac{1}{2}}$ and the dynamic head is proportional to y.

Equation (14), with an appropriate value for K, could be regarded as the first term of a series expansion representing the whole inner layer profile, the higher terms arising from the inertial forces and the gradual fall-off of the mixing length from the linear value assumed for it. Since the details of the mixing length behaviour could be determined only by recourse to experiment, it is particularly expedient for the present purpose, of calculating the separation position, to incorporate a single empirical factor, say 'β', in this first term, omitting higher terms whatever their source, and to obtain the factor from a special experiment. By omitting the higher terms in the profile expansion the profile has been over-idealized as regards its own shape, so that good agreement with experimental profiles would not be expected, but the empirical factor might be expected adequately to represent the effect on the separation criterion of the higher terms. The factor β will be used also to represent any effects which the pressure rise might have on the mixing length, effects which are discussed in more detail by Ludweig & Tillmann (1949), by Squire (1950), and by Stratford (1956, 1959).

For present purposes, therefore, the inner layer ($y < y_i$) is represented by the idealized profile

$$\tfrac{1}{2}\rho u^2 = \frac{2}{(0{\cdot}41\beta)^2}\frac{\partial p}{\partial x}y \quad (\tau_0 = 0,\ y < y_i), \tag{15}$$

0·41 being the flat plate value for the Karman constant.

Incidentally, the fact that $\partial\tau/\partial y > 0$ and $\partial^2 u/\partial y^2 < 0$ in this flow renders the vorticity transfer theory inapplicable.

4. The joining condition, and the preliminary result

At the join between the inner and outer layers continuity is specified in ψ, u and $\partial u/\partial y$. This is sufficient to determine the join, and the suggested algebra for so doing and for deriving the separation condition (equation 19a) is as follows.

At the join ψ and $\partial u/\partial y$ for the inner layer are equal to ψ and $\partial u/\partial y$ for the outer layer and, therefore, from the definition of corresponding points and from equation (6), ψ and $\partial u/\partial y$ for the inner layer at the join are equal to ψ (or ψ') and $\partial u'/\partial y'$ for the corresponding point on the comparison profile. Equating $\psi(\partial u/\partial y)^3$ and $\psi'(\partial u'/\partial y')^3$, calculated respectively from equations (15) and (5a), gives that the join at the separation position is such that its corresponding point satisfies

$$\left(\frac{y'}{\delta'}\right)^{(2n-4)/n} = \frac{3(0{\cdot}41\beta)^4}{(n+1)\,(n\delta'\,dC_p/dx)^2} \quad (\psi = \psi_i), \tag{16}$$

the join being thus determined. A further property of the join

$$u^2/u'^2 = 3/(n+1) \quad (\psi = \psi_i) \tag{17}$$

is obtained by comparing $u^2/(\psi\,\partial u/\partial y)$, calculated from equation (15), with the corresponding quantity calculated from equation (5a).

The separation condition may now be derived from equation (4) for, from that equation and equation (5a),

$$C_p = (y'/\delta')^{2/n}\,(1 - u^2/u'^2) \quad (\psi \geqslant \psi_i,\ C_p \leqslant [1 - u^2/u'^2]), \tag{18}$$

where $C_p = (p - p_0)/\tfrac{1}{2}\rho U_0^2$. Use of values at the join, as given by equations (16) and (17), followed by substitution of equations (5b) and (5c) for δ', leads to

$$(2C_p)^{\frac{1}{4}(n-2)}\left(x\frac{dC_p}{dx}\right)^{\frac{1}{2}} = 1{\cdot}06\beta(10^{-6}R)^{\frac{1}{16}} \quad \left(C_p \leqslant \frac{n-2}{n+1}\right), \tag{19a}$$

R being the Reynolds number based on the local value of the distance x and the peak velocity U_0. In obtaining equation (19a) the quantity

$$(n+1)^{\frac{1}{4}(n+1)}\,(n+2)^{\frac{1}{2}}/(n-2)^{\frac{1}{4}(n-2)}$$

has been replaced by $10{\cdot}7 \times (2{\cdot}00)^{\frac{1}{4}(n-2)}$, which is within 1 % of the former quantity when $6 \leqslant n \leqslant 8$.

The limitation $C_p \leqslant (n-2)/(n+1)$ results formally from the join of the inner layer with the outer layer reaching the edge of the boundary layer when using the idealized velocity profiles. The same limitation applies to the range over which β has been determined empirically.

The parameter β may be determined by comparison with the experiment which is described in the following paper (Stratford 1959). In this experiment the flow was maintained just at the separation condition throughout the pressure rise, as will be considered theoretically in the last section of the present paper. It is found that β is independent of C_p and has the value

$$\beta = 0{\cdot}66 \quad (\tau_0 \equiv 0,\ C_p \leqslant [n-2]/[n+1]). \tag{19b}$$

The qualification '$\tau_0 \equiv 0$' has been added because β will vary somewhat with the value of d^2p/dx^2 immediately prior to separation, this quantity having its greatest possible negative value in the experiment. The variation will be discussed in §5.

The quantity 'n' pertains to the flat plate comparison profile at $x = x_s$, suffix s being used to denote separation; the relevant Reynolds number is still

$$R_s = x_s U_0/\nu.$$

Now if $C_{p,s} = 0{\cdot}50$ equation (19a) is seen to be independent of n. Moreover, in general it is not sensitive to n, for example, a typical change from $n = 6$ to $n = 7$ has a 4% effect, and so the use of a reasonable value for n is sufficient. Analysis of a velocity profile obtained by Schubauer & Klebanoff (1950) suggests the value $n = 7$ at a Reynolds number of $1{\cdot}43 \times 10^7$, while as part of the experiment with continuously zero skin friction the value $n = 6$ was obtained for a Reynolds number of $0{\cdot}64 \times 10^6$. Comparison of the values of n with those of $\log_{10} R$ and consideration of the degree of accuracy required therefore suggests the use of

$$n = \log_{10} R_s, \tag{19c}$$

the errors thus introduced into the formula being expected to be usually less than 1%.

Except for the small effect of $(d^2p/dx^2)_s$, which will be discussed in §5, equations (19a) to (19c) are sufficient to determine whether separation will occur at any chosen point on a given pressure distribution. This is the principal result of the paper.

Some typical values, and comparison with the laminar boundary layer

Equations (19) demonstrate that the value of the pressure rise to separation is not highly sensitive to the value of the pressure gradient at separation. As a typical example, for a separating turbulent boundary layer the value of $x\,dC_p/dx$ is in the neighbourhood of unity and so the value of C_p at separation would be about 0·35, say between 0·3 and 0·5.

These results are to be compared with results for the laminar layer, which, according to Stratford's (1954) analysis, satisfies

$$C_p\left(x\frac{dC_p}{dx}\right)^2 \doteqdot 0{\cdot}0076 \quad \text{(laminar separation)}.$$

The pressure recovery of the laminar layer at separation is thus much more sensitive to pressure gradient. Values for $(x\,dC_p/dx)_s$ for a laminar boundary layer would usually range between 0·2 and 0·5, or higher, so that a typical pressure recovery is, say, 0·06.

Allowance for an initial region of favourable pressure gradient or laminar flow

For pressure distributions having an initial region of favourable pressure gradient, the value of x to be used in the above equations has to be an equivalent value, the flow with favourable gradient being replaced by one at constant pressure and with a mainstream velocity equal to the peak mainstream velocity U_0. The criterion of equivalence is the value of the boundary layer momentum thickness θ at the point of peak velocity. It may be shown semi-empirically (using the energy equation and the data of Schubauer & Klebanoff (1950)) that for a boundary layer turbulent from the leading edge this criterion leads approximately to

$$x_0 = \int_0^{X_0} \left(\frac{U}{U_0}\right)^3 dX, \tag{20}$$

where X and x are distances from the actual and the equivalent leading edges respectively.

For a boundary layer which is initially laminar the momentum thickness θ_1 at $X = X_1$ may be calculated from the following equation, which has been obtained with minor variations by Young & Winterbottom (1940), Walz (1943) and Thwaites (1949):

$$\theta_1 = 0{\cdot}664\left[\frac{\nu}{U_1}\int_0^{X_1}\left(\frac{U}{U_1}\right)^5 dX\right]^{\frac{1}{2}}. \tag{21}$$

The equivalent length of turbulent boundary layer can now be determined from equation (5*c*) on the standard assumptions of sudden transition and of conservation of momentum. For the final equivalent condition, in which both the boundary layer is entirely turbulent and the pressure is constant at p_0 until the rise of pressure commences, equations (5*c*), (20) and (21) lead to

$$x_0 = 38{\cdot}2\left(\frac{\nu}{X_t U_t}\right)^{\frac{1}{5}}\left(\frac{U_0}{U_t}\right)^{\frac{1}{5}}\left[\int_0^{X_t}\left(\frac{U}{U_0}\right)^5 d\left(\frac{X}{X_t}\right)\right]^{\frac{4}{5}} X_t + \int_{X_t}^{X_0}\left(\frac{U}{U_0}\right)^3 dX, \tag{22}$$

where X is the distance from the actual leading edge and suffix t indicates values at transition. Suffix 0 now refers to conditions at the position of peak velocity, or at transition, whichever is later. If, however, transition is immediately followed by a steep pressure rise leading to separation the present theory would only be roughly correct, as the turbulent flat plate profile assumed to exist at $x = x_0$ would not be properly formed.

The profiles at separation

The derivation of the preceding sections can be used to obtain the profiles at the separation position; these are shown in figure 4 in the form of dynamic head profiles. It will be noticed that there is an appreciable variation in the shape of the separation profile with variation in the value of $C_{p,s}$.

The value of the ratio θ_s/θ', where θ' is the momentum thickness of the comparison boundary layer, is plotted in figure 5 as a function of $C_{p,s}$. The absolute value of θ_s for any given pressure distribution may be found by using this figure together with the relation for θ' from equation (5*c*).

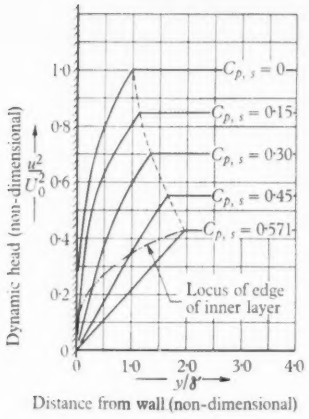

FIGURE 4. The idealized theoretical dynamic head profiles at separation, $R_s = 10^6$, δ' = thickness of the flat plate comparison profile.

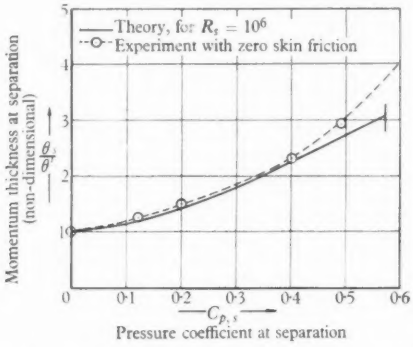

FIGURE 5. Momentum thickness of the boundary layer at separation, θ' = momentum thickness of the comparison profile.

5. Tests of the method and development of the formula to allow for variation of $(d^2p/d^2x)_s$

The formulae (19), of which formula (19*b*) strictly holds only for large negative values of d^2p/dx^2, will be applied to certain test pressure distributions and then a correction discussed for d^2p/dx^2.

The data are taken from von Doenhoff & Tetervin (1943) for the first three tests and from Schubauer & Klebanoff (1950) for the fourth; Schubauer & Klebanoff's measurements were made on a special surface in a large wind tunnel. In order to assist the assessment the experiment used for the empirical determination of β has been included as 'Test' 5. It should be noted that the experimental pressure distributions allow some range of interpretation as regards dp/dx, especially in the neighbourhood of a point of inflexion, and the effect on the theoretical prediction could be as much as $\pm 5\,\%$.

The results are shown in figures 6 and 7 and table 1 (pages 11–13).

It will be seen that in the main tests the prediction for the pressure recovery at separation is always too low. The discrepancy in β varies between 0 and 20 %; the discrepancy in $C_{p,s}$ is also in this range, but the precise value depends on how long the boundary layer 'hovers' (due to its softening of the pressure gradient) just close to the condition for separation, without actually separating.

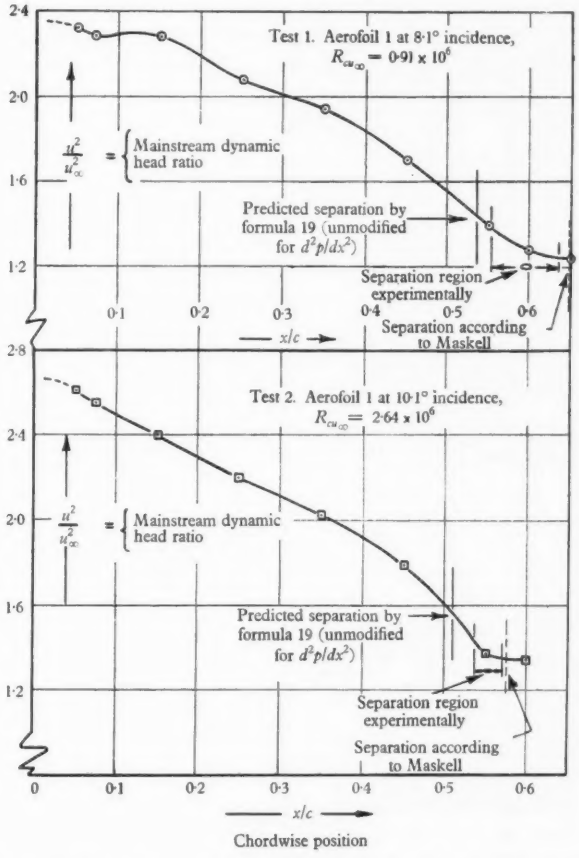
Test 1. Aerofoil 1 at 8·1° incidence,
$R_{cu_\infty} = 0{\cdot}91 \times 10^6$
$\frac{u^2}{u_\infty^2}$ = Mainstream dynamic head ratio
Predicted separation by formula 19 (unmodified for d^2p/dx^2)
Separation region experimentally
Separation according to Maskell
x/c
Test 2. Aerofoil 1 at 10·1° incidence,
$R_{cu_\infty} = 2{\cdot}64 \times 10^6$
$\frac{u^2}{u_\infty^2}$ = Mainstream dynamic head ratio
Predicted separation by formula 19 (unmodified for d^2p/dx^2)
Separation region experimentally
Separation according to Maskell
x/c
Chordwise position

FIGURE 6. Tests (1 and 2) of the method before its development to allow for the effect of d^2p/dx^2.

A closer examination of the results in conjunction with the pressure distribution shows that the error in the formulae increases with increase in the value of d^2p/dx^2 immediately prior to separation. Consideration of the theoretical analysis for the laminar boundary layer (Stratford 1954) shows that this is to be expected, and it would have been found in that case also that the use of the result obtained for flow with continuously zero skin friction would have caused a considerable error. At present, there is insufficient data to make full allowance for d^2p/dx^2 in the case

of the turbulent boundary layer, but a crude modification, that would about halve the error, would be to replace equation (19*b*) by

$$\left.\begin{aligned}\beta &= 0{\cdot}66 \quad (d^2p/dx^2 < 0),\\ \beta &= 0{\cdot}73 \quad (d^2p/dx^2 \geqslant 0),\end{aligned}\right\} \tag{23}$$

the relevant value of d^2p/dx^2 being that immediately prior to separation. The final result is then given by equations (19*a*), (19*c*) and (23). For the Reynolds numbers of the order of 10^6, the form quoted in the Summary is a convenient simplification.

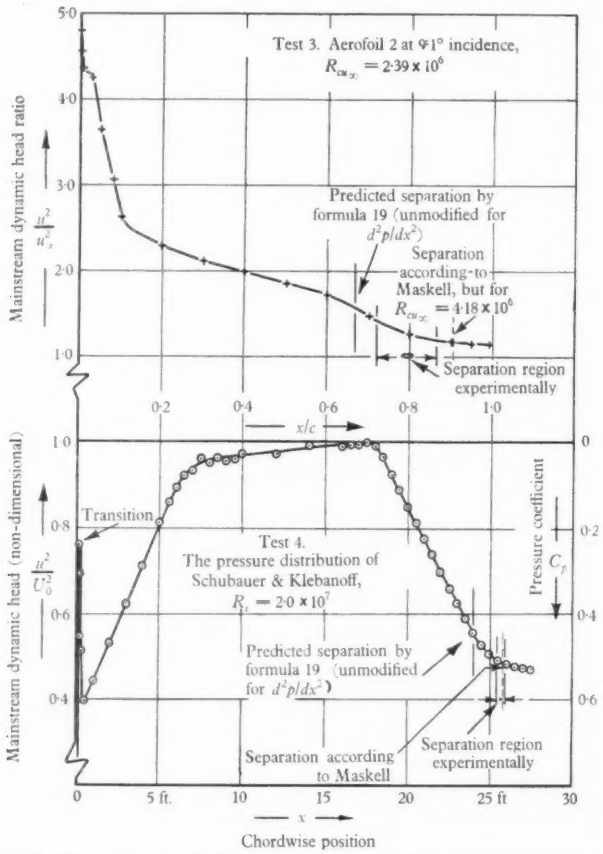

FIGURE 7. Tests (3 and 4) of the method before its development to allow for the effect of d^2p/dx^2.

Further tests would be desirable at extreme Reynolds numbers, in case, for example, the factor β should vary. At present β has been assumed to be independent of the Reynolds number.

As a further test of the basic theoretical concepts the theoretical predictions for the momentum thickness may be compared with the results taken from the experiment with continuously zero skin friction. The predictions are independent

of the empirical factor β when plotted in the form θ_s/θ' against C_p, as in figure 5; it is the more significant therefore that, as may be seen from the figure, the predictions are satisfactorily confirmed. The experiment also confirms the linear dynamic head close to the wall predicted by equations (10) and (14), at least for the special conditions of that experiment where there is no actual reverse flow. With flow reversal the softening of the pressure gradient, together with a new type of turbulence discovered while carrying out the experiment with zero skin friction, might tend to mask the linear dynamic head profile, although the criterion for separation would not be affected.

Test no. ...	1	2	3	4	5
Figure no.	6	6	7	7	4 of next paper
$R_s/10^6$	0·76	2·2	3·4	20	1·0 to 1·6
n (nominal value)	5·9	6·3	6·5	7·3	6·0
$C_{p,s}$ theory, before allowing for $(d^2p/dx^2)_s$	0·372	0·412	0·626	0·442	0 to 0·57, used for empirical fitting
$C_{p,s}$ experiment*	0·409 to 0·470	0·464 to 0·495	0·669 to 0·734	0·460 to 0·530	
Approx. increase in β required for theory to give agreement with experiment	+8 %	+20 %	+20 %	+2 %	0 %
d^2p/dx^2 immediately prior to separation	Slightly positive	Large and positive	Large and positive	Negative	Maximum negative

* The two experimental values quoted for $C_{p,s}$ for each test, correspond (except in test 5) respectively to the position where $C_p(x dC_p/dx)^{\frac{1}{2}}$ is a maximum (this is where the danger of separation is greatest according to the theory), and to the position where dC_p/dx has become zero (due to the separation destroying the pressure rise).

TABLE 1. Tests of the method using equations (19) without correction for $(d^2p/dx^2)_s$

Comparison with other methods

Results of calculations by the method of von Doenhoff & Tetervin (1943) and by that of Maskell (1951) are shown respectively in figure 8, and in figures 6 and 7. von Doenhoff & Tetervin's criterion for separation is that the shape parameter H should lie between 1·8 and 2·6 and this, it will be seen, leaves an indeterminacy of up to about 10 % in the predicted pressure rise to separation, i.e. about the same as for the present method. Maskell improves upon this accuracy mostly by using Ludweig & Tillmann's skin friction law, which, on extrapolation, gives the position of separation once the distributions of H and θ are known. Recently, Spence (1956*a*) has increased the usefulness of these types of analysis by developing a method whereby H may be more rapidly calculated. The accuracy of Maskell's predictions is probably highly satisfactory for most pressure distributions, although difficulty might be experienced with special pressure distributions such as very sharp pressure rises or the flow with continuously zero skin friction.

For most pressure distributions the present method probably would not be as accurate as either Maskell's method or the Maskell–Spence method until the

allowance for d^2p/dx^2 has been improved. However, it should be more accurate than those methods for the special types of pressure distribution mentioned above, and it could be employed generally, taking advantage of its considerably

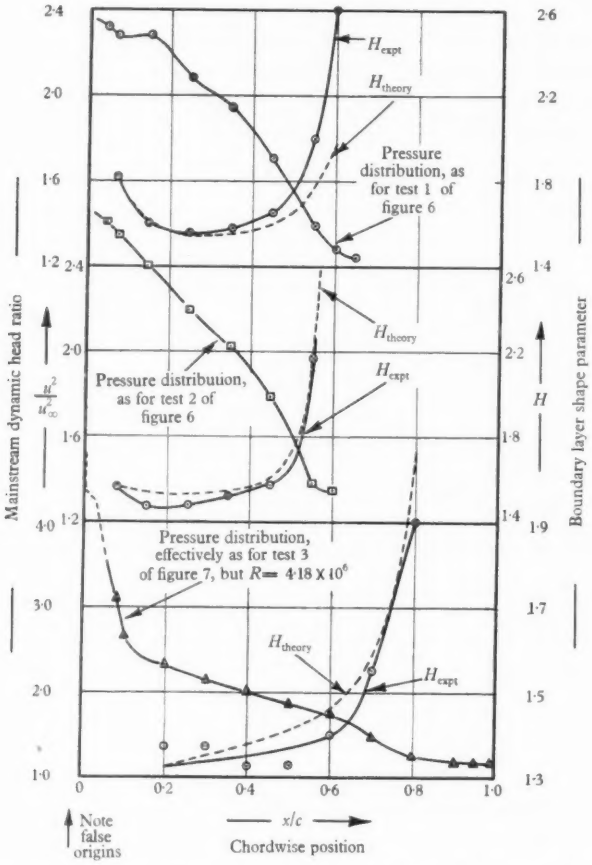
H_{expt}
H_{theory}
Pressure distribution, as for test 1 of figure 6
H_{theory}
H_{expt}
Pressure distribution, as for test 2 of figure 6
Pressure distribution, effectively as for test 3 of figure 7, but $R = 4{\cdot}18 \times 10^6$
H_{theory}
H_{expt}
Mainstream dynamic head ratio $\frac{u^2}{u_\infty^2}$
Boundary layer shape parameter H
Note false origins
x/c
Chordwise position

FIGURE 8. Results from the method of von Doenhoff & Tetervin (separation is assumed to occur when H is between 1·8 and 2·6).

greater speed, where its 10 % range of uncertainty is acceptable. Further claims for the present method are that it provides a better physical picture and understanding of the flow, and also a greater flexibility. The latter is demonstrated both by the ease with which may be seen the effects of any change in a given pressure distribution, and by the extension to flow with continuously zero skin friction, as obtained in § 6.

An example

We shall consider the case of a linear pressure rise starting at the leading edge, i.e. $C_p = x/c$. For simplicity it will be assumed that the Reynolds number R_s is

equal to 10^6. Since d^2p/dx^2 is zero, the value 0·73 is used in equation (23); equations (19*a*) and (19*c*) (or the equation of the Summary) then become

$$[(x/c)^{\frac{3}{2}}]_s = 0{\cdot}39,$$
$$x_s/c = C_{p,s} = 0{\cdot}53,$$
$$U_s/U_0 = 0{\cdot}68.$$

6. An extension to flow with continuously zero skin friction

If the separation condition of zero skin friction is reached at each point downstream of $x = x_0$, but separation itself is always just avoided, the separation criterion of equations (19) will apply at all positions and consequently will become a differential equation for the pressure distribution. On integration, neglecting the small variation of n with x, the pressure distribution is found to be

$$C_p = 0{\cdot}645\left\{0{\cdot}435R_0^{\frac{1}{5}}\left[\left(\frac{x}{x_0}\right)^{\frac{1}{5}} - 1\right]\right\}^{2/n} \quad \left(\tau_0 \equiv 0,\ C_p \leqslant \frac{n-2}{n+1}\right), \tag{24}$$

where $R_0 = x_0 U_0/\nu$, the coefficient 0·645 being a close fit (to $\frac{1}{2}$ % for $6 \leqslant n \leqslant 8$) to a function of n.

At a Reynolds number of $R_0 = 10^6$, when $n \doteqdot 6$, this pressure distribution becomes

$$C_p = 1{\cdot}23\left[\left(\frac{x}{x_0}\right)^{\frac{1}{6}} - 1\right]^{\frac{1}{3}} \quad (\tau_0 \equiv 0,\ C_p \leqslant \tfrac{4}{7}). \tag{25}$$

When $C_p = (n-2)/(n+1)$ the inner layer reaches the edge of the main boundary layer and equation (24) is at the limit of its validity. At greater pressure rises a solution could be sought in which the whole boundary layer retained a constant profile shape. Thus the simple form of the momentum equation is

$$\frac{d}{dx}(\rho U^2\theta) = \tau_0 + \delta^*\frac{dp}{dx}. \tag{26}$$

The value of the shape parameter H, $= \delta^*/\theta$, is put equal to a constant and, with the skin friction τ_0 equal to zero, the equation readily yields

$$\theta = \frac{\text{const.}}{(1-C_p)^{(1+\frac{1}{2}H)}}. \tag{27}$$

This may be transformed into a pressure distribution by direct resort to an argument based on similarity. Alternatively, the inner layer profiles of equations (10), (14) and (15) show that

$$\frac{dp}{dx} \propto \frac{\frac{1}{2}\rho u^2}{y},$$

and therefore, by similarity,

$$\frac{dp}{dx} \propto \frac{\frac{1}{2}\rho U^2}{\theta}. \tag{28}$$

Elimination of θ from equations (27) and (28), integration, and putting $H = 2{\cdot}0$, which would be the value for a linear dynamic head as used in the simplified inner layer profile, leads to

$$C_p = \left[1 - \frac{a}{(x+b)^{\frac{1}{2}}}\right] \quad \left(\tau_0 \equiv 0,\ C_p \geqslant \frac{n-2}{n+1}\right), \tag{29}$$

where a and b are constants, determined by continuity with the pressure distribution of equation (24). For a Reynolds number of $R_0 = 10^6$ continuity with equation (25) gives $a = 0{\cdot}39x_0^{\frac{1}{2}}$ and $b = -0{\cdot}78x_0$.

This extension of the theory has utilized the empirical value $\beta = 0{\cdot}66$ obtained from the experiment with zero skin friction; the closeness of the empirical fitting may be judged from the comparison shown in figure 4 of the following paper.

The work leading to the present paper was started in the Aeronautics Department of Imperial College and has been completed at the National Gas Turbine Establishment. The author is indebted to staff and colleagues who have given valuable criticism and advice, and to the Department of Scientific and Industrial Research for a grant which enabled the work to be initiated.

REFERENCES

VON DOENHOFF, A. E. & TETERVIN, N. 1943 *Rep. Nat. Adv. Comm. Aero., Wash.*, no. 772.

DURAND, W. F. (Ed.) 1943 *Aerodynamic Theory*, Vol. III. California Institute of Technology.

GOLDSTEIN, S. (Ed.) 1938 *Modern Developments in Fluid Dynamics*, Vols. I and II. Oxford University Press.

KALIKHMANN, L. E. 1943 *Dokl. Akad. Nauk, SSSR*, **38**, 165.

LUDWEIG, H. & TILLMANN, W. 1949 *Tech. Mem. Nat. Adv. Comm. Aero., Wash.*, no. 1285 (transl.).

MASKELL, E. C. 1951 *Aero. Res. Coun., Lond.*, Unpublished Paper no. **14**, 654.

ROTTA, J. 1953 Rep. no. 8. University of Göttingen.

SCHLICHTING, H. 1941 *Tech. Mem. Nat. Adv. Comm. Aero., Wash.*, no. 1218 (transl.).

SCHUBAUER, G. B. & KLEBANOFF, P. S. 1950 *Rep. Nat. Adv. Comm. Aero., Wash.*, no. 1030.

SPENCE, D. A. 1956*a* *Aero. Res. Coun., Lond.*, Unpublished Paper no. 18,261. (Modified method by Spence; also a review of methods including those of Garner, Schuh, Truckenbrodt, and Zaat.)

SPENCE, D. A. 1956*b* *J. Aero. Sci.* **23**, 3.

SQUIRE, H. B. 1950 *Rep. & Mem. Aero. Res. Coun., Lond.*, no. 2751.

SQUIRE, H. B. & YOUNG, A. D. 1937 *Rep. & Mem. Aero. Res. Coun., Lond.*, no. 1838.

STRATFORD, B. S. 1954 *Rep. & Mem. Aero. Res. Coun., Lond.*, no. 3002.

STRATFORD, B. S. 1956 *Curr. Pap. Aero. Res. Coun., Lond.*, no. 307.

STRATFORD, B. S. 1959 *J. Fluid Mech.* **5**, 17.

THWAITES, B. 1949 *Aero. Quart.* **1**, 245.

WALZ, A. 1943 U & M no. 3060. University of Göttingen.

YOUNG, A. D. & WINTERBOTTOM, N. E. 1940 *Rep. & Mem. Aero. Res. Coun., Lond.*, no. 2400.

An experimental flow with zero skin friction throughout its region of pressure rise

By B. S. STRATFORD
National Gas Turbine Establishment, Farnborough

(Received 17 July 1958)

A flow has been produced having effectively zero skin friction throughout its region of pressure rise, which extended for a distance of 3 ft. No fundamental difficulty was encountered in establishing the flow and it had, moreover, a good margin of stability. The dynamic head in the zero skin friction boundary layer was found to be linear at the wall (i.e. $u \propto y^{\frac{1}{2}}$), as predicted theoretically in the previous paper (Stratford 1959).

The flow appears to achieve any specified pressure rise in the shortest possible distance and with probably the least possible dissipation of energy for a given initial boundary layer. Thus an aerofoil which could utilize it immediately after transition from laminar flow would be expected to have a very low drag. A design pressure distribution (besides having the usual safety margin against stall) should have a slightly more gradual start to the pressure rise than in the present experiment, as small errors close to the discontinuity can cause difficulty.

1. Introduction

In aerodynamics there is a commonly occurring need to decelerate, or diffuse, the flow of fluid relative to a surface. On an aerofoil, for example, diffusion is likely to be necessary on the rearward upper surface whether the aerofoil be isolated, as for an aircraft wing, or in cascade, as for turbo-machinery. Moreover, the diffusion is required in a fairly short distance and with a minimum loss of energy. § 6 of the previous paper (Stratford 1959) considered a flow having continuously zero skin friction throughout its region of pressure rise and this flow, as it will be shown, might be expected to achieve diffusion in the shortest possible distance with probably the lowest possible loss. After a preliminary theoretical discussion an experiment will be described testing the flow.

The pressure distribution for the present flow has been derived by specifying that the boundary layer shall be just at the condition of separation, without actually separating, at all positions in the pressure rise. Now at the condition of separation the local pressure gradient is the steepest which can be applied to the boundary layer, because an attempt to apply a steeper gradient would cause actual separation and breakdown of the flow. The present pressure distribution might be expected, therefore, to attain any given pressure rise in the shortest possible distance for a given initial boundary layer. This may be confirmed formally by a simple extension of the theory of the previous paper.

The second property of interest concerns the energy loss. Since the present flow is at all points at the condition of separation, the skin friction is continuously zero. Now 'zero skin friction' might at first suggest low loss, but in fact losses due to the pressure gradient tend to compensate for the reduction in skin friction. It is not immediately clear from the momentum equation whether the present flow provides a net gain over other flows as the pressure gradient term, $\delta^* dp/dx$, is not readily calculated. However, consideration of the rate of energy dissipation by the shear forces throughout the boundary layer indicates that for a given local mainstream velocity the dissipation per unit length of surface would vary only slightly with the shape of the boundary layer profile (the latter determines the skin friction). Thus, flow with zero skin friction would have about the same loss per unit length as other flows, but, because it has the shortest possible length, it would have the least possible final loss. This argument, based upon the energy equation for the boundary layer, is not exact, and so the result will be verified in the next paragraph using the theory of the previous paper.

The previous paper shows that for any boundary layer in a pressure rise the total head in the outer layer is equal to that at the corresponding point in the comparison layer ($C_p = 0$). In the sub-layer, on the other hand, the total head is higher than in the comparison layer, the difference almost certainly being greater the greater the pressure rise; at the wall, clearly, the difference is equal to C_p. The energy loss in a flow with pressure rise is therefore less than in one without; moreover, the energy loss is least, at a given value of x, in the flow which has the greatest pressure rise, i.e. the present flow, which is continuously at the separation condition. It follows that the energy loss at a specified pressure rise will also be least in the present flow.

The advantage of minimum energy dissipation may not of itself be particularly significant in practical applications. On an aerofoil, for example, if the pressure gradient were shortened and, say, the region of constant pressure lengthened in order to maintain the lift unchanged, then for a fixed transition point the drag may not be appreciably different. A worthwhile gain would seem likely, however, if advantage were taken of the shortness of the pressure rise to increase the proportion of the chord over which the pressure gradient were favourable, in this way delaying transition. Such an aerofoil might be expected to represent the most efficient type that is possible without artificial boundary layer control. Wortmann (1955, 1957), Eppler (1955) and Speidel (1955) have already carried out a considerable volume of work on a similar type of aerofoil, this being based on the concepts of Wortmann using the boundary layer theory of Truckenbrodt (1952), and Wortmann (1957) has obtained improvements of the order of 20 % over certain previous low drag sections. Wortmann's pressure distribution appears to be more gradual than in the present experiment, as will be discussed later in the paper.

2. Apparatus and methods

The apparatus, sketched in figure 1, consisted of an open return wind tunnel having an 8 in. square-working section, a 9/1 ratio contraction, and a nominally 2/1 two-dimensional diffuser leading via transition sections to a fan. The speed

in the working section was approximately 55 ft./sec. The test boundary layer was that growing on one side wall of the working section and diffuser, and in this region the top wall of the apparatus was transparent.

The design shape of the test wall is shown in figure 2. The pressure distribution specified for the design was estimated from the evidence on boundary layer separation available at the time; the design geometry was then obtained from

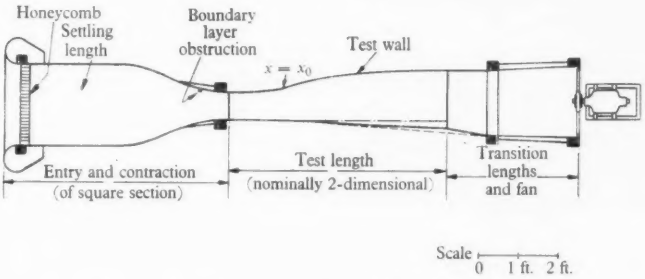

FIGURE 1. Plan-section sketch of the wind tunnel.

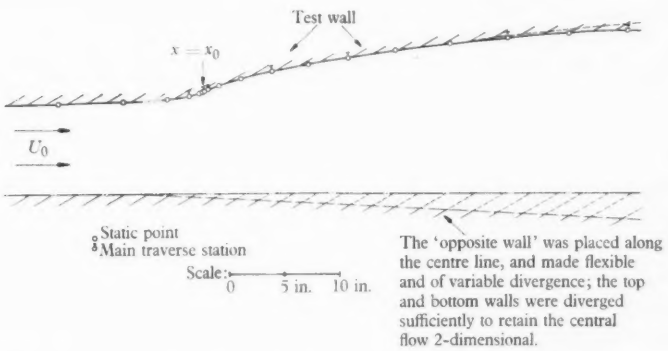
Test wall
$x = x_0$
U_0
Static point
Main traverse station
Scale: 0 5 in. 10 in.
The 'opposite wall' was placed along the centre line, and made flexible and of variable divergence; the top and bottom walls were diverged sufficiently to retain the central flow 2-dimensional.

FIGURE 2. Design of the test section.

this pressure distribution by applying corrections, based on physical arguments, to the shape that would be predicted from one-dimensional inviscid flow theory. Since the design method was only approximate and the correct pressure distribution was known only roughly before testing, and since the boundary layer itself would affect the pressure distribution, provision was made for varying the divergence and shape of the opposite wall, in conjunction, if necessary, with building up the surface of the test wall.

One embarrassing feature of the design was that the aspect ratio of the test wall was very low. This feature resulted when the test wall was made long in order that the test boundary layer should be thick and its measurement thereby facilitated. Consequently, precautions were necessary in order to ensure that the flow within the test region was two-dimensional. Thus the top and bottom walls of the diffuser were diverged in order to compensate the displacement

thickness of their boundary layers; by this means the effective span of the flow, as checked by traversing for the displacement thickness of the top and bottom boundary layers, was held constant for the main tests to within about 1 %. The principal measurements were made at mid-span, on either side of which the flow was of uniform total head; the minimum width of uniform flow was about 40 % of the span, as shown by the traverses of figure 3.

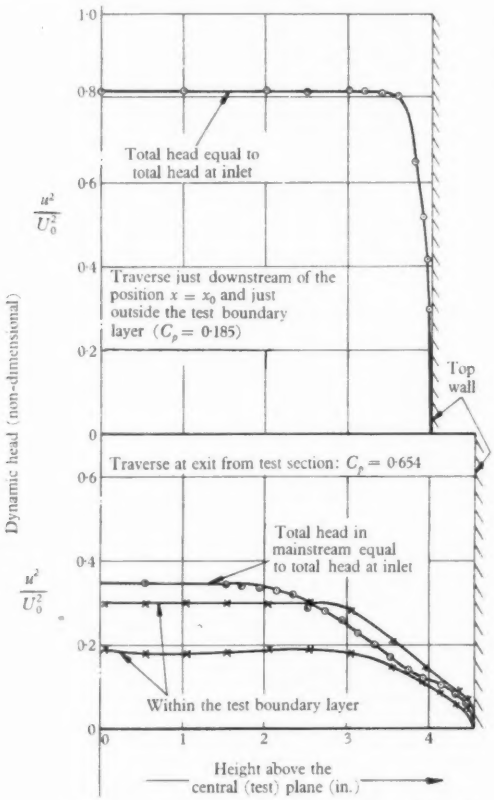

FIGURE 3. Spanwise variation of total head.

The method of finding the correct pressure distribution

The required flow was obtained by progressively earlier tripping of the test boundary layer in conjunction with the adjustments to the opposite flexible wall and slight building up of the test wall. In the final stages of this process the test boundary layer was thickened artificially just before entry to the working section. The correct and, at the time, unknown pressure distribution could thus be approached gradually even though the flow sought was everywhere close to separation.

The technique of artificial thickening was adopted when it was found desirable to shorten the original working section in order to reduce the thickness of the

boundary layers on the other walls. (Figure 1 is for the tunnel after shortening.) The artificial thickening resulted in an increase of 30 % in the value of the momentum thickness θ_0 at $x = x_0$. It was produced by a rectangular projection from the wall, this extending at first along the central 75 % of the span, but later along only the central 54 %. The projection had accurately ground surfaces in order to produce spanwise uniformity of loss, and it was preceded by a trip wire, this also being found necessary for obtaining spanwise uniformity. Traverses showed that despite the artificial thickening the test boundary layer had settled to a steady profile shape, to within about $2\frac{1}{2}$ % on velocity, well before reaching the region of pressure rise. Also its rate of growth $d\theta/dx$, and hence, presumably, its turbulence, was normal for a turbulent boundary layer without pressure gradient. The equivalent length x_0 of the test boundary layer in the main test was 35·2 in. giving a Reynolds number $x_0 U_0/\nu$ of $1{\cdot}0 \times 10^6$.

Simultaneously with the following through of the above process, small amounts of boundary layer control were applied to the other boundary layers, in particular at the corners, in order to prevent local separations or the development of large displacement thicknesses; these conditions could limit the pressure recovery attainable in the test section and even cause slight secondary flow on the test wall. Care was needed to prevent secondary flow near the control points themselves.

The process just outlined was straightforward in principle. In practice, however, it required much patient adjustment and modification. The greatest trouble that was encountered, apart from the embarrassments from the small aspect-ratio, occurred in correcting the pressure distribution near the discontinuity at $x = x_0$, the necessary correction itself being discontinuous at that point. A complicating factor was the sudden thickening of the test boundary layer on meeting the steep pressure gradient starting at the discontinuity.

The experimental pressure distribution obtained initially with a very thin boundary layer was quite close to design; the starting-point for the pressure rise was $\frac{1}{4}$ in. upstream of the design position, and the pressure coefficient at any given distance downstream of the starting-point was about 0·03 smaller than design. There was also a slight suction peak ($C_p = -0{\cdot}04$) just upstream of the discontinuity. The correct pressure distribution, i.e. that found necessary for giving continuously zero skin friction with the final thick boundary layer, had a pressure coefficient in most of the region of the pressure rise about 0·04 smaller than that of the initial experimental pressure distribution; this correct distribution was obtained as already described, the necessary distortions to the opposite wall being quite severe despite the smallness of the change required in C_p.

Observation techniques

Determination of the flow condition was based on the following techniques, the observations being considered in conjunction one with another.

(*a*) *Tuft behaviour.* Tufts indicated the steadiness and direction of the flow. The degree of unsteadiness became a good indication of the closeness to the separation condition.

(*b*) *Transition.* It being an open return tunnel, the chalk dust technique was used for indicating transition.

(*c*) *Static pressure distribution.* Readings from a multi-tube manometer indicated the smoothness of the distribution, its steadiness with time, and whether the maximum possible pressure rise was being obtained for a given initial boundary layer.

(*d*) *Substitution into the integrated momentum equation.* Ideally τ_0 could be obtained from the experiment by direct substitution into the momentum equation

$$\tau_0 = \frac{d}{dx}(\rho U_1^2 \theta) - \delta^* \frac{dp}{dx}. \tag{1}$$

However, the differentiation of the experimental values of $\rho U_1^2 \theta$ makes this method over-sensitive to error. A more satisfactory procedure is to integrate the momentum equation, thus obtaining

$$\left(\frac{\rho U_1^2 \theta}{\rho U_0^2 \theta_0}\right) = \left[1 + \int_{x_0}^{x} \frac{\delta^*}{2\theta_0} dC_p\right] + \frac{1}{\rho U_0^2 \theta_0} \int_{x_0}^{x} \tau_0 dx, \tag{2}$$

and to compare curves of the experimental values of

$$\frac{\rho U_1^2 \theta}{\rho U_0^2 \theta_0} \quad \text{and} \quad \left[1 + \int_{x_0}^{x} \frac{\delta^*}{2\theta_0} dC_p\right].$$

A difference between the curves indicates a non-zero skin friction force provided the flow is accurately two-dimensional.

(*e*) *Velocity traverses.* Standard theory for turbulent flow shows that there is a close relation between the skin friction and the height of the 'shoulder' which occurs very close to the wall in either the velocity profile or the dynamic head profile. Thus a qualitative estimate could be made of the closeness to separation just by looking at the Pitot traverse. The estimate could be made more precise by using the result of the previous paper that the skin friction is zero when, in effect, the shoulder in the dynamic head profile is zero or, more specifically, when the dynamic head close to the wall increases linearly from a zero value at the wall. However, since it was a part of the object of the experiment to verify this theory, agreement with it could be used only as additional corroboration.

The effect of turbulence on the Pitot reading

The Pitot readings have not been corrected for the effect of turbulence. Calculations for the main test suggest that the proportional effect on the local dynamic head could be appreciable, but that the effect on the momentum thickness should be small.

Variation of static pressure across the boundary layer

In positions very close to the discontinuity the wall is highly curved and the static pressure varies across the thickness of the boundary layer. Now the actual boundary layer at any station x would become the same as for an experiment which conformed to the conditions of the theoretical model (static pressure

constant across the thickness of the boundary layer at all positions) if both the static pressure at the station x were made constant and equal to that at the wall, and if it could be assumed that the difference upstream between the local and the wall static pressures did not affect significantly the total pressure in any streamtube at the station x. The latter would be reasonably true in the present experiment as the variation of static pressure across the boundary layer is found to be both small and confined to a short length of wall. Hence the present experimental results would correspond to those of an experiment conforming to the theoretical model if in the formula for θ,

$$\theta = \int_0^\infty (1-u/U)\,d\psi/U = \int_0^\infty (1-u/U)\,u\,dy/U, \tag{3}$$

the velocities were calculated from an equivalent dynamic head equal to the local total head minus the wall static pressure, the true volume flow, however, being retained in any streamtube. Consequently θ has been calculated on this basis.

3. Results

Characteristics of the flow

The flow had three important characteristics: (*a*) there was no fundamental difficulty in obtaining it, (*b*) it did appear to provide the shortest possible distance for a given pressure rise, and (*c*) it was stable.

(*a*) No fundamental difficulty was experienced in obtaining the flow with continuously zero skin friction; the relevant part of the test surface extended for just over 3 ft.

(*b*) The flow condition could be varied by altering the divergence and shape of the opposite wall. As far as could be ascertained, the condition for maximum pressure rise at any specified position on the test wall did coincide with the condition for continuously zero skin friction. For example, as the divergence of the diffuser was gradually increased the pressure rise at any given position on the test wall first increased to a maximum, which occurred when the skin friction had become effectively zero, it then remained almost constant for an appreciable range of divergence and, thereafter, it decreased. Attempts at improving upon the pressure rise given by the flow with continuously zero skin friction were never successful.

(*c*) The flow was found to be stable, and with the divergence just sufficient to reduce to zero the skin friction and to produce the maximum pressure rise, neither the losses, nor the steadiness of the pressure rise, were very sensitive to small changes in the passage divergence. In particular, a small increase in the divergence did not cause backflow. [Instead the displacement thickness of the test boundary layer increased sufficiently (up to a maximum of about 10 % of the total boundary layer thickness $\delta_{0{\cdot}99}$) to compensate the additional flow area, the skin friction remaining sensibly zero and the pressure distribution unaltered. This 'elasticity' in the boundary layer displacement thickness was made possible by the onset of a special regime of flow with a very high turbulence level close to the wall.]

The stability found for this flow is in contrast to the usual instability of turbulent flows near separation. In the present experiment the flow contained no dead-air region, while the boundary layers on the other three walls were controlled sufficiently to prevent separation; thus the geometry of the mainstream was virtually fixed. In most previous experiments, on the other hand, the mainstream geometry could vary either due to the presence of a dead-air region, or due to separation being imminent all round. Consequently, the usual instability found in previous experiments may be a result of the variable mainstream geometry rather than of the characteristics of the local boundary layer.

Quantitative results are shown in figure 4 onwards.

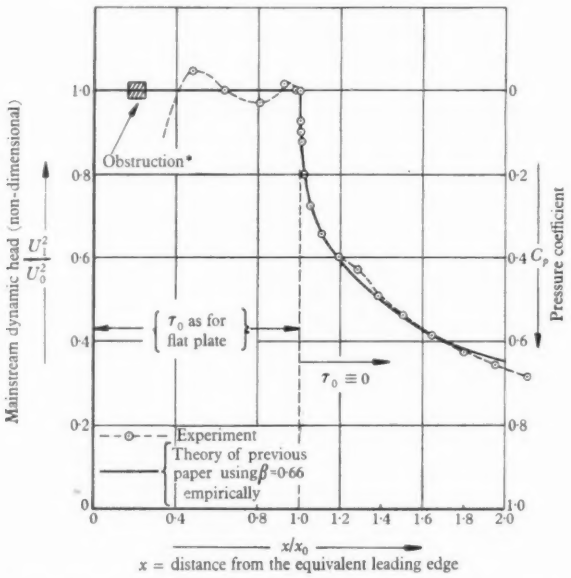

FIGURE 4. Pressure distribution for flow with zero skin friction ($R_0 = 10^6$). In the experiment the initial region (a length of about $\frac{1}{3}x_0$) was replaced by an equivalent obstruction, and the equivalence, including indirectly, the normality of the turbulence level, checked by boundary layer traverses.

4. Discussion of the results

The value of β

The immediate item of analytical data required from the experiment was the value of the factor 'β' necessary for completion of the theory. In figure 4 is shown a comparison of the experimental and 'theoretical' pressure distributions for producing continuously zero skin friction when a constant value of β, equal to 0·66, is used empirically in the theory; it will be seen that the fit of the curves is very good. (Most of the irregularities in the pressure distribution upstream of $x = x_0$ result from the distortions made in the opposite wall when setting the conditions in the main test length near and downstream of $x = x_0$.) The fact that β is of order unity supports the general concepts of the theoretical

method. It is notable how close an agreement is obtained using a value of β which is independent of x/x_0. The evidence is insufficient of course to show that there are not even small variations in β with x/x_0.

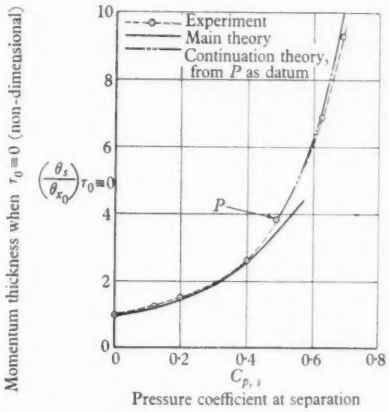

FIGURE 5. Momentum thickness of the boundary layer.

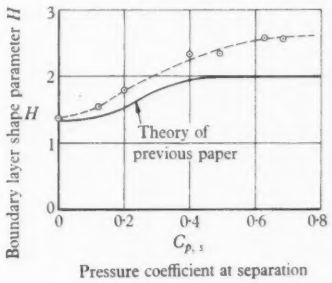

FIGURE 6. Values of the shape parameter $H = \delta^*/\theta$.

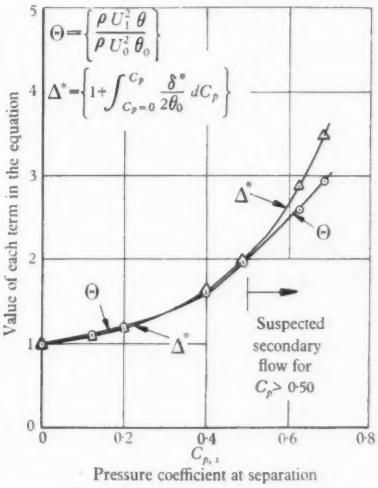
$\Theta = \left\{\frac{\rho U_1^2 \theta}{\rho U_0^2 \theta_0}\right\}$
$\Delta^* = \left\{1 + \int_{C_p=0}^{C_p} \frac{\delta^*}{2\theta_0} dC_p\right\}$
Value of each term in the equation
Δ^*
Θ
Suspected secondary flow for $C_p > 0{\cdot}50$
$C_{p,s}$
Pressure coefficient at separation

FIGURE 7. Substitution into the integrated momentum equation (2).

The main test

Some details from the main test, for which the pressure distribution was as in figure 4, are given in figures 5 to 8, together with the theoretical profiles for comparison in figure 9.

This main test provided the shortest pressure rise that it was found possible to achieve in the experiment, and it may be judged from the dynamic head profiles that the skin friction is zero, or very close to zero. The linear profile for the

dynamic head (figure 8), close to the wall in the inner layer, is visible particularly in the profiles for $C_p = 0{\cdot}122$, $C_p = 0{\cdot}200$ and $C_p = 0{\cdot}682$. The very slight shoulder in the profiles at $C_p = 0{\cdot}399$, $C_p = 0{\cdot}489$ and $C_p = 0{\cdot}624$, indicates an imperfection in setting the condition, so that the corresponding skin friction is still very slightly positive. (A special test to check that a linear profile is possible at these latter values for C_p was able to produce results such as curve 'b' of figure 12.)

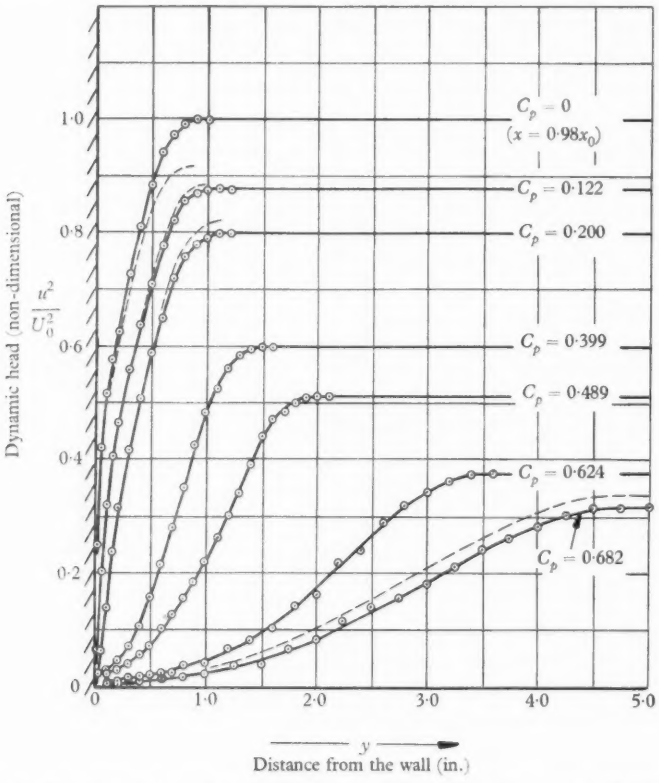

FIGURE 8. The dynamic head profiles. The full line profiles represent total pressure minus static pressure at the wall. Where the static pressure varies across the boundary layer the true dynamic head is represented by the broken lines. The C_p values refer to the wall.

At the condition of this test the tufts were beginning to become unsteady but there was no sign of backflow or serious oscillation. Examination of figure 7 shows that the flow is consistent with the integrated momentum equation with $\tau_0 \equiv 0$, up to $C_p = 0{\cdot}5$; above this value there is a discrepancy, the final momentum deficiency being about 15 % less than it apparently should be. Since the skin friction is certainly not negative it would seem that there was some loss of fluid from the later part of the test boundary layer, presumably by spanwise flow on that part of the test wall, despite the precautions taken; thus the results for this test are not accurate above, say, $C_p = 0{\cdot}5$.

When plotted against C_p, as in figure 5, the momentum thickness shows a very rapid increase above, say, $C_p = 0{\cdot}5$, at which position it has quadrupled its value at $x = x_0$. Comparison with figure 4 shows that the rate of increase with x would be greatest in the range just downstream of x_0. Figure 5 indicates reasonable agreement with the theoretical values for the momentum thickness. (If this is plotted as θ_s/θ_b against C_p, as in figure 5 of the previous paper, the theoretical values are independent of the empirical factor β. The agreement obtained, which is effectively the same as in the present figure 5, provides significant confirmation of the soundness of the theoretical concepts.)

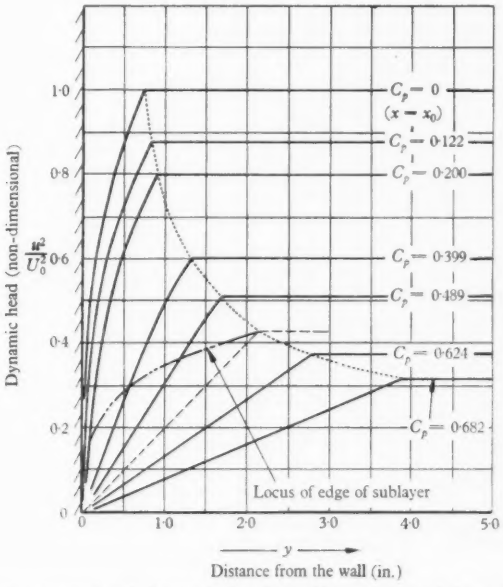

FIGURE 9. The theoretical dynamic head profiles calculated from the previous paper, for comparison.

The experiment confirms the linear dynamic head predicted theoretically for the inner layer near the wall. The experimental profiles, however, show a region of concavity. This is not surprising in view of the fact that the theoretical profiles have been idealized for simplicity of analysis. In terms of the theory the concavity is explained by a sharp fall-off in the value of the mixing length from the idealized linear value assumed for it. The conversion of a dynamic head profile with such a concavity to a velocity profile gives the hump characteristic of turbulent boundary layers near separation. (On the other hand, a hump is obtainable in the dynamic head profile itself as, for example, in the tests of figures 10 and 11, which will be discussed later.)

In using the results just quoted as confirmation of the theory the argument is not quite complete. Thus the theory suggests: first, that the skin friction falls to zero when the dynamic head becomes linear; and secondly, that the shortest possible pressure rise for a given initial boundary layer is obtained when the skin

friction is continuously zero. The experiment, on the other hand, verifies that the shortest possible pressure rise for a given initial boundary layer is obtained when the hump in the dynamic head profile close to the wall has been reduced to zero and the dynamic head has become linear, at all positions along the wall; it is only the almost circumstantial evidence provided by the behaviour of the tufts,

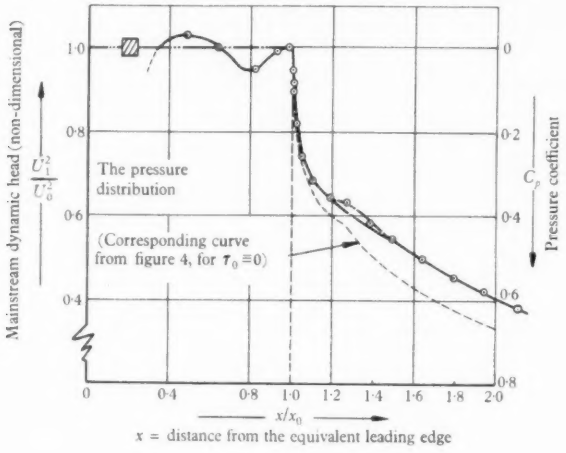

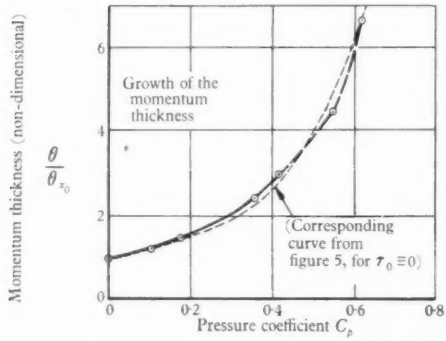

FIGURE 10. Details of the flow with a slightly slower pressure rise.

by substitution into the integrated momentum equation, by the steadiness of the pressure distribution, and by earlier qualitative ideas that the skin friction was related to the hump in the profile close to the wall, which confirms that this condition of a linear dynamic head coincides also with an effectively zero skin friction.

A slightly more gradual pressure rise

For comparison with the main test figures 10 and 11 show the effect of using a slightly more gradual pressure rise, the Reynolds number $x_0 U_0/\nu$ being maintained at the same value as before.

With the more gradual pressure rise the tufts indicated that the flow was very steady, the dynamic head profiles of figure 11 showing that it was appreciably away from separation. The effect of the skin friction on the increase of momentum deficiency was still small however, in comparison with the increase due to pressure gradient, as may be seen from the momentum equation in figure 11. It is not surprising, therefore, that the momentum thickness expressed as a

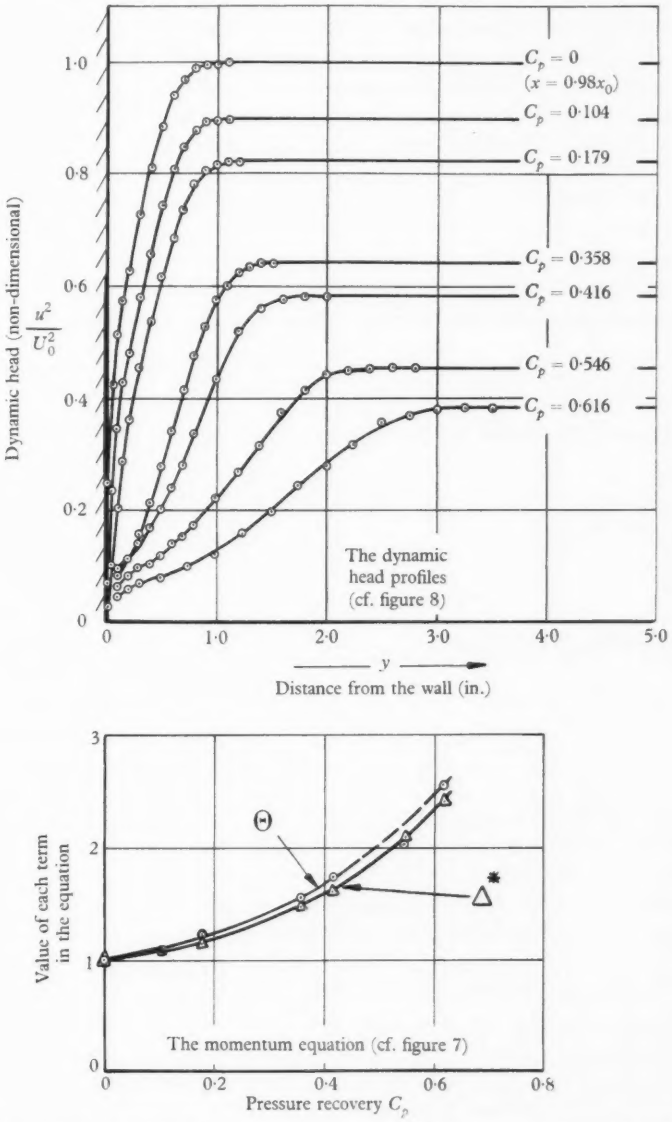

FIGURE 11. Further details of the flow with a slightly slower pressure rise.

function of pressure recovery, as in figure 10, was only a little greater than for the main test. (Considered from another viewpoint, θU_1^3 is related to the energy dissipation, which in turn may be related approximately to $\left[\int_0^x (U_1/U_0)^3\,dx\right]^{\frac{1}{3}}$. At, say, $C_p = 0{\cdot}5$, this last quantity had increased by only 8 % between the two tests.)

Although such a flow as represented in figures 10 and 11 would require a distance 50 % greater than for the flow with zero skin friction in order to achieve any specified pressure recovery, the pressure rise would still be very rapid, achieving, for example, a pressure recovery of $C_p = 0{\cdot}3$ in a length equal to 10 % of the length x_0, and $C_p = 0{\cdot}5$ in a length equal to two-thirds of x_0.

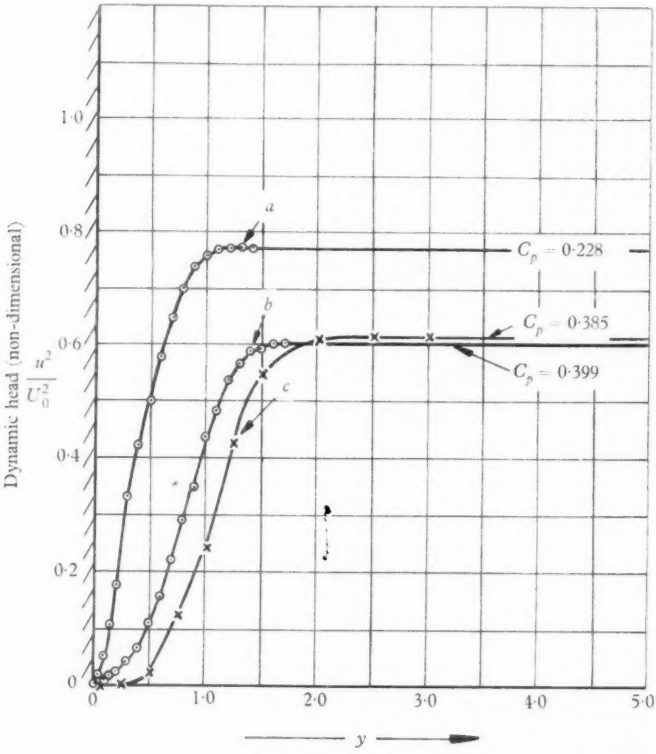

FIGURE 12. Some further dynamic head profiles.

Increased divergence—the regime with a very high turbulence level

Some further dynamic head profiles are shown in figure 12; these were all taken at different settings of the diffuser, profiles '*a*' and '*b*' each being for a slightly greater divergence rate than was used for the main test (figures 4 to 8).

Profile '*c*' of figure 12 is typical of the flow all along the test wall when the divergence was increased as much as was possible without producing a region

where the time-mean component of velocity was reversed. In this flow the tufts at the wall oscillated backwards and forwards violently indicating that the turbulence, if this name may be applied, was locally very intense. The static pressure as indicated by a sloping liquid manometer oscillated slightly; the maximum pressure recovery at each position was close to that for figures 4 to 8, while the minimum was approximately 7 % less, the time-mean being 0·01 or 0·02 less according to position. The flow as a whole, however, was still fairly steady. Since the pressure recovery at any specified position did not increase beyond that of the main test it follows that the increased divergence had been absorbed by an increase in the displacement thickness of the boundary layer. This is borne out by the shape of the profile; thus the dynamic head measurement was very close to zero for a depth of a $\frac{1}{4}$ in. from the wall, while the value of H, $= \delta^*/\theta$, had become 3·9, the largest measured in the experiment.

An increase in the divergence of the diffuser beyond that for profile '*c*' of figure 12 produced a narrow region of backflow all along the test wall; the pressure rise became erratic, although the maximum value at any position still remained close to that for the main test. At a still greater divergence a complete breakdown of the flow occurred, with loss of pressure recovery and severe large scale fluctuations in the flow pattern and pressure distribution.

From a practical designer's viewpoint it is reassuring to know that, for the flow with effectively zero skin friction, the boundary layer, by means of its 'elastic' displacement thickness, allows some tolerance in the positioning of the wall. The tolerance is of the order of 10 % of the local boundary length thickness $\delta_{0\cdot99}$. For a diffuser, the tolerance would be available presumably on only a part of the periphery, as otherwise the flow might become unstable, due to having exceeded the divergence for maximum (time-mean) pressure recovery.

Mixing length distributions

Finally, figure 13 shows the distributions of mixing length calculated from some of the profiles. By using the equation for the inner layer profile obtained in the previous paper the values of the mixing length near the wall are readily shown to be given by

$$\left(\frac{\partial L}{\partial y}\right)_0 = \left\{\frac{2dC_p/dx}{[\partial(u^2/U_0^2)/\partial y]_0}\right\}^{\frac{1}{2}}, \tag{4}$$

where suffix 0 indicates values at $y = 0$. The values away from the wall have been obtained with the aid of a semi-theoretical estimate of the inertia forces in the inner layer.

These distributions of mixing length will not be very accurate as two differentiations of experimental profiles are necessary, together with the assumption that the skin friction is precisely zero; moreover, for an examination of the flow which obtains before the onset of the intense turbulence the dynamic head profile must be just linear, a critical condition which is not easily set in the experiment. Of the distributions shown in figure 13 those for curve '*b*' of figure 12 and for '$C_p = 0{\cdot}200$' of figure 8 are close to this critical condition, for which the mixing length is seen to be not very different from that for the boundary layer on a flat plate. A more precise conclusion would not be justified by the evidence

available. For comparison Ludweig & Tillmann (1949) concluded for a turbulent boundary layer in a weak adverse pressure gradient that there was no change in the mixing length. On the other hand, for fully turbulent diffusers Squire (1950) and Stratford (1956) considered that the turbulence was greater than for the corresponding flow in a parallel pipe, Stratford (1956) suggesting that the increase

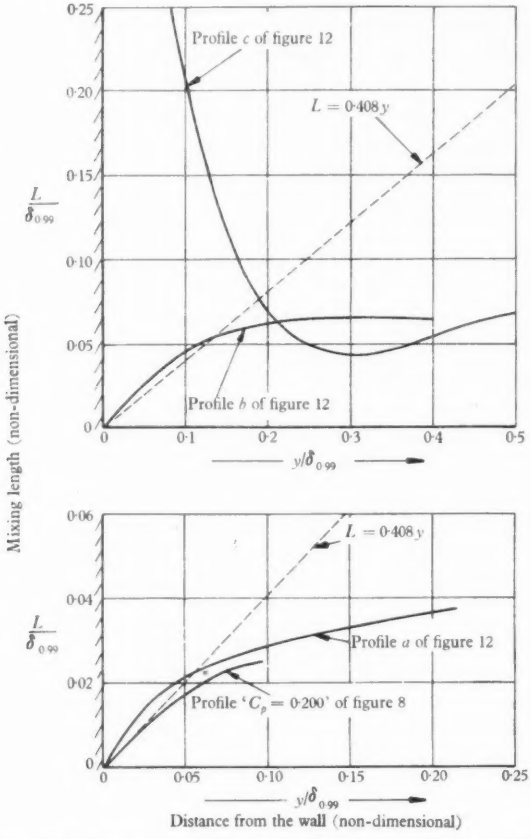
Profile c of figure 12
L = 0·408 y
Profile b of figure 12
L/δ0·99
y/δ0·99
Mixing length (non-dimensional)
L = 0·408 y
Profile a of figure 12
Profile 'Cp = 0·200' of figure 8
Distance from the wall (non-dimensional)

FIGURE 13. The turbulence level: some calculated mixing length distributions.

in the mixing length exceeded 30 %. It will be noticed that for none of the profiles in figure 13 is the value of $(\partial L/\partial y)_0$ less than 0·41, the value used for the flat plate boundary layer. The fact that β has been found to be less than unity in the present experiment is attributed to the rapid fall off in the mixing length away from the wall.

When the divergence is increased beyond that for the critical condition the turbulence as represented by $(\partial L/\partial y)_0$ at first increases, as for profile 'a' of figures 12 and 13, and eventually becomes of a higher order of magnitude, as shown for profile 'c', infinities nominally becoming involved. This type of behaviour supports the indication from the tufts.

Since the regime of intense turbulence does not cause an increase in the attainable pressure recovery at any position it does not affect the condition for separation; in particular it does not alter the theoretical prediction of the previous paper. There would, however, at a position of separation and flow reversal be a softening of the predicted discontinuity according to which $\partial u/\partial y$ at the wall changes from infinity positive to infinity negative.

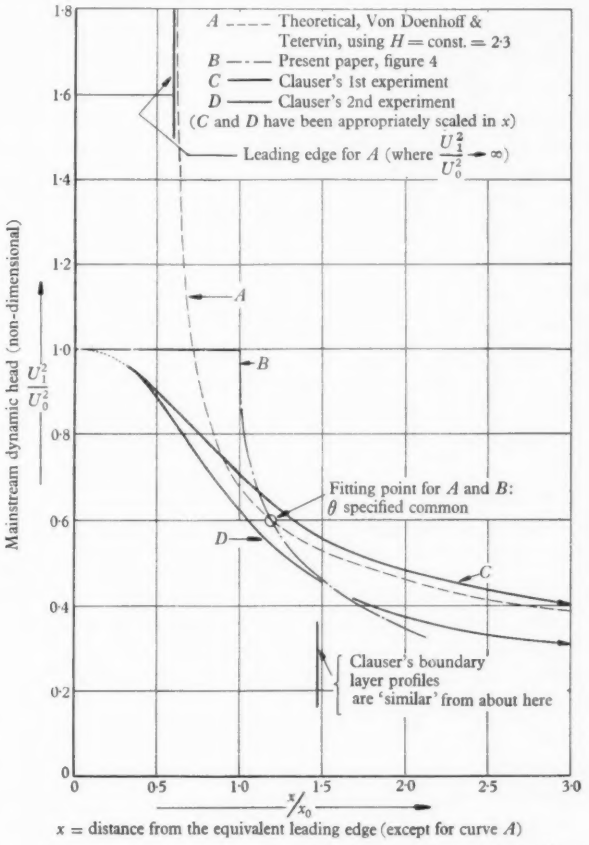
A ---- Theoretical, Von Doenhoff & Tetervin, using H = const. = 2·3
B —·— Present paper, figure 4
C —— Clauser's 1st experiment
D —— Clauser's 2nd experiment
(C and D have been appropriately scaled in x)
Leading edge for A (where U1²/U0² → ∞)
Mainstream dynamic head (non-dimensional) U1²/U0²
Fitting point for A and B: θ specified common
Clauser's boundary layer profiles are 'similar' from about here
x/x0
x = distance from the equivalent leading edge (except for curve A)

FIGURE 14. Comparison with other pressure distributions.

Comparison with other special pressure distributions

von Doenhoff & Tetervin (1943) have derived equations for a pressure distribution which would maintain the boundary layer at the separation condition, with similar velocity profiles, at all stations along the surface. In figure 14 this pressure distribution, calculated from their equations using the value $H = 2{\cdot}3$, is compared with the pressure distribution of the present paper. At the fitting point the values of H and θ are common to the two boundary layers, and so it might be expected that downstream of this point the pressure distributions should agree. In fact, they disagree.

Examination of von Doenhoff & Tetervin's analysis suggests that the derivation of this pressure distribution is not an appropriate application of their theory. Although the latter should be reasonably accurate for predicting separation when the profile shape is changing rapidly, there appears to be no evidence in support of their empirical auxiliary relations when a boundary layer near separation has a steady profile shape. In such a flow their relations become an extrapolation which, it would seem, could not be considered more than tentative.

In figure 14 are reproduced two experimental pressure distributions of Clauser (1954); each of these distributions gives a constant shape in the outer part of the boundary layer downstream of an initial settling length. For his first experiment Clauser considers that the bounday layer is far from separation while, for his second experiment, although this is closer to separation, he considers the skin friction still to be greater than zero. It would seem, therefore, that the pressure distribution of the present paper could be considered a reasonable extrapolation to zero skin friction from the two distributions of Clauser. The difference in the Reynolds number between Clauser's test and the present should cause only a very small effect. Comparison of velocity profiles using the variable adopted by Clauser, i.e. $(u-U_1)/u^*$, is not possible as $1/u^*$ $(=\sqrt{[\rho/\tau_0]})$ is infinite in the present test, where $\tau_0 = 0$.

Wortmann (1955, 1957) has produced pressure distributions for a constant form parameter H using the method of calculation of Truckenbrodt (1952). Although exact comparison is complicated by interpretation of the conditions at transition, Wortmann's experiments being for laminar flow aerofoils on which the close control of transition presented some difficulty, it would seem that the steepest pressure rise used by Wortmann is intermediate between Clauser's and that of the present experiment. Speidel's (1955) test of an aerofoil designed by Wortmann also appears to have a more gradual pressure rise than in the present experiment. Some of the difference in the rates of pressure recovery is probably due to the difference in Reynolds numbers.

The results of the present experiment check quite accurately both within themselves and with the predictions of the previous paper, and they are in at least qualitative agreement with Clauser's results and with the distributions of Wortmann. However, it would be desirable to have confirmatory evidence from a surface of larger aspect ratio before the accuracy of the present paper were regarded as established.

The value of n in the flat plate relationship, $u/U_0 = (y/\delta)^{1/n}$

Profiles were analysed for two positions upstream of the position $x = x_0$, figure 15 showing logarithmic and direct plots for a Reynolds number of $0{\cdot}64 \times 10^6$ $(= 10^{5{\cdot}8})$. It was concluded that the relation adopted in the previous paper, i.e. $n = \log_{10} R$, was reasonably satisfied near $R = 10^6$.

The experiment described in this paper was carried out in the Aeronautics Department of Imperial College, London. The author is indebted to the staff of that Department for stimulating criticism and advice, and to the Department of Industrial and Scientific Research for a grant which enabled the work to be undertaken.

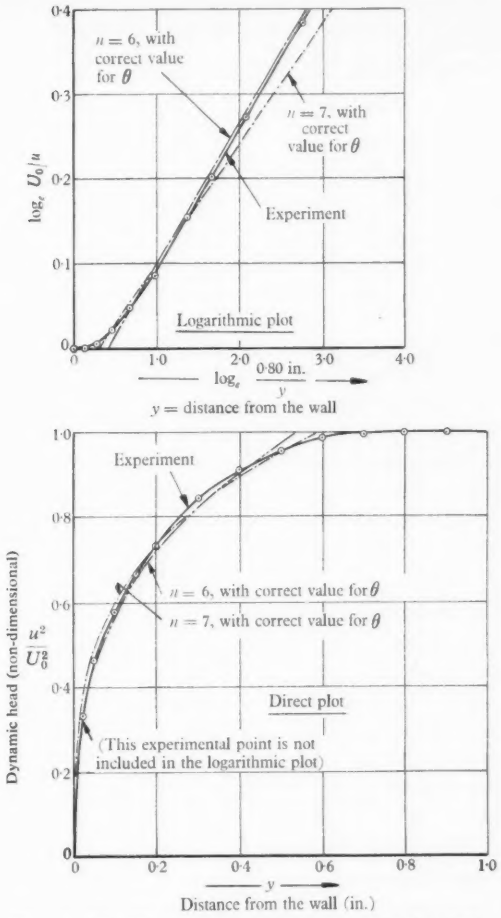
$n = 6$, with correct value for θ
$n = 7$, with correct value for θ
Experiment
Logarithmic plot
$\log_e \frac{U_0}{u}$
$\log_e \frac{0{\cdot}80 \text{ in.}}{y}$
y = distance from the wall
Experiment
$n = 6$, with correct value for θ
$n = 7$, with correct value for θ
Direct plot
(This experimental point is not included in the logarithmic plot)
Dynamic head (non-dimensional) $\frac{u^2}{U_0^2}$
Distance from the wall (in.) y

FIGURE 15. The value of 'n' when $R = 0{\cdot}64 \times 10^6$.

REFERENCES

CLAUSER, F. H. 1954 *J. Aero. Sci.* **21**, 91.

VON DOENHOFF, A. E. & TETERVIN, N. 1943 *Rep. Nat. Adv. Comm. Aero., Wash.*, no. 772.

EPPLER, R. 1955. *Z. Flugwiss.* **3**, 345 (British M.o.S. transl., in preparation).

LUDWEIG, H. & TILLMANN, W. 1949 *Tech. Mem. Nat. Adv. Comm. Aero., Wash.*, no. 1285 (transl.).

SPEIDEL, L. 1955 *Z. Flugwiss.* **3**, 353 (British M.o.S. transl., in preparation).

SQUIRE, H. B. 1950 *Rep. & Mem. Aero. Res. Coun., Lond.*, no. 2751.

STRATFORD, B. S. 1956 *Curr. Pap. Aero. Res. Coun., Lond.*, no. 307.

STRATFORD, B. S. 1959 *J. Fluid Mech.* **5**, 1.

TRUCKENBRODT, E. 1952 *Ingen.-Arch.* **20**, 211.

WORTMANN, F. X. 1955 *Z. Flugwiss.* **3**, 333 (British M.o.S. transl., in preparation).

WORTMANN, F. X. 1957 *Z. Flugwiss.* **5**, 228 (British M.o.S. transl., in preparation).

Two solutions for inviscid rotational flow with corner eddies

By CHIA-SHUN YIH
Department of Engineering Mechanics, University of Michigan

(Received 11 June 1958)

The steady rotational flow of an inviscid fluid in a two-dimensional channel or a circular tube toward a sink is treated. The velocity distribution at infinity is approximated by a cosine curve (which is nearly parabolic) for the two-dimensional case, and is taken as exactly parabolic for the axisymmetric case. The dependence of vorticity on stream-function is assumed to be everywhere the same as it is for streamlines coming from infinity upstream. The resulting linear equations of motion are solved exactly. The solutions show the rather unusual features of separating streamlines and regions of closed flow (corner eddies).

It is well known that, for a viscous fluid flowing in a channel or pipe with an abrupt contraction, eddies occur at the corners immediately preceding that contraction. The occurrence of such eddies, and their shape and size, are probably influenced strongly by the rotationality of the flow far upstream, and the intention in this note is to show two simple solutions which throw a little light on this influence. Since we are interested here in the effect of upstream vorticity only, the direct effect of viscosity will be ignored, although the distribution of vorticity far upstream will be assumed to be the same (or nearly so) as it would be for a fluid with viscosity. The particular flow to be studied is that of an inviscid homogeneous fluid in a long channel or pipe toward a sink in the middle of a wall across the channel. Under these assumptions, exact solutions of the governing differential systems (assumed to apply to the entire region of flow) will be seen to show the existence of separating streamlines and regions of closed flow or corner eddies. (For another instance of corner eddies, in stratified flow, see Yih (1958).) No singular surfaces occur in the flow (nor could they, in view of the assumption made about the dependence of vorticity on stream-function), and the solutions to be given are unlikely to represent the corresponding flow of a real fluid at large Reynolds number; this is part of the penalty for neglecting viscous forces entirely.

Two-dimensional flow into a line sink

In this section we consider steady two-dimensional flow in a long channel with half-width equal to unity terminating in a wall with a symmetrically placed line sink. The origin of a system of Cartesian co-ordinates is taken at the sink, with the centreline of the channel as the x-axis (see figure 1).

If ψ is Lagrange's stream function, the equation governing steady two-dimensional flow of an inviscid fluid is

$$\nabla^2\psi \equiv \frac{\partial^2\psi}{\partial x^2} + \frac{\partial^2\psi}{\partial y^2} = f(\psi), \tag{1}$$

where $-f(\psi)$ represents the vorticity and depends on ψ alone. The velocity distribution far upstream from the sink should be parabolic if it is to be made the same as that for the laminar flow of a viscous fluid in a long channel. However, a parabolic distribution of the upstream velocity would make equation (1) non-linear and preclude the possibility of a simple solution. Since we are looking here

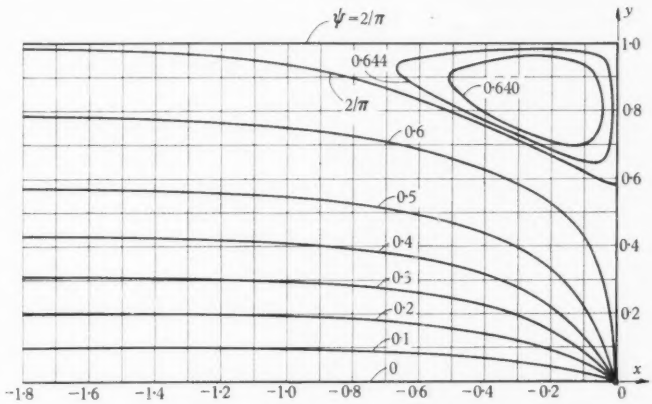

FIGURE 1. Pattern of two-dimensional flow into a sink.

for the effect of non-uniformity of the upstream velocity, a cosine distribution, which is nearly parabolic and makes equation (1) linear, can usefully be assumed. If the upstream velocity U is measured in terms of the centreline velocity $U_{\max}$, the dimensionless upstream velocity is then

$$u = U/U_{\max} = \cos\tfrac{1}{2}\pi y, \tag{2}$$

which vanishes at the walls ($y = \pm 1$). The corresponding (dimensionless) stream function far upstream is then

$$\psi = \int_0^y \cos\tfrac{1}{2}\pi y\, dy = (2/\pi)\sin\tfrac{1}{2}\pi y, \tag{3}$$

and the vorticity is

$$-\nabla^2\psi = \tfrac{1}{2}\pi\sin\tfrac{1}{2}\pi y = \tfrac{1}{4}\pi^2\psi. \tag{4}$$

Thus the function $f(\psi)$ is equal to $-\frac{1}{4}\pi^2\psi$ not only far upstream but everywhere, and equation (1) becomes

$$\nabla^2\psi = -\tfrac{1}{4}\pi^2\psi. \tag{5}$$

The boundary conditions on ψ are

(i) $\psi \to (2/\pi)\sin\frac{1}{2}\pi y$ as $x \to -\infty$,
(ii) $\psi = \pm(2/\pi)$ for $y = \pm 1$,
(iii) $\psi = \mp(2/\pi)$ for $y \lesssim 0$ and $x = 0$.

Solution of equation (5) by the method of separation of variables yields

$$\psi = (2/\pi)\sin\tfrac{1}{2}\pi y + \sum_{n=1}^{\infty} C_n \sin n\pi y \exp\{(n^2-\tfrac{1}{4})^{\frac{1}{2}}\pi x\}, \tag{6}$$

which satisfies (i) and (ii), and is an odd function of y. It is therefore only necessary to determine the C_n to satisfy

$$\sum_{n=1}^{\infty} C_n \sin n\pi y = (2/\pi)(1-\sin\tfrac{1}{2}\pi y) \quad (0 < y \leqslant 1), \tag{7}$$

which yields

$$C_n = \frac{4}{n\pi^2}\left(1+\frac{\cos n\pi}{4n^2-1}\right). \tag{8}$$

Equations (6) and (8) constitute the solution. The flow pattern for half of the channel is shown in figure 1, in which the corner eddy is evident. The point of separation is at infinity upstream.

It should be noted that, since the flow in the eddies does not originate at infinity, there is no *a priori* reason why equations (4) and (5) should govern the flow in the eddies. The details of the eddy flow may be significantly different from those given by equation (6) (see Batchelor 1956), and the solution (6) is likely to be valid for a viscous fluid at high Reynolds number only for the region outside the corner eddies.

Axisymmetric flow into a point sink

In this section we consider steady axisymmetric flow in a long circular pipe with unit radius terminating in a wall with a point sink at the centre. The point sink will be taken to be the origin of a set of cylindrical co-ordinates, with the centreline of the pipe as the z-axis and with the radial distance therefrom denoted by r (see figure 2).

If ψ is now Stokes's stream function, steady axisymmetric flow of an inviscid fluid is governed by the equation

$$\frac{\partial^2\psi}{\partial r^2} - \frac{1}{r}\frac{\partial\psi}{\partial r} + \frac{\partial^2\psi}{\partial z^2} = r^2 F(\psi), \tag{9}$$

where $rF(\psi)$ represents the vorticity and F depends on ψ alone (Lamb 1945). The velocity distribution far upstream can here be assumed to be parabolic, as for the laminar flow of a viscous fluid in a long pipe, so that the dimensionless velocity far upstream is

$$w = W/W_{\max} = r^2 - 1. \tag{10}$$

The corresponding dimensionless stream function far upstream is

$$\psi = \tfrac{1}{2}r^2 - \tfrac{1}{4}r^4, \tag{11}$$

and the vorticity there is $-2r$. Thus the function F is constant (-2) far upstream and hence everywhere, and the equation governing the flow everywhere is

$$\frac{\partial^2\psi}{\partial r^2} - \frac{1}{r}\frac{\partial\psi}{\partial r} + \frac{\partial^2\psi}{\partial z^2} = -2r^2. \tag{12}$$

The boundary conditions are

(i) $\psi \to \frac{1}{2}r^2 - \frac{1}{4}r^4$ as $z \to \infty$,
(ii) $\psi = \frac{1}{4}$ for $r = 1$,
(iii) $\psi = \frac{1}{4}$ for $z = 0$ $(0 < r \leqslant 1)$.

Solution of equation (12) by the separation of variables yields

$$\psi = \tfrac{1}{2}r^2 - \tfrac{1}{4}r^4 + \sum_{n=1}^{\infty} C_n r J_1(\lambda_n r) \exp(-\lambda_n z) \tag{13}$$

which satisfies (i) and (ii) if λ_n are the zeros of $J_1(\lambda)$. The coefficients C_n are determined by the condition (iii), and we find

$$C_n = \frac{1}{2\lambda_n J_0^2(\lambda_n)} \left(1 + \frac{8J_0(\lambda_n)}{\lambda_n^2}\right) \tag{14}$$

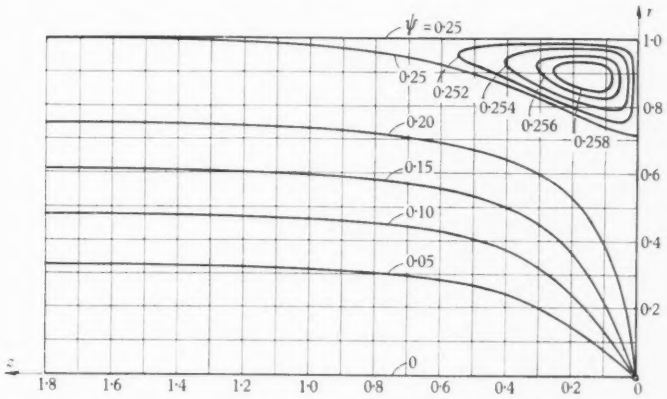

FIGURE 2. Pattern of axisymmetric flow into a sink.

by multiplying equation (13) (with $z = 0$) by $J_1(\lambda_m r)$, integrating between 0 and 1, and using the orthogonality of the functions $J_1(\lambda_n r)$. The detailed calculation for C_n involves integrations by parts and some known relationships for J_0 and J_1, and is omitted because it is straightforward. Equations (13) and (14) then constitute the solution.

The flow pattern for half of the meridianal plane is shown in figure 2, in which the ring-shaped corner eddy is evident. The point of separation is again at infinity. Again, the solution is strictly applicable to a fluid of small viscosity only outside the region of the ring eddy; equation (12) has been *assumed* to be valid for the whole field of flow, but the solution shows a region of closed flow where the vorticity is not determined by conditions far upstream and there is no *a priori* reason (other than convenience) why equation (12) should be applicable. We note that equation (12) does state that the vorticity is proportional to r everywhere, and therefore in the eddy in particular, which coincides with the exact result for flow with closed streamlines at high Reynolds number (Batchelor 1956); however, the constant of proportionality is also fixed by equation (12) and

is unlikely to have here the value that would be required for a fluid with non-zero viscosity. As in the two-dimensional case, the flow shown in figure 2 is free from singular surfaces.

The computational assistance rendered by Mr Wei Lai and Mr Walter R. Debler is much appreciated. Mr Lai's assistance was made available to the author through a faculty research fund granted by the Rackham Graduate School of the University of Michigan. Mr Debler's assistance was supplied by the Office of Ordnance Research, U.S. Army.

REFERENCES

BATCHELOR, G. K. 1956 On steady laminar flow with closed streamlines at large Reynolds number. *J. Fluid Mech.* **1**, 117.

LAMB, H. 1945 *Hydrodynamics.* New York: Dover.

YIH, C.-S. 1958 On the flow of a stratified fluid. *Proc. Third U.S. National Congress of Applied Mechanics* (to be published).

The structure of the jet-stream in a rotating fluid with a horizontal temperature gradient

By RUTH H. ROGERS
Department of Mathematics, University of Manchester*

(Received 28 June 1958)

The jet-stream in a rotating fluid is treated as a thermal boundary layer, but viscous effects are omitted from the first approximation. A theoretical justification for this treatment is presented, and a particular solution of the resulting equations is found. This solution is shown to give a reasonable picture of the flow in the neighbourhood of the stream far from solid boundaries.

1. Introduction

The problem of the convection of a rotating fluid subject to differential heating has been considered in recent years by workers in two fields. Meteorologists are concerned with a rotating atmosphere heated from below: heat is supplied at the equator, and is removed to outer space via the poles. Geophysicists are concerned with the motion of the earth's core, which also rotates and is assumed to be differentially heated. Both groups of workers have devised laboratory experiments to investigate the problem more thoroughly, and although the method of heating varies, the phenomena observed are essentially the same. The experiments have been described by Hide (1956, 1958), Fultz (1951) and Riehl & Fultz (1957).

In each case, the motion relative to the rotating apparatus is observed to be symmetrical about the axis of rotation (which is vertical) for sufficiently high Rossby numbers. The appropriate parameter, which is related to a Rossby number, has been expressed by Hide in the form†

$$\Theta = \frac{gd}{4\omega^2(b-a)^2}\frac{\Delta\rho}{\rho_0}, \tag{1}$$

where g is the acceleration due to gravity, d is the depth of the working fluid, ω is the angular velocity of the apparatus, a and b are the radii of the containing cylinders, $\Delta\rho$ is the applied horizontal density difference across the cylinders, and ρ_0 is the mean density of the fluid. He finds that the flow is symmetrical when Θ is greater than 0·4. When Θ is less than its critical value, the motion becomes asymmetric relative to the apparatus: most of the motion is concentrated into a narrow stream which meanders from boundary to boundary forming a number of equal lobes. A picture of the surface of a three-lobe formation obtained in experiments by the author at Manchester is shown in figure 1 (plate 1). By analogy with

* Now at Royal Aircraft Establishment, Farnborough, Hants.

† Hide defines Θ as four times the value given in (1).

similar narrow streams sometimes observed in the atmosphere, this is usually called the 'jet-stream'. There is some doubt as to the accuracy of this analogy, because there are so many more variables in the atmospheric motions than in the experimental flows (for example, in the atmosphere the Coriolis parameter varies, and there are considerable surface irregularities not present in the laboratory experiment). It seems likely, however, that some of the atmospheric jet-streams have similar causes to the experimental ones. There are slow circulations in the remainder of the fluid, but these are very small. Similar streams have been obtained by Fultz, although his method of heating is slightly different from that of Hide; he supplies heat from below the fluid, in an attempt to simulate more closely the conditions in the atmosphere.

The theory of the symmetrical mode of flow has been studied in detail by Davies (1953), by Lance & DeLand (1957), and by Lance (1958). The instability of this flow has been investigated by Davies (1956), Chandrasekhar (1953) and Kuo (1954). But no completely successful attempt has been made to solve the problem of the existence of the jet-stream itself. This paper is an attempt to find some simplifying assumptions which may help towards a solution of this problem, but does not claim to do more than suggest an approach.

The equations of motion are first put into a non-dimensional form containing the parameter Θ. Approximations are made by taking Θ to be small, and then expanding in powers of Θ. A particular solution of the first approximation is found in the form of a jet-stream, and this can be valid in the stream itself except where it meets the boundaries. The vertical velocity vanishes in the first approximation, but is given in the second. It is also shown that the equations of motion of the atmosphere can be reduced to a form identical with that discussed here, so that a similar solution exists in this case.

2. The equations of motion in the laboratory experiment

The liquid in which the motion takes place is assumed to have a constant coefficient of thermal expansion, α_0, so that its equation of state is given by

$$\rho = \rho_0 - \alpha_0(T - T_0), \tag{2}$$

where ρ is the density corresponding to the temperature T, and ρ_0, T_0 are reference density and temperature. This is a good approximation for all liquids except water near its freezing-point.

It is contained between coaxial cylinders of radii a and b, and has a depth d; the upper surface is free. The common axis of the cylinders is vertical, and the apparatus rotates with angular velocity ω about this axis. We choose a right-handed system of Cartesian axes $Oxyz$, which rotates with the apparatus; Ox is chosen to be along the surface jet-stream, and Oz to be vertically upwards. The sense of Ox is the same as the direction of rotation. A more precise specification of the axes will be given later: here we have only that the direction of motion is roughly along Ox, and that density and velocity gradients are essentially parallel to Oy. This is sufficient to allow us to make a boundary-layer type of approximation later.

It is easily shown that, in a liquid, the effect of variable density enters the equations of motion only in the buoyancy term. In the horizontal momentum equations, and in the equation of continuity, then, we can replace ρ by its mean value, which we choose to be the reference density ρ_0 of equation (2).

The effect of rotation is evident in the Coriolis and centrifugal terms in the horizontal momentum equations. Since only low rates of rotation are considered, the centrifugal terms are neglected, as is usual also in the equations of motion of the atmosphere. This is justified by the experimental observation that the surface of the rotating fluid does not assume the form of a paraboloid significantly different from the special case of a horizontal plane, for rotations at which the jet-stream occurs.

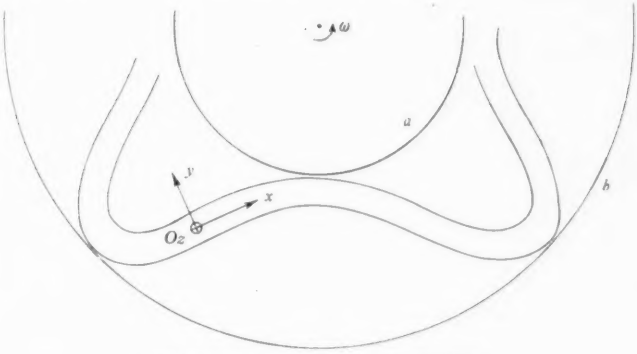

FIGURE 2. The co-ordinate system.

At this stage we can write the equations of horizontal momentum, the hydrostatic equation of vertical equilibrium, the equation of continuity, and the equation of heat transfer in the form

$$u\frac{\partial u}{\partial x}+v\frac{\partial u}{\partial y}+w\frac{\partial u}{\partial z}-2\omega v=-\frac{1}{\rho_0}\frac{\partial p}{\partial x}+\nu\left(\frac{\partial^2 u}{\partial x^2}+\frac{\partial^2 u}{\partial y^2}+\frac{\partial^2 u}{\partial z^2}\right), \tag{3}$$

$$u\frac{\partial v}{\partial x}+v\frac{\partial v}{\partial y}+w\frac{\partial v}{\partial z}+2\omega u=-\frac{1}{\rho_0}\frac{\partial p}{\partial y}+\nu\left(\frac{\partial^2 v}{\partial x^2}+\frac{\partial^2 v}{\partial y^2}+\frac{\partial^2 v}{\partial z^2}\right), \tag{4}$$

$$0=-g-\frac{1}{\rho}\frac{\partial p}{\partial z}, \tag{5}$$

$$\frac{\partial u}{\partial x}+\frac{\partial v}{\partial y}+\frac{\partial w}{\partial z}=0, \tag{6}$$

$$u\frac{\partial T}{\partial x}+v\frac{\partial T}{\partial y}+w\frac{\partial T}{\partial z}=\kappa\left(\frac{\partial^2 T}{\partial x^2}+\frac{\partial^2 T}{\partial y^2}+\frac{\partial^2 T}{\partial z^2}\right), \tag{7}$$

where p is the pressure at the point (x, y, z), u, v, w are the components of velocity of the fluid parallel to the axes at this point, ν is the kinematic viscosity of the liquid and κ its thermal diffusivity. It is assumed that the motion is steady, and that the frictional dissipation terms in the equation of heat transfer are negligible.

An immediate simplification to these equations can be made by the assumptions of boundary-layer theory. We note that v is very much smaller than u, and that

variations of the dependent variables in the direction of Oy are much more rapid than in the directions of Ox and Oz; but we assume that $\partial u/\partial x$ and $\partial v/\partial y$ are of the same order of magnitude. The momentum equations (3) and (4) then reduce to

$$u\frac{\partial u}{\partial x}+v\frac{\partial u}{\partial y}+w\frac{\partial u}{\partial z}-2\omega v=-\frac{1}{\rho_0}\frac{\partial p}{\partial x}+\nu\frac{\partial^2 u}{\partial y^2}, \tag{8}$$

$$2\omega u=-\frac{1}{\rho_0}\frac{\partial p}{\partial y}, \tag{9}$$

and the heat transfer equation (7) becomes

$$u\frac{\partial T}{\partial x}+v\frac{\partial T}{\partial y}+w\frac{\partial T}{\partial z}=\kappa\frac{\partial^2 T}{\partial y^2}. \tag{10}$$

We can incorporate the equation of state (2) in the hydrostatic equation (5) to give

$$g\rho_0-g\alpha_0(T-T_0)=-\frac{\partial p}{\partial z}. \tag{11}$$

The equations (6), (8), (9) and (11) can now be rearranged in the form

$$g\alpha_0 T=g(\rho_0+\alpha_0 T_0)+\frac{\partial p}{\partial z}, \tag{12}$$

$$u=-\frac{1}{2\omega\rho_0}\frac{\partial p}{\partial y}, \tag{13}$$

$$v=\frac{1}{2\omega\rho_0}\frac{\partial p}{\partial x}+\frac{\dfrac{1}{8\omega^3\rho_0^2}\left(\dfrac{\partial p}{\partial y}\dfrac{\partial^2 p}{\partial x\partial y}-\dfrac{\partial p}{\partial x}\dfrac{\partial^2 p}{\partial y^2}\right)+\dfrac{\nu}{4\omega^2\rho_0}\dfrac{\partial^3 p}{\partial y^3}-\dfrac{w}{4\omega^2\rho_0}\dfrac{\partial^2 p}{\partial y\partial z}}{1+\dfrac{1}{4\omega^2\rho_0}\dfrac{\partial^2 p}{\partial y^2}}, \tag{14}$$

$$\frac{\partial w}{\partial z}=-\frac{\partial}{\partial y}\left[\frac{\dfrac{1}{8\omega^3\rho_0^2}\left(\dfrac{\partial p}{\partial y}\dfrac{\partial^2 p}{\partial x\partial y}-\dfrac{\partial p}{\partial x}\dfrac{\partial^2 p}{\partial y^2}\right)+\dfrac{\nu}{4\omega^2\rho_0}\dfrac{\partial^3 p}{\partial y^3}-\dfrac{w}{4\omega^2\rho_0}\dfrac{\partial^2 p}{\partial y\partial z}}{1+\dfrac{1}{4\omega^2\rho_0}\dfrac{\partial^3 p}{\partial y^3}}\right]. \tag{15}$$

Formally, the problem is now solved: for (12) and (13) give T and u in terms of p, (15) can be solved to give w in terms of p, and then (14) used to give v in terms of p. It then remains only to substitute these expressions for T, u, v, w in the equation (10), and solve the resulting equation in p. Unfortunately, this is intractable, and we have to simplify further.

We look for further simplifying assumptions by defining non-dimensional co-ordinates (X, Y, Z), velocities (U, V, W), pressure P and temperature τ, as follows. We take first

$$x=k(b-a)\,X, \quad y=(b-a)\,Y, \quad z=dZ, \tag{16}$$

where k is a scale factor to be defined more precisely later; here we note only that k is very much greater than unity. Then we take for the velocities

$$u=2\omega(b-a)\,U, \quad v=\frac{2\omega(b-a)}{k}V, \quad w=\frac{2\omega d}{k'}W, \tag{17}$$

where k' is another scale factor; k occurs in the denominator of v, so that $\partial u/\partial x$ and $\partial v/\partial y$ are of the same order. Finally, we take

$$p = -g(\rho_0 + \alpha_0 T_0)z + (gd\,\Delta\rho)P, \quad \alpha_0 T = \Delta\rho\,\tau, \tag{18}$$

where $\Delta\rho$ is the density difference corresponding to the applied horizontal temperature difference ΔT. Substituting in the equations (12) to (15), we obtain

$$\tau = \frac{\partial P}{\partial Z}, \tag{19}$$

$$U = -\Theta\frac{\partial P}{\partial Y}, \tag{20}$$

$$V = \Theta\frac{\partial P}{\partial X} - \frac{k}{k'}\Theta W\frac{\partial^2 P}{\partial Y\,\partial Z} + \Theta^2\mathscr{P}, \tag{21}$$

where

$$\mathscr{P} = \frac{\dfrac{\partial P}{\partial Y}\dfrac{\partial^2 P}{\partial X\,\partial Y} - \dfrac{\partial P}{\partial X}\dfrac{\partial^2 P}{\partial Y^2} + \sigma\left(\dfrac{2\omega\kappa k\rho_0}{gd\,\Delta\rho}\right)\dfrac{\partial^3 P}{\partial Y^3}}{1 + \Theta\dfrac{\partial^2 P}{\partial Y^2}}, \tag{21a}$$

$$\frac{k}{k'}\frac{\partial W}{\partial Z} = -\Theta^2\frac{\partial \mathscr{P}}{\partial Y},$$

where $\sigma = \nu/\kappa$ is the Prandtl number of the fluid. Introducing the non-dimensional variables, and substituting for U and V, in (11), we have

$$-\frac{\partial P}{\partial Y}\frac{\partial T}{\partial X} + \frac{\partial T}{\partial Y}\left(\frac{\partial P}{\partial X} - \frac{k}{k'}W\frac{\partial^2 P}{\partial Y\,\partial Z} + \Theta\mathscr{P}\right) + \frac{k}{k'}W\frac{\partial T}{\partial Z} = \frac{2\omega\kappa k\rho_0}{gd\,\Delta\rho}\frac{\partial^2 T}{\partial Y^2}. \tag{22}$$

We can now be more specific about the scale factors k and k'. Since k' occurs only in the ratio k/k' when this multiplies W, we can take $k = k'$ without loss of generality. The factor k occurs only in the expression $2\omega\kappa k\rho_0/gd\,\Delta\rho$. It seems reasonable, then, to define

$$k = \frac{gd\,\Delta\rho}{2\omega\kappa\rho_0}. \tag{23}$$

This ratio was found to be of the order of 1000 in the experiments carried out in Manchester by the present author, and so satisfies the condition that k is very much greater than unity. This definition implies that the terms on both sides of equation (22) are of equal importance; that is, that transfer of heat occurs both by conduction and convection. It follows immediately from (21) and (21*a*), that the viscous terms are of the same order of magnitude as the inertia terms (as long as σ does not differ greatly from unity). If a smaller value of k is chosen so that the conduction term on the right of equation (22) is negligible, that is, if

$$1 \ll k \ll \frac{gd\,\Delta\rho}{2\omega\kappa\rho_0},$$

then the viscous term in the expression for $\mathscr{P}$ is also negligible compared with the inertia terms, unless σ is much greater than unity. If k is very much larger than the value given in (23), so that the convection terms on the left of equation (22)

are negligible, then the temperature field is independent of the velocity field, and viscous terms may be of importance. These are the assumptions made by Davies in his theories of the symmetrical regime and its instability. We now have the simpler expressions for V, $\mathscr{P}$ and $\partial W/\partial Z$, as follows:

$$V = \Theta\frac{\partial P}{\partial X} - \Theta W\frac{\partial^2 P}{\partial Y\partial Z} + \Theta^2\mathscr{P}, \tag{24}$$

where

$$\mathscr{P} = \frac{\dfrac{\partial P}{\partial Y}\dfrac{\partial^2 P}{\partial X\partial Y} - \dfrac{\partial P}{\partial X}\dfrac{\partial^2 P}{\partial Y^2} + \sigma\dfrac{\partial^3 P}{\partial Y^3}}{1 + \Theta\,\partial^2 P/\partial Y^2}, \tag{25}$$

$$\frac{\partial W}{\partial Z} = -\Theta^2\frac{\partial\mathscr{P}}{\partial Y}. \tag{26}$$

Equation (22) can be written

$$-\frac{\partial P}{\partial Y}\frac{\partial^2 P}{\partial X\partial Z} + \frac{\partial^2 P}{\partial Y\partial Z}\left(\frac{\partial P}{\partial X} - W\frac{\partial^2 P}{\partial Y\partial Z} + \Theta\mathscr{P}\right) + W\frac{\partial^2 P}{\partial Z^2} = \frac{\partial^3 P}{\partial Y^2\partial Z}. \tag{27}$$

The only parameter entering into this set of equations is Θ, and this is known to be small. It seems reasonable to look for a solution in powers of Θ. We write

$$P = P_0 + \Theta P_1 + \Theta^2 P_2 + \ldots,$$

so that

$$\begin{aligned}
\tau &= \tau_0 + \Theta\tau_1 + \Theta^2\tau_2 + \ldots,\\
U &= \Theta U_0 + \Theta^2 U_1 + \Theta^3 U_2 + \ldots,\\
V &= \Theta V_0 + \Theta^2 V_1 + \Theta^3 V_2 + \ldots,\\
W &= \Theta W_0 + \Theta^2 W_1 + \Theta^3 W_2 + \ldots.
\end{aligned}$$

These variables satisfy the equations

$$\tau_0 = \frac{\partial P_0}{\partial Z}, \quad \tau_1 = \frac{\partial P_1}{\partial Z}, \quad \tau_2 = \frac{\partial P_2}{\partial Z}, \ldots,$$

$$U_0 = -\frac{\partial P_0}{\partial Y}, \quad U_1 = -\frac{\partial P_1}{\partial Y}, \quad U_2 = -\frac{\partial P_2}{\partial Y}, \ldots,$$

$$V_0 = \frac{\partial P_0}{\partial X}, \quad V_1 = \frac{\partial P_1}{\partial X} + W_0\frac{\partial^2 P_0}{\partial Y\partial Z} + \mathscr{P}_0, \ldots,$$

$$\frac{\partial W_0}{\partial Z} = 0, \quad \frac{\partial W_1}{\partial Z} = -\frac{\partial\mathscr{P}_0}{\partial Y}, \ldots,$$

where

$$\mathscr{P}_0 = \frac{\partial P_0}{\partial Y}\frac{\partial^2 P_0}{\partial X\partial Y} - \frac{\partial P_0}{\partial X}\frac{\partial^2 P_0}{\partial Y^2} + \sigma\frac{\partial^3 P_0}{\partial Y^3}.$$

We have from (27) that

$$-\frac{\partial P_0}{\partial Y}\frac{\partial^2 P_0}{\partial X\partial Z} + \frac{\partial P_0}{\partial X}\frac{\partial^2 P_0}{\partial Y\partial Z} + W_0\left(\frac{\partial^2 P_0}{\partial Z^2} - \left(\frac{\partial^2 P_0}{\partial Y\partial Z}\right)^2\right) = \frac{\partial^3 P_0}{\partial Y^2\partial Z}, \tag{28}$$

and more complicated expressions relating W_1 and P_1, etc.

In the first approximation we have

$$\frac{\partial W_0}{\partial Z} = 0 \quad \text{or} \quad W_0 = \text{constant};$$

it follows at once that $W_0 = 0$ everywhere. Equation (28) now simplifies further to

$$-\frac{\partial P_0}{\partial Y}\frac{\partial^2 P_0}{\partial X \partial Z}+\frac{\partial P_0}{\partial X}\frac{\partial^2 P_0}{\partial Y \partial Z}=\frac{\partial^3 P_0}{\partial Y^2 \partial Z}. \tag{29}$$

If this equation can be solved, an expression for $\mathscr{P}_0$ can be obtained, which can be used to find the form of $\partial W_1/\partial Z$ without difficulty. We have

$$\frac{\partial W_1}{\partial Z}=-\frac{\partial}{\partial Y}\left(\frac{\partial P_0}{\partial Y}\frac{\partial^2 P_0}{\partial X \partial Y}-\frac{\partial P_0}{\partial X}\frac{\partial^2 P_0}{\partial Y^2}+\sigma\frac{\partial^3 P_0}{\partial Y^3}\right). \tag{30}$$

It is difficult to define precise boundary conditions at this stage; they will depend to a considerable extent on how much of the motion we try to describe by the above equations. Further discussion of this problem is postponed until a solution of (29) has been found.

T. V. Davies has pointed out that in the first approximation, the equation of heat transfer can be written in the form

$$-\frac{\partial p}{\partial y}\frac{\partial T}{\partial x}+\frac{\partial p}{\partial x}\frac{\partial T}{\partial y}=2\omega\rho_0\kappa\left(\frac{\partial^2 T}{\partial x^2}+\frac{\partial^2 T}{\partial y^2}\right),$$

where the term representing conduction in the vertical is now the only one omitted. This equation is left unchanged by a conformal transformation in the xy-plane. It follows that we lose no generality by taking rectangular axes, and assuming that the stream flows parallel to Ox; for any solution so obtained is still valid after a conformal transformation designed to transform Ox into some other curve.

If the first approximation is used with the equations in cylindrical polar form, and we assume that variations with respect to r are much greater than those with respect to θ, the fundamental equation to be solved for p is

$$-\frac{\partial p}{\partial r}\frac{\partial^2 p}{\partial \theta \partial z}+\frac{\partial p}{\partial \theta}\frac{\partial^2 p}{\partial r \partial z}=2\omega\rho_0\kappa\frac{\partial}{\partial r}\left(r\frac{\partial^2 p}{\partial r \partial z}\right).$$

Writing $R = \log r$, this reduces to the form

$$-\frac{\partial p}{\partial R}\frac{\partial^2 p}{\partial \theta \partial z}+\frac{\partial p}{\partial \theta}\frac{\partial^2 p}{\partial R \partial z}=2\omega\rho_0\kappa\frac{\partial^2 p}{\partial R \partial z}, \tag{31}$$

and this is of the same form as in local Cartesian co-ordinates with y replaced by $R = \log r$, and x replaced by θ.

3. A particular solution of the approximate equation

We have essentially to solve equation (29), but it is more convenient to return to physical variables at this stage. In the first approximation, we have to neglect all inertia terms and viscous terms in equation (8), put $w = 0$ in (10) and leave (9) and (11) as they stand. We can eliminate the hydrostatic part of the pressure from the problem by writing

$$p=-g(\rho_0+\alpha_0 T_0)z+p_0. \tag{32}$$

Then (11) becomes

$$\alpha_0 T=\frac{1}{g}\frac{\partial p_0}{\partial z}, \tag{33}$$

and equations (8) and (9) give

$$u = -\frac{1}{2\omega\rho_0}\frac{\partial p_0}{\partial y}, \quad v = \frac{1}{2\omega\rho_0}\frac{\partial p_0}{\partial x}. \tag{34}$$

The equation of continuity (6), is automatically satisfied, since $w = 0$. The heat transfer equation (10) now gives

$$-\frac{\partial p_0}{\partial y}\frac{\partial^2 p_0}{\partial x \partial z} + \frac{\partial p_0}{\partial x}\frac{\partial^2 p_0}{\partial y \partial z} = 2\omega\rho_0\kappa\frac{\partial^3 p_0}{\partial y^2 \partial z}. \tag{35}$$

One of the properties of the jet-stream of the experiments is its approximately constant width. This suggests a solution of the form

$$p_0 = p_1(x, z)\, p_2(y).$$

Such a solution of equation (35) is possible if

$$p_2\frac{dp_2}{dy} \propto \frac{d^2 p_2}{dy^2}.$$

This implies that *either* $p_2(y) = \tan(y/y_0)$, which does not correspond to the physical problem, *or*

$$p_2(y) = \tanh(y/y_0),$$

where y_0 is an arbitrary constant. Taking this value of p_2, (35) becomes

$$-p_1\frac{\partial^2 p_1}{\partial x \partial z} + \frac{\partial p_1}{\partial x}\frac{\partial p_1}{\partial z} = -\frac{4\omega\rho_0\kappa}{y_0}\frac{\partial p_1}{\partial z};$$

the general solution of this equation is

$$p_1 = -\frac{4\omega\rho_0\kappa}{y_0}\frac{F_1(x) + G_1(z)}{F_1'(x)},$$

where $F_1(x)$, $G_1(z)$ are arbitrary functions of x, z respectively. We have, therefore, a solution of the form

$$p_0 = -\frac{4\omega\rho_0\kappa}{y}\frac{F_1(x) + G_1(z)}{F_1'(x)}\tanh\frac{y}{y_0}. \tag{36}$$

The corresponding values of T, u, v are given by equations (33) and (34) in the form

$$\alpha_0 T = -\frac{4\omega\rho_0\kappa}{g y_0}\frac{G_1'(z)}{F_1'(x)}\tanh\frac{y}{y_0}, \tag{37}$$

$$u = \frac{2\kappa}{y_0^2}\frac{F_1(x) + G_1(z)}{F_1'(x)}\operatorname{sech}^2\frac{y}{y_0}, \tag{38}$$

$$v = -\frac{2\kappa}{y_0}\left[1 - \frac{F_1''(x)\{F_1(x) + G_1(z)\}}{\{F_1'(x)\}^2}\right]\tanh\frac{y}{y_0}. \tag{39}$$

This is the simplest solution we can find of the equation, and it is worth considering its nature. It certainly describes a jet-stream in the direction of Ox, which is a streamline, an isotherm, and a line of maximum velocity. There is a horizontal temperature gradient across the stream of magnitude

$$\frac{\partial T}{\partial y} = -\frac{4\omega\rho_0\kappa}{g\alpha_0 y_0^2}\frac{G_1'(z)}{F_1'(x)}\operatorname{sech}^2\frac{y}{y_0}, \tag{40}$$

FIGURE 1 (plate 1).

and the temperature itself approaches a limit on each side of the stream. The 'width' of the stream can be taken as $3y_0$, since $\operatorname{sech}^2 3 = 0{\cdot}01$ and $\tanh 3 = 0{\cdot}995$; so, for $|y|$ greater than or equal to $3y_0$, u and $\partial T/\partial y$ are less than 1 % of their values on $y = 0$, and T is within $\frac{1}{2}$ % of its limiting value. The cross-velocity, v, is an odd function of y, so that there is either an inflow towards $y = 0$, or an outflow from $y = 0$; this solution gives no velocity across $y = 0$.

The general functions $F_1(x)$ and $G_1(z)$ are difficult to determine, because of the lack of precise boundary conditions. It is convenient to discuss them in terms of the density difference across the stream

$$(\Delta\rho)' = \frac{8\omega\rho_0\kappa}{gy_0^2}\frac{G_1'(z)}{F_1'(x)}, \tag{41}$$

and the velocity on the x-axis

$$u_0 = \frac{2\kappa}{y_0^2}\frac{F_1(x)+G_1(z)}{F_1'(x)}. \tag{42}$$

The function $G_1'(z)$ can be left arbitrary: in the Chicago experiments of Fultz and his co-workers, where the fluid is heated from below, it is certainly not a constant; in the Cambridge and Manchester experiments, an attempt to make the boundary temperatures independent of z is made, but there are certainly vertical temperature gradients in the fluid. It is of interest, however, to note that there does exist a formal solution for the case in which there are no vertical temperature gradients; in this case, the velocity increases linearly with z. We note that the vertical conduction term $\partial^2 T/\partial z^2$ in the heat transfer equation is then identically zero (not merely negligible, as assumed in the derivation).

The function $F_1(x)$ is more troublesome. We note first that $F_1'(x)$ has always the same sign (or is zero), since $(\Delta\rho)'$, as given by (41), cannot change sign with x. It follows that $F_1(x)$ is a monotonic function of x, and cannot be periodic. Hence, either $F_1(x)/F_1'(x)$ or $F_1'(x)$ itself is monotonic, and u cannot be periodic in x as long as it is continuous. Since the jet-stream touches one or other boundary at certain values of x, and there is a sudden temperature change at such a point, it is not unreasonable to obtain discontinuities in the solution.

As a possible example, we consider

$$\frac{F_1(x)}{F_1'(x)} = A + B\cos 2mx \quad (B < A).$$

After integration and some manipulation, we obtain

$$\frac{1}{F_1'(x)} = \frac{A + B\cos 2mx}{C}\, e^{-\theta/m\alpha\beta},$$

where $$\alpha^2 = A + B, \quad \beta^2 = A - B, \quad \tan\theta = (\beta/\alpha)\tan mx.$$

If we always choose $-\frac{1}{2}\pi < \theta < \frac{1}{2}\pi$, then the exponential factor in the expression for $1/F_1'(x)$ is periodic, with a period in x of $\pi/2m$; the $\cos 2mx$ term has a period in x of π/m. As x increases, the exponential term decreases—this corresponds to a decrease in $1/F'(x)$, and hence in $(\Delta\rho)'$, as the stream gets further from a boundary. When it reaches the other boundary, there is a sudden increase in $(\Delta\rho)'$—that is, a discontinuous increase in $1/F_1'(x)$. The factor $(A + B\cos 2mx)$ oscillates about

the constant value A, never changing sign; it has twice the period of the exponential factor, and passes through the value A at each discontinuity of θ. The way in which θ varies with x is shown in figure 3.

We can consider one interval of this solution only, taking $-(\pi/2m) < x < (\pi/2m)$, say. If B is very much less than A, so that β is approximately equal to α, we can write $\theta = \beta mx/\alpha$ approximately within the interval; also, to this approximation

$$\frac{F_1(x)}{F_1'(x)} = A, \quad \frac{1}{F_1'(x)} = \frac{A}{C}e^{-x/A}, \quad \frac{F_1''(x)}{F_1'(x)} = \frac{1}{A}.$$

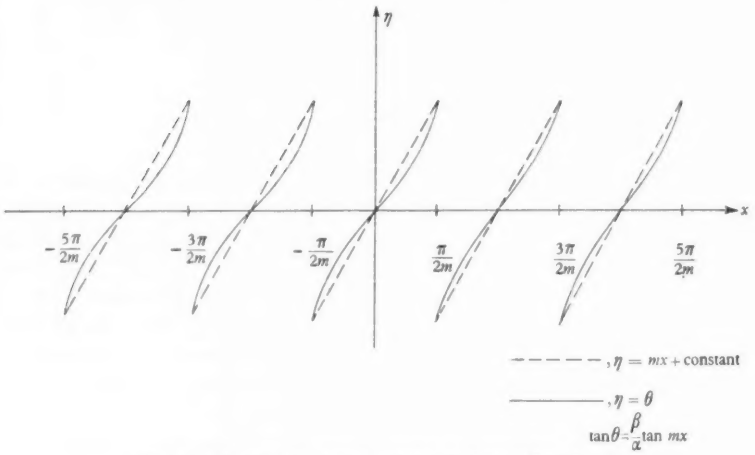

FIGURE 3. The variation of the function θ with x.

This gives, for T, u and v in any interval far from the boundary

$$\left.\begin{aligned} T &= -\frac{4\omega\rho_0\kappa}{\alpha_0 g y_0^2}\frac{A}{C}G_1'(z)\,e^{-x/A}\tanh y/y_0, \\ u &= \frac{2\kappa}{y_0^2}A\left(1+\frac{G_1(z)}{C}e^{-x/A}\right)\operatorname{sech}^2 y/y_0, \\ v &= \frac{2\kappa}{y_0}\frac{G_1(z)}{C}e^{-x/A}\tanh y/y_0. \end{aligned}\right\} \tag{43}$$

Such a solution implies that during the passage from one boundary to another, the temperature difference across the stream, and the velocity u decrease slightly, and that there is an outflow everywhere which also decreases in magnitude as x increases. (In the experiment, there is almost certainly a cross-flow, but this may appear in this solution only in the second approximation.) The approximate particular solution of equations (43) can be fitted into the experimental pattern as shown in figure 4, where the dotted lines indicate the slow circulations which take place outside the jet-stream.

It is not suggested that this is the best form of the function $F_1(x)$, but it is put forward as a possible one; it is probably the simplest. The jet-stream described by this solution does not obviously differ from that observed in a fundamental

way, although the mechanism of transition between the jet-stream and the slow circulations described above is not obvious.

We can relate the solution of equation (43) more closely to experiment, if we incorporate the constant C in the arbitrary function G_1, and write

$$\frac{4\omega\rho_0\kappa}{gy_0^2}A = \tfrac{1}{2}\Delta\rho,$$

or

$$A = \frac{gy_0\Delta\rho}{8\omega\rho_0\kappa}y_0. \tag{44}$$

Then we have

$$\alpha_0 T = -\tfrac{1}{2}\Delta\rho\, G_1'(z)\, e^{-x/A}\tanh y/y_0,$$

$$u = \frac{g\Delta\rho}{4\omega\rho_0}(1 + G_1(z)\, e^{-x/A})\operatorname{sech}^2 y/y_0,$$

$$v = \frac{2\kappa}{y_0}G_1(z)\, e^{-x/A}\tanh y/y_0.$$

We note that

$$\frac{u}{v} \sim \frac{gy_0\Delta\rho}{8\omega\kappa\rho_0} = \frac{A}{y_0},$$

and this is to be compared with the scale-factor k defined by equation (23). It is certainly smaller than k, by a factor of $y_0/4d$, but is probably still large enough to justify the retention of the conduction term. A study of the separate terms of the

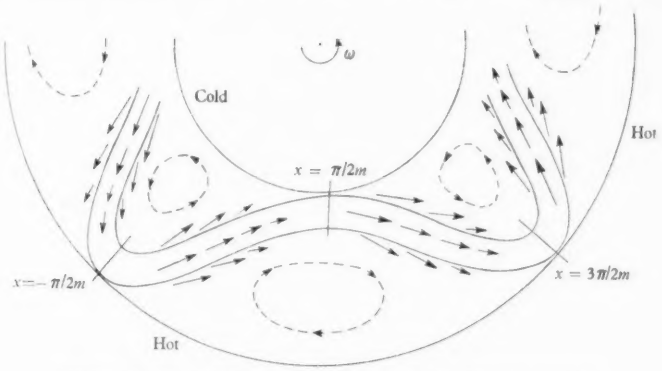

FIGURE 4. A particular solution of the first approximation.

heat-transfer equation indicate that the conduction is balanced entirely by the convection due to the part of u which is independent of z (this is true of the general equation); since u varies considerably with height, it seems likely that this is the smaller term, and this is consistent with a small conduction term.

We can equate A, which is essentially the scale of x, to $\pi(b+a)/n$, where n is the number of lobes in the pattern, and obtain an order of magnitude for the width of the jet-stream, $3y_0$. We have

$$\frac{\pi(b+a)}{n} = \frac{gy_0^2\Delta\rho}{8\omega\rho_0\kappa},$$

or

$$y_0^2 = \frac{8\pi\omega\rho_0\kappa(b+a)}{gn\Delta\rho} \sim 0{\cdot}4\,\text{cm}^2.$$

This gives y_0 of the order 0·6 cm, and the width of the stream of order 2 cm; this is in agreement with experiment.

In cylindrical polar co-ordinates, we can use equation (31) instead of (35), to obtain a solution of the form (37), (38) and (39), with x replaced by θ, and with $\tanh(y/y_0)$ replaced by

$$\tanh(\log r^\gamma) = (r^{2\gamma}-1)/(r^{2\gamma}+1),$$

where γ is an arbitrary constant. The necessary discontinuity with respect to θ makes this solution impracticable.

4. A generalization of this solution

By inspection, it is easy to generalize the solution (36) of equation (35) to the form

$$p_0 = -4\omega\rho_0\kappa\left\{\frac{F_1(x)+G_1(z)}{F_1'(x)}\left[\frac{1}{y_0(x)}\tanh\frac{y-y_1(x)}{y_0(x)} - F_2'(x)\right] + F_2(x)+G_2(z)\right\}, \tag{45}$$

where $F_1(x)$, $F_2(x)$, $y_0(x)$, $y_1(x)$ are arbitrary functions of x, and $G_1(z)$, $G_2(z)$ of z. The other variables are then given by

$$\alpha_0 T = -\frac{4\omega\rho_0\kappa}{g}\left\{\frac{G_1'(z)}{F_1'(x)}\left[\frac{1}{y_0(x)}\tanh\frac{y-y_1(x)}{y_0(x)} - F_2'(x)\right] + G_2'(z)\right\}, \tag{46}$$

$$u = \frac{2\kappa}{[y_0(x)]^2}\frac{F_1(x)+G_1(z)}{F_1'(x)}\operatorname{sech}^2\frac{y-y_1(x)}{y_0(x)}, \tag{47}$$

$$\begin{aligned} v = &-\frac{2\kappa}{y_0(x)}\left\{1-\frac{F_1''(x)[F_1(x)+G_1(z)]}{[F_1'(x)]^2}\right\}\tanh\frac{y-y_1(x)}{y_0(x)} \\ &+2\kappa\frac{F_1(x)+G_1(z)}{F_1'(x)}\left\{\frac{y_0'(x)}{[y_0(x)]^2}\tanh\frac{y-y_1(x)}{y_0(x)} + F_2''(x) - \frac{F_2'(x)F_1''(x)}{F_1'(x)}\right. \\ &\left.+\frac{1}{y_0(x)}\left[\frac{y_1'(x)}{y_0(x)}+\frac{\{y-y_1(x)\}y_0'(x)}{[y_0(x)]^2}\right]\operatorname{sech}^2\frac{y-y_1(x)}{y_0(x)}\right\}. \end{aligned} \tag{48}$$

We consider the effect of the new functions introduced into the solution, and shall show that most of them can be ignored.

The function $G_2(z)$ does not appear in the expression for the velocity; its effect is, then, to allow an overall variation of temperature (and hence pressure) in the vertical. As with the function $G_1(z)$, it is difficult to find suitable boundary conditions, and it may be left arbitrary. No doubt the form of $G_2(z)$ in experiments where heating is from below differs from that when the applied heating is purely radial. We note that the form of the function $G_2(z)$ does not alter the expression for the density difference $(\Delta\rho)'$ across the stream, as given in (41).

Since the width of the jet-stream is proportional to $y_0(x)$, we can regard this function as applying to a jet-stream of variable width. As stated in the previous section, the width of the stream in the experiments varies very little, and so we can take $y_0(x) = y_0$, a constant. In atmospheric jets, however, it may be necessary to retain the function, as shown in §6.

The jet form of the solution now has its maximum value of u about $y = y_1(x)$, instead of about $y = 0$; since the solution is based on the assumption that the jet is more or less parallel to $y = 0$, it follows that the two curves are nearly parallel. This means that $y_1'(x)$ cannot be large. We can introduce the function, then, to introduce a small curvature of the jet-stream. A large departure from $y = 0$ must be dealt with by means of a conformal transformation, as explained in § 2.

The nature of the function $F_2(x)$ can be seen most readily if we write

$$f'(x) = F_2'(x)/F_1'(x),$$

so that

$$f''(x) = \frac{F_2''(x)}{F_1'(x)} - \frac{F_2'(x)\,F_1''(x)}{[F_1'(x)]^2}.$$

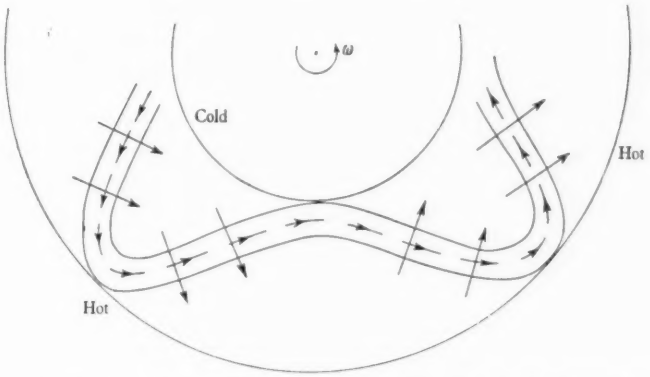

FIGURE 5. The cross-flow in a more general solution of the first approximation.

Then, if y_0 is a constant, we have

$$\alpha_0 T = -\frac{4\omega\rho_0\kappa}{g}\left\{\frac{G_1'(z)}{F_1'(x)}\frac{1}{y_0}\tanh\frac{y-y_1(x)}{y_0} - f'(x)\,G_1'(z) + G_2'(z)\right\}, \tag{49}$$

$$u = \frac{2\kappa}{y_0^2}\frac{F_1(x)+G_1(z)}{F_1'(x)}\operatorname{sech}^2\frac{y-y_1(x)}{y_0}, \tag{50}$$

$$v = -\frac{2\kappa}{y_0}\left\{1 - \frac{F_1''(x)\,[F_1(x)+G_1(z)]}{[F_1'(x)]^2}\right\}\tanh\frac{y-y_1(x)}{y_0}$$
$$+\frac{2\kappa}{y_0^2}\frac{F_1(x)+G_1(z)}{F_1'(x)}\,y_1'(x)\operatorname{sech}^2\frac{y-y_1(x)}{y_0} + 2\kappa[F_1(x)+G_1(z)]f''(x). \tag{51}$$

We see that the function $f'(x)$ implies an overall variation of T with x, and a cross-flow term in v. As the stream travels from the hot to the cold boundary, we would expect $f'(x)$ to decrease; it follows at once that $f''(x)$ is negative in this case, and a positive value of v results. Conversely, there is a negative value of v as the stream approaches the hot boundary. The cross-flow therefore corresponds to a small circulation of the whole fluid as shown in figure 5. This cross-flow is, of course, superposed on the out-flow or inflow corresponding to the solution of § 3.

We note that on the line $y = y_1(x)$, the slope of the isotherms and that of the streamlines are the same, and are given by the expression

$$\frac{dy}{dx} = y_1'(x) + y_0^2 F_1'(x) f''(x). \tag{52}$$

The line itself is not itself a streamline or an isotherm unless

$$y_1'(x) + y_0^2 F_1'(x) f''(x) = 0.$$

If this relation holds, however, the line is both a streamline and an isotherm, and this does not agree with experiment.

5. The second approximation: the vertical velocity

The variation of the vertical velocity with height is given in terms of the non-dimensional variables by (30); the corresponding relation in terms of the physical variables is

$$\frac{\partial w}{\partial z} = -\frac{1}{8\omega^3\rho_0^2}\frac{\partial}{\partial y}\left(\frac{\partial p_0}{\partial y}\frac{\partial^2 p_0}{\partial y \partial x} - \frac{\partial p_0}{\partial x}\frac{\partial^2 p_0}{\partial y^2} + 2\omega\rho_0\nu\frac{\partial^3 p_0}{\partial y^3}\right), \tag{53}$$

where p_0 is given in the first approximation. We can write this in the form

$$\frac{\partial w}{\partial z} = \frac{\partial w_i}{\partial z} + \frac{\partial w_v}{\partial z}, \tag{54}$$

where

$$\frac{\partial w_i}{\partial z} = -\frac{1}{8\omega^3\rho_0}\frac{\partial}{\partial y}\left(\frac{\partial p_0}{\partial y}\frac{\partial^2 p_0}{\partial x \partial y} - \frac{\partial p_0}{\partial x}\frac{\partial^2 p_0}{\partial y^2}\right) \tag{54a}$$

is dependent on the inertia terms, and

$$\frac{\partial w_v}{\partial z} = -\frac{\nu}{4\omega^2\rho_0}\frac{\partial^4 p_0}{\partial y^4} \tag{54b}$$

is due to the viscosity. Since this term contains a derivative of p_0 of higher order than the original equation for p_0, it is doubtful whether we can include the viscous effect in this form. An alternative method would be to replace the term $\nu\partial^2 u/\partial y^2$ in the x-momentum equation by Ku, where K is a friction constant. In this case we have

$$\frac{\partial w_v}{\partial z} = -\frac{K}{4\omega^2\rho_0}\frac{\partial^2 p_0}{\partial y^2}. \tag{54c}$$

Both forms of the term will be discussed.

Substituting the solution given in equations (50), (51) into (54a), and taking $y_0(x) = y_0$, a constant, we have

$$\frac{\partial w_i}{\partial z} = \frac{8\kappa^2}{\omega y_0^5}\frac{F_1(x)+G_1(z)}{F_1'(x)}\left\{1 - \frac{F_1''(x)\,[F_1(x)+G_1(z)]}{[F'(x)]^2}\right\}\operatorname{sech}^2\frac{y-y_1(x)}{y_0}\tanh^3\frac{y-y_1(x)}{y_0}$$
$$+\frac{4\kappa^2}{\omega y_0^4}\left[\frac{F_1(x)+G_1(z)}{F_1'(x)}\right]^2\left[F_2''(x) - \frac{F_1''(x)\,F_2'(x)}{F_1'(x)}\right]\left(3\operatorname{sech}^4\frac{y-y_1(x)}{y_0} - 2\operatorname{sech}^2\frac{y-y_1(x)}{y_0}\right). \tag{55}$$

We note that this can be expressed in the form

$$\frac{\partial w_i}{\partial z} = -\frac{2}{\omega y_0^2} uv \tanh^2 \frac{y - y_1(x)}{y_0} + \frac{3}{\omega} u^2 F_1'(x) f''(x). \tag{55a}$$

This consists of two terms, the first corresponding to the jet part of the solution, and the second to the cross-flow part introduced by the function $F_2(x)$ of §4. The sign of the cross-flow part is therefore negative (suggesting downflow) when the stream approaches a cold boundary, and positive (suggesting upflow) when

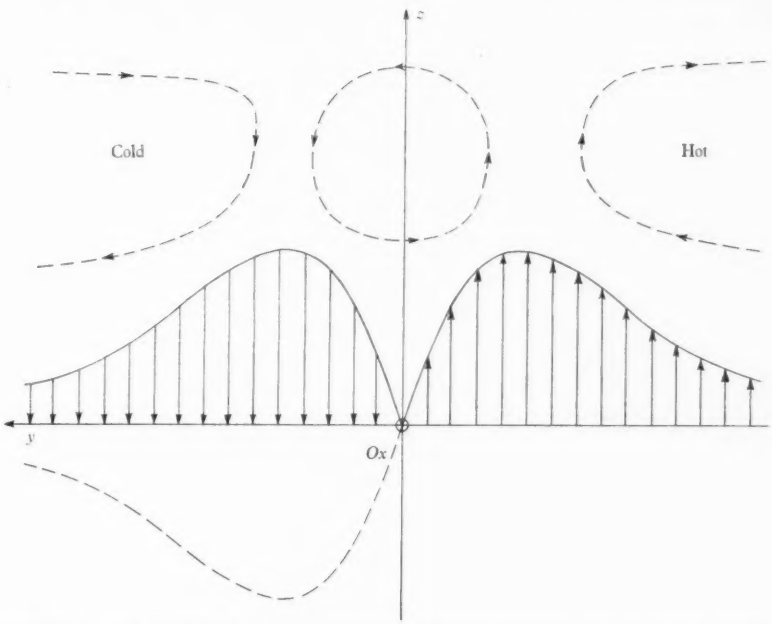

FIGURE 6. The cross-circulation in the second approximation, due to inertia forces.

the stream approaches a hot boundary. Its magnitude is large near $y = y_1(x)$, and falls off rapidly as $|y - y_1(x)|$ increases; it is an even function of $y - y_1(x)$. The jet part of (55*a*) has the same sign as uv; it varies across the stream like

$$-\operatorname{sech}^2 \frac{y - y_1(x)}{y_0} \tanh^3 \frac{y - y_1(x)}{y_0},$$

when there is outflow in the first approximate solution (as in the solution of equation (43)); this gives values for w near $z = 0$ as shown in figure 6. This suggests a cross-circulation as shown by the dotted lines, and this is consistent with the observations of Riehl & Fultz (1957). It is assumed that the velocities given by the second term of (55*a*) are superposed on this circulation, but do not alter it essentially; certainly in the mean with respect to x, they will not do so, as the term changes sign.

The viscous term as given by (54*c*) becomes

$$\frac{\partial w_v}{\partial z} = -\frac{2K\kappa}{\omega y_0^3}\frac{F_1(x)+G_1(z)}{F_1'(x)}\operatorname{sech}^2\frac{y-y_1(x)}{y_0}\tanh\frac{y-y_1(x)}{y_0}$$

$$= -2\frac{K}{\omega y_0}u\tanh\frac{y-y_1(x)}{y_0}.$$

This gives a cross-circulation similar in form to that of figure 6, though the maximum value of $|\partial w_v/\partial z|$ occurs for a different value of $|y-y_1(x)|$ from that for which $|\partial w_t/\partial z|$ is a maximum. It follows that, if this is the correct form for the viscous terms, the cross-circulation is similar to that given by figure 6.

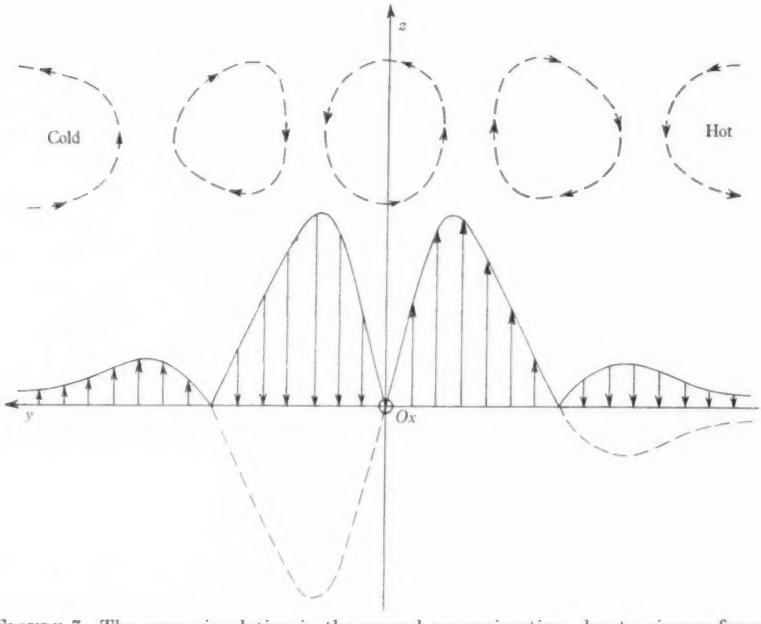

FIGURE 7. The cross-circulation in the second approximation, due to viscous forces proportional to $\partial^2 u/\partial y^2$.

If we can keep the viscous term in the form (54*b*), we have

$$\frac{\partial w_v}{\partial z} = \frac{8\nu\kappa}{\omega y_0^3}\frac{F_1(x)+G_1(z)}{F_1'(x)}\left(3\operatorname{sech}^4\frac{y-y_1(x)}{y_0}-\operatorname{sech}^2\frac{y-y_1(x)}{y_0}\right)\tanh\frac{y-y_1(x)}{y_0}$$

$$= \frac{4\nu}{\omega y_0}u\left(3\operatorname{sech}^2\frac{y-y_1(x)}{y_0}-1\right)\tanh\frac{y-y_1(x)}{y_0}.$$

This suggests a vertical velocity distribution and cross-circulation as shown in figure 7. This is not outstandingly different from that of figure 6, at least in the centre of the stream. In any case the two circulations must be superposed, and it seems likely that the small circulations away from the centre in figure 7 will be swamped by larger velocities of figure 6; if this is so, figure 6 again gives a qualitative picture of the circulation.

The validity of expanding the solution in powers of Θ is not discussed here; it is assumed that the expansion is possible, and the only justification given is that it gives a reasonable solution.

6. The corresponding problem in the atmosphere

Making assumptions similar to those of the first approximation in §2, and taking a similar choice of axes, the equations of motion and continuity in the atmosphere are

$$2\omega \sin\phi \,.\, u = -\partial h/\partial y,$$

$$2\omega \sin\phi \,.\, v = +\partial h/\partial x,$$

$$-\frac{1}{\rho} = \partial h/\partial p,$$

$$\frac{\partial u}{\partial x} + \frac{\partial v}{\partial y} = 0,$$

where $h = gz$ is the geopotential, and ϕ is the latitude of the origin of co-ordinates. In these equations, x, y and p are chosen as independent variables. The equation of state is now

$$p = R\rho T,$$

and the equation of heat transfer is still

$$u\frac{\partial T}{\partial x} + v\frac{\partial T}{\partial y} = \kappa \frac{\partial^2 T}{\partial y^2}.$$

The relation between T and p becomes

$$T = \frac{p}{R\rho} = -\frac{1}{R} p \frac{\partial h}{\partial p} = -\frac{1}{R}\frac{\partial h}{\partial q},$$

where $q = \log p$. The equations then reduce essentially to those of §2, and we have the equation for h:

$$-\frac{\partial h}{\partial y}\frac{\partial^2 h}{\partial x \partial q} + \frac{\partial h}{\partial x}\frac{\partial^2 h}{\partial y \partial q} = 2\omega\kappa \sin\phi \frac{\partial^3 h}{\partial y^2 \partial q}.$$

A solution of exactly similar form for T, u, v is therefore obtained.

The solution can be applied immediately to a local jet. In this case, the variation of the function $y_0(x)$ of §4 should be retained; it will decrease as x increases at the entry to the jet, and increase with x at the exit. The extra term in v which occurs in equation (48) by taking $y_0'(x)$ non-zero is an odd function of $y - y_1(x)$; this corresponds to an inflow to $y = y_1(x)$ at the entrance, and an outflow at the exit, as would be expected. We note also that u is proportional to $1/[y_0(x)]^2$, and so increases as the stream narrows. The mechanism is similar to that of the confluence theory suggested by Clapp & Namias (1949).

It is more difficult to apply the same solution to a jet which circumvents the earth, as there are now no boundaries where it is reasonable to take a discontinuity. A solution of the equations which does not involve discontinuities would, however, be applicable to both cases.

7. Some difficulties of the present solution

Any complete solution of the problem of the jet-stream must give a satisfactory account of the transfer of angular momentum, and of heat, across the fluid. The present theory is at first sight unsatisfactory in both respects, but since the solution does not pretend to describe the flow completely, this is not a serious defect. It may be of interest to give a brief indication of the transport of these quantities across the stream.

The transfer of momentum behaves like the product uv, and is zero across the line $y = y_1(x)$, unless the function $F_2(x)$ is retained. Even in this case the transport is in opposite directions across the stream, according to whether the stream approaches the inner or the outer boundary, so that the mean with respect to x is zero. But the effect of the boundaries where the stream touches them is of considerable importance in practice, and the present theory takes no account of this.

No simple form for the transfer of heat across the stream exists, and it is impossible to interpret fully the appropriate expression to the solution of §4. It is clear, however, that in the mean with respect to x, the transfer of heat across the line $y = y_1(x)$ is entirely by conduction. Again, the exchange of heat between the stream and the boundaries, which is omitted from the solution, is of major importance.

In order to describe the motion properly, then, we must find solutions for the parts of the jet-stream where it touches the boundaries, and also for the circulations in the remainder of the fluid. In principle this should be possible, but in practice it seems to be intractable.

The solution is of interest, however, because it does give a stream with the right kind of transverse variation in temperature and velocity. This suggests that the basic assumptions made in §2 are valid, and a more general solution should be sought.

The author wishes to thank Prof. M. J. Lighthill for his continued interest in her work, and Prof. T. V. Davies for the benefit of several discussions during the preparation of this paper.

REFERENCES

CHANDRASEKHAR, S. 1953 The instability of a layer of fluid which is heated from below and subject to Coriolis forces. *Proc. Roy. Soc.* A, **217**, 306–326.

CLAPP, P. F. & NAMIAS, J. 1949 Confluence theory of the high tropospheric jet-stream. *J. Met.* **6**, 330–336.

DAVIES, T. V. 1953 The forced flow of a rotating viscous liquid which is heated from below. *Phil. Trans.* A, **246**, 81–112.

DAVIES, T. V. 1956 The forced flow due to heating of a rotating liquid. *Phil. Trans.* A, **249**, 27–64.

FULTZ, D. 1951 Experimental analogies to atmospheric motions. *Compendium of Meteorology*, pp. 1235–1248.

HIDE, R. 1956 Fluid motion in the earth's core and some experiments on thermal convection in a rotating fluid. *Symposium on Geophysical Fluid Dynamics.* Baltimore, 1953.

HIDE, R. 1958 An experimental study of thermal convection in a rotating liquid. *Phil. Trans.* A, **250**, 441–478.

KUO, H.-L. 1954 Symmetrical disturbances in a thin layer of fluid subject to a horizontal temperature gradient and rotation. *J. Met.* **11**, 399–411.

LANCE, G. N. 1958 The effect of a vertical lapse rate of temperature on the spiral flow of a fluid in a heated rotating cylinder. *J. Fluid Mech.* **3**, 523.

LANCE, G. N. & DELAND, E. C. 1957 The steady, axially symmetric flow of a viscous fluid in a deep rotating cylinder heated from below. *Univ. Calif. Publ. Engng*, **5**, 159–176.

RIEHL, H. & FULTZ, D. 1957 Jet streams and long waves in a steady rotating-dishpan experiment: structure of the circulation. *Quart. J. Roy. Met. Soc.* **83**, 215–231.

The effect of wall shape on the degree of reinforcement of a shock wave moving into a converging channel

By G. A. BIRD

Aerodynamics Division, Weapons Research Establishment, Salisbury, South Australia

(Received 22 June 1958)

The one-dimensional theory for the interaction between a normal shock wave and a discontinuous reduction in area is applied to the flow in a two-dimensional channel. It is shown that, for a given overall area ratio, a channel shape consisting of two equal discontinuous reductions in area produces a larger gain in shock strength than a channel having a single discontinuity. The gain in shock strength continues to increase with the number of steps, until the ideal limiting case of an infinite number of vanishingly small changes in area is reached.

A drum camera was used to measure, in a shock tube, the increase in speed of normal shock waves passing through two-dimensional converging channels of different wall shape. It was found that a single discontinuous change produced a gain in shock strength which was less than half that given by the one-dimensional analysis. However, the gain increased as the area change was made more gradual and for long smooth nozzles the value for the ideal case was nearly attained.

1. Introduction

It is not possible to analyse completely the two-dimensional flow associated with the motion of a strong shock wave through a channel of arbitrary wall shape as repeated Mach reflexion usually occurs (see, for example, Kahane, Warren, Griffith & Marino, 1954). However, if the assumption is made that the flow is one-dimensional, the interaction between a normal shock wave and a discontinuous area change can be analysed. Chisnell (1957) obtained a solution of this one-dimensional flow for a single infinitesimal change in area and then integrated this relationship to obtain the shock strength as a function of area. He applied this solution to the special cases of cylindrical and spherical shock waves and showed that the results given by this approach agree closely with those of Guderley (1942) and Butler (1954) which are exact for very strong waves.

The most general flow diagram for the interaction of a normal shock wave with a discontinuous reduction in area is shown in figure 1. This flow pattern is termed Type (a) and occurs when the flow in Region 2 is either supersonic or high subsonic, and the area ratio is too large for isentropic flow to occur through the area change without sonic conditions being reached. A strong reflected shock wave is produced and the flow behind it in Region 3 is subsonic, its velocity being fixed by the area ratio of the change, as the flow at the start of

the reduced section 4 must be sonic. The flow then expands through a rarefaction fan which has its leading edge stationary at 4. A contact surface divides the flow consisting of gas which was originally in the wide section from that which was originally in the narrow section and a transmitted shock wave moves into the narrow section. When the flow behind the shock wave is supersonic, there is a limiting value of the area ratio below which the reflected shock wave is not sufficiently strong to move upstream. However, when this condition is reached, a modification to the flow pattern is possible, as the area ratio is small enough for

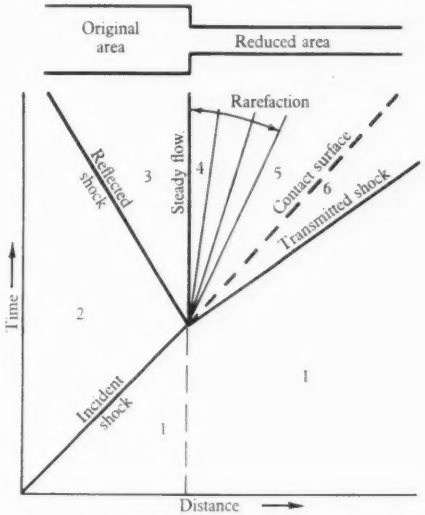

FIGURE 1. Wave diagram of general case of interaction between normal shock wave and discontinuous reduction in area.

steady isentropic compression of the supersonic flow in Region 2 to take place without critical conditions being reached in the area change. No reflected shock wave occurs and the rarefaction is carried downstream as the flow at the start of the reduced section is still supersonic. A contact surface and a transmitted shock wave are, of course, again formed and this flow pattern is termed Type (*b*) flow. There are combinations of shock strength and area ratio for which both types of flow are possible. A further modification which is called Type (*c*) flow occurs when the incident shock wave is weaker. The rarefaction fan is then not necessary and the flow in all regions, with the possible exception of the region between the contact surface and the transmitted shock wave, is subsonic.

A solution may be found for any particular problem by assuming one of the flow patterns, estimating the strength of one of the waves, writing down the relationships between the variables across the other waves and applying an iterative procedure until all the regions of the flow match and the boundary conditions are satisfied. Some results of this numerical analysis, which is similar to that used earlier on the same problem by Laporte (1954), are shown in

figure 2, where the strength of the transmitted shock wave is plotted against the strength of the incident shock wave for interactions with area changes of a number of different ratios. Here, the strength of a shock wave has been defined as the pressure ratio across it. It can be seen that, when a shock wave of strength 7·0 is incident on an area change of ratio 10:1 a transmitted wave of strength 10·7 is produced. However, when the same wave meets a change of $\sqrt{(10)}$:1 a transmitted shock wave of strength 9·4 is produced, and when this wave meets another change of ratio $\sqrt{(10)}$:1 a final transmitted shock wave of strength 12·8 is produced. Therefore, when the reduction in area takes place in two equal steps the increase in shock strength is greater than if it takes place in one step of the same overall area ratio.

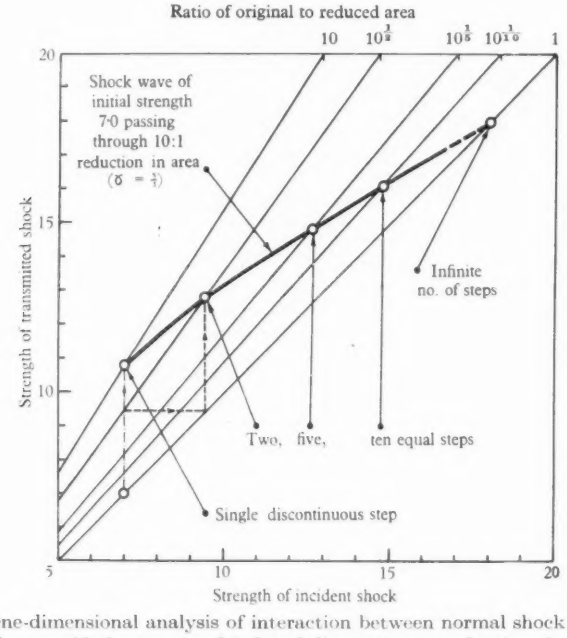

FIGURE 2. One-dimensional analysis of interaction between normal shock waves in a gas with a specific heat ratio of 5:3 and discontinuous reductions in area.

This general graphical procedure can be extended to any number of steps, and figure 2 shows the results for five and ten steps. The locus of these points may be extrapolated to the line of no area change and this gives a transmitted shock strength of 17·9. This corresponds to the ideal case of an infinite number of vanishingly small steps and is equivalent to Chisnell's analytical solution. Care must be taken when applying this graphical method to very strong waves, since the reflected shock wave in Type (*a*) flow causes non-isentropic losses which do not occur in Type (*b*) flow and the transition between the two is not continuous. In this example, a small region of Type (*b*) flow is possible for very small area ratios when the shock strength is above 9·27, but the reflected shock wave in the immediately adjacent region of Type (*a*) flow is sufficiently weak to be

regarded as isentropic, so that the transition between the two regions is effectively continuous.

These considerations may be applied to the motion of a shock wave through converging channels of arbitrary wall shape, and it would be expected that the increase in shock strength for a given overall area change would be intermediate between that for a single discontinuous change and that for the 'ideal' channel. An experimental investigation was therefore undertaken to measure the speed and the strength of shock waves as they passed through two-dimensional converging channels of various wall shapes.

2. Experimental arrangements

The experiments were carried out in a shock tube using air as the high-pressure driving gas and argon as the low-pressure gas. The tube had a rectangular cross-section of 41 × 66 mm and the lengths of the high- and low-pressure sections were 0·75 and 3·0 m, respectively. Gas bottles were used to supply both sections, the low-pressure section being evacuated by a vacuum pump before the argon was admitted. The high and low pressures were set as near as possible to 2·4 and 0·032 atm., respectively, so that the nominal pressure ratio across the diaphragm was 75:1. Cellulose aceto-butyrate of 0·25 mm thickness forming the diaphragm was ruptured by remote control using a solenoid operated pricker. The theoretical shock strength for a diaphragm pressure ratio of 75:1 is 7·25 and the actual strengths ranged from 6·4 to 7·3, the scatter being primarily due to difficulties in accurately setting the pressure. The symmetrical nozzle blocks were carefully fitted in the working section which was 50 cm long and had windows which were 30 cm long and 1·2 cm wide. Nozzles 1–6 (table 1) were made of steel, while 7 was of polished wood; the area ratio of the contraction was 9·9:1 in all cases.

The image of a double mirror schlieren system was projected on to the film in a drum camera, so that a record of the flow was obtained in the distance–time plane. The light source for the schlieren was a water-cooled mercury arc lamp. As this provided a continuous source, an electromagnetically operated shutter was placed directly behind the slit so that the light could be allowed to pass for less than one revolution of the drum. A pulse generator in the camera produced 50 pulses each revolution of the drum; these were counted in the drum-camera control unit and the result was displayed on a frequency meter, which therefore gave a measure of the speed of rotation of the drum. This speed was set to the desired value by an adjustable transformer. A piece of thin aluminium foil was placed across the diaphragm and, when ruptured, provided a signal to the control unit. This signal initiated a time delay after which a pulse was passed to open the shutter. The shutter remained open until 16 pulses from the drum camera had been counted and then shut. The times were set so that the shutter was open and a record was produced by the camera while the shock wave was passing through the working section.

A number of the records obtained from the drum camera are reproduced in figure 3 (plate 1). The flow pattern in figure 3*a* is generally similar to that shown in figure 1 and the nature of the waves in this camera record may be deduced by

comparing the two. The flow patterns in the other records are generally similar, although the discontinuities become more diffuse as the area change is made more gradual. The optical reduction of the schlieren system and the speed of rotation of the drum were known so that the speed, q, of the shock was easily

Nozzle blocks [Two-dimensional symmetrical area ratio 9·9 : 1]			Shock wave strength			
No.	Shape	Description	Incident	Transm.	% increase	Mean % increase
1	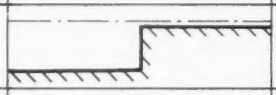	90°, sharp corner	7·3	9·1	25	25
2	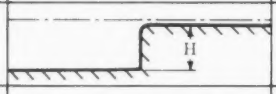	90°, 0·1 H radius corner	7·1	9·1	29	29
3	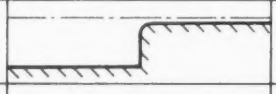	90°, 0·2 H radius corner	7·0 7·2	9·3 9·6	33 33	33
4	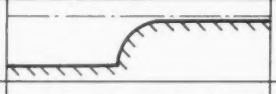	Quadrant shaped	6·4	11·0	72	72
5		45°, straight	6·8 6·4	12·8 11·9	88 86	87
6	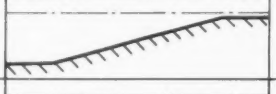	15°, straight	6·6 7·2 7·3	14·6 15·8 16·2	121 119 122	121
7		15°, rounded	6·9 7·3	16·1 16·5	133 126	130

TABLE 1. Results of experiments on interaction between normal shock waves in argon and converging nozzles

obtained from the camera record. The speed of sound, a, in the undisturbed gas ahead of the shock, was also known and the strength, z, of the shock waves followed from the expression

$$z = \frac{2\gamma}{\gamma+1}\left(\frac{q}{a}\right)^2 - \frac{\gamma-1}{\gamma+1},$$

where γ is the ratio of the specific heats of the gas.

The initial change in the shock speed in the records for the 15° nozzles appears almost discontinuous as the windows showed only the portion of the shock at the centreline of the tube. No change in shock speed was therefore observed until the intersection point of the Mach reflexions from the top and bottom nozzles

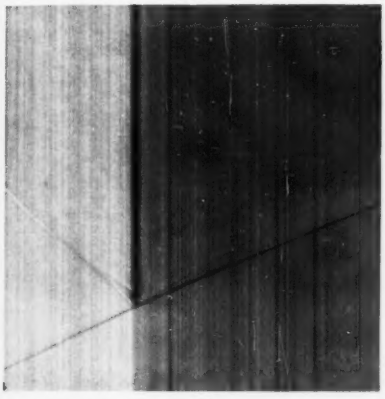

(*a*)

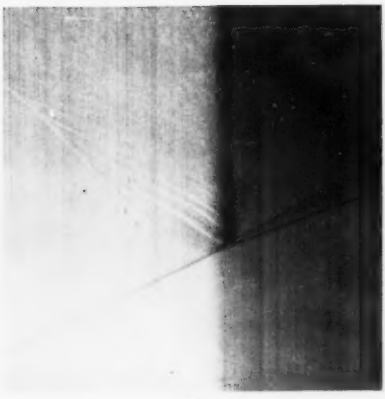

(*b*)

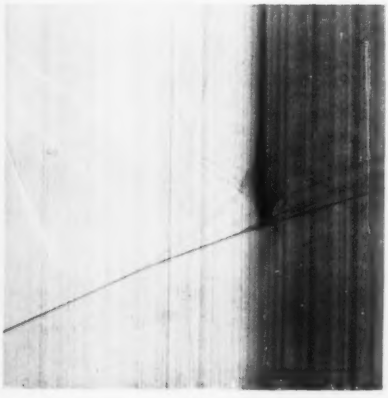

(*c*)

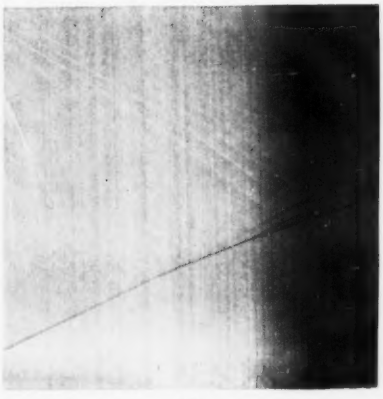

(*d*)

FIGURE 3 (plate 1). (*a*) 90°, 0·1 H radius corner nozzle blocks. (*b*) Quadrant-shaped nozzle blocks. (*c*) 15°, straight nozzle blocks. (*d*) 15°, rounded nozzle blocks.

(*Facing p.* 64)

met at the centre. The darkening of the background in the reduced area section of the records was caused by the nozzle blocks protruding over the edge of the windows.

3. Experimental results and discussion

The experimental results are summarized in table 1. It is estimated that the error in the strengths of the incident and transmitted shock waves was of the order of 1 %. In the cases where the tests were repeated, the results were consistent within the order of accuracy of the measurements. The variations in the incident shock strength are unimportant as the percentage increase in shock strength is not sensitive to them.

The 90°, sharp corner nozzle gave an increase in shock strength of only 25 % compared with the theoretical value (see figure 2) for a discontinuous area change of 53 %. This discrepancy can be accounted for as the theory assumes inviscid isentropic steady flow across the contraction and this could not possibly be approached in this nozzle. In addition, the shock would have to travel a distance equal to several tube widths past the change before this flow pattern could become established. It was noted on the record that the shock did not attain its final speed until it had moved some distance past the area change, its initial behaviour corresponding to an interaction with an area change of lower area ratio. Small radii of one-tenth and one-fifth of the height of the nozzle blocks increased the shock strength reinforcement to 29 and 33 %, respectively.

When the radius was increased to the full height of the nozzle blocks (i.e. quadrant shaped nozzle) the gain in shock strength rose to 72 % which is well above the theoretical value for a single discontinuous area change. The 45° straight nozzle which had the same area transition length as the quadrant nozzle produced a larger gain of 87 %. This indicates that the overall change in shock strength is sensitive to the initial strength of the reflected shock wave, which would be greater for the quadrant shaped blocks. For comparison, the theoretical values of the increase in shock speed for the two, five and ten equal area change cases are 83, 100 and 128 %, respectively.

When the transition region was greatly lengthened by the use of the 15° straight blocks the gain in shock strength rose to 121 %. In order to avoid the losses caused by the sharp corners on this nozzle it was then replaced by one with the same general shape, but with the corners rounded and the gain in shock strength rose to 130 %. This approaches the theoretical value of 156 % for the ideal case of an infinite number of vanishingly small area changes. Chisnell pointed out that this theory assumes that the effects of the reflected and re-reflected disturbances on the primary shock wave may be neglected and these experimental results seem to provide some further justification for this assumption.

4. Conclusions

The degree of reinforcement of a shock wave moving into a converging channel was shown to depend critically upon the wall shape and the extreme values of the percentage increase in shock strength for a contraction of a fixed

area ratio differed by a factor of five. The most effective set of nozzle blocks produced a gain in shock strength, which was more than twice as great as the theoretical value for a single discontinuous area change, and approached that for the ideal case of an infinite number of vanishingly small area changes. This indicates that a converging section could well be incorporated in the design of those shock tubes in which the strongest possible shock waves are desired. Care would have to be taken in positioning the area change to ensure that the downstream travelling waves, produced by the interaction between the reflected waves from the area change and the contact surface from the diaphragm, do not overtake the primary shock wave in the working section.

Acknowledgement is made to the Chief Scientist, Department of Supply, Australia, for permission to publish this article.

REFERENCES

Butler, D. 1954 *Rep. Armament Research and Development Est.* no. 54/54.

Chisnell, R. F. 1957 *J. Fluid Mech.* **2**, 286.

Guderley, G. 1942 *Luftfahrtforschung*, **19**, 302.

Kahane, A., Warren, W. R., Griffith, W. C. & Marino, A. A. 1954 *J. Aero. Sci.* **21**, 505.

Laporte, O. 1954 *Rep. Los Alamos Scientific Laboratory*, L.A. 1740.

The structure of a hydromagnetic shock in steady plane motion

By G. S. S. LUDFORD
University of Maryland and Harvard University

(Received 31 May 1958)

In this paper we discuss the structure of those oblique shocks which occur in plane hydromagnetic flow. We find that not all pairs of states satisfying the shock conditions can be linked by a one-dimensional flow of a viscous, electrically conducting fluid, while other pairs can be linked in more than one way. In the latter case a particular transition is singled out when further information is given concerning the three-dimensional problem of which the plane motion is an idealization.

Introduction

We consider the steady plane motion of an electrically conducting, perfect, viscous gas in the presence of a magnetic field in its own plane, on the basis of classical continuum theory. The local behaviour of the gas at a shock is studied by considering transitions in which all quantities, as functions of one co-ordinate x, change from finite initial values at $x = -\infty$ to finite final values at $x = +\infty$.

This problem was studied by Marshall (1955) for the particular case in which the x-component of the magnetic field (i.e. normal to the shock front) is zero throughout, so that the y-component of velocity may be taken zero also. He found that for a given initial state at $x = -\infty$ there is not only a unique final state at $x = +\infty$ but also a unique transition. In the general (oblique) case discussed in the present paper we find that there can be as many as three final states, with, moreover, an infinite number of transitions ending at one of them. The former indeterminacy is implied in several discussions of the necessary conditions which hold across a discontinuity surface in the flow of an inviscid, perfectly conducting fluid, and is presumably resolved in any particular problem by specifying further boundary conditions. However, such treatments can never discover whether two states satisfying these necessary conditions can in fact be joined by a transition solution, much less whether it is unique. Indeed, we shall also find that some pairs of states cannot be joined. In brief, the shock conditions are not sufficient to ensure that there is a unique transition joining any two states satisfying them [cf. the corresponding situation for the purely gas-dynamical shock as described by von Mises (1958)].

We consider in detail two particular cases, the first of which is Marshall's. The second corresponds simultaneously to switch-on (fast), switch-off (slow), and transverse shock discontinuities as identified by Friedrichs (1957). There is no

transition solution for the last-mentioned and we must conclude that the transverse shock cannot occur in plane motion. Here we also encounter the lack of uniqueness mentioned in the last paragraph, which seems to point to the necessity of specifying how the current lines (lying along the z-direction) are closed at infinity, this constituting additional information about the three-dimensional problem of which the plane motion is an idealization. In fact, when we assume that the motion is the limit (at large radial distances) of an axially symmetric flow, for which the current lines are closed in the fluid (circles), the difficulty resolves itself.

Special interest lies in the behaviour of a transition solution in the limit of vanishing viscosity with non-zero resistivity. Marshall indicated that in his case a purely gas-dynamical discontinuity can appear (the Rankine–Hugoniot conditions are satisfied and the magnetic field is continuous), upstream of which there is an adjustment region to hydromagnetic values. We show explicitly that the adjustment may take place upstream or downstream, the former occurring in his case and for the switch-on shock, the latter for the switch-off shock.

Governing the motion are the Navier–Stokes equations, now containing terms arising from the Maxwell stresses and with the Joule heat appearing as a new source of dissipated energy, and Maxwell's equations supplemented by Ohm's law for a moving medium. The charge accumulation is neglected and, for simplicity, all material coefficients are assumed constant.

The argument is concerned with a phase plane, in which the transition solutions are represented by curves joining singular points of a certain system of differential equations. Any pair of singular points satisfies the shock conditions, and it is a question of deciding how many curves (if any) join the pair.

1. Equations of motion

We consider a motion in which the velocity $\mathbf{v}$ and the magnetic field $\mathbf{H}$ are given by

$$\mathbf{v} = (u, v, 0), \quad \mathbf{H} = (H_n, H, 0), \tag{1}$$

where all components are functions of x alone. It then follows from $\operatorname{div} \mathbf{H} = 0$ that

$$H_n = \text{constant}, \tag{2}$$

and from $\mathbf{J} = \operatorname{curl} \mathbf{H}$ that the current lies in the z-direction:

$$\mathbf{J} = (0, 0, J), \quad J = H'(x). \tag{3}$$

If we now assume the conduction equation

$$\mathbf{J} = \sigma(\mathbf{E} + \mu \mathbf{v} \times \mathbf{H}), \tag{4}$$

then the electric field $\mathbf{E}$ also lies in the z-direction (since both $\mathbf{J}$ and $\mathbf{v} \times \mathbf{H}$ do):

$$\mathbf{E} = (0, 0, E_0), \quad E_0 = \text{constant},$$

where the constancy of E_0 follows from $\operatorname{curl} \mathbf{E} = 0$.

Under these conditions the equations of continuity and momentum* reduce to

$$\left.\begin{aligned} \frac{d}{dx}(\rho u) &= 0, \\ \rho u \frac{du}{dx} &= -\frac{dp}{dx} + \mu_1 \frac{d^2u}{dx^2} - \mu H \frac{dH}{dx}, \\ \rho u \frac{dv}{dx} &= \mu_2 \frac{d^2v}{dx^2} + \mu H_n \frac{dH}{dx}, \end{aligned}\right\} \tag{5}$$

where μ_2 is the coefficient of shear viscosity while $\mu_1 - 4\mu_2/3$ is the coefficient of bulk viscosity. Similarly, under the assumption that a fluid element receives energy only by heat conduction (coefficient k) and by viscous and electrical dissipation, and assuming the gas to be perfect, we find the specifying equation

$$\rho u \frac{d}{dx}\left[\tfrac{1}{2}(u^2+v^2) + \frac{p}{(\gamma-1)\rho} + \frac{\mu}{2\rho}(H_n^2+H^2)\right] + \frac{d}{dx}\left[pu - \mu_1 u\frac{du}{dx} - \mu_2 v\frac{dv}{dx} - \frac{\mu}{2}\{(H_n^2-H^2)u + 2H_n Hv\} - \frac{1}{\sigma}H\frac{dH}{dx}\right] = k\frac{d^2T}{dx^2}, \tag{6}$$

where γ has its usual meaning.

To these must be added the conduction equation (4) with **J** given by (3)

$$\frac{dH}{dx} = \sigma[E_0 + \mu(uH - vH_n)]. \tag{7}$$

These five equations (for u, v, p, ρ, H) immediately integrate to give $\rho u = m$ (constant) and

$$\mu_1 \frac{du}{dx} = mu + p + \tfrac{1}{2}\mu H^2 - A,$$

$$\mu_2 \frac{dv}{dx} = mv - \mu H_n H - B,$$

$$k\frac{dT}{dx} = C + Au + Bv + m\left[\frac{p}{(\gamma-1)\rho} - \tfrac{1}{2}(u^2+v^2)\right] - HE_0 - \tfrac{1}{2}\mu H(uH - 2H_n v),$$

$$\frac{1}{\sigma}\frac{dH}{dx} = E_0 + \mu(uH - vH_n),$$

where A, B, C are constants. Without loss in generality we may take $u > 0$ and hence $m > 0$, and, since we are interested only in flows which tend to uniform conditions ($d/dx = 0$), we also have $A > 0$. When the dimensionless variables

$$U = \frac{m}{A}u, \quad V = \frac{m}{A}v, \quad h = \sqrt{\left(\frac{\mu}{2A}\right)}H, \quad \Theta = \frac{m^2 p}{A^2\rho} = \frac{m^2 RT}{A^2}$$

* In this paragraph see Goldstein (1957) for the complete equations.

are introduced, the equations become

$$\left.\begin{aligned} \frac{\mu_1}{m} U \frac{dU}{dx} &= -U + \Theta + U^2 + Uh^2, \\ \frac{\mu_2}{m} \frac{dV}{dx} &= a + V - 2h_n h, \\ \frac{k}{mR} \frac{d\Theta}{dx} &= b + U - aV + \frac{\Theta}{\gamma - 1} - e_0 h - \tfrac{1}{2}(U^2 + V^2) + 2h_n Vh - Uh^2, \\ \frac{m\eta}{A} \frac{dh}{dx} &= \tfrac{1}{2} e_0 + Uh - h_n V, \end{aligned}\right\} \tag{8}$$

where $\eta = 1/\mu\sigma$ is the magnetic diffusivity, and

$$a = -\frac{B}{A}, \quad b = \frac{mC}{A^2}, \quad e_0 = m\sqrt{\left(\frac{2}{\mu A^3}\right)} E_0, \quad h_n = \sqrt{\left(\frac{\mu}{2A}\right)} H_n.$$

Solutions of the system (8) are represented by curves in (U, V, Θ, h)-space on which x is a parameter. In order to visualize their geometry we make the following simplifications. (i) In the third of equations (8) k is set equal to zero; it is known that in the purely gas-dynamical case the neglect of heat conduction has no effect on the general character of shock transition solutions (see Gilbarg 1951). (ii) In the second equation (8) we put $\mu_2 = 0$; this corresponds to the physically unrealistic assumption of zero shear viscosity and non-zero bulk viscosity, but again this is justified in the purely gas-dynamical case (in fact the relevant solution is the same: $V = -a$, whether μ_2 is zero or not). Under these assumptions the system (8) reduces to

$$\left.\begin{aligned} \frac{\mu_1}{m} U \frac{dU}{dx} &= f(U,h) \equiv (\gamma - 1)\beta - \gamma U + 2(\gamma - 1)\alpha h + \frac{\gamma + 1}{2} U^2 - 2(\gamma - 1) h_n^2 h^2 + \gamma U h^2, \\ \frac{m\eta}{A} \frac{dh}{dx} &= g(U,h) \equiv \alpha - h(2h_n^2 - U), \end{aligned}\right\} \tag{9}$$

when V and Θ are eliminated; here

$$\alpha = ah_n + \tfrac{1}{2} e_0, \quad \beta = -(b + \tfrac{1}{2} a^2).$$

2. The singular points

In the (U, h)-plane the infinite isocline of the system (9) is the cubic $f = 0$. The zero isocline is formed by the rectangular hyperbola* $g = 0$ and the h-axis: $U = 0$. We are concerned with integral curves lying in the right half of the plane: $U > 0$, and in particular those joining the singular points given by $f = 0$, $g = 0$. These points are also the intersections of the ellipse

$$f - \gamma hg \equiv \frac{\gamma + 1}{2}\left[U - \frac{\gamma}{\gamma + 1}\right]^2 + 2h_n^2\left[h - \frac{(2 - \gamma)\alpha}{4h_n^2}\right]^2 + \left[\beta(\gamma - 1) - \frac{(2 - \gamma)^2 \alpha^2}{8h_n^2} - \frac{\gamma^2}{2(\gamma + 1)}\right] = 0, \tag{10}$$

* For $\alpha = 0$ the results which follow must be understood in an appropriate limit sense.

which is not an isocline, and the rectangular hyperbola (see figure 1). Therefore, there are 0, 2 or 4 real singular points, of which an even number lie on each branch of the hyperbola. On eliminating U between $f = 0$ and $g = 0$, we find that their ordinates are given by the quartic equation

$$F(h) \equiv 2h_n^2 h^4 - (2-\gamma)\alpha h^3 + [2(\gamma+1)h_n^4 - 2\gamma h_n^2 + (\gamma-1)\beta]h^2 - \alpha[2(\gamma+1)h_n^2 - \gamma]h + \tfrac{1}{2}(\gamma+1)\alpha^2 = 0. \quad (11)$$

We now investigate the nature of the singular points, since it is this which determines the way in which a transition flow tends to the corresponding uniform conditions at infinity.

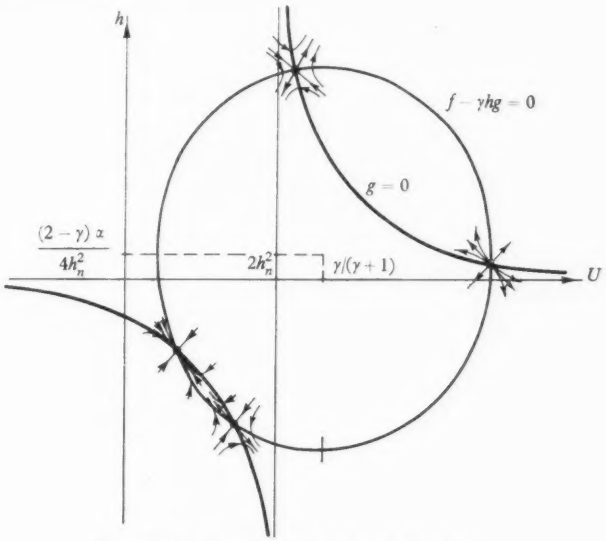

FIGURE 1. Singular points in phase plane.

In order of decreasing $|h|$ the points (in $U > 0$) with $h > 0$ are alternatively saddle and nodal, and similarly for those with $h < 0$. For the characteristic equation of (9) at a singular point (U_0, h_0) is*

$$\kappa^2 - (\bar{f}_U + \bar{g}_h)\kappa + (\bar{f}_U \bar{g}_h - \bar{f}_h \bar{g}_U) = 0, \quad (12)$$

where $\bar{f} = mf/\mu_1 U$, $\bar{g} = Ag/m\eta$ and all values are to be taken at the point, i.e.

$$\bar{f}_U = \frac{m}{\mu_1 U_0}[-\gamma + (\gamma+1)U_0 + \gamma h_0^2], \quad \bar{f}_h = \frac{2m}{\mu_1} h_0 \quad (13a)$$

and

$$\bar{g}_U = \frac{A}{m\eta} h_0, \quad \bar{g}_h = -\frac{A}{m\eta}\frac{\alpha}{h_0}. \quad (13b)$$

The discriminant of this equation is

$$(\bar{f}_U - \bar{g}_h)^2 + 4\bar{f}_h \bar{g}_U,$$

* This equation determines the exponential solutions ($e^{\kappa x}$) of (9) when the right-hand sides are linearized in the neighbourhood of the point (cf. §5).

which is positive since $\bar{f}_h$ and $\bar{g}_U$ have the same sign; hence the roots of (12) are real. Also the constant term has the same sign as

$$-\frac{1}{U_0 h_0}[\alpha\{-\gamma+(\gamma+1)U_0+\gamma h_0^2\}+2U_0 h_0^3]$$
$$=-\frac{1}{U_0 h_0^2}[4h_n^2 h_0^4-(2-\gamma)\alpha h_0^3+\alpha\{2(\gamma+1)h_n^2-\gamma\}h_0-(\gamma+1)\alpha^2]$$
$$=-\frac{h_0}{U_0}\left[\frac{d}{dh}\left(\frac{F(h)}{h^2}\right)\right]_{h=h_0}, \tag{14}$$

where $F(h)$ is given in (11). Now $h\,d[F(h)/h^2]/dh$ is clearly positive for sufficiently large $|h|$ and has opposite signs at consecutive zero of $F(h)/h^2$ on the same side of the U-axis. Since a negative constant term implies a saddle point, and a positive one a nodal point, the result follows.

Since there may be two nodal points in the region of interest the possibility arises of there being an infinity of integral curves joining them, i.e. a family of transitions between given states at $x = \pm\infty$. We shall discuss two particular cases; in the first this does not occur, in the second it does.

3. The case $H_n = 0$

This was discussed first by Marshall (1955) and then by Burgers (1957). The former did not completely discuss the limit of vanishing viscosity; the latter assumed zero viscosity from the start and hence had to introduce extraneous assumptions.

We return for a moment to the original equations (8), with μ_2 not necessarily zero, and set $h_n = 0$. Then the second of these can be integrated explicitly, the only relevant solution being $V = -a$ (all others are exponentially large at $x = +\infty$). But this is precisely what is used to eliminate V and obtain equations (9) when $\mu_2 = 0$. Hence, in the present case our discussion is in fact independent of the assumption $\mu_2 = 0$.

The rectangular hyperbola becomes

$$g \equiv \alpha + hU = 0,$$

and the ellipse (10) degenerates into the parabola

$$f-\gamma hg \equiv \frac{\gamma+1}{2}\left[U-\frac{\gamma}{\gamma+1}\right]^2-(2-\gamma)\alpha h+\left[(\gamma-1)\beta-\frac{\gamma^2}{2(\gamma+1)}\right]=0.$$

Since the system (9) is unaltered on replacing α, h by $-\alpha, -h$ we may take $\alpha \leqslant 0$. Then these curves will lie as in figure 2, always having an intersection 3 at which $U < 0$, and, for suitable values of α, β, another two intersections 1, 2 at which U is always positive. This can be read off from (11), which also shows that the fourth intersection lies at infinity on the lower branch of the hyperbola.

Only the points 1 and 2 are of physical interest. Between them f is negative ($= f-\gamma hg$) on the hyperbola and positive ($= \gamma hg$) on the parabola. Hence the infinite isocline: $f = 0$ lies above the hyperbola and below the parabola. Since each horizontal cuts it in at most two points (see (9)), it has just one extremum (a maximum) between 1 and 2 if it has positive slope at 2 and none if it

has negative slope. From (13*a*) the condition for a maximum is therefore $U_2^2-\gamma U_2(1-U_2-h_2^2) = U_2^2-\gamma\Theta_2 < 0$, or in the original variables: $u_2^2 < \gamma p_2/\rho_2 = a_2^2$. Within the region R bounded by the arcs 1 2 of $f = 0$ and $g = 0$ the integral curves have negative slope, with x increasing in the negative U-direction on each.

We saw in the last section that 2 is a saddle point and 1 is a nodal point. The singular directions at either point are determined by

$$Q(m) \equiv \bar{f}_h m^2 + (\bar{f}_U - \bar{g}_h)\, m - \bar{g}_U = 0;$$

hence, since $Q(0) < 0$ and $Q(\pm\infty) > 0$ (see (13)), one has positive slope and the other negative. It now follows, as in the purely gas-dynamical case (see Gilbarg 1951), that there is a unique transition solution joining the points 1 and 2, which

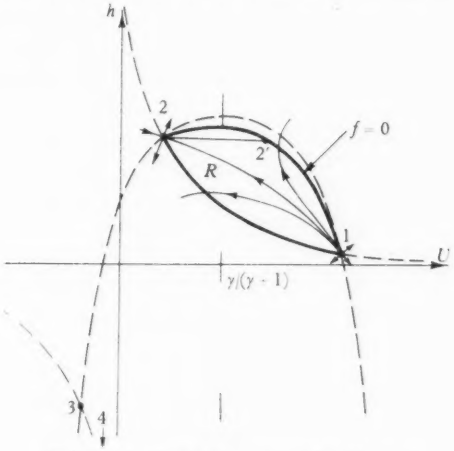

FIGURE 2. Transition curve for $H_n = 0$.

correspond to $x = -\infty$ and $x = +\infty$, respectively,* and this curve lies in R. Moreover, when the infinite isocline is monotonic between 1 and 2, the limiting transition as $\mu_1 \to 0$ follows this isocline; whereas when there is a maximum, it follows the isocline until attaining (at 2′) the same ordinate as 2 and then the horizontal into 2. This second behaviour is due to the fact that no integral curve can attain positive slope in R.

The straight segment 2 2′ corresponds to a purely gas-dynamical shock (x constant in limit); across it the Rankine–Hugoniot conditions hold. For $f = 0$ is the result of eliminating V and Θ between the equations obtained by setting the right sides (with $h_n = 0$) of the first three equations (8) equal to zero. Hence

$$U_2 + \frac{\Theta_2}{U_2} = 1 - h_2^2 = 1 - h_{2'}^2 = U_{2'} + \frac{\Theta_{2'}}{U_{2'}},$$

$$\tfrac{1}{2}U_2^2 + \frac{\gamma}{\gamma-1}\Theta_2 = -b + aV_2 + e_0 h_2 + \tfrac{1}{2}V_2^2 = -b + aV_{2'} + e_0 h_{2'} + \tfrac{1}{2}V_{2'}^2$$

$$= \tfrac{1}{2}U_{2'}^2 + \frac{\gamma}{\gamma-1}\Theta_{2'},$$

* The sign of (14) expresses that u^2 is greater than $\gamma p/\rho + \mu H^2/\rho$ at 1 and less at 2, i.e. the transition flow is initially supersonic and finally subsonic.

which, combined with $\rho_2 u_2 = \rho_{2'} u_{2'}$ and expressed in the original variables, are precisely the Rankine–Hugoniot conditions. The point 2 also corresponds to the whole uniform limit state behind the shock.

Thus, we see that a transition flow in an electrically conducting fluid of vanishingly small viscosity contains a gas-dynamical shock if and only if the final state is subsonic (in the gas-dynamical sense), and that when it does the whole adjustment region (to hydromagnetic values) lies upstream of the shock. The magnetic field is continuous across the shock, though dH/dx undergoes a jump $\sigma(E_0 + \mu u_{2'} H_2)$.

4. The case $H = 0$ in initial state

One possibility is that $H \equiv 0$. The transition is then a purely fluid-dynamical one with no interaction between flow and magnetic field. We shall see immediately, however, that this is not the only possibility under certain circumstances; indeed, our assumption only implies $\alpha = 0$ in (9).

Clearly the present section covers Friedrichs' switch-on shock discontinuities ($H = 0$ initially but not finally); it also covers his switch-off ($H = 0$ finally but not initially), and transverse (H changes sign but not magnitude) shock discontinuities, since either assumption concerning the end-points leads to $\alpha = 0$ also.

The zero isocline degenerates into the pair of straight lines

$$U = 2h_n^2, \quad h = 0,$$

while the infinite isocline

$$\left[U - \frac{2(\gamma-1)}{\gamma} h_n^2\right]\left[\frac{\gamma+1}{2} U + \gamma h^2 + \frac{\gamma^2-1}{\gamma} h_n^2 - \gamma\right] = 2(\gamma-1) h_n^2 \left[1 - \frac{\gamma^2-1}{\gamma^2} h_n^2\right] - (\gamma-1)\beta$$

represents a hyperbola in the (U, h^2)-plane. [We use this rather than the (U, h)-plane in the present section.] The three points of intersection are

$$1, 2: \quad U = \frac{\gamma}{\gamma+1}(1 \pm k), \quad h^2 = 0,$$

$$3: \quad U = 2h_n^2, \quad h^2 = \frac{\gamma^2}{4(\gamma+1) h_n^2}\left[k^2 - \left(1 - \frac{2\sqrt{\gamma+1}\, h_n^2}{\gamma}\right)^2\right],$$

where $k = \sqrt{\{1 - 2(\gamma^2-1)\beta/\gamma^2\}}$ (which must be real, by assumption).

Thus, there are five ranges of the parameter h_n to consider:*

(i) $$2h_n^2 < \frac{\gamma}{\gamma+1}(1-k) = U_2,$$

(ii$a$) $$\frac{\gamma}{\gamma+1}(1-k) < 2h_n^2 < \frac{\gamma^2}{\gamma^2-1}(1-k),$$

(ii$b$) $$\frac{\gamma^2}{\gamma^2-1}(1-k) < 2h_n^2 < \frac{\gamma}{\gamma+1}(1+k) = U_1,$$

* From the first of equations (8), $\Theta_1 = U_1(1-U_1)$. Hence, with positive temperature at 1, k is less than $1/\gamma$.

(iii$a$) $$\frac{\gamma}{\gamma+1}(1+k) < 2h_n^2 < \frac{\gamma^2}{\gamma^2-1}(1+k),$$

(iii$b$) $$2h_n^2 > \frac{\gamma^2}{\gamma^2-1}(1+k).$$

The different situations are illustrated in figures 3–6. In case (i) (figure 3), the point 3 is discarded and 1, 2 lie on the same branch of the hyperbola with 1 a nodal and 2 a saddle point. For (ii), 3 is a saddle point, while the points 1 and 2 are nodal, lying on the same branch when (ii$a$) holds (figure 4) and on different branches when (ii$b$) holds (figure 5). With (iii) (figure 6), the point 3 is again discarded, the point 1 is a saddle, and point 2 a node, and the latter lie on different or the same branches of the hyperbola according as (iii$a$) or (iii$b$) holds. The integral curves are easily sketched once the singular directions at 1, 2 and 3 have been determined and the signs of dU/dx and dh/dx in the various regions found.

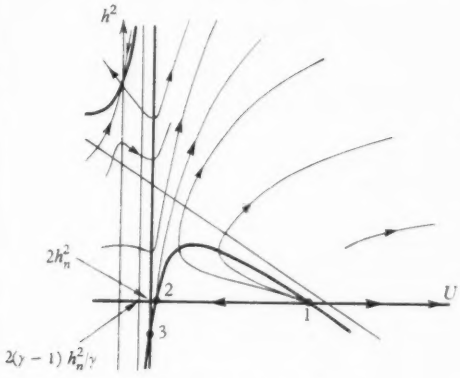

FIGURE 3. Integral curves for $\alpha = 0$; case (i).

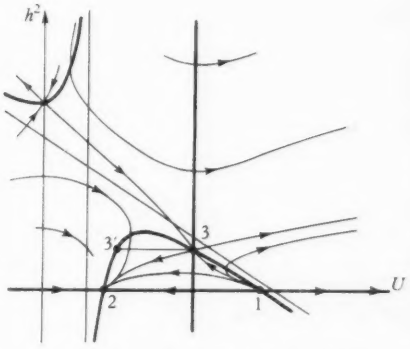

FIGURE 4. Integral curves for $\alpha = 0$; case (ii$a$).

When (i) or either of (iii) holds there is a unique transition: it starts at 1 and ends at 2, and has $H = 0$ throughout, so that there is no interaction between the fluid motion and the magnetic field. The end-points 1 and 2 satisfy the ordinary Rankine–Hugoniot shock conditions. The same transition can occur in case (ii), but now there is not only a second end-point* 3 (to which the transition is unique), but also a whole family of possible transitions from 1 to 2. Within each, H^2 increases from zero to a maximum and then decreases to zero again.

Before discussing this lack of uniqueness in greater detail we make one further observation. If the initial state and magnetic field are chosen so as to give the point 3 in figure 4, there will be a unique transition ending at the point† 2. Now the hyperbola has its maximum‡ to the left of 3, so that as $\mu_1 \to 0$ this transition

* The pair 1, 3 represents the switch-on shock, while the two images of 3 in the (U, h)-plane represent the transverse shock. There is clearly no integral curve joining the latter.

† The pair 3, 2 in figures 4, 5 represent the switch-off shock.

‡ For smaller h_n the maximum lies on the right side; the change takes place as u_3 increases through $a_3 = \sqrt{(\gamma p_3/\rho_3)}$.

will tend to follow the horizontal 3 3′ and then the infinite isocline to 2. A proof quite similar to that at the end of § 3 shows that 3 and 3′ satisfy the ordinary gas-dynamical shock conditions. However, in contrast to § 3 the whole adjustment region now lies downstream of the shock.

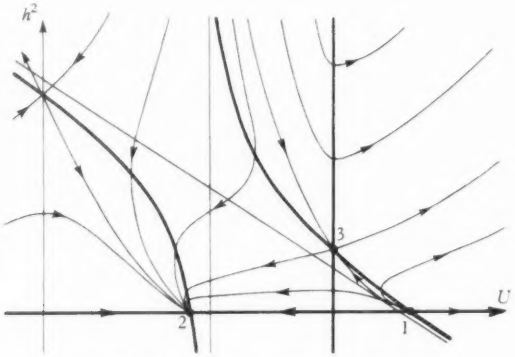

FIGURE 5. Integral curves for $\alpha = 0$; case (ii$b$).

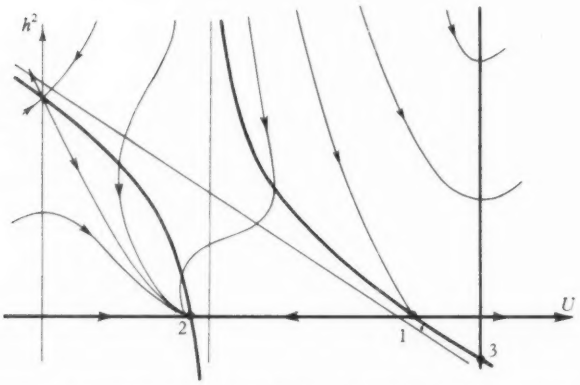

FIGURE 6. Integral curves for $\alpha = 0$; case (iii$a$). In case (iii$b$) the hyperbola has the same form as in figures 3 and 4, the points 1 and 2 now lying on the upper branch.

5. Axially symmetric flow

A simple way to close the current lines is to consider a flow in which the velocity **v** and magnetic field **H** are given by (1) in a cylindrical co-ordinate system (x, r, θ), where now all components are functions of x and r but not of θ. Then (2) is replaced by

$$\frac{\partial H_n}{\partial x} + \frac{1}{r}\frac{\partial}{\partial r}(rH) = 0, \tag{15}$$

and the currents form closed loops (circles) in the fluid with

$$\mathbf{J} = (0, 0, J), \quad J = \frac{\partial H}{\partial x} - \frac{\partial H_n}{\partial r}.$$

From (4) we then see that **E** has only a θ-component:

$$\mathbf{E} = \left(0, 0, \frac{E_0}{r}\right), \quad E_0 = \text{constant}, \tag{16}$$

where curl $\mathbf{E} = 0$ has been used to obtain the form of this component.

We now consider the ways in which a uniform stream: $u = u_0$, $v = 0$, $p = p_0$, $\rho = \rho_0$ with $H = 0$ and $H_n = H_{n0}$, at $x = -\infty$ can be disturbed. In the one-dimensional case such disturbances are represented by the integral curves leaving a point such as 1 in figures 3–6. Here we discuss only the immediate behaviour and hence replace all coefficients in the non-linear equations of continuity, momentum, energy balance, and electric conduction by their zero values. Using u, v, p, ρ, H and H_n for their own disturbances now, we find (5), (6) and (7) replaced by

$$\rho_0 \frac{\partial u}{\partial x} + u_0 \frac{\partial \rho}{\partial x} + \frac{\rho_0}{r} \frac{\partial}{\partial r}(rv) = 0, \tag{17a}$$

$$\rho_0 u_0 \frac{\partial u}{\partial x} = -\frac{\partial p}{\partial x} + \mu_1 \frac{\partial}{\partial x}\left[\frac{\partial u}{\partial x} + \frac{1}{r}\frac{\partial}{\partial r}(rv)\right], \tag{17b}$$

$$\rho_0 u_0 \frac{\partial v}{\partial x} = -\frac{\partial p}{\partial r} + \mu_1 \frac{\partial}{\partial r}\left[\frac{\partial u}{\partial x} + \frac{1}{r}\frac{\partial}{\partial r}(rv)\right] + \mu H_{n0}\left(\frac{\partial H}{\partial x} - \frac{\partial H_n}{\partial r}\right), \tag{17c}$$

$$\frac{\partial p}{\partial x} - a_0^2 \frac{\partial \rho}{\partial x} = 0, \quad a_0^2 = \gamma \frac{p_0}{\rho_0}, \tag{17d}$$

$$\eta\left[\frac{\partial H}{\partial x} - \frac{\partial H_n}{\partial r}\right] = u_0 H - H_{n0} v; \tag{17e}$$

in obtaining this last equation from (4) we must set $E_0 = 0$ in (16) to ensure that $\partial H/\partial x \to 0$ as $x \to -\infty$.

The six functions u, v, p, ρ, H_n, H must therefore satisfy equations (15) and (17). For reference we first determine the corresponding solution in the one-dimensional case, which is obtained by replacing all $\partial/\partial r$ terms by zero. The resulting homogeneous system is solved by setting all variables proportional to $e^{\lambda x}$, where either $\lambda = 0$ (which we exclude) or $H_n = 0$ and*

$$\lambda = \frac{\rho_0 u_0}{\mu_1}\left(1 - \frac{a_0^2}{u_0^2}\right) = \lambda_1 \quad \text{or} \quad \lambda = \frac{u_0}{\eta}\left(1 - \frac{\mu H_{n0}^2}{\rho_0 u_0^2}\right) = \lambda_2.$$

The complete (relevant) solution is

$$p = a_0^2 \rho = -\frac{\rho_0 a_0^2}{u_0} u, \quad v = \frac{\mu H_{n0}}{\rho_0 u_0} H, \quad H_n = 0,$$
$$u = A e^{\lambda_1 x}, \quad H = B e^{\lambda_2 x}, \tag{18}$$

where A and B are arbitrary constants. Each ratio $A:B$ determines a different disturbance of the initially uniform stream, the remaining scale factor corresponding to choice of the origin of x.

* At the point 1 in figures 4 and 5, λ_1 and λ_2 are both positive of course. At the point 3 they are both negative, confirming that the latter is approached as $x \to +\infty$.

We now set all variables proportional to $e^{\lambda x}$ in (15) and (17), denoting the factor in each case (a function of r) by the variable itself. Then from (15), (17a), (17d) and (17e) we find

$$\left.\begin{aligned} p = a_0^2\rho = -\frac{\rho_0 a_0^2}{u_0}\left[u+\frac{1}{\lambda}P\left\{-\frac{\eta}{\lambda H_{n0}}\frac{\partial}{\partial r}P+\frac{1}{H_{n0}}(u_0-\lambda\eta)\right\}H\right], \\ v = \left[-\frac{\eta}{\lambda H_{n0}}\frac{\partial}{\partial r}P+\frac{1}{H_{n0}}(u_0-\lambda\eta)\right]H, \quad H_n = -\frac{1}{\lambda}PH, \end{aligned}\right\} \tag{19}$$

where $P \equiv \dfrac{1}{r}\dfrac{\partial}{\partial r}r$ and from (17b), (17c) u, H must satisfy

$$A_1 u + \left(C_1 + D_1 P\frac{\partial}{\partial r}\right)PH = 0, \tag{20a}$$

$$A_2\frac{\partial u}{\partial r} + \left(B_2 + C_2\frac{\partial}{\partial r}P + D_2\frac{\partial}{\partial r}P\frac{\partial}{\partial r}P\right)H = 0, \tag{20b}$$

with

$$A_1 = \rho_0 u_0 - K, \quad C_1 = -\frac{KL}{\lambda H_{n0}}, \quad D_1 = \frac{\eta K}{\lambda^2 H_{n0}},$$

$$A_2 = -K, \quad B_2 = \frac{\lambda}{H_{n0}}(\rho_0 u_0 K - \mu H_{n0}^2), \quad C_2 = -\frac{1}{\lambda H_{n0}}[KL + \rho_0 u_0(u_0 - L) + \mu H_{n0}^2],$$

$$D_2 = \frac{\eta K}{\lambda^2 H_{n0}}, \quad K = \frac{\rho_0 a_0^2}{u_0} + \mu_1\lambda, \quad L = u_0 - \eta\lambda.$$

When $\lambda = \lambda_1$ the coefficient A_1 is zero and (20a) becomes

$$\left(C_1 + D_1 P\frac{\partial}{\partial r}\right)PH = P\left(C_1 + D_1\frac{\partial}{\partial r}P\right)H = 0,$$

so that

$$H = \frac{A}{r} + \mathscr{C}_1(mr), \quad m = \sqrt{\frac{C_1}{D_1}}, \tag{21}$$

where $\mathscr{C}_1$ is the general solution of Bessel's equation of order one, and A is an arbitrary constant. Pending further discussion, we take $\mathscr{C}_1 = 0$; then from (20b)

$$u = -\frac{B_2}{A_2}A\log r + B.$$

Similarly, for $\lambda = \lambda_2 : B_2 = 0$ and

$$H = Cr + \frac{D}{r}, \quad u = -\frac{2D_1}{A_1}C,$$

where C and D are arbitrary constants and zero has been taken as the solution of a Bessel equation.

The general disturbance is therefore given by (19) and

$$u = \left[-\frac{B_2}{A_2}A\log r + B\right]e^{\lambda_1 x} - \frac{2D_1}{A_1}C\,e^{\lambda_2 x},$$

$$H = \frac{A}{r}e^{\lambda_1 x} + \left[Cr + \frac{D}{r}\right]e^{\lambda_2 x}.$$

Thus for $r \to \infty$, (i) with $s = x + (\log r)/\lambda_2$ fixed, we find

$$u = 0, \quad H = C\,e^{\lambda_2 s};$$

(ii) with $C = 0$ and $s = x + (\log\log r)/\lambda_1$ fixed

$$u = -\frac{B_2}{A_2} A\, e^{\lambda_1 s}, \quad H = 0;$$

(iii) with $C = A = 0$ and $s = x$ fixed

$$u = B e^{\lambda_1 s}, \quad H = 0;$$

and, finally, (iv) with $C = A = B = 0$ and $s = x - (\log r)/\lambda_1$ fixed

$$u = 0, \quad H = D e^{\lambda_2 s}.$$

We conclude that the only one-dimensional disturbances which are the limits as $r \to \infty$ of axially symmetric ones are those corresponding to $A = 0$ or $B = 0$ in (18). This singles out what may be called the two principal solutions of (9) through the point 1 in figures 4 and 5, and it is clear that one of the principal solutions is the purely fluid-dynamical transition $H = 0$. The other may be ignored, at least for small enough η/μ_1.*

The reason for excluding the Bessel function in (21) is now clear. For large r, the corresponding solution would either oscillate, and hence not have a one-dimensional form, or else behave exponentially (small or large): $e^{\tau r}/r^{\frac{1}{2}}$, $\tau = \pm im$. For the latter we would have to take $s = x + \tau r - (\log r)/2\lambda_1$, which corresponds to a shock front at an oblique angle to the incident stream.

Final remarks

The lack of uniqueness found in §4 cannot be attributed to the unrealistic assumption $\mu_2 = 0$; without this assumption there is still an infinite number of integral curves in (U, V, h)-space joining the points 1 and 2 in figures 4 and 5, which are now a nodal and nodal-saddle point, respectively. Also the discussion in §5 need not be restricted in this way and the (three) principal solutions through 1 are again singled out.†

Moreover, the same results are obtained in the limit $\mu_1, \mu_2 \to 0$ as for our special case $\mu_2 = 0$, $\mu_1 \to 0$. For a limiting transition curve in (U, V, h)-space clearly follows the curve obtained by setting the right sides of the first three equations (8) equal to zero, except possibly for a segment lying in a plane $h =$ constant whose ends lie on this curve (cf. end of §3). At these ends the value of $V = -a + 2h_n h$ is the same, so that V is constant along the segment; otherwise dV/dx would have to change sign on transition curves at points outside the plane

$$V - 2h_n h + a = 0. \tag{22}$$

Thus in the limit $\mu_1, \mu_2 \to 0$ the transition curve lies in the plane (22) and follows the same path as for $\mu_1 \to 0$, $\mu_2 = 0$.

* Its slope at 1 is $dh^2/dU = [U_1(U_1 - 2h_n^2) - \frac{1}{2}(\gamma+1)\,\epsilon(U_1 - U_2)]/\epsilon[\gamma U_1 - 2(\gamma-1)\,h_n^2]$, where $\epsilon = m^2\eta/A\mu_1$. Thus for $\epsilon < 2U_1(U_1 - 2h_n^2)/(\gamma+1)\,(U_1 - U_2) = \epsilon_0$ the curve leaves 1 with positive slope and joins 1 to 2 below the U-axis (figures 4 and 5 were drawn for ϵ large); such a join must be rejected (h is imaginary). As ϵ increases past ϵ_0 we may expect the curve to continue to join 1 and 2, but now above the U-axis. It would then provide an alternative transition to $H \equiv 0$.

† And similarly at 2, where one of the solutions may be discarded since the point is approached as $x \to -\infty$.

The author is indebted to S. Goldstein for valuable discussion at each stage of the present investigation, and to M. Krook for his helpful interest. This research was supported in part by the United States Air Force under Contract AF 49(638)–154 monitored by the AF Office of Scientific Research of the Air Research and Development Command. Support from the Guggenheim Foundation is gratefully acknowledged.

REFERENCES

BURGERS, J. 1957 Penetration of a shock wave into a magnetic field. *Magnetohydrodynamics* (Ed. R. K. M. Landshoff), pp. 36–56, Stanford University Press.

FRIEDRICHS, K. O. 1957 Nonlinear wave motion in magnetohydrodynamics. *Los Alamos Rep.* no. 2105.

GILBARG, D. 1951 The existence and limit behavior of the one-dimensional shock layer. *Amer. J. Math.* **73**, 256–274.

GOLDSTEIN, S. 1957 Lectures on fluid mechanics. *Proc. Sem. Appl. Math.* (*A.M.S.*), *Boulder, Colorado.* New York: Interscience (in the Press).

MARSHALL, W. 1955 The structure of magneto-hydrodynamic shock waves. *Proc. Roy. Soc.* A, **233**, 367–376.

VON MISES, R. 1958 *Mathematical Theory of Compressible Fluid Flow* (completed by Hilda Geiringer and G. S. S. Ludford), pp. 436–442. New York: Academic.

An experimental investigation of the stability of Poiseuille flow

By RICHARD J. LEITE
University of Michigan, Ann Arbor, Michigan

(Received 23 April 1958)

An axially symmetric laminar flow of air was established in a long smooth pipe. This flow was steady up to Reynolds numbers of about 20,000, the capacity of the system. Small, nearly axially, symmetric disturbances were superimposed by longitudinally oscillating a thin sleeve adjacent to the inner wall of the pipe. Hot-wire anemometer measurements consisting of radial and longitudinal traverses were made downstream of the sleeve. These measurements indicated that within the Reynolds number range investigated (up to 13,000), the flow is stable to small disturbances. In general, the radial distribution of disturbance amplitudes was not independent of distance downstream; while the disturbances, as generated, exhibited imperfect axial symmetry, the non-symmetric part decayed more rapidly than the symmetric part. Results were interpreted in such a way that rates of propagation and rates of decay of the disturbances could be compared with those given by a recent theoretical stability analysis. It was found that the rates of decay are predicted fairly satisfactorily by the theory; however, the rates of propagation are not. In addition, it was found that transition to turbulent flow occurs whenever the amplitude of the disturbance exceeds a threshold value which decreases with increasing Reynolds number. Due to the departures from axial symmetry in the amplitude of the disturbance, it was not possible to obtain a quantitative measure of the threshold. A mathematical idealization of the disturbances, believed to be more akin to experimental perturbations than the classical model used in small-perturbation analyses, is proposed.

1. Introduction

The purpose of the experimental work reported here was to study the initial stability of Poiseuille flows. More precisely the intent was to determine the evolution in time of small controlled disturbances in the laminar velocity profile.

In the early work following Reynolds's investigations, it was observed (see, for instance, Prandtl & Tietjens 1934) that the Reynolds number of transition could be made to increase apparently without bounds if great attention was paid not to disturb the laminar flow upstream of the pipe. This indicated clearly that the initial state of the laminar flow bears on the transition process. While many experiments have contributed in other ways to an understanding of transition (see, in particular, Rotta (1956); and Webb & Harrington (1956)), no measurements have been reported on the manner in which a smooth laminar

regime amplifies or damps small residual disturbances which are unavoidably present in any flow.

On the other hand, small-disturbance stability theory has been applied several times to Poiseuille flow (e.g. Sexl 1927*a*, *b*; Pretsch 1941; Pekeris 1946). Neither the rigour nor the generality of these efforts have been universally granted. But all the analyses produced so far have concluded that axially symmetric Poiseuille flow is stable. A renewed interest in the theoretical aspects of the problem (Corcos 1952) led to the experimental work reported presently.

We might expect to learn from an experiment whether small disturbances are always damped or sometimes amplified in Poiseuille flows. Then we might wish to go beyond this purely qualitative consideration and describe the decay or amplification of a disturbance in time. To do this practically we should first classify our disturbances in some systematic way; for a disturbance is in general a three-dimentional vector function of x, y, z and t. It can be viewed more profitably as the synthesis of a large number of more elementary disturbances each of which can be characterized in time and space by a finite number of parameters. This is a point of view peculiar to small (i.e. linear) perturbation analysis which can be exploited both by theory and experiment. Unfortunately, what has been chosen traditionally as an elementary disturbance in the theoretical analysis of the problem is not what the experimenter would regard as simple. For Poiseuille flows, disturbances have been assumed to be axially symmetric (Sexl 1927*a*) and such that their stream function is given by

$$\Psi = \phi(r)\, e^{i\alpha(x-ct)}, \tag{1}$$

where α is real and c is complex.

Such a disturbance would have to be imposed at an initial instant everywhere in the pipe and, in particular, periodically in the axial direction—a requirement which was judged impracticable. The elementary disturbances generated in the pipe for the experiment reported presently were, of necessity, of a different kind. They were induced along a short length of the pipe wall and they were periodical in time. By traversing the pipe downstream of the disturbance generator in the radial and the axial direction and along different azimuths, it was possible to measure the amplitude distribution of the disturbances, and, by comparing the instantaneous signal at various points, to establish the phase relationship between neighbouring points. Thus, the space description of the disturbance at a given time was recorded, together with the frequency at which this pattern was sinusoidally varied in time.

A description of the experimental apparatus and procedure is given first. The results are then summarized and discussed. Some attention is paid to a comparison with the results of a recent analysis. Finally, a few observations are reported on the behaviour of larger periodic disturbances.

2. Experimentation

Apparatus

Experiments were conducted in a horizontal Lucite pipe, 1·25 in. in diameter and 73 ft. (700 diameters) long. Figure 1 is a schematic diagram of the equipment. High-pressure air (90 lb./in.^{2}) from the laboratory supply line was passed

through a separator to remove most of the oil and water present in the incoming air. From the separator, the air proceeded through an activated alumina dryer to a pressure-regulating valve which controlled the pressure in a 100 cu.ft. storage tank used as a constant pressure source for the air supply system. Air flowed from the tank through a flow meter to the settling chamber and thence through a smooth contraction into the pipe.

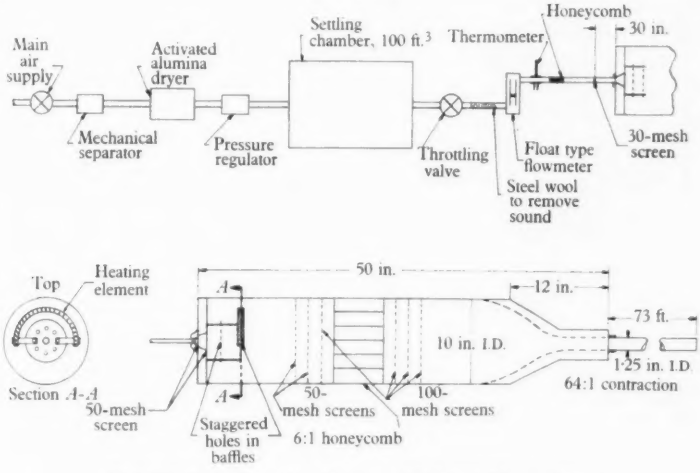

FIGURE 1. Schematic diagram of air supply system.

Uniformity of the internal diameter and concentricity of the pipe, as supplied by the manufacturer, were found to be within 0·005 in. for all sections of the pipe. The length of each section was approximately 50 in. To eliminate any adverse effects due to curvature along the length of the pipe, a theodolite was used to align and level the pipe. This method of alignment resulted in a system which departed at most only a few hundredths of an inch from true alignment over the entire length of the pipe.

The capacity of the laboratory air supply allowed operation at a maximum Reynolds number of approximately 20,000. No natural transition to turbulent flow was observed up to that Reynolds number. However, the supply pressure varied widely for the higher flow rates and therefore stability measurements were not attempted beyond a Reynolds number of 13,000.

All measurements were made with a hot-wire anemometer by conventional methods. In order to limit the size of the probe, only a U-meter was used. The wires were calibrated in a free jet. Figure 2 (plate 1) shows a typical hot-wire probe assembly used to make radial surveys inside the pipe. The hot-wire probe was accurately positioned in the radial direction by a micrometer gauge to which the probe was attached. The azimuth of the probe could be changed by merely rotating the entire probe assembly about the axis of the pipe. The hot-wire element itself was a platinum wire (Wollaston process) approximately 0·04 in. in length and 0·0002 in. in diameter. It could be placed at any radial position, relative to the wall of the pipe, with an accuracy of 0·003 in.

To take measurements at various axial positions while keeping a fixed radial distance from the wall, a probe was constructed which could be made to slide along the wall of the pipe. This probe is shown in the foreground of figure 2 and was called the 'bug'. By means of the 'bug', measurements of signal amplitudes and phase angles could be made as a function of distance along the pipe.

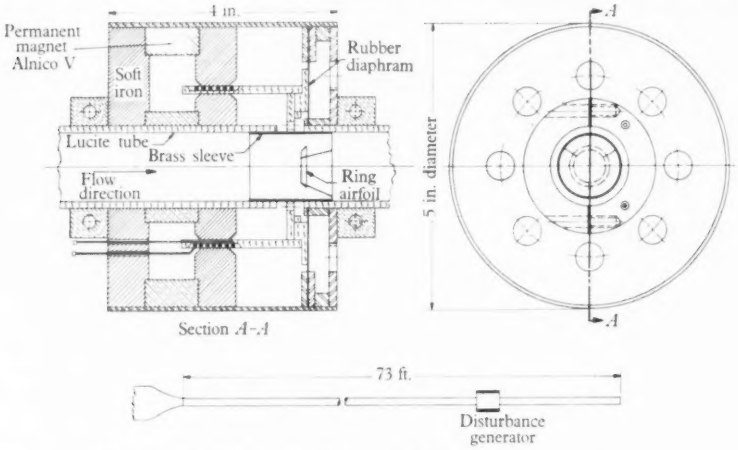

FIGURE 3. Schematic diagram of disturbance generator.

The disturbance generator was an electro-magnetic transducer which introduced velocity fluctuations of controllable amplitude and frequency into the flow within the pipe. Figure 3 is a schematic cross-section of the generator. The moving element was a thin (0·002 in.) cylindrical sleeve which lined the inner wall of the pipe over a length of 2 in. and was mounted concentrically to a coil located in a permanent magnetic field. An alternating current from a sinusoidal oscillator excited the coil and drove both coil and sleeve in longitudinal oscillations. The motion of the sleeve altered the boundary conditions at the wall and superimposed disturbance velocities upon the axially symmetric parabolic flow field.

Another means of generating axially symmetric disturbances, suitable for larger amplitudes, was to mount a ring airfoil within the cylindrical sleeve (see figure 3). The airfoil had a chord of 0·10 in. and a thickness of 0·003 in. The ring had a diameter of approximately 0·9 in. and was formed by truncating a cone having an apex angle of 6°.

Procedure

The laminar velocity profile of the undisturbed flow was checked before each series of disturbance measurements. Upon satisfactorily establishing that the mean flow was axially symmetric and parabolic, preliminary surveys were made to determine the range of disturbance frequencies which appeared least stable, i.e. those which decayed least with downstream distance. Then radial and longitudinal surveys of the disturbances were made downstream of the disturbance generator and at various azimuth angles.

A stationary hot-wire probe was used to observe any variation in the characteristics of the disturbance during each series of stability measurements. The ideal location for this probe would have been immediately downstream of the disturbance generator. However, since the wake of the probe would have greatly interfered with the disturbance, it was located instead in the test region diametrically opposite the test probe.

The hot wire was operated at a constant mean temperature. The mean square values of the disturbance amplitude were read on a millivoltmeter which was driven by a thermocouple attached to the output of the hot-wire voltage amplifier. Relative phase angles of the disturbance were determined as a function of radial and longitudinal separation distance by means of a dual beam cathode-ray oscilloscope. By applying the input voltage to the disturbance generator on one beam of the oscilloscope and the hot-wire signals on the other beam, relative phase angles of the disturbance velocities could be determined with an accuracy of approximately plus or minus five degrees.

Undisturbed pipe flow

(A) *The parabolic profile*

The velocity distribution of a steady laminar flow through a pipe, sufficiently far downstream of the entrance, is the well-known axially symmetric parabolic velocity profile of Poiseuille. When this profile was measured, deviation from axial symmetry was found throughout the pipe. The maximum velocity was not found to be on the geometric axis, the distribution being skewed as shown in figure 4. Radial surveys taken slightly downstream of the pipe inlet indicated that the asymmetry probably originated in the settling chamber; for the velocity of the core was not found to be uniform but slightly greater near the bottom of the pipe. Radial surveys of temperature and velocity were made within the settling chamber. However, the variation of these quantities was so minute that the results were inconclusive.

A systematic reorientation of the various components of the settling chamber and a modification of the settling chamber inlet failed to affect the pipe velocity profile. The conclusion was reached that the configuration of the settling chamber was not to blame and that the trouble was thermal rather than geometrical.

In order to combat distortions due to thermal effects, a heat source consisting of a nichrome wire wound on a curved glass tube, which spanned an arc of approximately 150°, was placed at the upstream end of the settling chamber (see figure 1). By varying the heating current supplied to this element, one could fix the location of the maximum in the velocity profile, far downstream, above or below the centreline; added current displaced the profile upwards. The average amount of heat added was approximately 10 W; assuming that half of the air passing through the settling chamber was heated uniformly, the total temperature rise would have been 2·3 °C at $R = 13{,}000$. The amount of heating current necessary was found to be an increasing function of the room temperature, which undoubtedly influenced the temperature of the air in the storage tank. It also depended somewhat on the Reynolds number.

Thereafter, this method of improving the velocity profile in the pipe was used. Prior to conducting stability measurements, velocity profiles were measured at the stations where the experiments were to be conducted, and the heating current was adjusted as required. Typical examples of velocity profiles with and without heat added are shown in figure 4.

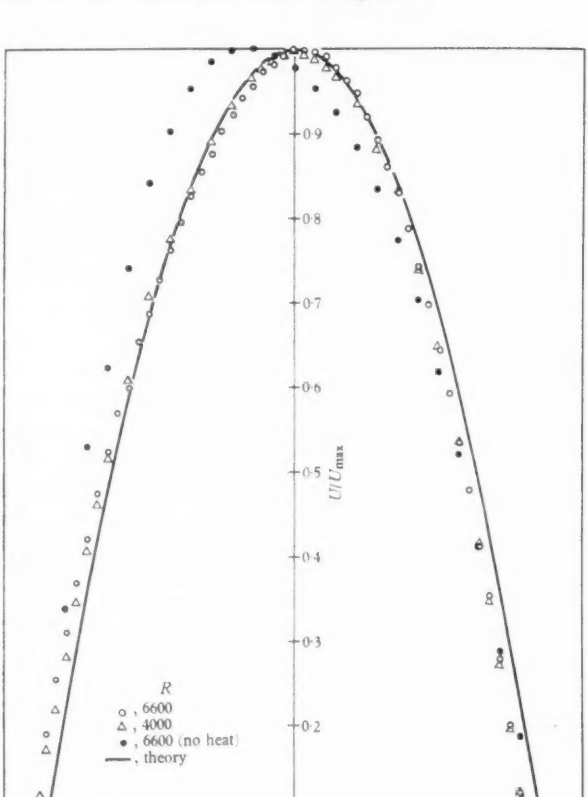

FIGURE 4. Mean velocity profiles, R = 4000 and 6600.

(B) *Residual unsteadiness*

Small residual disturbances were found to provide a noise background in the flow. The mean amplitude of their axial component u'/U was measured. It had a maximum value of approximately 10^{-4}. These disturbances were believed to be largely caused by radiated sound, because their amplitudes varied little across the pipe.

(C) *The entrance flow*

Some velocity profiles were obtained at several Reynolds numbers in the laminar transition region of the pipe, where the entrance flow evolves into a fully-developed parabolic profile. These profiles were compared with the calculated results of Boussinesq (1891). Satisfactory agreement existed at the lower Reynolds numbers; however, at higher Reynolds numbers, the formula gave values for the length of the pipe required for the development of a parabolic profile which seemed to be too large. For instance, at $R = 13{,}000$, the required length for a satisfactory profile was only 0·8 times the predicted length.

The small discrepancies found between experimental and theoretical profiles near the walls were believed to be due to the interference between the hot-wire probe and the boundary. Regardless of the source, however, the discrepancies did not appear large enough to influence the results significantly.

3. Results and discussion

The small disturbances introduced by the periodic motion of the sliding sleeve decayed as they travelled downstream for all the Reynolds numbers at which the measurements were taken (i.e. up to $R = 13{,}000$). Larger disturbances introduced by the motion of the ring airfoil did not decay at all Reynolds numbers. The part of the investigation, relating to the dynamics of these larger disturbances, is taken up separately later. Presently the behaviour of the small disturbances is discussed.

The data offered below covers a rather narrow band of frequencies. Preliminary tests indicated that frequencies above 45 c/s were damped so rapidly that accurate measurements could not be taken, while frequencies below 25 c/s caused difficulties related to the power requirements and to trace synchronization on the scope. Qualitative tests were made at frequencies ranging from 2 to 15 c/s. The disturbances at these frequencies always decayed as they proceeded downstream.

Axial symmetry

While axial symmetry was attempted both for the mean flow and for the disturbances, the disturbance amplitude recorded and shown in figure 5 is not independent of azimuth angle. This departure from axial symmetry could be caused by a number of factors such as small deviations of the fully developed flow from axial symmetry, small leaks around the disturbance generator allowing the generator to pump when in motion, and imperfections in the shape of the sleeve.

While departures from axial symmetry somewhat complicated the measurements, they lent greater generality to the results. In particular, it appears from figure 5 that the disturbances become more, or at least no less, axially symmetric as they proceed downstream. Thus, if one considers the perturbations to be the sum of an axially symmetric and a non-axially symmetric part, it appears that the latter decays at a faster rate than the former, as it proceeds downstream,

so that at least for the kind of disturbance tested the assumption of axial symmetry (as it is used in theoretical treatments of the problem) is not unreasonably restrictive.

General features of the disturbances

The peripheral surveys, which were used to determine the degree of axial symmetry of the disturbances, appeared to indicate that the disturbances possessed the same general character, as a function of azimuth angle, at each streamwise station. This fact supported previous measurements which indicated the absence of swirl in the pipe.

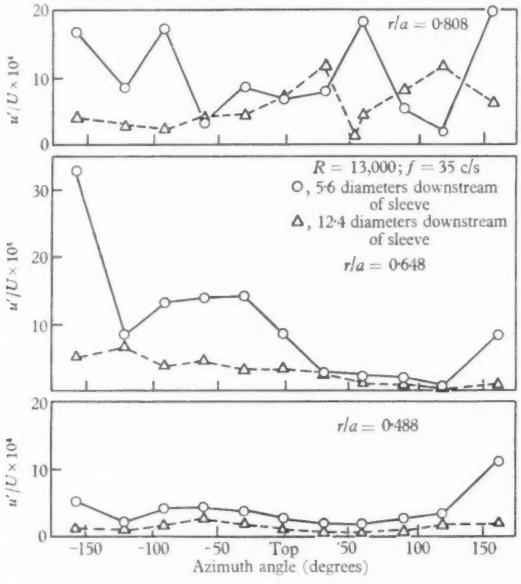

FIGURE 5. Peripheral distribution of amplitude of disturbances, $R = 13{,}000$.

Typical radial distributions of disturbance amplitude are given in figures 6 and 7. These disturbances seem to have, on the whole, the same shape except near the wall where a second amplitude peak occurs in some cases.

Inspection of the r.m.s. amplitude curve reveals that the u' component of the disturbance velocity approaches zero not only at $r = a$ (as is required by the no-slip condition at the wall) but also at $r = 0$. There seems to be no *a priori* reason to expect this result.

The amplitude curves also indicate that the amplitude of u' is a somewhat different function of r for different downstream distances. In general, the peak amplitude moves inwards as the disturbance propagates downstream. Figure 7 shows that the peak amplitude approaches an equilibrium position, but it is doubtful that similarity is really achieved before the disturbance is dissipated.

Radial variation of phase angle is given for several downstream distances in figures 8 and 9. The reference signal was measured at a different downstream station for each radial survey because of mutual interference of the two probes, hence, direct comparison between phase angles, at fixed radii for different stations, could not be made. However, 'bug' measurements, together with the driving voltage supplied to the disturbance generator, were used to establish

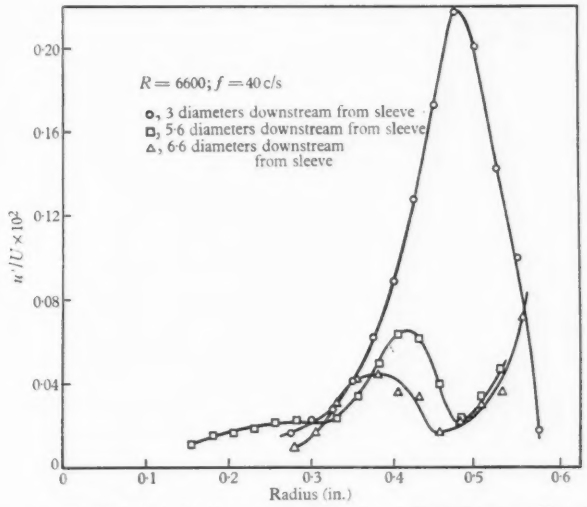

FIGURE 6. Radial distributions of amplitude of disturbances, $R = 6600$.

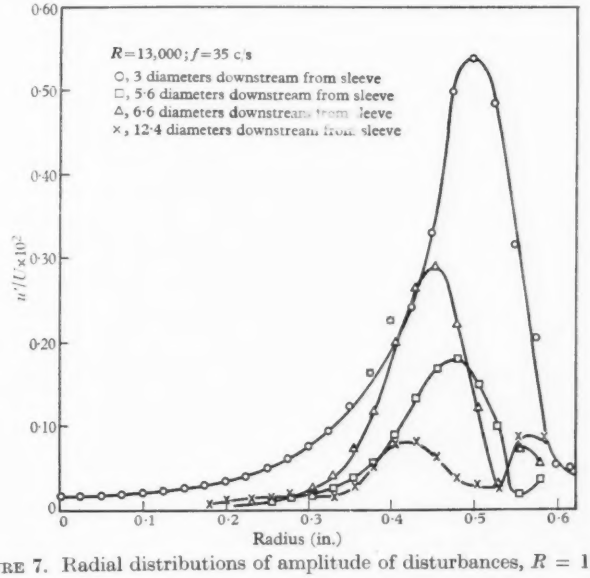

FIGURE 7. Radial distributions of amplitude of disturbances, $R = 13{,}000$.

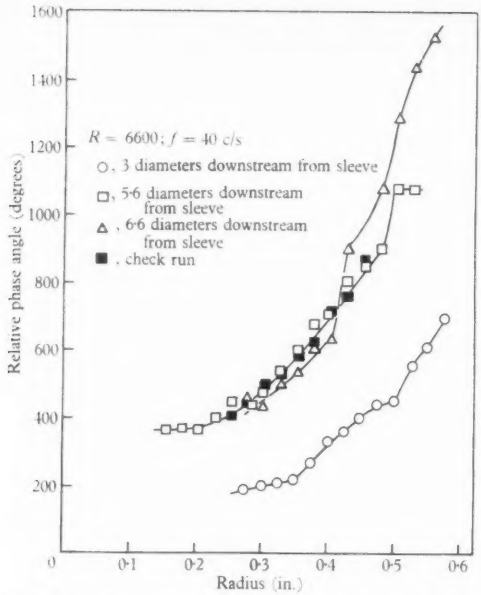

FIGURE 8. Radial distributions of phase angles of disturbances, R = 6600.

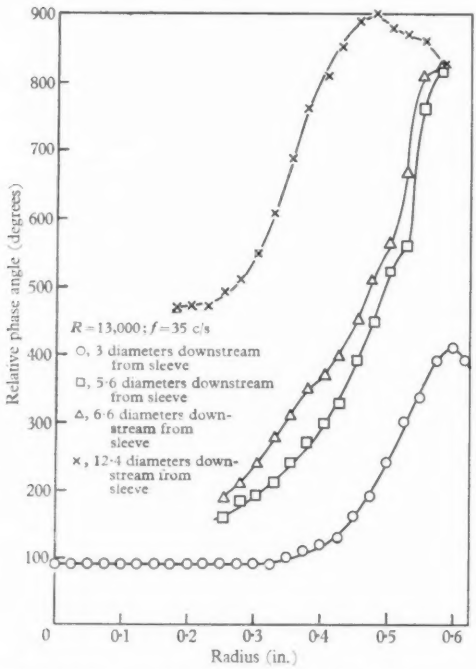

FIGURE 9. Radial distributions of phase angles of disturbances R = 13,000.

longitudinal phase distributions of the reference probe at fixed radial positions. Therefore, by adjusting the radial-survey phase measurements, in such a manner that they corresponded with the 'bug' measurements, at prescribed radii, the actual radial phase distribution at each station was recorded. Typical results are shown in figures 8 and 9. From these curves, it appears that there is an inward convection of the disturbances, and that at least in first approximation the convection velocity depends little upon r and therefore little on the local stream velocity.

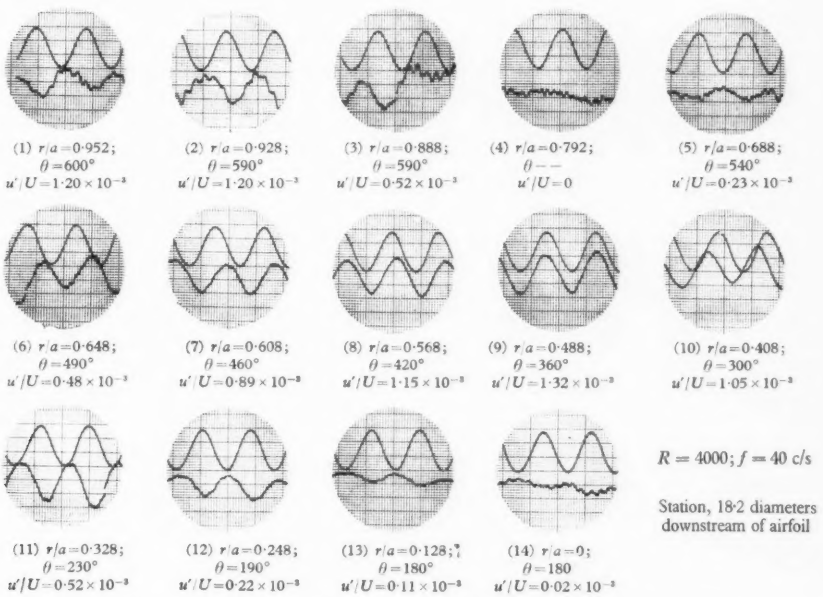

FIGURE 10. Radial distribution of disturbances (pictorial), $R = 4000$.

Several of the curves (see figures 6 and 8, 7 and 9) show a rather abrupt phase shift of approximately 180°. The corresponding amplitude curves reveal that a velocity minimum occurs at the same radial position. A torroidal vortex would betray its presence in just such a way. It would, however, exhibit no phase shift except at its centre where the amplitude is nil. In our case, the disturbance is somewhat more complex. It appears first near the wall and then propagates radially inwards.

Figure 10 reproduces the traces which appeared on the dual-beam cathode-ray oscilloscope during a typical radial survey. The top trace represents the driving voltage supplied to the disturbance generator. This signal provided a common reference for all phase-angle measurements. The time scale runs left to right. The relative amplitude of the disturbance is indicated at each radial position. These pictures illustrate that the signal phase lags as r decreases, and they give an example of a null occurring at $r/a = 0{\cdot}792$, together with a phase shift of approximately 180°.

Longitudinal surveys yielded rates of decay of the amplitude with x. These measurements, made with the 'bug', were quite sensitive to small orientation errors of the probe and great care had to attend them. Figure 11 shows, on the assumption that the decay in x is exponential, that there are two distinct rates of decay. The first one is believed to be associated with the radial redistribution of the disturbance amplitude and the second one with the characteristics of reasonably general disturbance profiles.

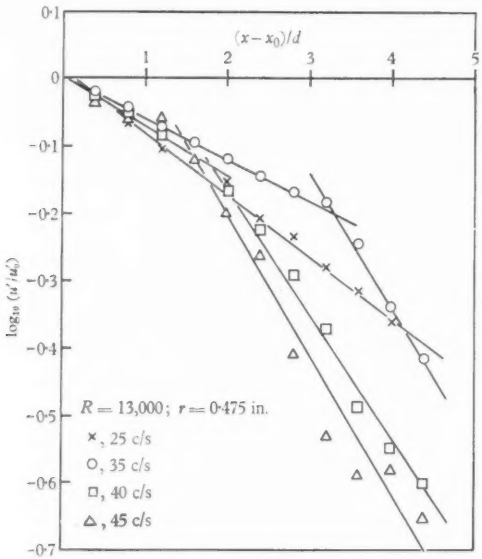

FIGURE 11. Decay of u-component of disturbances, $R = 13{,}000$.

The comparison of the phase angles of the signal, at various x-wide stations, with that of a reference signal at a fixed but arbitrary position (figure 12) supports the view that the disturbances are convected downstream at a rate which is independent of x.

An idealization of the experimental disturbances

In the Introduction it was noted that the disturbances generated for the experiment reported presently were unavoidably different from the elementary disturbances assumed in the linear perturbation theory. It can be seen from figures 6 and 7 that in the experiment the disturbance amplitude is far from homogeneous in the x-direction. Since, in fact, the disturbance amplitude decays largely in one wavelength, it is natural to suspect that an x-wise homogeneous representation might be seriously unrealistic. We have seen that, in view of the data, the assumptions of axial symmetry and of constant convective speed were not too restrictive. In addition, if one neglects the initial radial readjustment of disturbances, the assumption of radial similarity would seem

tolerable. In view of these facts a first-order description of the experimental disturbances generated in the present experiment might be

$$\Psi = \phi(r)\, e^{-\nu x + i\omega t},$$

where ν is complex and ω is real. This is the stream function of a disturbance periodic as well as exponential in x and periodic in t. It is clear that such disturbances lend themselves to small perturbation analysis, since they were formally

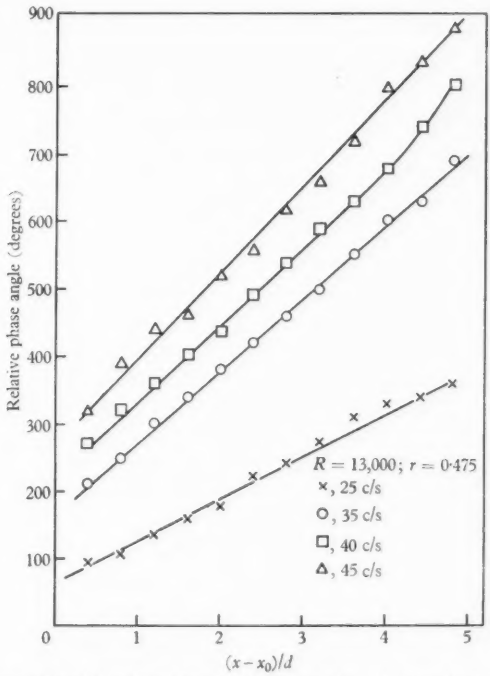

FIGURE 12. Longitudinal distributions of phase angles of disturbances, $R = 13{,}000$.

identical to the disturbances which satisfy the Orr–Sommerfeld equation (or rather the corresponding equations for fully developed pipe flow). The analysis would define the dependence of the real and imaginary part of ν (the x-rate of decay and the wavelength, respectively) on the frequency ω and the Reynolds number. Such quantities would be more directly comparable to those measured here. However, it was thought of interest to attempt a comparison of the present results with those of the recent theoretical analysis due to Corcos & Sellars (1959). In particular, in view of the fact that the disturbances are convected downstream at a uniform rate, it is possible to compare the measured convection-speeds with those of the theory. In addition, one may consider the rates of decay in x as time rates of decay for an observer travelling with the disturbances. Accordingly, the values of the damping factor c_i were obtained from the slopes of curves similar to those shown on figure 11.

From equation (1), the streamwise component of the velocity can be written

$$u = -\frac{\phi'(r)}{r} e^{\alpha c_i t} e^{i\alpha(x-c_r t)}. \tag{2}$$

Here c has been written $c = c_r + ic_i$.

The change in amplitude with respect to time can be expressed, using (2), as

$$\frac{u_2}{u_1} = \exp\left\{\int_{t_1}^{t_2} \alpha c_i \, dt\right\}. \tag{3}$$

In figure 11, x_0 corresponds to a station 3·6 diameters downstream from the sleeve. The r.m.s. amplitude of the disturbance velocity is u_0' at x_0 and u' at stations downstream of x_0.

Writing (3) in terms of the measured quantities, we get

$$\frac{u'}{u_0'} = \exp\left\{\int_{t(x_0)}^{t(x)} \alpha c_i \, dt\right\}$$

or

$$2{\cdot}3 \log_{10} \frac{u'}{u_0'} = \int_{t(x_0)}^{t(x)} \alpha c_i \, dt.$$

Differentiating with respect to t and using the relation $dx/dt = c_r$, this equation then becomes

$$c_i = \frac{2{\cdot}3 c_r}{\alpha} \frac{d}{dx}\left(\log_{10} \frac{u'}{u_0'}\right), \tag{4}$$

where $\alpha = 2\pi a/\lambda$. The non-dimensional wave velocities c_r were determined from curves similar to those shown in figure 12. The longitudinal distance the 'bug' had to be displaced to observe a 360° phase shift was called the wavelength λ of the disturbance. Then, by definition,

$$c_r = \frac{\lambda f}{U_{\max}}, \tag{5}$$

where f is the frequency of the disturbance and $U_{\max}$ is the maximum undisturbed stream velocity. Figure 13 compares both c_r and c_i with the values given by the theory of Corcos & Sellars (1959). The values of the propagation velocity c_r, which were deduced from the present measurements, are seen to be generally higher than those predicted by the theory for streamwise-homogeneous disturbances. On the other hand, the values of the damping factor given by the experiment agree rather well with the predictions of the theory. A fair amount of scatter appears in the measurements, in part because radial phase differences are large and a small amount of radial convection or readjustment introduces fairly large errors in apparent axial phase shift.

Ring airfoil: larger disturbances and transition

It has been shown above that small disturbances decayed at all Reynolds numbers investigated. Upon introducing the ring airfoil, disturbance amplitudes were increased appreciably and the stability characteristics of the flow changed markedly. At low Reynolds numbers comparison with theory is no longer possible and at higher Reynolds numbers the wake from the ring airfoil, when held stationary, was sufficient to cause transition to turbulent flow.

Results of measurements at a Reynolds number of 4000 are shown in figure 13. These results indicate that the larger disturbances propagate at a greater speed and decay more slowly than those generated by the sleeve and they stand far from results of the theory. Tests made at $R = 8000$ showed that transition was induced when the airfoil was oscillated with the smallest possible amplitude. At $R = 12{,}000$, with the airfoil held stationary, the induced disturbances were amplified, as they propagated downstream, with transition to fully turbulent flow finally resulting. A detailed description of this phase of the work was presented by Kuethe (1956).

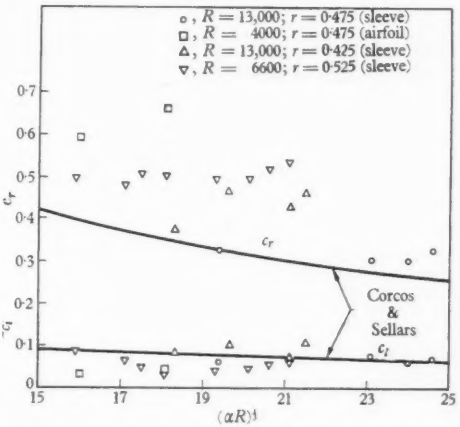

FIGURE 13. Comparison of experimental results with theoretical predictions; c_r and $-c_i$ *vs* $(\alpha R)^{\frac{1}{2}}$.

5. Conclusions

The following conclusions can be drawn from the present investigation.

1. Axially symmetric Poiseuille flow was found to damp the small disturbances introduced, whether they be axially symmetric or not, up to a Reynolds number of 13,000.

2. Experimental values of rate of decay were found to agree satisfactorily with those given by a recent theoretical analysis, even though assumptions of axial symmetry and longitudinal homogeneity of the disturbance are assumed in the latter.

3. To a first approximation, the propagation velocity of the disturbance does not depend upon radial position, hence upon local stream velocity, and is independent of distance downstream.

4. It has been found that small disturbances decay at all Reynolds numbers investigated and that large disturbances are unstable. Therefore, for fixed Reynolds numbers some disturbance of intermediate amplitude must be marginally stable.

The author is greatly indebted to Prof. Arnold M. Kuethe and Dr John R. Sellars for their advice, guidance and constructive criticism during the entire course of this work and to Dr Gilles M. Corcos for his helpful suggestions during

the preparation of the manuscript. This paper is based upon a dissertation submitted by the author to the University of Michigan in partial fulfilment of the requirements for the degree of Doctor of Philosophy. The work was sponsored, under the supervision of Prof. Kuethe, by the United States Air Force, through the Office of Scientific Research of the Air Research and Development Command under Contract No. AF 18(600)-350.

REFERENCES

Boussinesq, J. 1891 *C.R. Acad. Sci., Paris*, **113**, 9 & 49.

Corcos, G. M. 1952 *On the Stability of Poiseuille Flows.* Ph.D. Thesis, University of Michigan.

Corcos, G. M. & Sellars, J. R. 1959 *J. Fluid Mech.* **5**, 97.

Kuethe, A. M. 1956 *J. Aero. Sci.* **23**, 446.

Pekeris, C. L. 1946 *Proc. Nat. Acad. Sci., Wash.*, **34**, 285.

Prandtl, L. & Tietjens, O. G. 1934 *Applied Hydro and Aero Mechanics.* New York: McGraw-Hill.

Pretsch, J. 1941 *Z. angew. Math. Mech.* **21**, 204.

Rotta, J. 1956 *Ing.-Archiv.* **24**, 4, 258.

Sexl, Th. 1927*a* *Ann. Phys., Lpz.*, **83**, 835.

Sexl, Th. 1927*b* *Ann. Phys., Lpz.*, **84**, 807.

Webb, W. H. & Harrington, R. P. 1956 *J. Aero. Sci.* **23**, 792.

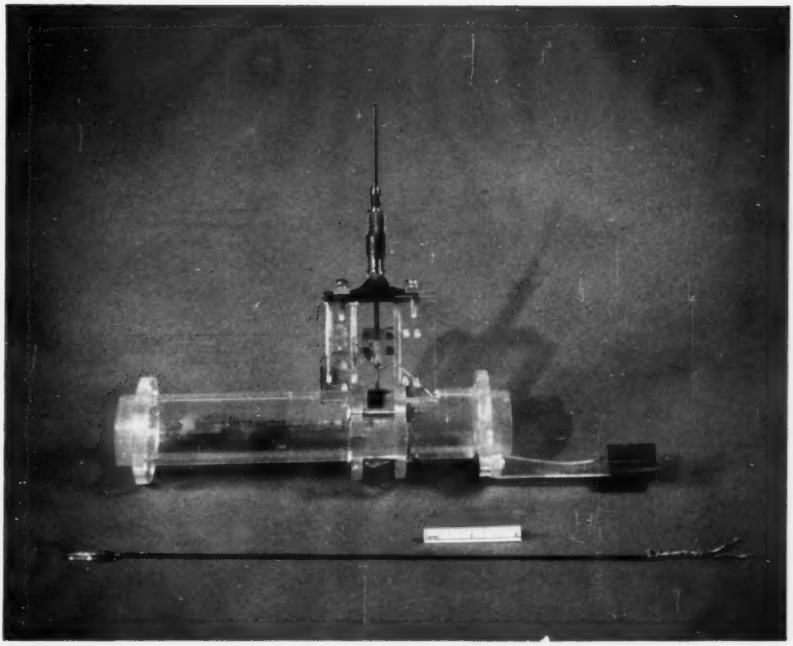

FIGURE 2 (plate 1). Photograph of hot-wire probe and 'bug'.

On the stability of fully developed flow in a pipe

By GILLES M. CORCOS AND JOHN R. SELLARS

The University of California and The Ramo-Wooldridge Corporation

(Received 23 April 1958)

The stability of infinitesimal axially symmetric disturbances in fully developed pipe flow is examined anew. The classical eigenvalue problem is treated in part by asymptotic methods and leads to an algebraic relation between the eigenvalue c, the disturbance wavelength $2\pi/\alpha$, and the Reynolds number. Examination of the limiting cases of this relation reveals the existence of two families of characteristic numbers, the value of which tends to unity and to zero as the Reynolds number increases without bounds. For the latter, a more accurate solution is required and given. It is found that all eigenvalues yield stable solutions and that for a given wave number and Reynolds number only a finite number of eigenvalues exists.

The limitations of the analysis are discussed in the light of a recent experimental study of the same problem.

1. Introduction

It is generally believed that fully developed flow in a pipe is stable at any Reynolds number when it is excited by infinitesimally small axially symmetric disturbances. While several authors have considered this problem, the proof of stability offered by Sexl (1927, 1928) has served as a standard reference. A recent investigation by Pekeris (1948*a*) points out that certain *a priori* assumptions about the nature of the stability criteria (the eigenvalues) damaged the rigour of Sexl's proof. The same paper gave an independent demonstration of stability. It has been shown that Sexl's work may be criticized on other grounds as well (Corcos 1952), and the present paper shows that Pekeris' work is incomplete in the sense that he only investigated one class or family of modes while two distinct classes of modes can be found. These two sets of modes are very similar to those found by Pekeris (1948*b*) in connexion with two-dimensional Poiseuille flows. In the latter problem, one of the sets is always stable while the other contributes the unstable perturbations at some Reynolds numbers. In our case, as the following development will undertake to show, both sets are stable or positively damped.

Nevertheless, the second set of modes deserves to be studied because it generates the least stable disturbances, because it is germane to the unstable set of the two-dimensional problem, and because it corresponds rather well with a set of modes which is observed experimentally (Leite 1959).

In the following, the eigenvalues corresponding to any mode are given as functions of Reynolds number and wavelength, and it is shown that the number of modes present (i.e. the number of eigenvalues) is finite and depends for a given wavelength of the disturbances upon the Reynolds number.

2. The formulation of the problem

Let the mean flow be an axially symmetric pipe flow, and let the disturbances be axially symmetric and periodic in the direction of flow, i.e. the stream function has a perturbation of the form

$$\psi(x, r, t) = \phi(r)\, e^{i\alpha(x-ct)}.$$

Then the appropriate differential equation for the eigen function $\phi(r)$ (Sexl 1927) is

$$(W-c)\left(\phi'' - \frac{\phi'}{r} - \alpha^2\phi\right) + \phi\left(\frac{W'}{r} - W''\right) = -\frac{i}{\alpha R}\left[\phi^{\mathrm{iv}} - \frac{2}{r}\phi''' + \frac{3}{r^2}\phi'' - \frac{3}{r^3}\phi' - 2\alpha^2\left(\phi'' - \frac{\phi'}{r}\right) + \alpha^4\phi\right]. \tag{2.1}$$

Here $c = c_r + ic_i$ is the eigenvalue, α is the wave-number of the disturbance, $W = W(r)$ is the non-dimensional main stream velocity profile, and $R =$ (centre velocity) (radius of pipe)/(kinematic viscosity) is the Reynolds number of the flow. Primes indicate differentiation with respect to r. The boundary conditions at the origin (centre of the pipe) require that the disturbance be axially symmetric and bounded, i.e.

$$\lim_{r\to 0}\frac{\phi}{r} = 0 \quad \text{and} \quad \lim_{r\to 0}\frac{\phi'}{r} \quad \text{is bounded.} \tag{2.2a}$$

On the walls, the kinematic and no-slip conditions are equivalent to

$$\phi(1) = \phi'(1) = 0. \tag{2.2b}$$

A stable disturbance is characterized by $c_i < 0$, a neutral disturbance by $c_i = 0$, and an unstable disturbance by $c_i > 0$.

In general, the differential equation (2.1) will have four linearly independent solutions. The method of approach adopted herein will enable us to eliminate immediately those solutions which are not sufficiently regular near the origin. The remaining two solutions we will denote by ϕ_i and ϕ_a. Then the appropriate solution may be written as a linear combination of ϕ_i and ϕ_a

$$\phi = C_1\phi_i + C_2\phi_a. \tag{2.3}$$

Applying the boundary conditions (2.2), we will obtain two homogeneous equations for the constants C_1 and C_2. In order for a non-trivial solution to exist, the determinant of the coefficients C_1 and C_2 must vanish. We thus obtain

$$F(\alpha, \alpha R, c) = \begin{vmatrix} \phi_i(1) & \phi_a(1) \\ \phi_i'(1) & \phi_a'(1) \end{vmatrix} = 0. \tag{2.4}$$

This equation gives the functional dependence of c on α and αR and thus indicates for what Reynolds number, if any, disturbances will grow in time.

3. The determination of the 'inviscid' solutions

For Poiseuille flow, $W(r) = 1-r^2$, and the differential equation (2.1) may be written conveniently as

$$f''-\frac{1}{r}f'-\alpha^2 f-i\alpha R(1-r^2-c)f=0, \tag{3.1}$$

where

$$\phi''-\frac{\phi'}{r}-\alpha^2\phi=f. \tag{3.2}$$

This form has been previously utilized by both Sexl and Pekeris.

Clearly $f=0$ is a solution of (3.1); substituting in (3.2) we obtain ϕ in terms of Bessel functions of order unity, of the first and of the second kind, i.e.

$$\phi_1 = rJ_1(i\alpha r), \quad \phi_2 = rY_1(i\alpha r). \tag{3.3}$$

These are two linearly independent exact solutions of (2.1), and they are usually referred to as the inviscid solutions, since they are solutions of the perturbation equation for $R=\infty$. The second solution ϕ_2 is rejected immediately in conformity with the boundary conditions at the origin, and thus we obtain

$$\phi_i = rJ_1(i\alpha r). \tag{3.4}$$

4. The determination of the second independent solution

Equation (2.1) has power series solutions which are convergent throughout the interval $0 \leqslant r \leqslant 1$. However, these solutions converge very slowly because positive powers of αR (a large number) occur as coefficients in the series. This type of expansion is therefore of little use to us for an explicit solution. Instead, we resort to an asymptotic development due to Heisenberg. We look for a solution of the form

$$\phi = e^g, \tag{4.1}$$

and we assume that for large enough values of αR we can express g by the asymptotic series

$$g = (\alpha R)^n g_0 + g_1 + (\alpha R)^{-n} g_2 + \ldots. \tag{4.2}$$

Substituting (4.1) and (4.2) in (2.1) and equating coefficients of equal powers of αR, we find that

$$n=\tfrac{1}{2}; \quad g_0 = \pm\int_{r_0}^{r}\sqrt{\{i(W-c)\}}\,dr; \quad g_1 = \log\frac{r^{\frac{1}{2}}}{(W-c)^{\frac{1}{4}}}.$$

Making use of the first and second approximations only, we write

$$\phi_a = r^{\frac{1}{2}}(W-c)^{-\frac{1}{4}}[A\chi_+(r_0,r)+B\chi_-(r_0,r)], \tag{4.3}$$

where

$$\chi_+(a,b) = \exp\left\{+\int_a^b\sqrt{\{i\alpha R(W-c)\}}\,dr\right\},$$

$$\chi_-(a,b) = \exp\left\{-\int_a^b\sqrt{\{i\alpha R(W-c)\}}\,dr\right\},$$

and where the ratio A/B will now be determined around the origin by comparing ϕ_a with a regular (viscous) solution valid in the neighbourhood of $r = 0$.

We note that $i\alpha R(1-r^2-c) \doteq i\alpha R(1-c)$ for small values of r. Making this approximation in (3.1), and neglecting α^2 compared to αR, we can write the solution of (3.1) directly in terms of Bessel functions of order one. Thus

$$f = hrJ_1(i\gamma r) + lrY_1(i\gamma r), \tag{4.4}$$

where $\gamma = \{i\alpha R(1-c)\}^{\frac{1}{2}}$ and h and l are constants. From (3.2), this gives directly

$$\phi_a = h_1 rJ_1(i\gamma r) + l_1 rY(i\gamma r) \tag{4.5}$$

provided $\gamma \neq \alpha$, which will always be true in any of the cases of interest.

The boundary conditions at the origin require that l_1 be zero, and thus ϕ_a must be represented near the origin by

$$\phi_a = h_1 rJ_1(i\gamma r). \tag{4.6}$$

Even though this representation is restricted to small values of r, if αR is sufficiently large, we may make γr large enough to use the asymptotic form of the above Bessel function. Then we have

$$\phi_a = h_2 r^{\frac{1}{2}}[\exp\{-\langle i\alpha R(1-c)\rangle^{\frac{1}{2}} r + \tfrac{3}{4}\pi i\} + \exp\{+\langle i\alpha R(1-c)\rangle^{\frac{1}{2}} - \tfrac{3}{4}\pi i\}], \tag{4.7}$$

provided $$-\pi < \arg i\{i\alpha R(1-c)\}^{\frac{1}{2}} < 2\pi.$$

On the other hand, if $r_0 = 0$, (3.3) becomes for very small r (bounded from zero)

$$\phi_a = r^{\frac{1}{2}}(1-c)^{-\frac{1}{4}}[A_0 \exp\{+\langle i\alpha R(1-c)\rangle^{\frac{1}{2}} r\} + B\exp\{-\langle i\alpha R(1-c)\rangle^{\frac{1}{2}} r\}], \tag{4.8}$$

where the notation A_0 and B_0 is intended to indicate that r_0 in (4.3) is taken as zero. A comparison of (4.8) and (4.7) gives

$$\frac{A_0}{B_0} = i. \tag{4.9}$$

The ratio A/B has now been evaluated so that ϕ_a corresponds to the solution with the proper behaviour near the origin, but we must impose certain restrictions upon the use of (4.3) with (4.9). First, it is clear that (4.3), an asymptotic approximation for large αR, fails at $r = 0$; although it is valid (in the sense of being a good approximation) arbitrarily close to $r = 0$ for sufficiently large αR. This point will be dealt with later. Then since (4.3) contains a singularity for $W = c$, which is a regular point of the differential equation (2.1), the asymptotic representation fails there also. Finally, we should not expect the ratio A/B as found in (4.9) to remain the same for the whole interval, particularly in the neighbourhood of the singularity $W = c$. The reason can be set forth as follows. Our asymptotic representation must be single-valued if it is to approximate an exact solution of (2.1). On the other hand, the functions χ_+ and χ_- have branch cuts and are multi-valued functions of the complex argument r.

Thus a single linear combination of χ_+ and χ_- would yield a non-unique solution. On the other hand, it is possible to chose the coefficients of χ_+ and χ_- corresponding to various parts of the complex r plane in such a manner as to

satisfy the two requirements that we must place upon the solution: (*a*) that it be unique; (*b*) that it be continuous, or at least that discontinuities in the solution be of the order of the errors made by an asymptotic approximation.

The question is examined in detail in the Appendix. The need to modify the linear combinations of asymptotic solutions here and there (in our case on three discrete lines) was first described by Stokes, and the lines on which solutions are connected to each other are termed the Stokes lines.

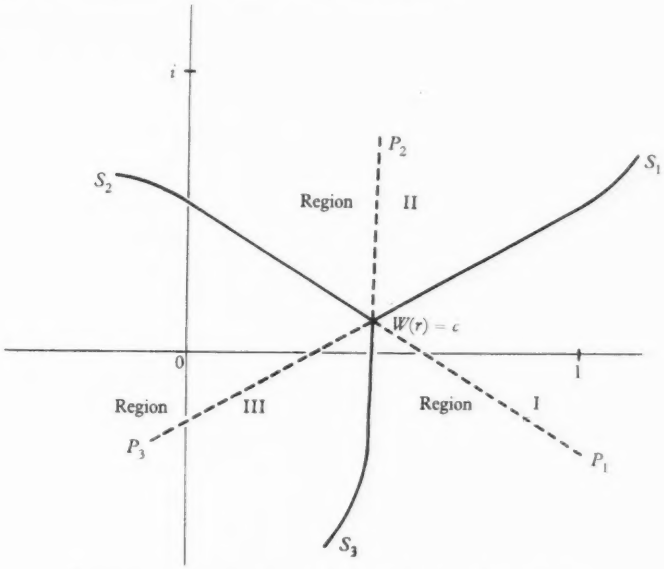

FIGURE 1. The complex r-plane and the Stokes regions.

The Appendix shows that Stokes lines originate at the complex value of r for which $W = c$, that they divide the complex r plane into three regions (figure 1), and that we should expect $r = 0$ to be in Region III and $r = 1$ to be in Region I. Furthermore, the connexion formulae taken together with (4.9) yield

$$\frac{A_1}{B_1} = i[1 - e^Q], \tag{4.10}$$

where

$$Q = 2\int_k^0 \sqrt{\{i\alpha R(W-c)\}}\, dr = e^{\frac{3}{4}\pi i}(\alpha R)^{\frac{1}{2}}\, \tfrac{1}{2}\pi k^2, \tag{4.11}$$

with

$$k^2 = 1 - c.$$

5. The eigenvalue equation

Henceforth in evaluating integrals of the type

$$\int_k^1 \sqrt{\{i\alpha R(W-c)\}}\, dr \quad \text{and} \quad \int_k^0 \sqrt{\{i\alpha R(W-c)\}}\, dr,$$

we shall choose our arguments in conformity with the convention adopted when we defined the Stokes regions (see Appendix). Proceeding with this in mind, we

may write the determinant (2.4) explicitly. We thus obtain an algebraic eigenvalue equation. Simplifying a little, we get

$$(1-e^{Q})e^{P} = -i\left[\frac{e^{-\frac{1}{4}\pi i}\sqrt{(\alpha Rc)} + \dfrac{[d/dr\{rJ_1(i\alpha r)\}]_{r=1}}{J_1(i\alpha)} + \dfrac{5}{2c} - \dfrac{1}{2}}{e^{-\frac{1}{4}\pi i}\sqrt{(\alpha Rc)} - \dfrac{d/dr\{rJ_1(i\alpha r)\}_{r=1}}{J_1(i\alpha)} - \dfrac{5}{2c} + \dfrac{1}{2}}\right], \tag{5.1}$$

where $$P = \int_k^1 \sqrt{\{i\alpha R(W-c)\}}\,dr = e^{-\frac{1}{4}\pi i}\sqrt{(\alpha R)}\left[c^{\frac{1}{2}} - k^2 \log\frac{1+c^{\frac{1}{2}}}{k}\right],$$

and where we have taken

$$-\pi < \arg(c) \leqslant \pi \quad \text{and} \quad -\pi < \arg k \leqslant \pi.$$

The solution of (5.1) will determine c as a function of α and of αR.

Equation (5.1) has to be solved by trial and error for any value of α and αR, and a representative tabulation would be very time consuming. However, the important conclusions can be drawn without resorting to extensive numerical work. It is sufficient to note the general behaviour of the eigenvalues and to develop formulae for the interesting limiting cases.

We shall successively assume that c is non-vanishing as $\alpha R \to \infty$ and that $c \to 0$ as $\alpha R \to \infty$, and we shall thus get two different limiting representations for the eigenvalues. These representations we shall call families of eigenvalues.

6. The first limiting form

Let us first assume that c is non-vanishing as $\alpha R \to \infty$. Then for large αR the right-hand side of (5.3) is approximately $-i$, while the term $\exp(P)$ grows very large. Thus the term $(1-e^{Q})$ must be very nearly zero. We have for this case

$$\begin{aligned} e^{Q} &= 1, \\ Q &= -2\pi N i, \\ c &= 1 + \frac{4N}{(\alpha R)^{\frac{1}{2}}}\,e^{-\frac{1}{4}(3\pi i)} \quad (N = 1, 2, 3 \ldots). \end{aligned} \tag{6.1}$$

It is seen that all values of c given by (6.1) correspond to damped disturbances. We have taken only positive values of N in (6.1) because negative values would give values of c which are inconsistent with our connexion formulae.

The family of eigenvalues given by (6.1) requires that $c \to 1$ as $\alpha R \to \infty$. As a consequence, the Stokes point approaches the boundary $r = 0$ for increasing values of αR and the following question should be raised. Is the matching of our asymptotic solutions with Bessel functions in the neighbourhood of the origin legitimate? In the neighbourhood of the origin the argument of the Bessel functions used is $i\{i\alpha R(1-c)\}^{\frac{1}{2}}r$. The question is whether there is in Region III a neighbourhood of $r = 0$ for which the argument is large enough to justify the use of asymptotic expansions. Substituting for c from (6.1), we get for the representation in the neighbourhood of the origin

$$\phi_a = rJ_1[E(\alpha R)^{\frac{1}{4}}r],$$

where E is a constant. Now it is true that $r = 0$ is, in addition, only a distance of order $(\alpha R)^{-\frac{1}{2}}$ away from the Stokes point. However, use is made of the asymptotic expansions not at $r = 0$ but in a neighbourhood of it which can be chosen for convenience anywhere in Region III provided that in this neighbourhood $r \ll 1$, say, $|r| \gg (\alpha R)^{-\frac{1}{2}}$. It is therefore evident that the matching to the Bessel function at the origin can always be made even for the family of eigenvalues (6.1), provided αR is large enough. In addition, an obvious restriction to the use of (6.1) is that $4N \ll \alpha R$, so that only a relatively small number of modes is given with accuracy by (6.1).

Pekeris (1948*a*) derived an equation identical to (6.1) to the proper order of approximation by an independent method.* However, this method did not yield the other family of eigenvalues, namely, that for which $c \to 0$ as $\alpha R \to \infty$. This is the case to which we now turn.

7. The second limiting form

For small c we find that

$$P \cong \tfrac{2}{3}(\alpha R)^{\frac{1}{2}} c^{\frac{3}{2}} e^{-\frac{1}{4}i\pi},$$

and note that

$$e^Q \to 0 \quad \text{as} \quad \alpha R \to \infty.$$

Defining

$$\delta = (2i\alpha R)^{\frac{1}{3}} c,$$

we are able to write the eigenvalue equation in the following form:

$$\exp\left\{\frac{\sqrt{2}}{3} i\delta^{\frac{3}{2}}\right\} = -i\left\{\frac{i2^{\frac{1}{2}}\delta^{\frac{3}{2}} - 5}{i2^{\frac{1}{2}}\delta^{\frac{3}{2}} + 5}\right\}.$$

This leads to the formula

$$\delta^{\frac{3}{2}} = \frac{3\pi}{2^{\frac{3}{2}}}\left[4N + 1 - \frac{4\theta}{\pi}\right] \quad (N = 0, 1, 2 \ldots), \tag{7.1}$$

where

$$\theta = \arctan \frac{\sqrt{2}}{5} \delta^{\frac{3}{2}}.$$

There are discrete values of δ corresponding to the various modes; and as δ increases, $4\theta/\pi$ rapidly tends to 2, so that for the higher modes

$$c = \frac{1}{2(2i\alpha R)^{\frac{1}{3}}} [3\pi(4N + 1)]^{\frac{2}{3}}. \tag{7.2}$$

Again, we see that we have a set of eigenvalues corresponding to damped disturbances. We must again restrict the value of N in (7.1) so that $|c| \ll 1$. Figure 2 now gives an approximate picture of the eigenvalues in the complex c-plane for a given value of αR. At each end of the interval there are a finite number of eigenvalues described by (6.1) and (7.1). In between we cannot simplify the eigenvalue equation, but a few numerical computations at given Reynolds numbers suffice to give the behaviour of the solution. The results indicate that in the middle region there is again a finite number of eigenvalues. The actual number

* Pekeris' third term (1948*a*, equation (44)) is of the order of $(\alpha^2/\alpha R)$ and can be obtained by the present method if one proceeds as above after defining in (2.1) and (3.1) a quantity $c = c + i\alpha^2/\alpha R$, instead of neglecting α^2 compared to $i\alpha R$.

of solutions possible for a given Reynolds number and a given wave-number is relatively small but increases, of course, as αR increases. For instance, there are about eighteen eigenvalues for $\alpha R = 10{,}000$.

The same sort of objection can be made to (7.1) as was made to (6.1). The Stokes point approaches the boundary $r = 1$ as $R \to \infty$; hence, is the asymptotic representation valid? Here the objection is more serious, and a little reasoning (Corcos 1952, p. 25) shows that the argument of the asymptotic expressions is, at least for lower modes (N small), of the order of unity no matter how large αR is. Therefore, we will now obtain a more accurate representation of the family for which $c \to 0$.

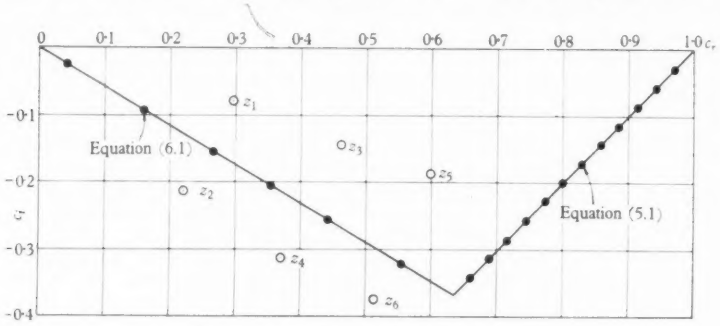

FIGURE 2. c_i *vs* c_r, for $\alpha R = 10{,}000$.

8. Expansion in terms of a convergent series

We will attempt to connect the preceding work with an alternate development which should give a more accurate representation of the viscous solution when the boundary is in the immediate vicinity of the Stokes point. We will use a notation suggestive of the corresponding quantities in the work of Lin (1945) in order that some of his results may be utilized.

We will first translate our origin of co-ordinates to the wall so that the slope of the velocity profile will be positive near the wall to correspond to the convention used in plane Poiseuille flow. We define

$$y = 1 - r.$$

Thus, the Stokes point is given by

$$y_k = 1 - k.$$

Further, following Lin, we take

$$\epsilon\eta = (y - y_k)$$

and

$$(W - c) = W_k'\eta\epsilon + \frac{W_k''}{2!}(\eta\epsilon)^2 + \ldots,$$

where $\epsilon = (\alpha R)^{-\frac{1}{3}}$. We then express (2.1) in terms of η and look for a solution of the form

$$\phi = \phi_0 + \epsilon\phi_1 + \epsilon^2\phi_2 + \ldots.$$

We find that ϕ_0 satisfies the differential equation

$$-i\phi_0^{\text{iv}} = W_k'\eta\phi_0''.$$

The viscous solutions are given by the particular solutions (Lin 1945; equation (4.9))

$$\phi_3 = \int_{+\infty}^{\eta} d\xi \int_{+\infty}^{\xi} d\mu\, \mu^{\frac{1}{2}} H_{\frac{1}{3}}^{(1)}[\tfrac{2}{3}(i\alpha_0\mu)^{\frac{3}{2}}]$$

and

$$\phi_4 = \int_{-\infty}^{\eta} d\xi \int_{-\infty}^{\xi} d\mu\, \mu^{\frac{1}{2}} H_{\frac{1}{3}}^{(2)}[\tfrac{2}{3}(i\alpha_0\mu)^{\frac{3}{2}}], \tag{8.1}$$

where

$$\alpha_0 = \left(\frac{dW}{dy}\right)^{\frac{1}{3}}_{y=y_k},$$

and $H_{\frac{1}{3}}^{(1,2)}$ represent Hankel functions of the first and second kind of order one-third. Our problem is to connect these solutions with the asymptotic viscous solutions. For small values of c we have seen that e^Q is very small. If e^Q is taken as being exactly zero, we have in Region I (near the wall)

$$\phi_a = A_1 \frac{r^{\frac{1}{2}}}{(W-c)^{\frac{1}{4}}}[\chi_+(k,r) - i\chi_-(k,r)]. \tag{8.2}$$

We may ask what combination corresponds to this in Region III. From (8.2) we take $B_1 = iA_1$ in the connexion formula (4.11), which yields

$$A_{\mathrm{III}} = A_{\mathrm{I}}, \quad B_{\mathrm{III}} = 0.$$

This shows that near the Stokes point only one of the viscous terms in Region III has significance. We then have

$$\phi_a = \frac{Ar^{\frac{1}{2}}}{(W-c)^{\frac{1}{4}}}\chi_+(k,r)$$

for r near the Stokes point in Region III. Near the Stokes point this solution may be rewritten approximately as

$$\phi_a = \text{const.} \times \frac{e^{\frac{2}{3}i(i\alpha_0\eta)^{\frac{3}{2}}}}{\eta^{\frac{1}{4}}}.$$

Similarly, ϕ_3 as given by (8.1) may be expressed asymptotically for large values of η by

$$\phi_3 = \text{const.} \times \frac{e^{\frac{2}{3}i(i\alpha_0\eta)^{\frac{3}{2}}}}{\eta^{\frac{1}{4}}}.$$

So it can be seen that the viscous solution is expressed (to the proper order of approximation) by ϕ_3. Since ϕ_3 is analytic in the region about the Stokes point it must represent the solution everywhere in that neighbourhood. In particular, it is valid on the boundary, and we may formulate our eigenvalue determinant in terms of this solution and the inviscid solution $rJ_1(i\alpha r)$.

9. An alternative determination of the eigenvalues

Writing the eigenvalue problem in terms of ϕ_3 leads us to the expression

$$\left(\frac{\phi_3}{\phi_3'}\right)_{y=0} = (k-1)\,F(z) = \frac{-J_1(i\alpha)}{[d/dr\{rJ_1(i\alpha r)\}]_{r=1}}, \tag{9.1}$$

where $z = (1-k)\,(\alpha R)^{\frac{1}{3}}\,(2k)^{\frac{1}{3}}$ and $F(z)$ is the Tietjens function

$$F(z) = \frac{\int_{\infty}^{-z} d\xi \int_{\infty}^{\xi} d\mu\, \mu^{\frac{1}{2}} H_{\frac{1}{3}}^{(1)}[\frac{2}{3}(i\mu)^{\frac{3}{2}}]}{-z\int_{\infty}^{-z} d\mu\, \mu^{\frac{1}{2}} H_{\frac{1}{3}}^{(1)}[\frac{2}{3}(i\mu)^{\frac{3}{2}}]}$$

which has been tabulated by Tietjens and by Lin for real values of z corresponding to neutral disturbances. Since

$$J_1(i\alpha)/[d/dr\{rJ(i\alpha r)\}]_{r=1}$$

is real and positive for all values of α, a neutral disturbance would require that $F(z)$ be real and positive for z positive. According to the tabulation of $F(z)$ given by Lin (1945, p. 140), this can only occur at $z = 2{\cdot}5$, $F(z) = 0{\cdot}51$. These values substituted in (9.1) are found to require α to be of the order of $(\alpha R)^{\frac{1}{3}}$. For this case the whole treatment is invalid. However, the work of Synge (1939) indicates that very short wavelength disturbances can be expected to be stable from energy considerations. Thus, we conclude that there is no neutral disturbance. A very interesting and significant comparison can be made between this family of eigenvalues and those of Couette flow. The inviscid solutions for Couette flow are $\sinh \alpha y$ and $\cosh \alpha y$. Using these, Lin's formula (1945, equation (6.13)) becomes

$$\left(\frac{\phi_3}{\phi_3'}\right)_{y=0} = -\frac{\sinh\alpha}{\alpha\cosh\alpha} - \left(\frac{\phi_4}{\phi_4'}\right)_{y=1}\frac{\cosh\alpha}{\alpha\sinh\alpha}. \tag{9.2}$$

If we look for solutions of this equation for which c is small, the second right-hand term can be neglected since

$$\left(\frac{\phi_4}{\phi_4'}\right)_{y=1} = \theta[(\alpha R)^{-\frac{1}{2}}].$$

The resulting eigenvalue problem

$$\frac{\phi_3(0)}{\phi_3'(0)} = -\frac{\sinh\alpha}{[d/dy(\sinh\alpha y)]_{y=1}} \tag{9.3}$$

is remarkably similar to equation (9.1). This means that Couette flow has one set of modes given by an equation similar to equation (7.2). Another set of modes will be found for which $c \to 1$ as $\alpha R \to \infty$. These two sets correspond to the dominance of the term

$$\frac{\phi_3(0)}{\phi_3'(0)},$$

or the term

$$\frac{\phi_4(1)}{\phi_4'(1)}$$

respectively in equation (9.2). For c in the middle region, these terms are of equal importance and the whole equation must be considered. The eigenvalues are given qualitatively by a figure similar to figure 2, but are symmetrical about $c = \frac{1}{2}$. We may now determine the eigenvalues of both Couette flow and pipe flow for which $c \to 0$ as $\alpha R \to \infty$, using the Tietjens function. Since the terms involving

the wave number are independent of αR and c, $F(z)$ must grow large without bounds if $y - y_k \to 0$. This happens when z satisfies the equation

$$\int_{\infty}^{-z} d\mu\, \mu^{\frac{1}{3}} H_{\frac{1}{3}}^{(1)}[\tfrac{2}{3}(i\mu)^{\frac{3}{2}}] = 0, \tag{9.4}$$

where for Poiseuille flows

$$z = [1 - \sqrt{(1-c)}]\,(1-c)^{\frac{1}{6}}\, 2^{\frac{1}{3}}(\alpha R)^{\frac{1}{3}},$$

and for Couette flows $\qquad z = c(\alpha R)^{\frac{1}{3}}.$

Equation (9.4) gives a discrete set of values for z, which we will denote by z_n. These zeros lie in pairs which are very nearly reflexions in the ray $(\arg z) = \frac{1}{6}\pi$. The first pair is approximately

$$z_{1,2} = 4{\cdot}23e^{(-\frac{1}{6}\pi \pm \frac{1}{12}\pi)i}, \tag{9.5}$$

a result obtained by a numerical integration using tabulated values of the integrand (Furry 1945). Other values are

$$z_{3,4} = 6{\cdot}8e^{(-\frac{1}{6}\pi \pm 12°)i}, \quad z_{5,6} = 9{\cdot}5e^{(-\frac{1}{6}\pi \pm 8°)i}.$$

The most critical of these values, $z_i = 4{\cdot}23e^{-\frac{1}{12}\pi i}$, was checked on a differential analyser; the others are only rough estimates. Figure 2 is a plot of the eigenvalues corresponding to $\alpha R = 10{,}000$ and belonging to both families (i.e. the family $c \to 0$ as $\alpha R \to \infty$ obtained by integrating (9.4) and the family $c \to 1$ as $\alpha R \to \infty$ given by (6.1)). In the region where the two families join, neither representation is accurate, and the complete equation (5.1) should be used. Nevertheless, figure 2 illustrates quite well the fact that there exists only a finite number of modes for any αR.

It is interesting to note that for the first few modes an asymptotic formula such as the one given by Hopf (1914) in the case of Couette flow is very inaccurate. For $n > 6$ the roots of (9.4) are given to sufficient accuracy by the asymptotic equation

$$\exp\{\tfrac{2}{3}e^{-\frac{1}{4}\pi} z^{\frac{3}{2}} - \tfrac{5}{12}\pi i\} - \exp\{-\tfrac{2}{3}e^{-\frac{1}{4}i\pi} z^{\frac{3}{2}} - \tfrac{11}{12}\pi i\} + \frac{3{\cdot}03}{0{\cdot}853} z^{\frac{1}{2}} e^{\frac{17}{24}\pi i} = 0,$$

$$\tfrac{1}{2}\pi > (\arg z) > -\tfrac{2}{3}\pi. \tag{9.6}$$

Thus $$z_1 = 4{\cdot}23e^{-\frac{1}{12}\pi i} = \{1 - \sqrt{(1-c)}\}\,(1-c)^{\frac{1}{6}}\, z^{\frac{1}{3}}(\alpha R)^{\frac{1}{3}} \tag{9.7}$$

yields the most critical value of c, that which corresponds to the *least* damped solution. The results, calculated by means of (9.7) are compared to corresponding values from a differential analyser (Corcos 1952) in figure 3. Unfortunately, it was not possible to operate the analyser above $\alpha R = 1250$, and thus $(\alpha R)^{\frac{1}{3}}$ cannot be said to be extremely large for this case. Nevertheless, the results agree surprisingly well. The small amount of scatter in the computer data should be charged to the computer itself.

The close concurrence between the results of the differential analyser and the analytical formula (9.7) derived above give considerable confidence in the accuracy of the asymptotic methods. At low Reynolds numbers, the problem lends itself especially well to study with a differential analyser. It was noted in the course of the computer study that there were few eigenvalues corresponding

to a given value of α and αR, and that the solutions yielded large decays in time. It was also clear from the character of the solutions of the differential equations that none would meet the boundary conditions with a negative value of c_i (corresponding to an unstable eigenvalue).

Thus it must be concluded that Poiseuille flow damps infinitesimal axially symmetric disturbances of the type assumed here.

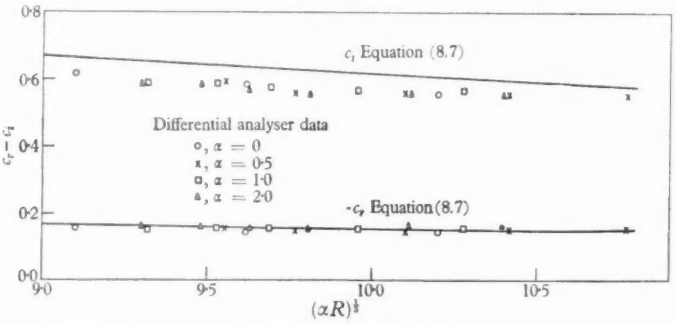

FIGURE 3. c_r, c_i *vs* $(\alpha R)^{\frac{1}{3}}$.

10. Conclusions

The purpose of a stability analysis is to provide information about the phenomenon of transition from a laminar flow to a turbulent one. In recent years it has been more fully realized that while the small-disturbance theory has a legitimate basis in fact (Schubauer & Skramstadt 1947; Liepmann 1943; Laufer 1956), it plays only a fragmentary role in the description of transition.

To begin with, if the oscillations grow, they eventually reach an amplitude beyond which linearization of the equations of motion is inadmissible. At this point we lose even qualitative information about the further development of the disturbances. They may grow, settle at some finite amplitude or decay. They may appear as localized turbulent spots or spearheads (Emmons 1951; Schubauer & Klebanoff 1955; Rotta 1956), and these may or may not spread. Here an entirely different type of analysis seems to be required to describe the spatial growth of a finite, even fully developed disturbance rather than the temporal growth of an infinitesimal one. Finally, even when small disturbances are guaranteed not to grow within a region of flow, disturbances of finite (but not necessarily large) amplitude may be 'imported'. The free stream turbulence of a wind tunnel may induce in boundary layers oscillations large enough to invalidate the conclusions of a small-disturbance analysis. In the problem which occupies us, finite disturbances may very well propagate downstream from the entrance of the pipe. There are good grounds (Tatsumi 1952) for believing that, for some Reynolds numbers, as the boundary layer grows on the walls of the pipe entrance, it is capable of amplifying infinitesimal disturbances before they reach the downstream portion of the pipe where fully developed parabolic flow prevails. Are we able to deduce from the analysis presented here that contamination from upstream is indeed the only means by which disturbances in a pipe can acquire a finite

amplitude? Unfortunately, this analysis taken by itself does not justify such strong conclusions. On the other hand, a recent set of experiments performed by Leite (1959) on fully developed pipe flow usefully complements the analysis.

There are three main reasons why one might hold that the small-disturbance analysis of fully developed pipe flow is incomplete.

(*a*) Axially symmetric disturbances have been assumed. This is an arbitrary albeit necessary restriction designed to permit separation of variables. No analytic considerations have been advanced to bolster the hope that asymmetric disturbances behave as symmetric ones do. However, Leite (1959) purposely introduced small disturbances with no symmetry. They became more axially symmetric as they progressed downstream. Thus the asymmetric part of the disturbances decayed faster than the symmetric part.

(*b*) It has been pointed out that the analysis yields a finite set of eigenvalues and hence of eigenfunctions for any given value of α and of αR. This means that arbitrary initial disturbances which are held to satisfying continuity cannot be represented as we have assumed by a sum of elemental solutions of the form

$$\psi(r, x, t) = \phi(r)\, e^{i\alpha x}.$$

For instance,

$$\psi_{\text{initial}} = f(r, R) \cos \alpha_1 x,$$

where $f(r, R)$ is an arbitrary continuous function of r subject to our boundary conditions, cannot be represented in the analysis since, according to our results, $f(r)$ can only be the linear combination of a finite number of eigenfunctions, i.e.

$$f(r) = \sum_{1}^{n} A_n \phi_n(\alpha_1, R, r).$$

Leite found that the rate of decay for the disturbances he introduced was given with relatively good accuracy by the present analysis. This would seem to indicate that the rates of decay are not very sensitive to the form of the disturbance so long as its amplitude is small.

(*c*) Finally, in the analysis disturbances are assumed periodic for

$$-\infty < x < \infty.$$

This is only one class of perturbations. For instance, disturbances introduced by a small roughness on the wall or artificially as in Leite's pipe occur, instead, at a given downstream section. If they are heavily damped or heavily amplified, say if the amplitude varies appreciably in one wavelength, the distinction may be important. This criticism naturally applies also to the study of boundary layer stability. One should perhaps not expect as good agreement between theory and experiment when the decay or amplification rates are large as say for the determination of a neutral curve. For pipe flows, since the experiments suggest heavy damping, it might be instructive to analyse the problem anew with disturbances of the form

$$\psi(r, x, t) = \phi(r)\, e^{-\nu x + i\omega t},$$

where ν is complex and ω is real.

Leite's experiments and the present work taken together do not amount to a proof that small disturbances cannot grow in a fully developed pipe flow, but they provide a very strong indication that this is the case.

Appendix

The Stokes phenomenon

Since, in general, the point $W = c$ corresponds to a complex value of r, we shall extend r into the complex domain by analytic continuation, and we shall make use of the fact that a true (i.e. exact) solution of (2.1) is single-valued analytic and continuous at and around the 'Stokes point' $W = c$. This avoids the indeterminacy introduced with the asymptotic solutions. The following development which is related to some of Langer's work is essentially due to Furry (1947), and the general approach is known as the W.K.B. method.

Let $W = c$ when $r = k$ and define

$$U = \int_k^r \sqrt{\{i(W-c)\}}\, dr.$$

Then if $(r-k) = \beta$, we have in the close neighbourhood of k

$$U = \int_0^{r-k} \sqrt{\{-i(2k)\beta\}}\, d\beta = \tfrac{2}{3}\sqrt{(-2ik)}\,\beta^{\frac{3}{2}}.$$

We seek the lines in the complex plane for which U is a pure real number. If we define $\arg(i) = \frac{1}{2}\pi$, the approximate expression for U above shows that at least in the vicinity of k these lines are such that

$$\arg\beta = -\tfrac{1}{2}\pi + \tfrac{2}{3}N\pi + \arg\sqrt{k}.$$

That is, there are three such lines which make 120° angles with each other near the Stokes point (figure 1). Away from the Stokes point these lines will be curved, because the approximation for U above will not hold for β-large. The sign of U alternates from line to line, so that for a given line it depends on the number of revolutions around the point k. These lines will be designated as the Stokes lines. In a similar way, U is purely imaginary near the Stokes point on lines such that $\arg(\beta) = \frac{1}{2}\pi + \frac{2}{3}N\pi + \arg\sqrt{k}$. As one proceeds out along a Stokes line the exponential terms $\exp[\sqrt{(\alpha R)}\,U]$, $\exp[-\sqrt{(\alpha R)}\,U]$ in the asymptotic expressions become either very large or very small depending on the sign of U associated with that line. This a consequence of the assumption that αR is a large number. Thus, if we were to traverse the β-plane in such a manner as to cross Stokes lines, we would successively see the coefficient of A in (4.3) become much larger than the coefficient of B, then the coefficient of B overpower the coefficient of A, etc. When one is on a Stokes line, the small exponential term is in fact smaller than the order of approximation of the asymptotic representation. On the other hand, on the lines of pure imaginary U, the coefficients of A and B have precisely the same magnitude. It is apparent from this observation that if we need to change our coefficients A and B within the interval, the proper place to modify them will be on the Stokes lines. There the coefficient of the small term could be modified without materially altering the value of the sum of the two asymptotic expressions, and thus without introducing a discontinuity in the representation.

We now inquire whether the original ratio A/B need be modified within the interval $(0 < r < 1)$. We define the Stokes lines and the lines of pure imaginary

U as shown in figure 1. Further we choose $U > 0$ on S_1, hence $U < 0$ on S_2, $U > 0$ on S_3, for the first revolution; and $U < 0$ on S_1' after one complete revolution from S_1. If the asymptotic solution (4.3) is represented in Region I by

$$\phi_a = \frac{r^{\frac{1}{2}}}{(W-c)^{\frac{1}{4}}}[A_1\chi_+(k,r)+B_1\chi_-(k,r)],$$

it can be represented in any Stokes region by a linear combination of the two terms. Thus

$$A_{\rm II} = aA_1+bB_1, \quad B_{\rm II} = cA_1+dB_1,$$

where a, b, c, d are constants. However, the continuity of our representation requires that the coefficient of the small term only be modified on the corresponding Stokes lines. Therefore, according to our convention we have

$$\begin{aligned} A_{\rm II} &= A_1, \\ B_{\rm II} &= B_1+\alpha A_{\rm I}, \\ A_{\rm III} &= A_{\rm II}+\mu B_{\rm II} = A_1+[B_1+\alpha A_1]\mu, \\ B_{\rm III} &= B_{\rm II} = B_{\rm I}+\alpha A_{\rm I}, \end{aligned}$$

and at the initial Stokes line after a full revolution counterclockwise

$$\begin{aligned} A_{\rm I}' &= A_{\rm III} = A_{\rm I}+\mu[B_1+\alpha A_1], \\ B_{\rm I}' &= B_{\rm III}+\gamma A_{\rm III} = B_1+\alpha A_{\rm I}+\gamma\{A_1+\mu[B_1+\alpha A_1]\}. \end{aligned}$$

On the other hand, after one revolution A has become the coefficient of the small term, B that of the large term, and the argument of the expression $(W-c)^{\frac{1}{4}}$ has gained an angle $5\pi/2$. For the solutions on $A_{\rm I}$ and $A_{\rm I}'$ to be the same requires that

$$\begin{aligned} A_{\rm I}' &= iB_1, \\ B_{\rm I}' &= iA_1. \end{aligned}$$

All the above relations will be compatible only if

$$\alpha = \mu = \gamma = i. \tag{A 1}$$

The present arguments show that for the representation to be continuous, one of the constants A or B must be modified every time a Stokes line is crossed. This property is known as the Stokes phenomenon. We now have a series of connexion formulae which permit us to evaluate this discontinuity in A and B on the Stokes lines. Which connexion formula will be used depends on the Stokes regions within which the end points $r = 0$ and $r = 1$ fall, and thus on the eigenvalue yet to be found. Once an arbitrary decision is made, it can be checked *a posteriori*; i.e. it is a correct choice only if it yields eigenvalues consistent with the assumptions. There are obviously nine cases to be considered, but it is now a simple matter to determine which is acceptable. One is guided partly by the expectation that the phase velocity of the disturbance (c_r) is positive and less than the maximum velocity of the main flow: $0 < c_r < 1$. This suggests that $r = 0$ is either in Region II or III. A systematic investigation by the authors indicated that eigenvalues existed only if they were such that $r = 0$ belonged to Region III and $r = 1$ to Region I. For this case our connexion formulae yield

$$A_1 = iB_{\rm III}+A_{\rm III}, \quad B_1 = -iA_{\rm III}. \tag{A 2}$$

If A_{III} and B_{III} are known, A_{I} and B_{I} are given by (A 2) and hold from the neighbourhood of the singularity to the wall. According to equations (4.9) and (4.3), reversing the order of integration, and changing the lower limit of integration, we find that

$$\begin{aligned} A_1 &= C_2[\exp(\tfrac{3}{4}\pi i)\,\chi_-(k,0) - i\exp(-\tfrac{3}{4}\pi i)\,\chi_+(k,0)], \\ B_1 &= C_2[-i\exp(\tfrac{3}{4}\pi i)\,\chi_-(k,0)], \end{aligned} \tag{A 3}$$

where C_2 is a constant.

REFERENCES

Corcos, G. M. 1952 *On the Stability of Poiseuille Flows.* Ph.D. Thesis, University of Michigan.

Emmons, H. W. 1951 *J. Aero. Sci.* **18**, 490.

Furry, W. H. 1945 *Modified Hankel Functions of Order One-Third.* Harvard Computing Laboratory.

Furry, W. H. 1947 *Phys. Rev.* **71**, 361.

Hopf, L. 1914 *Ann. Phys., Lpz.*, **44**, 1.

Laufer, J. 1956 *J. Aero. Sci.* **23**, 184.

Leite, R. 1959 *J. Fluid Mech.* **5**, 81.

Liepmann, H. W. 1943 *Wartime Rep. Nat. Adv. Comm. Aero., Wash.*, no. W–107.

Lin, C. C. 1945 *Quart. Appl. Math.* **3**, 117.

Pekeris, C. L. 1948*a* *Proc. U.S. Nat. Acad. Sci.* **34**, 285.

Pekeris, C. L. 1948*b* *Phys. Rev.* **74**, 191.

Rotta, J. 1956 *Proc. 9th Int. Congr. Appl. Mech., Brussels.*

Schubauer, G. B. & Klebanoff, P. S. 1955 *Tech. Note Nat. Adv. Comm. Aero., Wash.*, no. 3489.

Schubauer, G. B. & Skramstad, H. K. 1947 *J. Aero. Sci.* **14**, 69.

Sexl, T. 1927 *Ann. Phys., Lpz.*, **83**, 835.

Sexl, T. 1928 *Ann. Phys., Lpz.*, **84**, 807.

Synge, J. L. 1939 *Proc. 5th Int. Congr. Appl. Mech., Cambridge, Mass.*

Tatsumi, T. 1952 *Proc. Phys. Soc. Japan*, **7**, 489.

Small-scale variation of convected quantities like temperature in turbulent fluid

Part 1. General discussion and the case of small conductivity

By G. K. BATCHELOR

Cavendish Laboratory, University of Cambridge

(Received 1 June 1958)

When some external agency imposes on a fluid large-scale variations of some dynamically passive, conserved, scalar quantity θ like temperature or concentration of solute, turbulent motion of the fluid generates small-scale variations of θ. This paper describes a theoretical investigation of the form of the spectrum of θ at large wave-numbers, taking into account the two effects of convection with the fluid and molecular diffusion with diffusivity κ. Hypotheses of the kind made by Kolmogoroff for the small-scale variations of velocity in a turbulent motion at high Reynolds number are assumed to apply also to small-scale variations of θ.

Previous contributions to the problem are reviewed. These have established that the spectrum of θ varies as $n^{-\frac{5}{3}}$ (n being wave-number) at the low wave-number end of the equilibrium range, but there has been some confusion about the wave-number marking the upper end of the range of validity of this relation. The existence of a conduction 'cut-off' near $n = (\epsilon/\kappa^3)^{\frac{1}{4}}$ as put forward by Obukhoff and Corrsin is shown to hold only when $\nu \ll \kappa$, and that near $n = (\epsilon/\nu\kappa^2)^{\frac{1}{4}}$ put forward by Batchelor is shown to apply only when $\nu \gg \kappa$. In the case $\nu \ll \kappa$, the remaining problem is to determine the form of the spectrum of θ beyond the conduction cut-off; this is done in Part 2. In the case $\nu \gg \kappa$, the conduction cut-off occurs at wave-numbers much higher than $(\epsilon/\nu^3)^{\frac{1}{4}}$, which is where the energy spectrum is cut off by viscosity, and where the spectrum of θ ceases to vary as $n^{-\frac{5}{3}}$.

The form of the spectrum of θ in this latter case is determined over the range $n > (\epsilon/\nu^3)^{\frac{1}{4}}$ by analysing the effect of the velocity field, regarded as effectively a persistent uniform straining motion for these small-scale variations of θ, and of molecular diffusion on a single Fourier component of θ. The wave-number of this sinusoidal variation of θ is changed (and generally increased in magnitude) by the straining motion and the amplitude is diminished by diffusion. By supposing that the level of the spectrum of θ is kept steady at wave-numbers near $(\epsilon/\nu^3)^{\frac{1}{4}}$ by some mechanism of transfer from lower wave-numbers, the linearity of the equation for θ then allows the determination of the spectrum for $n > (\epsilon/\nu^3)^{\frac{1}{4}}$, the result being given by (4.8). The same result is obtained, using essentially the same approximation about the velocity field, from a different kind of analysis in terms of velocity and θ correlations. Finally, the relation between this work and Townsend's model of the small-scale variations of vorticity in a turbulent fluid is discussed.

1. Introduction

When the temperature of a fluid in turbulent motion is not uniform (although with such small variations that buoyancy forces are negligible), the temperature field is made random by the irregular movements of the fluid and acquires statistical properties which are directly related to those of the turbulent motion. Quite apart from its intrinsic interest as an aspect of a general study of turbulence, the distribution of temperature, and of other similarly conserved scalar physical quantities, in a turbulent fluid has a direct bearing on a number of problems in geophysics, mostly concerned with the scattering of either sound or electromagnetic waves. In these scattering problems it often happens, for extraneous reasons concerned with the choice of wavelength of the waves concerned, that the small-scale structure of the distribution of temperature (or whatever quantity is responsible for the variations in refractive index) is of particular interest. This is a fortunate circumstance, because these small-scale components may be expected, on the basis of arguments parallel to those used in Kolmogoroff's theory, to have a measure of universality and to have statistical properties which depend only weakly on the large-scale features of the distribution. It is probable that considerations of the fine structure of the distribution of quantities like temperature also have a bearing on industrial problems concerned with the mixing of one fluid in another of approximately the same density by means of turbulent motion. This paper will give a theoretical discussion of the small-scale components of quantities like temperature, 'small' being taken here to mean that the components concerned have characteristic length-scales small compared with the length-scale of the eddies containing the bulk of the kinetic energy of the turbulent motion, without regard for any of the possible applications of the results.

The dominant feature of the action of the turbulent motion on the temperature distribution is a continual reduction of the length-scale of temperature variations. The random convection of material elements of the fluid is inevitably accompanied by distortion of these elements, and, in the absence of molecular conduction, a (statistical) increase in the gradients of temperature. This process was described clearly by Obukhoff (1949), and has been analysed in terms of the way in which surfaces of constant temperature are increased in area and brought closer together (Batchelor 1952). Unless temperature variations on some definite length-scale are supplied continually by some external agency, the statistical properties of the temperature distribution cannot be exactly steady; however, the properties of the small-scale components of the temperature distribution will be approximately steady in general, because the process of convective distortion and increase of temperature gradients takes place much more quickly than the over-all decay of the temperature field. The continual increase in the magnitude of temperature gradients due to random convection will ultimately be checked by the smoothing action of thermal conduction, and no further refinement of the temperature distribution can occur; in this way, a length-scale characterizing the smallest temperature 'eddies' is determined.

There are only two properties of the quantity temperature which are relevant to these mechanical processes. One is the property of invariance of the tempera-

ture of a material element of fluid in the absence of molecular conduction; the other is that the temperature is subject to molecular conduction characterized by a diffusivity κ (of dimensions velocity by length). In these respects, temperature is no different from many other physical quantities, such as water-vapour content of air, salt concentration of water, and electron density in the ionosphere, although the numerical values of κ will be different in each case. To the extent that they do not depend on special values of κ, all the remarks and results of this paper will apply to all such dynamically passive conserved scalar quantities, the terminology associated with the typical case of temperature being employed sometimes for conciseness.

The problem to be studied is thus as follows. A quantity $\theta(x, t)$ has a distribution in the fluid which is governed by the equation

$$\frac{\partial \theta}{\partial t} + \mathbf{u}.\nabla\theta = \kappa\nabla^2\theta, \tag{1.1}$$

where $\mathbf{u}$ is the velocity of the fluid and is independent of θ. The fluid, taken as incompressible, is in turbulent motion at high Reynolds number, and the length-scale characterizing the energy-containing eddies is L. We wish to determine the statistical properties of those components of the spatial distribution of θ that have a length-scale small compared with L, and in particular to determine the wave-number spectrum of the distribution of θ. This is a familiar kind of objective in the theory of turbulence, although not one which is often achieved convincingly. It will be shown that a reasonably complete description of the spectrum of θ can be obtained, partly by the use of simple new ideas and partly by the use of old ideas in a new context, this success being made possible by the linearity in θ of all terms in (1.1). No measurements appear to be available for comparison with the theoretical results.

2. Previous work on the problem

The few published contributions that bear directly on the problem need to be described before the new work is presented. The first relevant papers seem to be those in which Obukhoff (1949; see also Yaglom 1949) and Corrsin (1951) pointed out the primary features of the effect of random convection on the spatial distribution of θ. These authors realized that the general increase of gradients of θ accompanying the irregular stirring action of the turbulence, which is a consequence of the quadratic term in (1.1), can also be thought of as a transfer between different Fourier components of the distribution of θ. If both $\mathbf{u}$ and θ are written in the form of Fourier integrals, the term $\mathbf{u}.\nabla\theta$ leads to the generation of new harmonic components of θ, and in particular to the growth of components of ever-increasing wave-number. This effective transfer from Fourier components of the θ-distribution at low wave-number to those at high wave-number is mathematically similar to that which acts on the turbulent velocity distribution, and Obukhoff and Corrsin made the plausible assumption (which will also be adopted here) that the hypotheses of Kolmogoroff's universal equilibrium theory apply equally well to the θ-distribution as to the $\mathbf{u}$-distribution. The arguments in favour of this extension of Kolmogoroff's hypotheses to apply to a temperature

distribution need not be given, since they are identical in form with, and neither stronger nor weaker in rigour than, those well-known arguments concerning the velocity distribution.

On the basis of these hypotheses, and with the assumptions that the Reynolds number of the turbulence is sufficiently high and that there are no external sources of variations of θ on a small length-scale, the statistical properties of the small-scale components of the θ-distribution are homogeneous, isotropic and steady, irrespective of the properties of the components with length-scale of the order of L. Moreover, owing to the dependence of the distribution of θ on that of $\mathbf{u}$, the components of the θ-distribution having these properties will be defined by the same condition as the components of the $\mathbf{u}$-distribution having the same properties, namely, that their linear size is small compared with L; the two distributions have a common 'equilibrium range' of wave-numbers. It is thus possible to define a spectrum function for the (small-scale components of the) spatial distribution of θ as

$$\Delta(\mathbf{n}) = \frac{1}{8\pi^3}\int S(\mathbf{r})\, e^{-i\mathbf{n}.\mathbf{r}}\, d\mathbf{r}, \tag{2.1}$$

where $\mathbf{n}$ is the vector wave-number and $S(\mathbf{r}) = \overline{\theta\theta'} = \overline{\theta(\mathbf{x})\,\theta(\mathbf{x}+\mathbf{r})}$ is the covariance of θ as a function of position ($\overline{\theta}$ being taken as zero for convenience). In view of the isotropy, Δ and S are functions of the magnitudes n and r alone, and the spectrum function giving the distribution with respect to wave-number magnitude is

$$\Gamma(n) = 4\pi n^2\Delta(n) = \frac{2n}{\pi}\int_0^\infty S(r)\, r \sin nr\, dr; \tag{2.2}$$

it follows from the transform of (2.1) that

$$\overline{\theta^2} = \int_0^\infty \Gamma(n)\, dn.$$

The statistical properties of the small-scale components of the θ-distribution are also independent of the detailed form of the properties of the large-scale components, according to the usual hypotheses,* and are affected by these large-scale components only inasmuch as the latter determine the magnitude of the rate of transfer from large-scale to small-scale components. In order to see exactly what is being transferred between different parts of the θ-spectrum, it is necessary to note only that the quadratic term in (1.1) makes no contribution to $\partial\overline{\theta^2}/\partial t$. Thus, when one Fourier component of the θ-distribution is changed by interaction between the θ and $\mathbf{u}$ fields, other Fourier components are changed simultaneously in such a way that the sum of the (necessarily independent) contributions to $\overline{\theta^2}$ from all Fourier components remains the same. This shows that what is transferred across the θ-spectrum, and conserved while being transferred, when the turbulent motion distorts the temperature distribution, is a contribution to $\overline{\theta^2}$ from Fourier components; for lack of a suitable word, let us call it θ^2-stuff.

Following the usual line of argument of the Kolmogoroff theory, we now suppose that the diffusivity κ is so small as to make the effect of conduction

* Which, however, are now challenged by Kraichnan (1958, 1959).

negligible for some of the Fourier components (namely, those at the small wave-number end of the range) comprising the group whose statistical properties are steady and isotropic. The part of the equilibrium range of wave-numbers for which the Fourier components of the **u**-distribution are independent of viscosity is usually termed the 'inertial subrange', and an appropriate term for the part of the equilibrium range for which the Fourier components of the θ-distribution are independent of molecular diffusion is the 'convection subrange'. No actual destruction of $\overline{\theta^2}$-stuff takes place at wave-numbers in, or smaller than those in, the convection subrange; all the destruction takes place at higher wave-numbers as a result of the action of molecular diffusion, the total rate of destruction of the $\overline{\theta^2}$-stuff in unit volume of fluid being

$$2\kappa\overline{\theta\nabla^2\theta} = -2\kappa\overline{(\nabla\theta)^2} = -\chi, \quad \text{say.} \tag{2.3}$$

We assume that, as in the case of the dissipation of kinetic energy by viscosity, the value of χ is determined by statistical interaction of the Fourier components of **u** and θ each with wave-numbers of order L^{-1}, and is a 'given' quantity so far as considerations of the small-scale components alone are concerned.

Thus the mean rate at which $\overline{\theta^2}$-stuff is transferred from wave-numbers smaller than, to wave-numbers larger than, any wave-number in the convection subrange, per unit volume of the fluid, is χ, and this is one of the parameters on which the form of the θ-spectrum in the convection subrange depends. The only other parameters on which the θ-spectrum in the convection subrange can depend are those which determine the Fourier components of the velocity distribution in the equilibrium range of wave-numbers, that is, the total rate of viscous dissipation of kinetic energy per unit mass of fluid, ϵ, and the kinematic viscosity ν. Provided the Reynolds number of the turbulence is so large that viscous effects, as well as conduction effects, are unimportant at at least some of the wave-numbers in the convection subrange, dimensional requirements lead to

$$\Gamma(n) \propto \chi\epsilon^{-\frac{1}{3}}n^{-\frac{5}{3}} \tag{2.4}$$

for $n \gg L^{-1}$ and n less than some upper limit yet to be determined. Thus the θ-spectrum here has the same dependence on n as the **u**-spectrum in the inertial subrange, namely,

$$E(n) \propto \epsilon^{\frac{2}{3}}n^{-\frac{5}{3}}, \tag{2.5}$$

as was demonstrated by Obukhoff (1949) and independently by Corrsin (1951).

A relation different from (2.4) has been put forward by Inoue (1950, 1951, 1952). Inoue appears to have thought of the various components, of different linear dimensions, into which the temperature distribution is resolved as being physical entities, and of the conserved quantity which is transferred between different components as a result of the stirring motion of the fluid as being heat—or, equivalently, since the fluid is of uniform heat capacity per unit volume, temperature. A dimensional argument like that leading to (2.4), but using a quantity specifying a rate of heat transfer in place of χ, then gives $\Gamma(n)$ as proportional to $n^{-\frac{7}{3}}$. This argument of Inoue's does not seem to be sound; the

'components' of a random spatial field are not entities relating to different portions of the fluid but are (or, at any rate, should be, if the concept is to be self-consistent) different members of an appropriate set of orthogonal functions. In his discussion of a temperature field Obukhoff (1949) pointed out that, for small fluctuations about the mean, $\overline{\theta^2}$ is a measure of the deficiency of entropy of the fluid relative to a state in which the temperature is uniform with the same mean value, and that this supplies a physical interpretation of the $\overline{\theta^2}$-stuff that is transferred across the spectrum. However, all that is strictly relevant to the above argument is that the value of θ for a material particle is unchanged by convection and that the different Fourier components of the distribution of θ make independent contributions to $\overline{\theta^2}$.

The papers by Obukhoff, Corrsin and Inoue, already referred to, appear to be the only published works on the form of the θ-spectrum in the equilibrium range of wave-numbers, apart from a rather unplausible suggestion by Villars & Weisskopf (1955) that $[\overline{(\theta-\theta')^2}]^{\frac{1}{2}}$ is proportional to r and to the gradient of $\overline{\theta}$ when conduction is unimportant. (The simple mixing process on which this suggestion is based is sound enough in itself, but I think the authors have overlooked the fact that the part of the fluctuating gradient of θ due to components with length-scale larger than r is much larger than the mean gradient of θ, and that the magnitude of this fluctuating gradient determines $\overline{(\theta-\theta')^2}$.) Obukhoff and Inoue gave expressions for the θ-spectrum only in the convection subrange. Corrsin obtained (2.4), like Obukhoff, and noted further that if one supposes the transfer across both the θ-spectrum and the **u**-spectrum to be representable mathematically as an eddy diffusion process in the manner suggested by von Weizsäcker and Heisenberg, with the smaller-scale components of **u** acting as the transfer agent for the larger-scale components of both θ and **u**, then both the θ-spectrum function $\Gamma(n)$ and the **u**-spectrum function $E(n)$ are proportional to n^{-7} at large wave-numbers beyond both the viscous and conduction cut-off wave-numbers. Since Corrsin's paper was published, the von Weizsäcker–Heisenberg hypothesis has come to be regarded, on both deductive and empirical grounds, as of doubtful value for predictions about the **u**-spectrum over the part of the equilibrium range for which viscous effects are important, and consequently the above prediction about the θ-spectrum is not now convincing.

The position is thus that the form of the θ-spectrum in that part of the equilibrium range in which neither viscous forces nor conduction effects are important is reasonably well established (assuming, as is done here, that the Kolmogoroff theory in general is reasonably well established), but that the form at larger wave-numbers is not known.

The range of validity of (2.4)

Obukhoff (1949) and Corrsin (1951) have also said something about the magnitude of the wave-number marking the upper end of the range of validity of the relation (2.4) for the θ-spectrum. Obukhoff remarked that the relation (2.4), for the stated range of wave-numbers, is equivalent to a relation

$$\overline{(\theta-\theta')^2} \propto \chi\epsilon^{-\frac{1}{3}}r^{\frac{2}{3}}, \tag{2.6}$$

valid for $r \ll L$ and for r bounded below in some way as yet unknown, and that when r is sufficiently close to zero there is available the exact relation (see (2.3))

$$\overline{(\theta - \theta')^2} = \frac{1}{6}\frac{\chi}{\kappa} r^2. \tag{2.7}$$

Equations (2.7) and (2.6) are asymptotic relations valid for 'small' and 'large' values of r respectively (the 'large' values being subject to the restriction $r \ll L$). Obukhoff argued that the two ranges of r concerned will be contiguous, in which case the dividing value of r will be given approximately by the solution of

$$\frac{1}{6}\frac{\chi}{\kappa} r^2 = \chi \epsilon^{-\frac{1}{3}} r^{\frac{2}{3}}$$

(the constant of proportionality in (2.6) being assumed as usual to be of order unity). Thus Obukhoff's conclusion is that (2.6) is valid for $(\kappa^3/\epsilon)^{\frac{1}{4}} \ll r \ll L$, or, equivalently, that the relation (2.4) for the θ-spectrum is valid for

$$L^{-1} \ll n \ll (\epsilon/\kappa^3)^{\frac{1}{4}}. \tag{2.8}$$

Corrsin's argument is apparently different in form, but leads to the same conclusion. He supposed that the relation (2.4) ceases to be valid when n is so large that the effect of molecular diffusion becomes important, and that this will happen when the Péclet number appropriate to the Fourier components of the θ-distribution with wave-number n becomes of order unity. The Péclet number in general is a measure of the ratio of convection to conduction effects, and Corrsin assumes this measure to be given by $E^{\frac{1}{2}}/(n^{\frac{1}{2}}\kappa)$, with the **u**-spectrum function $E(n)$ having the inertial subrange form (2.5). The conclusion is that conduction effects render (2.4) invalid when n is of order $(\epsilon/\kappa^3)^{\frac{1}{4}}$, in agreement with Obukhoff.

The inertial subrange, within which the relation (2.5) for the **u**-spectrum holds, is known to be specified by $L^{-1} \ll n \ll (\epsilon/\nu^3)^{\frac{1}{4}}$. Obukhoff and Corrsin thus hold that the variations of the θ and **u**-spectra as $n^{-\frac{5}{3}}$ are cut off, in the sense that at higher wave-numbers the two spectra begin to fall off more rapidly as a result of molecular diffusion being important, at wave-numbers whose ratio is given, to order of magnitude, by $(\nu/\kappa)^{\frac{3}{4}}$. The two arguments from which this result was found seem acceptable when ν and κ are of the same order of magnitude, or when $\nu \ll \kappa$, but I do not think they can be expected to hold when $\nu \gg \kappa$. When $\nu \gg \kappa$, the effect of viscosity on the **u**-spectrum becomes important at wave-numbers lower than those at which conduction first affects the θ-spectrum, and so the θ-spectrum is dominated by convection processes at wave-numbers up to and beyond the largest wave-number for which (2.5) is valid. There is a limitation in Obukhoff's argument inasmuch as he assumes that (2.4) is valid for *all* wave-numbers less than that at which conduction becomes important (expressed as contiguity of the ranges for which (2.6) and (2.7) are valid); this is not likely to be a valid assumption when $\nu \gg \kappa$, because the neglect of ν in the dimensional argument on which (2.4) was based is not then permissible for the higher wave-numbers in this range. Corrsin's argument is limited in effectively the same way, in that he employs (2.5) to evaluate the Péclet number appropriate to Fourier

components for wave-numbers which, when $\nu \gg \kappa$, are so large as to be beyond the range for which the inertial subrange relation (2.5) is valid.

In another paper which is relevant in this connexion (Batchelor 1952), the effect of molecular diffusion on the distribution of θ was regarded as a kind of perturbation of the effect of convection. When κ is zero, the surfaces of constant θ move as material surfaces and convective extension of these surfaces, with consequent decrease of their distance apart, leads to an increase in $\overline{(\nabla\theta)^2}$ at an (asymptotic) rate of order $\overline{(\boldsymbol{\omega}^2)^{\frac{1}{2}}}\,\overline{(\nabla\theta)^2}$ (where $\overline{(\boldsymbol{\omega}^2)^{\frac{1}{2}}}$ is the root-mean-square vorticity and is a measure of the mean rate of extension of material lines). If now a small molecular diffusivity is introduced, and if the effect of convection is not changed in form by the existence of the conduction, the value of $\overline{(\nabla\theta)^2}$ can be stationary only if the two terms in the expression for the rate of change of $\overline{(\nabla\theta)^2}$ (obtained in the usual way from (1.1)), namely,

$$\overline{(\boldsymbol{\omega}^2)^{\frac{1}{2}}}\,\overline{(\nabla\theta)^2} \quad \text{and} \quad \kappa\overline{(\nabla\theta).\nabla(\nabla^2\theta)},$$

are of the same order. On assuming that the values of these two weighted integrals of the θ-spectrum are determined by the wave-number at which the spectrum begins to fall off very rapidly as a result of conduction effects, we find that this wave-number must be of order $\overline{(\boldsymbol{\omega}^2)^{\frac{1}{4}}}/\kappa^{\frac{1}{2}}$, that is, of order $(\epsilon/\nu\kappa^2)^{\frac{1}{4}}$.

There is an apparent disagreement between this result and that obtained by Obukhoff and Corrsin, and at the time when my own paper was written I thought the conflict was real. However, I see now*—and the work to be described in the following sections will amplify the explanation—that each result is correct in its own context. Obukhoff and Corrsin found that conduction effects cut off the θ-spectrum at a wave-number of order $(\epsilon/\kappa^3)^{\frac{1}{4}}$; in finding this expression for the cut-off wave-number they assumed that one or other of the relations (2.4) and (2.5) is valid up to this cut-off wave-number, and, as shown above, this is likely to be permissible only when $\nu \ll \kappa$ or when ν/κ is of order unity. My work, on the other hand, assumes that the mechanics of the convection process is not changed by the existence of conduction and, in particular, that the distance between surfaces of constant θ is decreased by convection at a rate which is of the same order as that for material surfaces; this will be valid, when applied to a consideration of particular Fourier components of the θ-distribution, only when the wave-numbers concerned lie beyond the range in which the stretching effect of the velocity field lies, that is, only when the conduction cut-off of the θ-spectrum lies well beyond the viscous cut-off of the $\mathbf{u}$-spectrum, that is, finally, only when $\kappa \ll \nu$. The two different expressions for the wave-number at which the conduction cut-off occurs reduce to the same form when ν/κ is of order unity.

The position, as now seen after this discussion of previous work, is briefly as follows. With the usual proviso that the Reynolds number of the turbulence is large, it may be expected that the θ-spectrum has a form depending only on ϵ, χ, ν and κ in the equilibrium range specified by the condition $n \gg L^{-1}$. Provided κ and ν are both so small that some of the Fourier components of θ and $\mathbf{u}$ in this range are unaffected by conduction and viscous forces respectively, the

* Helped by some valuable discussions with Mr I. D. Howells.

θ-spectrum has the form (2.4) for $n \gg L^{-1}$ and n small compared with some wave-number which depends on the ratio ν/κ. When $\nu \ll \kappa$, the convection subrange is not as extensive as the inertial subrange and is specified by $L^{-1} \ll n \ll (\epsilon/\kappa^3)^{\frac{1}{4}}$. When ν/κ is of order unity, the convection and inertial subranges may be expected to be of comparable extent and to be specified by $L^{-1} \ll n \ll (\epsilon/\nu^3)^{\frac{1}{4}}$. In both these cases the θ-spectrum falls off more rapidly than as $n^{-\frac{5}{3}}$ at the end of the convection subrange as a consequence of conduction becoming important. When $\nu \gg \kappa$, convection effects dominate the θ-spectrum at wave-numbers beyond the inertial subrange and conduction does not become important until wave-numbers of order $(\epsilon/\nu\kappa^2)^{\frac{1}{4}}$ are reached; thus in this case there are two distinct parts to the convection subrange. In the part at the lower wave-number end, in convection subrange A say, specified by $L^{-1} \ll n \ll (\epsilon/\nu^3)^{\frac{1}{4}}$, the relations (2.5) and (2.4) hold; at the higher wave-number end, in convection subrange B specified by

$$(\epsilon/\nu^3)^{\frac{1}{4}} \ll n \ll (\epsilon/\nu\kappa^2)^{\frac{1}{4}},$$

neither (2.5) nor (2.4) holds because viscosity has an effect on the **u**-spectrum.

Part of the purpose of this paper is to review past work, to clear up some real and apparent conflicts and to assess the conditions under which the available results may be expected to be valid; this has now been done. The other intention is to complete the picture just described by obtaining expressions for the θ-spectrum in ranges where none is available.

3. The cases $\nu \ll \kappa$ and ν/κ is of order unity

When $\nu \ll \kappa$, the θ-spectrum has the form (2.4) over the entire convection subrange, and begins to fall off more rapidly at wave-numbers near $(\epsilon/\kappa^3)^{\frac{1}{4}}$ as a result of the effect of conduction. The remaining problem here is to determine the shape of the θ-spectrum in the neighbourhood of, and beyond, the conduction cut-off wave-number $(\epsilon/\kappa^3)^{\frac{1}{4}}$, and in particular to ascertain whether the cut-off is sharp. For many purposes it will be sufficient to know merely that the θ-spectrum begins to fall off more rapidly than as $n^{-\frac{5}{3}}$ when n is of order $(\epsilon/\kappa^3)^{\frac{1}{4}}$, but for other purposes (for example, the calculation of high-order integral moments of the θ-spectrum) more precise information about the spectrum will be useful. In Part 2 of this paper a specific mechanism for the effect of the velocity distribution on the Fourier components of θ is proposed, and from it the unknown form of the θ-spectrum at wave-numbers beyond the conduction cut-off is determined; no further reference to the case $\nu \ll \kappa$ will be made here.

When κ is not very different from ν, the convection and inertial subranges both terminate at wave-numbers near $(\epsilon/\nu^3)^{\frac{1}{4}}$, and it is known that the **u**-spectrum subsequently falls off sharply owing to the effect of viscosity. The exact forms of the two spectra in the neighbourhood of this cut-off wave-number are not known, and may be different. It is possible that some exact relation between the two spectra exists for the special case $\nu = \kappa$; however, it does not matter much if the precise form of $\Gamma(n)$ near $n = (\epsilon/\nu^3)^{\frac{1}{4}}$ is not known, since the coincidence of conduction and viscosity effects in this neighbourhood makes it virtually certain that the cut-off of the θ-spectrum is sharp (and, in all probability, sharp enough to make integral moments of $\Gamma(n)$ of all orders converge).

4. The case $\nu \gg \kappa$: Lagrangian analysis in terms of Fourier components

When $\nu \gg \kappa$, the convection subrange is more extensive than the inertial subrange, and, as explained in §2, consists of two distinct parts. In the part defined by $L^{-1} \ll n \ll (\epsilon/\nu^3)^{\frac{1}{4}}$, the result (2.4) holds. In the part defined by $(\epsilon/\nu^3)^{\frac{1}{4}} \ll n \ll (\epsilon/\nu\kappa^2)^{\frac{1}{4}}$, which is a range of wave-numbers lying beyond the viscous cut-off of the **u**-spectrum, the shape of the θ-spectrum is affected indirectly by viscosity, in a manner to be established here. It turns out to be possible to do more than this and to find the form of $\Gamma(n)$ for all $n \gg (\epsilon/\nu^3)^{\frac{1}{4}}$, that is, for a range embracing the convection subrange B and higher wave-numbers at which conduction effects are important.

The essential fact underlying the analysis that follows is that the spatial rate of change of the fluid velocity is approximately uniform over regions with linear dimensions not much smaller than $(\nu^3/\epsilon)^{\frac{1}{4}}$. In the inertial subrange the spectrum of $\partial u_i/\partial x_j$ rises slowly (as $n^{\frac{1}{3}}$), reaching a maximum near the wave-number $(\epsilon/\nu^3)^{\frac{1}{4}}$, and falls off sharply at higher wave-numbers, so that wave-numbers less than $(\epsilon/\nu^3)^{\frac{1}{4}}$ make a dominant contribution to the area under this spectrum curve. As more direct evidence, it can readily be calculated from the equation for the balance of mean-square vorticity, using the hypotheses of Kolmogoroff's theory and with an empirical value of about $-0{\cdot}3$ for the skewness factor of $\partial u_1/\partial x_1$, that

$$\overline{\left(\frac{\partial u_i'}{\partial x_j'}-\frac{\partial u_i}{\partial x_j}\right)^2}\Big/\overline{\left(\frac{\partial u_k}{\partial x_l}\right)^2} \approx 0{\cdot}03\,\frac{r^2}{(\nu^3/\epsilon)^{\frac{1}{2}}} \tag{4.1}$$

(the repeated indices on the left being summed) for small values of r; this shows that r does not need to be much less than $(\nu^3/\epsilon)^{\frac{1}{4}}$ for the velocity gradient to be approximately uniform over a region of linear dimensions r. If now we imagine a material element of fluid of linear dimensions somewhat less than $(\nu^3/\epsilon)^{\frac{1}{4}}$ to be chosen and followed in its motion, the internal distortion of this element, and of any distribution of θ contained in it, will be at any instant approximately a pure straining motion.

Theoretical work does not yet seem to have thrown any light on the degree of persistence of this straining motion, but Townsend (1951*b*) has made some valuable inferences from observations of the rate at which the temperature of small hot fluid elements decreases owing to the combined effect of convective distortion and conduction. He finds that the local straining motion is remarkably persistent, and that the time-scale of change of the principal rates of strain and of change of the directions, relative to the fluid, of the principal axes of the straining motion, is large compared with $(\nu/\epsilon)^{\frac{1}{2}}$ (largeness here presumably implying variation as some positive fractional power of the Reynolds number of the turbulence), this latter quantity being the only one with the dimensions of time which can be formed from the parameters determining the equilibrium range of the **u**-spectrum. That the principal axes of the rate of strain rotate only slowly relative to the fluid is also suggested by pictures of the position of portions of marked fluid at different instants, like those for two-dimensional motion published by Welander (1955); on the whole, the marked fluid is drawn out into long thin

streaks, of ever-increasing length, which do not show the small-scale wriggles and rapid variations in curvature that would result from local rotation of the principal axes of rate of strain relative to the fluid and from consequent local rotation of a small part of the streak relative to the remainder. (It is possible that this persistence of the stretching of a material line is no more than a reflexion of the fact that material lines tend to set themselves in the direction of the greatest local principal rate of strain (Batchelor 1952), and that if the principal axis of greatest rate of strain should rotate relative to the fluid, the material line with which it coincided initially would automatically turn and tend to align itself with the new direction of the principal axis of greatest rate of strain.) The conclusion, to be adopted here, is that the effect of convection on the spatial distribution of θ within a material element of suitably small size is approximately the same as that of a pure straining motion of constant magnitude and form relative to the fluid, so far as temporal changes of the distribution of θ on a time scale of order $(\nu/\epsilon)^{\frac{1}{2}}$ are concerned.

This picture of the convective distortion of small elements of the fluid has been used by Townsend (1951*a*) in a theory of the form of the **u**-spectrum at very large wave-numbers, and by Batchelor (1952; see also the review by Batchelor & Townsend 1956) in a discussion of the way in which material line elements in the fluid are extended and material surface elements are increased in area. The use to which it will be put in this and the following section has links with both of these earlier investigations, although there are also some new features.

The basic idea of the investigation is to make use of the linearity of the equation (1.1) for θ and to examine the effect of both convection and conduction on each Fourier component of the θ-distribution, the Fourier analysis being carried out with respect to axes which move with the fluid locally in translation and rotation and which in effect are distorted with the fluid locally. We consider any material element of fluid with linear dimensions somewhat less than $(\nu^3/\epsilon)^{\frac{1}{4}}$ and resolve the instantaneous distribution of θ within this element into its Fourier components. This material element moves in translation and rotation and is subjected to a pure straining distortion, and at the end of a finite time it will have a different position and orientation and will have experienced a finite pure strain. Only the straining of the element affects the distribution of θ within the element, and this straining will be regarded as representative of the effect of fluid convection on the Fourier components of θ with wave-numbers large compared with $(\epsilon/\nu^3)^{\frac{1}{4}}$. Of course, the way in which the distribution of θ is continued beyond the material element and joins up with other material elements which are being translated, rotated and strained also has an influence on Fourier components of θ, but this influence may be expected to be important only for components with wave-numbers of order $(\epsilon/\nu^3)^{\frac{1}{4}}$ or less (since $(\nu^3/\epsilon)^{\frac{1}{4}}$ is the characteristic length-scale for spatial variations of the rotational and straining motions).

Consider first the changes in an initially sinusoidal variation of θ throughout the material element. We choose Cartesian axes which translate with the element and which are always principal axes of the rate of strain of the element. According to the approximation explained above, these axes are fixed in the fluid, and the

principal rates of strain α, β, γ are constant, for time intervals at least as large as $(\nu/\epsilon)^{\frac{1}{2}}$. Then, the distribution of θ is governed by the equation

$$\frac{\partial\theta}{\partial t}+\alpha x\frac{\partial\theta}{\partial x}+\beta y\frac{\partial\theta}{\partial y}+\gamma z\frac{\partial\theta}{\partial z}=\kappa\nabla^2\theta, \tag{4.2}$$

and the initial condition is $\theta = A_0\sin(\mathbf{l}.\mathbf{x})$ at $t = 0$. This equation is satisfied by

$$\theta(\mathbf{x}, t) = A(t)\sin[\mathbf{m}(t).\mathbf{x}], \tag{4.3}$$

with

$$\frac{dA}{dt}=-\kappa m^2 A,$$

$$\frac{dm_1}{dt}=-\alpha m_1,\quad \frac{dm_2}{dt}=-\beta m_2,\quad \frac{dm_3}{dt}=-\gamma m_3,$$

where m_1, m_2, m_3 are components of $\mathbf{m}$. Thus the solution is

$$\theta(\mathbf{x}, t) = A_0\exp\left[\frac{\kappa}{2\alpha}(m_1^2-l_1^2)+\frac{\kappa}{2\beta}(m_2^2-l_2^2)+\frac{\kappa}{2\gamma}(m_3^2-l_3^2)\right]\sin(\mathbf{m}.\mathbf{x}), \tag{4.4}$$

in which

$$m_1 = l_1 e^{-\alpha t},\quad m_2 = l_2 e^{-\beta t},\quad m_3 = l_3 e^{-\gamma t}. \tag{4.5}$$

The planes of constant θ are turned so that the direction of their normal approaches asymptotically the direction of the greatest rate of contraction in the fluid, and, if $\alpha > \beta > \gamma$ (which implies $\alpha > 0$, $\gamma < 0$, since $\alpha+\beta+\gamma = 0$ by the continuity equation) we have

$$m^2 = m_1^2+m_2^2+m_3^2 \to l_3^2 e^{-2\gamma t},\quad \theta \to A_0\exp\left(\frac{\kappa m^2}{2\gamma}\right)\sin(\mathbf{m}.\mathbf{x}) \tag{4.6}$$

(provided $l_3 \neq 0$) as $t \to \infty$. The duration of time for which the principal axes of strain remain fixed relative to the fluid and α, β, γ remain constant is limited, but these asymptotic relations become quite accurate long before $t = 10/|\gamma|$ (except for certain special choices of l_2, l_3 and β/γ) and since $|\gamma|$ is of order $(\epsilon/\nu)^{\frac{1}{2}}$ the use of the asymptotic relations as being *typical* of what is happening to Fourier components of θ is consistent with the approximation described above.

All Fourier components of the initial distribution of θ in the material element will be changed in this way, and the distribution of θ at a time t subsequent to the initial instant can be obtained by superimposing the changed Fourier components. The distribution of θ tends towards a one-dimensional form with variation only in the direction of the principal axis of least rate of strain. Gradients of θ in the z-direction are made steeper by the convection process (by crests of the distribution being squeezed together), but are simultaneously made more gradual by conduction effects, and ultimately all the variation of θ is erased by conduction. However, it will be noticed that the smaller the value of κ, the longer is the time required for erasure of the variations of θ and the greater are the gradients of θ which are built up in the meantime.

This information about the way in which the convective distortion converts a Fourier component of certain wave-number into one of larger wave-number, the magnitude of the coefficient being diminished meanwhile by conduction, can now be used to find an expression for the steady θ-spectrum at wave-numbers large

compared with $(\epsilon/\nu^3)^{\frac{1}{4}}$. This is made possible by the fact that the convective modulation of Fourier components of the θ-distribution is entirely one-way as soon as the process of alignment of the wave-number vectors is nearly complete; $\overline{\theta^2}$-stuff is transferred wholly to components of larger wave-number. In the neighbourhood of the small wave-number end of the range in which the above approximations about the effect of the velocity field on Fourier components of θ are valid, this end being given by wave-number magnitude n_0 say, we may suppose that the level of the θ-spectrum is kept constant by a continual supply of $\overline{\theta^2}$-stuff from lower wave-numbers (the exact mechanism of this supply being irrelevant at the moment). The Fourier components with wave-numbers larger than n_0 are derived from those at smaller wave-number by the straining process, and the asymptotic relations (4.6) show that the $\overline{\theta^2}$-stuff which is spread over the wave-number range dn', at a wave-number (magnitude) n' at which the alignment of the wave-number vectors is nearly complete, is spread over the range $n\,dn'/n'$ at a later stage at which the Fourier component with wave-number n' has been distorted to that with wave-number n, and that during the time required for this change this amount of $\overline{\theta^2}$-stuff is reduced, at those places in the fluid where the least principal rate of strain has the value γ, by the factor $\exp[\kappa(n^2-n'^2)/\gamma]$ owing to the action of conduction. The principal rates of strain will not be uniform throughout the fluid, so we are obliged to assume that γ is an effective average value of the least principal rate of strain. The constant level of the θ-spectrum at wave-numbers well above n_0 is then given by

$$\Gamma(n)\frac{n}{n'}dn' = \Gamma(n')\,dn'\exp\left[\frac{\kappa}{\gamma}(n^2-n'^2)\right],$$

that is,

$$\Gamma(n) \propto \frac{1}{n}\exp\left(\frac{\kappa}{\gamma}n^2\right); \tag{4.7}*$$

the θ-spectrum is also isotropic at these wave-numbers in view of the isotropic distribution of the straining motion.

The dimensional factors in the constant of proportionality in (4.7) can be obtained by noticing that when $n \ll (-\gamma/\kappa)^{\frac{1}{2}}$—and such values of n can exist when κ/ν is sufficiently small, notwithstanding the existing restrictions on n—the exponential factor is approximately constant and $\Gamma(n) \propto n^{-1}$. At these values of n the effects of conduction are unimportant and the decrease of Γ with n is due entirely to the spreading of $\overline{\theta^2}$-stuff over a wider wave-number range by convective straining. The only parameters relevant to the form of $\Gamma(n)$ are then χ

* For simplicity this relation has been obtained from a consideration of the changes occurring in one Fourier component whose wave-number vector becomes aligned with the direction of the greatest rate of compression. There are, of course, some wave-number vectors which take a long time to become aligned (namely, those for which l_3 is small in (4.5)), and it is desirable to verify that the relation (4.7) is not affected by these untypical Fourier components. It is readily established, in fact, that if a continuous isotropic θ-spectrum with most of the $\overline{\theta^2}$-stuff at wave-numbers with magnitudes near n_0 is maintained by transfer from smaller wave-numbers, the steady spectrum produced at much larger wave-numbers by combined convective straining and conduction has the form (4.7), except in the particular case in which $\beta = \gamma$, when the form is different at wave-numbers of order $(-\gamma/\kappa)^{\frac{1}{2}}$.

and γ, and the dimensional part of the proportionality constant is thus χ/γ. Furthermore, the numerical part must have the value -1 in order that (4.7) should be consistent with the identity

$$\int_0^\infty n^2\Gamma(n)dn = \frac{\chi}{2\kappa}.$$

Several estimates of the average value of the least principal rate of strain in the fluid have been made (Batchelor & Townsend 1956), and they are all in the neighbourhood of $-0{\cdot}5(\epsilon/\nu)^{\frac{1}{2}}$. The final expression for the θ-spectrum in the wave-number range $n \gg (\epsilon/\nu^3)^{\frac{1}{4}}$ is therefore

$$\Gamma(n) = -\frac{\chi}{\gamma n}\exp\left(\frac{\kappa n^2}{\gamma}\right), \quad \text{with} \quad \gamma \approx -0{\cdot}5\left(\frac{\epsilon}{\nu}\right)^{\frac{1}{2}}. \tag{4.8}$$

According to this relation, in the wave-number range designated earlier as convection subrange B and specified by $(\epsilon/\nu^3)^{\frac{1}{4}} \ll n \ll (\epsilon/\nu\kappa^2)^{\frac{1}{4}}$, the θ-spectrum is given by

$$\Gamma(n) \approx -\frac{\chi}{\gamma n}. \tag{4.9}$$

It is worth noting that this latter relation could have been predicted (apart from a numerical constant) on dimensional grounds right at the beginning, provided the thesis adopted here, that the primary effect of the convection on variations of θ on a length-scale small compared with $(\nu^3/\epsilon)^{\frac{1}{4}}$ is a uniform straining at a rate of order $(\epsilon/\nu)^{\frac{1}{2}}$, be granted. The parameters in the constant of proportionality in (4.9) are consistent with the need for the relation (4.9) to join smoothly on to the relation (2.4) at lower wave-numbers; for the join occurs at values of n near $(\epsilon/\nu^3)^{\frac{1}{4}}$, when both relations show Γ to be of order $\chi\nu^{\frac{5}{4}}\epsilon^{-\frac{3}{4}}$.

The relation (4.9) describes a comparatively slow rate of decrease of θ as n increases, even slower than that holding at smaller wave-numbers in convection subrange A. The rate of decrease is so slow that $\int_0^n \Gamma(n)dn$ does not converge, as $n \to \infty$, for a fluid such that $\kappa = 0$—which is to be interpreted as meaning that, in a fluid with a very small value of κ/ν, a statistically steady state for the small-scale components of the θ-distribution can be set up only if there is a sufficiently large reservoir of $\overline{\theta^2}$-stuff in the large-scale components of θ and if sufficient time is available. The amount of $\overline{\theta^2}$-stuff in convection subrange B, as given by (4.9), is of order

$$-\frac{\chi}{2\gamma}\log\frac{\nu}{\kappa}, \tag{4.10}$$

and this may be larger than the amount in the large-scale components of θ without violating in any way the assumptions on which the analysis is based (although $\overline{\theta^2}$ would then not be a measure of the $\overline{\theta^2}$-stuff associated with Fourier components with wave-numbers of order L^{-1}). The time required for a stationary state to be set up over convection subrange B can be estimated from the time required for a Fourier component of θ with wave-number of order $(\epsilon/\nu^3)^{\frac{1}{4}}$ to be

deformed by the straining process into one with wave-number of order $(\epsilon/\nu\kappa^2)^{\frac{1}{4}}$ and is

$$-\frac{1}{\gamma}\log\frac{\nu}{\kappa}$$

(in agreement with (4.10) in view of the definition of χ), and this may be larger than the time scale of the large-scale components of θ again without inconsistency.

The relation (4.9) can also be interpreted in terms of the formation of steep spatial gradients of θ in the fluid. If $|\nabla\theta|$ became infinite (or as near infinite as the small conductivity allowed) at a finite number of points in unit volume of the fluid as a result of the effect of convection, $\Gamma(n)$ would vary as n^{-2}. The divergence of $\overline{(\nabla\theta)^2}$ as given by (4.9) is stronger than this, corresponding to the fact that convection actually steepens the gradient of θ, and does so persistently, throughout typical material elements of fluid; large values of $|\nabla\theta|$ thus appear, not at isolated points, but over a finite fraction of the whole fluid.

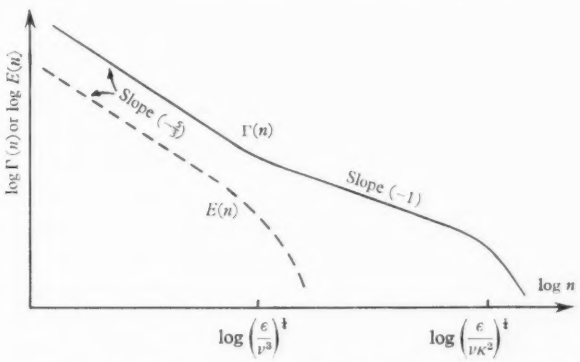

FIGURE 1. Spectra of θ and $\mathbf{u}$ in the equilibrium range of wave-numbers for the case $\nu \gg \kappa$.

The conduction cut-off given by (4.8) is sharp, and occurs, as expected, at wave-numbers of order $(\epsilon/\nu\kappa^2)^{\frac{1}{4}}$. The available information about $\Gamma(n)$ in the equilibrium range in the case $\nu \gg \kappa$ is shown schematically in figure 1. Finally, it is worth noting that these results about the form of $\Gamma(n)$ beyond the viscous cut-off wave-number do not require the Reynolds number of the turbulence to be so large that an inertial subrange exists. Whatever the Reynolds number of the turbulence, the distortion of sufficiently small material elements of fluid will be approximately a pure straining motion. Thus the first part of the relation (4.8) will still hold, although the estimate of the straining rate γ may not be accurate at low Reynolds number.

5. The case $\nu \gg \kappa$: Eulerian analysis in terms of correlations

Inasmuch as the analysis presented in the preceding section contains some novel features and may not carry immediate conviction, it may be useful to show how the same results can be obtained in a quite different way from essentially the same assumptions about the effect of the fluid motion on small-scale features of

the θ-distribution. This time the analysis involves mean values of products of θ and $\mathbf{u}$, and is rather more direct, although the character of the action of convection on the θ-distribution is not revealed so explicitly.

The expression for rate of change of the temperature covariance is readily found from (1.1) to be

$$\frac{\partial \overline{\theta\theta'}}{\partial t} = \frac{\partial}{\partial r_i}\overline{(u_i\theta\theta' - u_i'\theta\theta')} + 2\kappa\nabla^2\overline{\theta\theta'}, \tag{5.1}$$

where θ' is written for $\theta(\mathbf{x}+\mathbf{r}, t)$, and statistical homogeneity of θ and $\mathbf{u}$ has been assumed (as is appropriate for the small-scale features of their spatial distributions). When the distance r between the points to which θ, $\mathbf{u}$ and θ', $\mathbf{u}'$ refer is sufficiently small, we have

$$u_i' \approx u_i + r_j\frac{\partial u_i}{\partial x_j}, \tag{5.2}$$

the restriction on r being that it should be somewhat less than $(\nu^3/\epsilon)^{\frac{1}{4}}$ as established in the paragraph containing (4.1). Moreover, in accordance with the description of the convection process given in the preceding section for this same case $\nu \gg \kappa$, there are some values or r, at the upper end of this range, for which $\theta' - \theta$ is not linear in r because the θ-distribution has a finer structure than the $\mathbf{u}$-distribution. We shall therefore employ the approximation (5.2) in (5.1), without introducing a similar approximation for $\theta' - \theta$. Also, we shall approximate the left-hand side of (5.1) by $-\chi$, on the understanding (and in view of the results obtained in §4, there is need for care in the wording here) that we are investigating a distribution of θ which is stationary so far as the small-scale components are concerned and that the rate at which $\overline{\theta^2}$ and $\overline{\theta\theta'}$ are decreasing is due entirely to a decrease of $\overline{\theta^2}$-stuff in the large-scale components with length-scale L at a rate χ (or equivalently that $\overline{\theta^2}$-stuff is being supplied to these large-scale components at a rate χ in a case in which the whole of the θ-distribution is statistically stationary). Equation (5.1) then becomes

$$\begin{aligned} -\chi &= -r_j\frac{\partial \overline{u_i}}{\partial x_j}\frac{\partial \overline{\theta\theta'}}{\partial r_i} + 2\kappa\nabla^2\overline{\theta\theta'} \\ &= \tfrac{1}{2}(\mathbf{r}.\nabla\mathbf{u}).\nabla\overline{(\theta-\theta')^2} - \kappa\nabla^2\overline{(\theta-\theta')^2}. \end{aligned} \tag{5.3}$$

where ∇ is everywhere a gradient with respect to $\mathbf{r}$ alone, $\mathbf{x}$ being held constant where necessary.

The next step in the argument is to approximate to the first term on the right-hand side of (5.3), with the help of hypotheses about the persistence of the extension of material surfaces as in §4. The effect of the uniform straining motion which exists everywhere in the neighbourhood of a material point in the fluid is to turn the local surfaces of constant θ so that the directions of their normals approach that of the least principal rate of strain. Provided the material surfaces on which θ is constant continue to be extended—that is, provided the angle between the normal to the surfaces of constant θ and the direction of the least principal rate of strain continues to be small—for a time long compared with $(\nu/\epsilon)^{\frac{1}{2}}$ (which is the time characteristic of the straining motion and which is therefore a measure of the

time required for approximate alignment of the normals to the surfaces of constant θ), as is believed to be so on the basis of the evidence discussed in the preceding section, the direction of $\nabla(\theta-\theta')^2$ at each point of the fluid and at all times will tend to be aligned in the direction of the local least principal rate of strain. Of the two contributions to $\mathbf{r}.\nabla\mathbf{u}$, one from rigid rotation of the fluid about the point $\mathbf{x}$ and one from the pure straining motion, only the latter is related statistically to the distribution of θ. The contribution to $\mathbf{r}.\nabla\mathbf{u}$ from the pure straining motion has a component in the direction of the least principal rate of strain equal to $r\gamma\cos\phi$, where ϕ is the angle between $\mathbf{r}$ and the principal axis of least rate of strain.

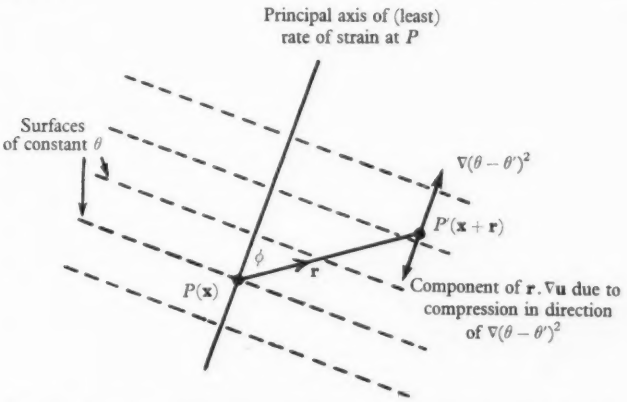

FIGURE 2. To illustrate the uniform straining motion near P and its effect on the distribution of θ.

Thus, if we assume that the process of orientation of $\nabla(\theta-\theta')^2$ along a principal axis of rate of strain is complete at all times and positions, as illustrated in figure 2, and that the fluctuations in γ are a negligible fraction of the mean value, we have

$$\overline{(\mathbf{r}.\nabla\mathbf{u}).\nabla(\theta-\theta')^2} = r\gamma\cos\phi\,\overline{|\nabla(\theta-\theta')^2|} = \gamma r\frac{\partial\overline{(\theta-\theta')^2}}{\partial r}. \tag{5.4}$$

These two assumptions are over-simplifications, so that, as in §4, γ must be regarded as an effective average value of the least principal rate of strain. The equation (5.3) for the covariance of θ now becomes

$$-\chi = \tfrac{1}{2}\gamma r\frac{\partial\overline{(\theta-\theta')^2}}{\partial r} - \kappa\left(\frac{\partial^2}{\partial r^2}+\frac{1}{r}\frac{\partial}{\partial r}\right)\overline{(\theta-\theta')^2}, \tag{5.5}$$

that is,
$$\frac{\chi}{\kappa}r^2\exp\left(-\frac{\gamma r^2}{4\kappa}\right) = \frac{\partial}{\partial r}\left[r^2\frac{\partial\overline{(\theta-\theta')^2}}{\partial r}\exp\left(-\frac{\gamma r^2}{4\kappa}\right)\right].$$

One integration gives

$$\frac{\partial\overline{(\theta-\theta')^2}}{\partial r} = \frac{\chi}{\kappa r^2}\exp\left(\frac{\gamma r^2}{4\kappa}\right)\int_0^r r^2\exp\left(-\frac{\gamma r^2}{4\kappa}\right)dr,$$

and, from a second,

$$\overline{(\theta-\theta')^2} = \frac{2\chi}{\gamma}\int_0^r\left[-\frac{1}{r}+\frac{1}{r^2}\exp\left(\frac{\gamma r^2}{4\kappa}\right)\int_0^r\exp\left(-\frac{\gamma r^2}{4\kappa}\right)dr\right]dr. \tag{5.6}$$

When $r^2 \ll 4\kappa/|\gamma|$, this relation reduces to

$$\overline{(\theta-\theta')^2} \approx \frac{\chi}{6\kappa}r^2, \tag{5.7}$$

as is required by the definition of χ (see (2.3)). At the other extreme, when $r^2 \gg 4\kappa/|\gamma|$ (although r must continue to be suitably small), we have

$$\overline{(\theta-\theta')^2} \sim -\frac{\chi}{\gamma}\log\left(-\frac{\gamma r^2}{\kappa}\right). \tag{5.8}$$

As in §4, γ can be replaced by its estimated value $-0{\cdot}5(\epsilon/\nu)^{\frac{1}{2}}$, in which case the asymptotic relation (5.8) becomes

$$\overline{(\theta-\theta')^2} \sim \chi\left(\frac{\nu}{\epsilon}\right)^{\frac{1}{2}}\log\left(\frac{\epsilon r^4}{\nu\kappa^2}\right), \tag{5.9}$$

valid for $(\nu^3/\epsilon)^{\frac{1}{4}} > r \gg (\nu\kappa^2/\epsilon)^{\frac{1}{4}}$. This logarithmic form for $\overline{(\theta-\theta')^2}$ lies between the parabolic form (5.7) in the immediate neighbourhood of the origin and a variation as $r^{\frac{2}{3}}$ at values of r such that $L \gg r \gg (\nu^3/\epsilon)^{\frac{1}{4}}$.

It remains to show that the result (5.8) is effectively the same as (4.8). This can be done by beginning with the identity (see (2.1))

$$\begin{aligned}\overline{(\theta-\theta')^2} &= \frac{1}{2\pi}\int\frac{\Gamma(n)}{n^2}(1-e^{-i\mathbf{n}.\mathbf{r}})d\mathbf{n}\\ &= 2\int_0^\infty\Gamma(n)\left(1-\frac{\sin nr}{nr}\right)dn.\end{aligned}$$

On substituting for $\Gamma(n)$ from (4.8), we find

$$\begin{aligned}\frac{\partial\overline{(\theta-\theta')^2}}{\partial r} &= \frac{2\chi}{\gamma}\int_0^\infty\exp\left(\frac{\kappa n^2}{\gamma}\right)\left(\frac{\cos nr}{nr}-\frac{\sin nr}{n^2r^2}\right)dn\\ &= \frac{2\chi}{\gamma}\left[-\frac{1}{r}-\frac{2\kappa}{\gamma r^2}\int_0^\infty\exp\left(\frac{\kappa n^2}{\gamma}\right)\sin nr\,dn\right]\\ &= \frac{2\chi}{\gamma}\left[-\frac{1}{r}+\frac{i\kappa}{\gamma r^2}\exp\left(\frac{\gamma r^2}{4\kappa}\right)\int_0^\infty\left\{\exp\frac{\kappa}{\gamma}\left(n+\frac{ir\gamma}{2\kappa}\right)^2-\exp\frac{\kappa}{\gamma}\left(n-\frac{ir\gamma}{2\kappa}\right)^2\right\}dn\right]\\ &= \frac{2\chi}{\gamma}\left[-\frac{1}{r}+\frac{1}{r^2}\exp\left(\frac{\gamma r^2}{4\kappa}\right)\int_0^r\exp\left(-\frac{\gamma r^2}{4\kappa}\right)dr\right],\end{aligned}$$

thus reproducing (5.6).

6. Comments on a different model of small-scale variations of θ in the case $\nu \gg \kappa$

In his theory of the form of the energy spectrum at very large wave-numbers, Townsend (1951*a*) made use of the same notion that the action of the whole

flow field on small-scale variations of any quantity—vorticity, in his case—is primarily to impose a uniform persistent straining motion. The action of a steady uniform rate of strain on weak variation of vorticity is to increase the gradient of the perturbation vorticity in the direction of the least principal rate of strain and to amplify the component of vorticity in the direction of the greatest principal rate of strain; this latter effect due to stretching of vortex lines is absent in the case of scalar quantities like temperature, but there is otherwise a fairly close analogy between the two cases. Townsend made a further assumption in his work on vorticity, and this has not been employed in the preceding discussion of the θ-spectrum for the case $\nu \gg \kappa$. Since the reasons for not using this extra assumption are not self-evident, and since they throw an interesting light on the nature of the assumption, a brief comparison of the foregoing results with the form they would take with an additional assumption like Townsend's will be given.

Guided by the observation that small-scale variations of vorticity seem to have an uneven spatial distribution, some parts of the fluid being relatively free from such variations, Townsend put an intermittent variation into his model by assuming that small-scale variations of vorticity exist mainly as isolated steady vortex sheets or 'line vortices' of small thickness. Each of these sheets or lines is steady under the opposing actions of molecular diffusion and stretching of vortex lines (the occurrence of two positive principal rates of strain giving rise to a vortex sheet, and one positive principal rate of strain to a line vortex, the former being the more probable), and the variations of vorticity on length scales small compared with $(\nu^3/\epsilon)^{\frac{1}{4}}$ were supposed to occur in the form of a random distribution of such sheets or lines. The sheets or lines were assumed to be separated by distances large compared with their thickness (which is of order $(\nu/|\gamma|)^{\frac{1}{2}}$), so that amalgamation of sheets or lines which are swept together by the straining motion happens only infrequently. The steady distribution of vorticity in a sheet or line can readily be calculated in terms of the principal rates of strain and so the spectrum of vorticity, and thence of velocity, can be determined at large wave-numbers. There is an arbitrary multiplicative constant in the resulting vorticity spectrum, representing the product of the number of sheets or lines per unit volume and their strength; the value of this constant is determined by the way in which inertia forces generate vorticity perturbations on a larger length-scale and lies outside the scope of the theory.

In exactly the same way one could assume that variations of θ on a small scale occur as randomly distributed, isolated, thin layers in which the distribution of θ is steady under the combined actions of molecular diffusion and uniform straining. Just as a uniform straining motion with one negative principal rate of strain (γ) converts (asymptotically) an arbitrary transition between two regions of uniform (and different) perturbation velocity into a steady vortex sheet of thickness of order $(\nu/|\gamma|)^{\frac{1}{2}}$, so it converts an arbitrary transition between two regions of uniform θ into a layer in which the steady distribution of θ is given by

$$\frac{\partial\theta}{\partial x} = \frac{\partial\theta}{\partial y} = 0, \quad \frac{\partial\theta}{\partial z} = \left(-\frac{\gamma}{2\pi\kappa}\right)^{\frac{1}{2}} A \exp\left(\frac{\gamma z^2}{2\kappa}\right), \tag{6.1}$$

A being a constant measuring the size of the jump in θ across the layer. The spectrum of θ for an array of such layers throughout the fluid, random with respect to both position and orientation, then follows as

$$\Gamma(n) = \frac{\chi}{(-\pi\gamma\kappa)^{\frac{1}{2}}} \frac{1}{n^2} \exp\left(\frac{\kappa n^2}{\gamma}\right), \tag{6.2}$$

where the multiplicative constant equal to the product of A^2 and the total layer area in unit volume of fluid has been determined from the requirement that the total rate of destruction of $\overline{\theta^2}$-stuff in unit volume of fluid be χ. (Note that this method of determining the constant is consistent with the model when $\kappa \ll \nu$, because the length-scale on which destruction of $\overline{\theta^2}$-stuff takes place is much smaller than the size of regions of the fluid over which the rate of strain is uniform. Such a determination of the multiplicative constant is not available in the case of the vorticity spectrum.) This result for the θ-spectrum should be compared with (4.8), which was obtained by considering the changes in all Fourier components of θ due to the actions of distortion and molecular diffusion and without assuming the existence of isolated layers of rapid change of θ.

It is not difficult to see that (6.2) cannot be correct. The spectrum function given by (6.2) is of order $\chi\nu^{\frac{7}{4}}/\epsilon^{\frac{3}{4}}\kappa^{\frac{1}{2}}$ at the wave-number $(\epsilon/\nu^3)^{\frac{1}{4}}$ marking the transition from convection subrange A to convection subrange B, and this is different by a factor $(\nu/\kappa)^{\frac{1}{2}}$ from the order of Γ (at the same wave-number) as determined by the relation (2.4) valid in convection subrange A. Another way of stating this difficulty in joining the relation (6.2) to the relation valid at smaller wave-numbers is to remark that, according to (6.2), the value of Γ at wave-numbers not near the conduction cut-off (that is, for $n \ll (-\gamma/\kappa)^{\frac{1}{2}}$) increases indefinitely as $\kappa \to 0$. The relation (6.2) has this behaviour because the steady rate of destruction of $\overline{\theta^2}$-stuff per unit area of a single layer across which there is a jump in θ is proportional to $\kappa^{\frac{1}{2}}$ (the gradients of θ increase, as $\kappa \to 0$, in such a way as to keep the local rate of destruction per unit volume of fluid in a layer constant, but the thickness of the layer decreases as $\kappa^{\frac{1}{2}}$), and the same average total rate of destruction of $\overline{\theta^2}$-stuff per unit volume of fluid can be achieved, as $\kappa \to 0$, only by an increase in the size of the jump in θ across the sheet or in the number of sheets in unit volume. A dependence of either of these quantities on κ is not possible, in fact, because the conditions leading to the formation of sheets are supposed to be generated by purely convective effects at wave-numbers smaller than those at which conduction is important.

The essential difference between the two theoretical models seems to be that in that leading to (6.2) the time-dependent effects accompanying the continual reduction in distance between neighbouring sheets and their ultimate amalgamation are ignored, as would be justified if the sheets were usually so far apart as to effect the form of Γ only at values of n of order $(\epsilon/\nu^3)^{\frac{1}{4}}$ (and this assumption, as seen, is open to the objection that the size of the jump in θ or the density of the layers must be supposed to increase as $\kappa \to 0$ in order to give the right total rate of destruction of $\overline{\theta^2}$-stuff), whereas in that leading to (4.8) the distribution of θ is always unsteady and the typical form of θ-variation is one in which neighbouring crests are continually approaching each other and 'amalgamating'. It might be

thought that since the model leading to (6.2) incorporates explicitly an intermittent small-scale variation of θ, objections to the spectral form (6.2) are equivalent to objections to an intermittent type of variation. This is not so, however; the model leading to (4.8) is consistent with an intermittent variation of θ provided that the region in which $\nabla\theta$ fluctuates should not be a vanishingly small fraction of the total volume as $\kappa \to 0$, the existence of intermittency of this kind having no influence on the result (4.8). It is now pertinent to inquire whether Townsend's assumption that small-scale variations of vorticity occur mainly in the form of isolated sheets or lines of concentrated vorticity was necessary, but that is another story.

REFERENCES

Batchelor, G. K. 1952 *Proc. Roy. Soc.* A, **213**, 349.

Batchelor, G. K. & Townsend, A. A. 1956 Article in *Surveys in Mechanics*, p. 352. Cambridge University Press.

Corrsin, S. 1951 *J. Appl. Phys.* **22**, 469.

Inoue, E. 1950 *Geophys. Notes, Tokyo*, **3**, no. **34**.

Inoue, E. 1951 *J. Phys. Soc. Japan*, **6**, 392.

Inoue, E. 1952 *J. Met. Soc. Japan*, **30**, 289.

Kraichnan, R. H. 1958 *Phys. Rev.* **109**, 1407.

Kraichnan, R. H. 1959 *J. Fluid Mech.* (in the Press).

Obukhoff, A. M. 1949 *Izv. Akad. Nauk, SSSR, Geogr. i Geofiz.*, **13**, 58.

Townsend, A. A. 1951*a* *Proc. Roy. Soc.* A, **208**, 534.

Townsend, A. A. 1951*b* *Proc. Roy. Soc.* A, 418.

Villars, F. & Weisskopf, V. F. 1955 *Proc. Inst. Radio Engrs, N.Y.*, **43**, 1232.

Welander, P. 1955 *Tellus*, **7**, 141.

Yaglom, A. M. 1949 *Dokl. Akad. Nauk, SSSR*, **69**, 743.

Small-scale variation of convected quantities like temperature in turbulent fluid

Part 2. The case of large conductivity

By G. K. BATCHELOR, I. D. HOWELLS AND A. A. TOWNSEND
Cavendish Laboratory, University of Cambridge

(Received 1 July 1958)

The analysis reported in Part 1 is extended here to the case in which the conductivity κ is large compared with the viscosity ν, the conduction 'cut-off' to the θ-spectrum then being at wave-number $(\epsilon/\kappa^3)^{\frac{1}{4}}$. It is shown, with a plausible and consistent hypothesis, that the convective supply of $\overline{\theta^2}$-stuff to Fourier components of θ with wave-numbers n in the range $(\epsilon/\kappa^3)^{\frac{1}{4}} \ll n \ll (\epsilon/\nu^3)^{\frac{1}{4}}$ is due primarily to motion on a length scale of order n^{-1} acting on a uniform gradient of θ of magnitude $[(\overline{\nabla\theta})^2]^{\frac{1}{2}}$. The consequent form of the θ-spectrum within this same wave-number range is $\Gamma(n) = \frac{1}{3}C\chi\epsilon^{\frac{2}{3}}\kappa^{-3}n^{-\frac{17}{3}}$.

The way in which conduction influences (and restricts) the effect of convection on the distribution of θ at these wave-numbers beyond the conduction cut-off is discussed.

It was shown in Part 1 (Batchelor 1959) that, when $\nu/\kappa \ll 1$, there is a convection subrange of wave-numbers defined by $L^{-1} \ll n \ll (\epsilon/\kappa^3)^{\frac{1}{4}}$ within which the θ-spectrum has the form

$$\Gamma(n) \propto \chi\epsilon^{-\frac{1}{3}}n^{-\frac{5}{3}} \tag{1}$$

(the notation being everywhere as in Part 1). The direct effect of molecular conduction is unimportant at wave-numbers within this range, but becomes important when n is of order $(\epsilon/\kappa^3)^{\frac{1}{4}}$. Over the more extensive inertial subrange of wave-numbers defined by $L^{-1} \ll n \ll (\epsilon/\nu^3)^{\frac{1}{4}}$, the velocity spectrum has the form

$$E(n) = C\epsilon^{\frac{2}{3}}n^{-\frac{5}{3}}; \tag{2}$$

the direct effect of viscosity becomes important at wave-numbers of order $(\epsilon/\nu^3)^{\frac{1}{4}}$, and causes $E(n)$ then to fall off much more rapidly than according to the power law (2).

The problem here is to find the form of the θ-spectrum at wave-numbers beyond those for which (1) is valid. Provided we confine attention to the wave-number range $L^{-1} \ll n \ll (\epsilon/\nu^3)^{\frac{1}{4}}$—which is not a serious practical limitation, since wave-numbers of order $(\epsilon/\nu^3)^{\frac{1}{4}}$ lie well beyond the conduction 'cut-off' of the θ-spectrum and the corresponding values of $\Gamma(n)$ will presumably be extremely small—the parameters relevant to the form of the θ-spectrum are ϵ, χ and κ, so that the general form of $\Gamma(n)$ is

$$\Gamma(n) = \chi\epsilon^{-\frac{1}{3}}n^{-\frac{5}{3}} \times \text{function of } (\kappa^{\frac{1}{4}}\epsilon^{-\frac{1}{4}}n),$$

the function being a constant when $n \ll (\epsilon/\kappa^3)^{\frac{1}{4}}$. In order to find the analytical form of this function it will be necessary to consider the specific mechanism by which the various Fourier components of the spatial distribution of θ are acted on by the velocity field.

The equation governing local variations of θ is

$$\frac{\partial\theta}{\partial t} + \mathbf{u}.\nabla\theta = \kappa\nabla^2\theta, \tag{3}$$

and, if $\mathbf{A}(\mathbf{n})$ and $B(\mathbf{n})$ are Fourier coefficients of the spatial distributions of $\mathbf{u}$ and θ, an equivalent equation is

$$\frac{\partial B(\mathbf{n})}{\partial t} + i\int n_i' A_i(\mathbf{n}-\mathbf{n}')\, B(\mathbf{n}')\, d\mathbf{n}' = -\kappa n^2 B(\mathbf{n}). \tag{4}$$

Thus a steady θ-spectrum can be maintained at wave-number $\mathbf{n}$ against the purely dissipative action of conductivity only by a net gain of $\overline{\theta^2}$-stuff resulting from the interaction of pairs of Fourier components represented by $\mathbf{A}(\mathbf{n}-\mathbf{n}')$ and $B(\mathbf{n}')$. The essence of a theory of the effect of a turbulent velocity field on the θ-field lies in a correct estimate of the values of $\mathbf{n}'$ for which the interaction of the corresponding pairs of Fourier components makes a dominant contribution to the supply of $\overline{\theta^2}$-stuff.

Now over the range $(\epsilon/\kappa^3)^{\frac{1}{4}} \ll n \ll (\epsilon/\nu^3)^{\frac{1}{4}}$ the θ-spectrum probably falls off rapidly as a consequence of the direct action of conductivity, whereas the $\mathbf{u}$-spectrum falls off at the relatively slow rate given by (2). This difference in the behaviour of the amplitudes of $\mathbf{A}$ and B can be made the basis for a hypothesis about the values of $\mathbf{n}'$ at which the dominant contributions to the integral in (4) are made when $(\epsilon/\kappa^3)^{\frac{1}{4}} \ll n \ll (\epsilon/\nu^3)^{\frac{1}{4}}$. For these dominant contributions will presumably come from values of $\mathbf{n}'$ at which $|B(\mathbf{n}')|$ does not have the small values resulting from the action of conduction, that is, from values of n' of order $(\epsilon/\kappa^3)^{\frac{1}{4}}$ or less. Further discussion of the hypothesis that these are the important values of n' will be given after the consequences have been examined. Notice that the restriction $n \ll (\epsilon/\nu^3)^{\frac{1}{4}}$ is significant because only for such values of n does $|\mathbf{A}(\mathbf{n})|$ vary so (relatively) slowly that the dominant range is determined by the behaviour of $|B|$ alone.

Before determining the spectrum of θ with the help of this hypothesis, we shall show that the time derivatives in (3) and (4) are negligible. Equation (3) can be thought of as equivalent to an equation for the temperature in a solid of conductivity κ with the second term on the left-hand side representing a distributed source of heat. If this source were steady in time, a Fourier component of θ with wave-number $\mathbf{n}$ would become steady in a time of order $\kappa^{-1}n^{-2}$ subsequent to the imposition of arbitrary initial conditions. The source term is not in fact steady, since the velocity field varies with t. However, it has been supposed that the relevant Fourier components of $\mathbf{u}$ in (4) are those with wave-number near $\mathbf{n}$; for those components the characteristic time (n being a wave-number magnitude within the inertial subrange) is $\epsilon^{-\frac{1}{3}}n^{-\frac{2}{3}}$, which is large compared with $\kappa^{-1}n^{-2}$ when $n \gg (\epsilon/\kappa^3)^{\frac{1}{4}}$. Thus, the source term is *approximately* steady, and the time derivative in (4) can be dropped when $(\epsilon/\kappa^3)^{\frac{1}{4}} \ll n \ll (\epsilon/\nu^3)^{\frac{1}{4}}$. Time derivatives like $\partial\Gamma(n)/\partial t$

are in any case negligible at large wave-numbers within the equilibrium range, but we have now shown that it is possible to go further and neglect terms like $[\partial B(\mathbf{n})/\partial t]^2$.

It now follows from (4) that

$$\kappa^2 n^4 \overline{B(\mathbf{n})\overset{*}{B}(\mathbf{n})} = \iint n_i' n_j'' \overline{A_i(\mathbf{n}-\mathbf{n}')\overset{*}{A}_j(\mathbf{n}-\mathbf{n}'')\, B(\mathbf{n}')\overset{*}{B}(\mathbf{n}'')}\, d\mathbf{n}'\, d\mathbf{n}'', \tag{5}$$

where the star denotes a complex conjugate. As explained, the integral in (4) is assumed to be dominated by values of $\mathbf{n}'$ such that $|\mathbf{n}-\mathbf{n}'| \gg n'$; in these circumstances, the statistical connexion between $\mathbf{A}(\mathbf{n}-\mathbf{n}')$ and $B(\mathbf{n}')$ may be neglected (although both quantities have non-negligible connexions with $B(\mathbf{n})$) and the mean value on the right-hand side of (5) splits into two. Then, on making use of the orthogonality of Fourier coefficients, we have

$$\kappa^2 n^4 \overline{B(\mathbf{n})\overset{*}{B}(\mathbf{n})} = \int n_i' n_j' \overline{A_i(\mathbf{n}-\mathbf{n}')\overset{*}{A}_j(\mathbf{n}-\mathbf{n}')}\; \overline{B(\mathbf{n}')\overset{*}{B}(\mathbf{n}')}\, d\mathbf{n}'. \tag{6}$$

A further consequence of the relation $|\mathbf{n}-\mathbf{n}'| \gg n'$ is that

$$\overline{A_i(\mathbf{n}-\mathbf{n}')\overset{*}{A}_j(\mathbf{n}-\mathbf{n}')} \approx \overline{A_i(\mathbf{n})\overset{*}{A}_j(\mathbf{n})},$$

so that

$$\kappa^2 n^4 \overline{B(\mathbf{n})\overset{*}{B}(\mathbf{n})} \approx \overline{A_i(\mathbf{n})\overset{*}{A}_j(\mathbf{n})}\, \frac{\partial\theta}{\partial x_i}\frac{\partial\theta}{\partial x_j},$$

$$= \tfrac{1}{3}\overline{A_i(\mathbf{n})\overset{*}{A}_i(\mathbf{n})}(\nabla\theta)^2, \tag{7}$$

in view of the isotropy of the (small-scale part of the) θ-field. The form of the θ-spectrum for wave-numbers in the range $(\epsilon/\kappa^3)^{\frac{1}{4}} \ll n \ll (\epsilon/\nu^3)^{\frac{1}{4}}$ is therefore given in terms of the kinetic energy spectrum function $E(n)$ by

$$\kappa^2 n^4 \Gamma(n) = \tfrac{2}{3}E(n)\frac{\chi}{2\kappa}, \tag{8}$$

that is, by

$$\Gamma(n) = \tfrac{1}{3}C_\chi \epsilon^{\frac{2}{3}}\kappa^{-3} n^{-\frac{17}{3}}. \tag{9}$$

This relation is certainly consistent with our assumption that $\Gamma(n)$ falls off rapidly at wave-numbers beyond $(\epsilon/\kappa^3)^{\frac{1}{4}}$ and that, so far as may be estimated from a consideration of *magnitudes* of Fourier coefficients, the supply of $\overline{\theta}^2$-stuff to Fourier components of θ with wave-numbers n in the range $(\epsilon/\kappa^3)^{\frac{1}{4}} \ll n \ll (\epsilon/\nu^3)^{\frac{1}{4}}$ will be dominated by direct interaction of components of $\mathbf{u}$ with wave-numbers in this same range and components of θ with smaller wave-numbers (of order $(\epsilon/\kappa^3)^{\frac{1}{4}}$ or less). Again we note that the same assumption cannot be made about the supply of $\overline{\theta}^2$-stuff to Fourier components of θ with wave-numbers of order $(\epsilon/\nu^3)^{\frac{1}{4}}$ or larger, because at these wave-numbers the energy spectrum $E(n)$ is also falling off rapidly (in fact, if both $E(n)$ and $\Gamma(n)$ fall off faster than exponentially at these high wave-numbers where both viscosity and conduction have important effects, as seems quite probable, the values of $\mathbf{n}'$ at which the integrand in (4) is greatest will lie in the neighbourhood of some fraction of $\mathbf{n}$, the fraction being $\frac{1}{2}$ if the two functions happen to diminish in the same way). Nor does the argument

give the form of $\Gamma(n)$ in the region of transition from the power-law (1) to the power-law (9) at wave-numbers of order $(\epsilon/\kappa^3)^{\frac{1}{4}}$ (where (1) and (9) do agree in giving the order of magnitude of $\Gamma(n)$ as $\chi\kappa^{\frac{3}{4}}\epsilon^{-\frac{3}{4}}$). However, neither of these limitations of the argument is of much importance. The available information about $\Gamma(n)$ is shown schematically in figure 1.

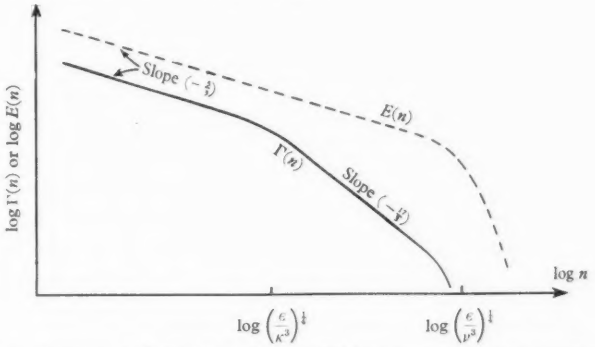

FIGURE 1. Spectra of θ and $\mathbf{u}$ in the equilibrium range of wave-numbers for the case $\nu \ll \kappa$.

It may be useful if we defend the argument against the possible objection that the contribution to the integral in (4) from small values of n' may actually be less than that from values of $\mathbf{n}'$ near $\mathbf{n}$. The mean square modulus of the latter contribution can be shown, by a calculation similar to that given for the former contribution, to be $\frac{1}{3}\overline{\mathbf{u}^2}n^2B(\mathbf{n})\overset{*}{B}(\mathbf{n})$. It is possible to make $\overline{u^2}$ arbitrarily large, for fixed values of ϵ, χ, ν and κ, simply by increasing the length scale L in such a way as to keep $(\overline{\mathbf{u}^2})^{\frac{3}{2}}/L$ constant, and by increasing $\overline{\theta^2}$ in proportion to $\overline{\mathbf{u}^2}$. Thus it would appear that, for any fixed n, $\overline{\mathbf{u}^2}$ could be made so large that the contribution from values of $\mathbf{n}'$ near $\mathbf{n}$ would dominate. However, the validity of the result which has been obtained is not affected, because in the circumstances in which this contribution from values of $\mathbf{n}'$ near $\mathbf{n}$ seems to be dominant the term $\partial B/\partial t$ is no longer negligible, and in fact cancels out this part of the integral. The reason for this is that the Fourier transforms are taken with respect to fixed axes, and the small-scale fluctuations in temperature, and the small eddies which cause them, are consequently being translated at a speed of order $(\overline{\mathbf{u}^2})^{\frac{1}{2}}$ by the large eddies. The integral in (4) therefore has one part which expresses the rates of change of Fourier components due to observation from fixed axes, and one part which expresses the actual production of fluctuations of temperature at wave-number $\mathbf{n}$ to balance the conductive decay; thus we can ignore the term $\partial B/\partial t$, and the corresponding part of the integral in (4), and the calculation leading to (9) remains valid.

The above hypothesis about the interaction between the fields of $\mathbf{u}$ and θ may be given another interpretation, which is mechanically more direct and consequently more illuminating. It will be noticed from (7) that the interaction has been calculated as if equation (3) were replaced by

$$\mathbf{u}.\nabla T = \kappa\nabla^2\theta, \tag{10}$$

where ∇T is independent of position $\mathbf{x}$ and fluctuates isotropically from one realization to another with a mean-square value

$$\overline{(\nabla T)^2} = \overline{(\nabla\theta)^2} = \chi/2\kappa. \tag{11}$$

In other words, we have assumed in effect that the supply of $\overline{\theta^2}$-stuff to θ-variations on any length scale between $(\kappa^3/\epsilon)^{\frac{1}{4}}$ and $(\nu^3/\epsilon)^{\frac{1}{4}}$ comes primarily from the convection due to motion on the same length scale in the presence of a uniform gradient of θ, this gradient being equal in magnitude to the root-mean-square value of $\nabla\theta$. The requirement that the length scale be small compared with $(\kappa^3/\epsilon)^{\frac{1}{4}}$ is needed because the gradient on which the convection acts would not otherwise be uniform with magnitude $[\overline{(\nabla\theta)^2}]^{\frac{1}{2}}$, and the requirement that it be large compared with $(\nu^3/\epsilon)^{\frac{1}{4}}$ is needed because the motion acting on the gradient would otherwise be too feeble for this to be the dominant method of supplying $\overline{\theta^2}$-stuff. The action of a velocity field of length scale n^{-1} on a uniform gradient of θ of magnitude ∇T produces variations of θ which are described accurately by the equation

$$\frac{\partial\theta}{\partial t} + \mathbf{u}.\nabla\theta + \mathbf{u}.\nabla T = \kappa\nabla^2\theta,$$

and, so it appears, approximately by the low Péclet number form (10) when $n \gg (\epsilon/\kappa^3)^{\frac{1}{4}}$.

An interesting aspect of this state of affairs is that the action of convection is directly influenced by the conduction process and cannot be considered separately. The effect of conduction is so strong as to 'balance' approximately any tendency for the convection to change the distribution of θ. An example of a case in which (10) is the appropriate equation is provided by Townsend's calculation (unpublished, and used in a paper by Clarke & Rothschild 1957) of the increase in the rate of diffusion of oxygen down a concentration gradient in semen caused by the swimming of spermatozoa; as (10) shows by its form, the magnitude of the fluctuations in θ is proportional to κ^{-1} and the transfer of oxygen by convective movement—which may be expressed by an eddy conductivity—is likewise proportional to κ^{-1}. The transfer of $\overline{\theta^2}$-stuff across the θ-spectrum due to the action of convection, as described above, may also be represented in terms of an 'eddy conductivity' (in the sense made familiar by Heisenberg). The total rate of destruction of $\overline{\theta^2}$-stuff in all Fourier components with wave-numbers above n by conductivity is seen from (8) to be given by the alternative expressions

$$\begin{aligned} 2\kappa\int_n^\infty n^2\Gamma(n)\,dn &= \frac{\chi}{\kappa}\int_n^\infty \frac{2E(n)}{3\kappa n^2}\,dn \\ &\approx 2\int_n^\infty \frac{2E(n)}{3\kappa n^2}\,dn\int_0^n n^2\Gamma(n)\,dn, \end{aligned} \tag{12}$$

showing that the effective eddy conductivity due to eddies of length scale smaller than n^{-1} acting on components of θ with length scale greater than n^{-1} is

$$\frac{2}{3\kappa}\int_n^\infty \frac{E(n)}{n^2}\,dn = \frac{C\epsilon^{\frac{2}{3}}}{4\kappa n^{\frac{4}{3}}}, \tag{13}$$

again inversely proportional to κ. The absence of any dependence of the effective transfer of kinetic energy on molecular viscosity in the corresponding expression for the eddy viscosity put forward by Heisenberg, namely

$$\text{const.} \times \int_n^\infty \left[\frac{E(n)}{n^3}\right]^{\frac{1}{2}} dn,$$

is presumably the reason for its failure at large values of n at which the effective Reynolds number is small, as has been suggested elsewhere (Townsend 1951).

REFERENCES

Batchelor, G. K. 1959 *J. Fluid Mech.* **5**, 113.
Clarke, E. W. & Rothschild, Lord 1957 *Proc. Roy. Soc.* B, **147**, 316.
Townsend, A. A. 1951 *Proc. Roy. Soc.* A, **208**, 534.

Experimental search for the effect of compressibility in unsteady Couette flow

By LESLIE HROMAS AND HAROLD DEGROFF
Purdue University, Lafayette, Indiana

(Received 18 June 1958)

Solution of the compressible Rayleigh problem involving an impulsively moved flat plate indicates that transverse velocities can be generated by a purely longitudinal shearing motion. It would be desirable to demonstrate the existence of these waves, and to do so was the motivation for the present investigation. However, the geometry for the Rayleigh problem is prohibitive; and since it was noticed that a similar behaviour should occur for the case of unsteady compressible Couette flow, this was considered for the present investigation. An experimental search for the existence of the transverse velocities was conducted using concentric rotating cylinders to generate the flow. Since these transverse velocities were too small to be measured directly, a temperature gradient was created across the annulus to take advantage of the much greater sensitivity of a hot-wire to temperature fluctuations produced by the fluctuation in the transverse velocity. The periodic temperature fluctuations noted were converted to equivalent transverse velocities. Experimental values obtained agreed qualitatively with the theory. Finally, the role of extraneous effects in the experimental apparatus was considered.

1. Introduction

Relation to the Rayleigh problem

The results of the classical incompressible Rayleigh problem, an infinite plate moved impulsively from rest parallel to its own plane, indicate that the resulting fluid motion is everywhere parallel to the plate and can be expressed rather simply in terms of the error function. Recently this problem has been re-examined for compressible fluids by a number of authors. In this case the conservation equations are coupled, basically through the viscous dissipation terms, and a non-zero transverse velocity occurs. In fact, as Stewartson (1955) shows, a strong shock wave travelling away from the plate can be generated. The total flow field is made up of three regions: a viscous boundary layer close to the moving plate, a disturbed inviscid region between the boundary layer and shock, and an undisturbed region beyond the shock wave. Mathematically the problem is to obtain separate solutions in these regions, and then to match them at the boundaries.

Illingworth (1950) has given a boundary layer solution suitable for large time and arbitrary Mach number. Howarth (1951) was able to obtain an expression for the pressure field in the compressible case by a linearization process, and he

also examined the initial motion without recourse to linearization. Van Dyke (1952) treated the non-linear problem and obtained a solution valid for small Mach numbers. He obtained a solution for the boundary layer region and the outer flow field to the third approximation by iterating between the two solutions. His process could be repeated indefinitely, except that the shock discontinuity in the outer flow field would have to be included. Finally, Stewartson (1955) considered the flow field for large Mach numbers, on the assumptions that the outer inviscid flow field and the boundary layer could be treated separately. A detailed summary of the existing theories is given by Stewartson (1955).

Van Dyke's and Stewartson's solutions together cover the complete Mach number range for the impulsive plate problem. Stewartson (1955) has compared the two solutions and found that even though there is a discontinuity, the agreement is fairly close, and that they can be matched by an approximate solution.

In each of the papers on the Rayleigh problem the distinguishing feature between the incompressible and compressible case is emphasized. This, of course, is the presence of the outflow velocity in the compressible case arising from the fact that viscous dissipation heats the fluid and a corresponding expansion occurs. Typical values of this outflow velocity $\bar{v}$ can be computed from the analyses mentioned. For example, Van Dyke (1952) gives the following expression for the small Mach number range in terms of the Mach number, time, and fluid properties:

$$\bar{v} = \frac{\gamma - 1}{\sqrt{(2\pi)}} M^2 \sqrt{\left(\frac{\nu}{t}\right)}, \tag{1}$$

where γ is the ratio of the specific heats and ν the kinematic viscosity. Assuming first, as an upper limit, $M = 1$ and t arbitrary—say $\frac{1}{4}$ sec, equation (1) gives for air $\bar{v} = 4 \times 10^{-3}$ ft./sec. For a low speed $M = 0{\cdot}01$, equation (1) gives

$$\bar{v} = 4 \times 10^{-7} \text{ ft./sec.}$$

It should be noticed that these are extremely small values. However, the overall results of the compressible Rayleigh problem indicate that transverse waves, or velocities, can be generated by a pure longitudinal shearing motion. It would be desirable to demonstrate the existence of these transverse waves experimentally. This was the motivation for the present investigation.

Experimental verification with a very large impulsive movement of a plate would be difficult, and so the question was raised as to whether the same phenomenon could be demonstrated with a different geometry, although in an analogous fashion. Examination of the basic equations for compressible plane Couette flow reveal the same degree of coupling as for the impulsive plate, i.e. transverse waves should occur in the channel for an unsteady motion of the moving walls. Also, for Couette flow the wall motion need not be impulsive, but could be a small oscillation superimposed on a uniform mean motion.

This reasoning led to the use of concentric rotating cylinders (outer cylinder rotating) to assimilate the plane Couette motion. It is realized that steady flow between concentric cylinders does not result in a linear velocity profile, but the deviation from linearity is small, i.e. 3 to 4 %, with the geometry which was adopted. The oscillation of the outer wall is primarily felt in a small region close

to it, and so the approximation with circular cylinders was found to be quite satisfactory.

With the circular geometry the problem was then to determine whether any periodic transverse velocity existed which could be traced to the wall velocity perturbation.

2. Analytical discussion of the Couette problem

Unsteady incompressible solution

So far it has not been possible to obtain a solution for unsteady compressible plane Couette flow which is suitable for comparison with experimental results. For the incompressible case, DeGroff (1955) has given a solution, and because of its significance in the present investigation it will be reviewed here. The equations of motion reduce to the diffusion equation (as for the incompressible Rayleigh problem)

$$\frac{\partial \bar{u}}{\partial t} = \nu \frac{\partial^2 \bar{u}}{\partial y^2}, \tag{2}$$

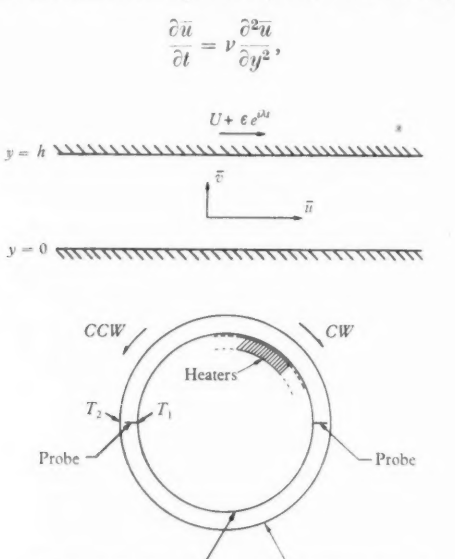

FIGURE 1. Notation for unsteady plane Couette flow and orientation of circular cylinders.

with the boundary conditions $\bar{u}(0,t) = 0$ and $\bar{u}(h,t) = U + \epsilon e^{i\lambda t}$. The co-ordinate system and notation are as shown in figure 1. In this case, as for the Rayleigh problem, conservation of mass for incompressible fluid motion precludes the existence of a transverse velocity.

The real part of the solution to (2) with the boundary conditions applied is given by

$$\bar{u}(y,t) = \frac{U}{h}y + \frac{\epsilon}{4A}\{e^{\alpha(h+y)}\cos(\lambda t + \alpha y - \alpha h) - e^{-\alpha(h-y)}\cos(\lambda t + \alpha y + \alpha h) - e^{\alpha(h-y)}\cos(\lambda t - \alpha y - \alpha h) + e^{-\alpha(h+y)}\cos(\lambda t - \alpha y + \alpha h)\}, \tag{3}$$

where $A = \sinh^2 \alpha h \cos^2 \alpha h + \cosh^2 \alpha h \sin^2 \alpha h$ and $\alpha = \sqrt{(\lambda/2\nu)}$. The first part of the solution is the linear steady-state Couette profile, and the second part is the contribution from the real part of the perturbation on the wall. It is interesting to note that the solution is made up of four components at different phase angles. Since $0 \leqslant y \leqslant h$ and generally $\alpha \gg 1$, it can be seen that in the outer portion of the channel the first term in the brackets is by far predominant over the other three.

Analytical determination of the transverse velocity

The compressible case differs from the incompressible in that the conservation equations are highly coupled and the full set of five must be solved simultaneously. One of the means of coupling is afforded through viscous dissipation, with the result that the velocity plays an important role in the energy equation. Also (2), which expresses conservation of momentum in the direction of $\bar{u}$, now involves both velocities $\bar{u}$ and $\bar{v}$ and the density $\bar{\rho}$. Thus,

$$\bar{\rho}\bar{u}_t + \bar{\rho}\bar{v}\bar{u}_y = \mu \bar{u}_{yy}, \tag{4}$$

where the subscripts denote partial differentiations.

Linearization of the equations is one means of attack used by Howarth (1951) for the flat plate, and if this is done here a particular characteristic of the present problem is seen. The linearization here is performed on the basis of a perturbation superimposed on the steady incompressible motion. The linearizing relations are $\bar{\rho} = \rho_0 + \rho$, $\bar{v} = v$ and $\bar{u} = (Uy/h) + u$; hence, if squares of the perturbation quantities ρ, v and u are neglected, there results from (4)

$$u_t + \frac{U}{h} v = \frac{\mu}{\rho_0} u_{yy}. \tag{5}$$

It is to be noted that the transverse velocity is retained in this equation, and thus the linearized equations are still coupled. This is in contrast with the linearized Rayleigh problem which depends on viscous dissipation for the coupling. It suggests that viscous dissipation can be completely neglected while still allowing an examination of coupling effects. This was done in the present case, with the viscous dissipation being made small experimentally due to the low air-flow velocities considered.

The coupling in the Rayleigh problem depends primarily on a thermodynamic mechanism, whereas the Couette case is seen to exhibit a strong dynamical mechanism. From the left-hand side of (5) it can be seen that for an inviscid fluid a transverse velocity must exist to satisfy the fluid acceleration in unsteady shear flows ($u_t \neq 0$, $u_y \neq 0$).

The linearization of (4) indicates that u_t and Uv/h should be of the same order of magnitude. A complete solution confirming this is not available; however, it is possible to compare the two terms by the following approximate analysis.

Even though there is no boundary layer in the usual sense, the region near the upper wall which is primarily affected by the perturbation can be considered as one, and from this a suitable 'boundary layer displacement thickness' defined. As an order of magnitude approximation this displacement thickness can be

found using the incompressible solution; and since it is a time-dependent function, its time rate of change is indicative of the transverse velocity.

Following this procedure, the displacement thickness δ^* is defined as

$$\delta^* = \int_0^h \frac{u}{\epsilon} dy. \tag{6}$$

Obtaining u from (3) and integrating with respect to y results in

$$\delta^* = \frac{1}{8A\alpha}\{2\sinh 2\alpha h(\cos\lambda t + \sin\lambda t) - 2e^{\alpha h}[\cos(\lambda t - \alpha h) + \sin(\lambda t - \alpha h)] + 2e^{-\alpha h}[\cos(\lambda t + \alpha h) + \sin(\lambda t + \alpha h)] + \sin 2\alpha h(-\cos\lambda t + \sin\lambda t)\}. \tag{7}$$

The first term will, in general, be much larger than the last three, so that

$$\delta^* = \frac{1}{2\alpha}(\cos\lambda t + \sin\lambda t) = (\nu/2\lambda)^{\frac{1}{2}}(\cos\lambda t + \sin\lambda t). \tag{8}$$

The value of δ^* for a flat plate oscillating alone in an infinite fluid is given by $\delta^* = \sqrt{(2\nu/\lambda)}$, which is $\sqrt{2}$ times the maximum value for the present problem. This is reasonable, since it would be expected that the present thickness would be smaller due to the proximity of the fixed plate.

Next, since $v = d\delta^*/dt$, differentiation of (7) gives

$$v = \frac{\lambda}{4A\alpha}\{\sinh 2\alpha h(\cos\lambda t - \sin\lambda t) - e^{\alpha h}[\cos(\lambda t - \alpha h) - \sin(\lambda t - \alpha h)] + e^{-\alpha h}[\cos(\lambda t + \alpha h) - \sin(\lambda t + \alpha h)] + \sin 2\alpha h(\cos\lambda t + \sin\lambda t)\}. \tag{9}$$

Again the first term is dominant near the outer wall; and if the time is chosen so that v is maximum, then

$$v_{\max} = \frac{\lambda}{\sqrt{2}\alpha} = \sqrt{(\lambda\nu)}. \tag{10}$$

Returning to (3), the value of u_t can be computed. At the wall this will simply be $\epsilon\lambda\sin\lambda t$ from the boundary condition. The order of magnitude for the ratio of the first two terms in (5) is then given by

$$\frac{u_t}{Uv/h} = O\left[\frac{h\epsilon}{U}\sqrt{(\lambda/\nu)}\right] = O\left[\frac{\epsilon}{U}\frac{h}{\delta^*}\right]. \tag{11}$$

Evaluated at the wall, where u_t is a maximum, (11) gives a ratio of $(u_t h)/(Uv) = 2$ for the experimental range of variables used here. If the ratio is to be found in the region where the experimental measurements were made, u_t must be computed using (3) as indicated above, evaluating the derivative at the co-ordinate desired. If $y = 0{\cdot}9h$ is arbitrarily chosen, $(u_t h)/(Uv) = 0{\cdot}5$. The transverse velocity as obtained here is independent of the co-ordinate y. However, the result should give the right order of magnitude. The results indicate that even at the wall, or at maximum u_t, the two terms are of the same order of magnitude; and thus the coupling due to the shear field is important and cannot be neglected.

The quantity h does not have any significance in the impulsive plate problem, but if the transverse velocity v is arbitrarily multiplied by a scale factor U/h, then

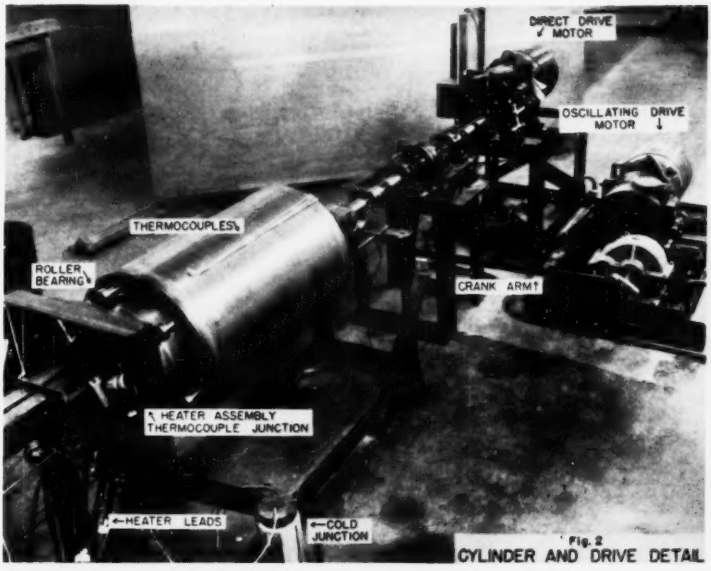

FIGURE 2 (plate 1). View of cylinder and drive.

for Van Dyke's solution (1) we have $(u_t h)/(Uv) \sim 10^6$ for the range of variables used above. This is much larger than for the present case. Since u_t is the same order of magnitude for the two cases, a much larger v should be obtained experimentally in the present case than the 4×10^{-7} ft./sec indicated by (1).

3. Experimental verification

Apparatus

The two metal cylinders used were 11·14 in. and 14·40 in. in diameter and were placed with their axes horizontal. The resulting annulus was 1·63 in. across and 22 in. in axial length. Profile velocity and temperature measurements were made in the horizontal plane at the axial mid-point of the annulus. The geometry and co-ordinate system for the cylinders are shown in figure 1. A photograph of the apparatus along with the driving mechanisms is shown in figure 2, plate 1. The report by Hromas & Thompson (1956), which deals with the steady-state heat transfer between the cylinders, gives a complete description of the apparatus.

All the measurements were made with hot-wire anemometers used as resistance thermometers for temperature measurements and in the normal manner for velocity measurements. The development and calibration of the probes has been described in the report by Hromas & Kentzer (1955).

Experimental technique

The objective was to examine the unsteady motion in the annulus, and, in particular, to determine whether any transverse velocity existed due to the imposed perturbation. At the outset one primary factor concerning the phenomenon was realized. This was that any existing transverse velocity would be very small, and hence any deviation from an incompressible behaviour would be slight. Therefore, the longitudinal velocity profile data should agree fairly well with the relatively simple incompressible solution.

With this fact in mind, the first step was to obtain a series of longitudinal velocity profile measurements for several shaking frequencies, and to compare them with the incompressible analysis.

The results indicated that any transverse velocity was indeed small, which led to the realization that it would not be suitable to attempt to measure the transverse velocity component directly. It was then proposed that it might instead be possible to measure v indirectly through its effect on another variable. In particular, it was thought that, since temperature changes could be detected on a much smaller scale than velocity, temperature fluctuations might be detected due to the oscillating wall. Using the hot-wire as a resistance thermometer, it was conjectured that if a temperature gradient were to be placed across the flow, any transverse velocity component would have a magnified effect on the temperature. From data obtained during the previous steady-state heat-transfer experiments of Hromas & Thompson (1956), suitable gradients were chosen such that the effect of free convection was known to be negligible.

When a temperature gradient was placed across the flow, definite temperature fluctuations were noted to occur at the frequency of the perturbation oscillation of the rotating cylinder. In order to extend the range of data, several different

temperature gradients were used with temperature traces being recorded at various gap settings in the annulus for each gradient. Instrumentation response determined the lowest gradient usable, and free convection the largest.

It was concluded that by this indirect method the existence of a transverse velocity was demonstrated for the problem involved. Assuming that $v\Delta T$ is indicative of the forced convection, and then knowing the temperature gradient, the frequency of oscillation, and the magnitude of the temperature fluctuations, average values for the transverse velocity were computed.

Comparison between theory and experiment

The first data obtained were the resultant velocity traces for various frequencies and gap settings. For both of these the cylinder walls were at room temperature. The experimental data are compared in figure 3 with the theoretical results for unsteady incompressible plane Couette flow. It can be seen that the experimental data agreed very closely with the analysis. The maximum discrepancy corresponds to a velocity of 0·07 ft./sec; and as the sensitivity limit of the instrumentation was 0·05–0·07 ft./sec, this error is not significant.

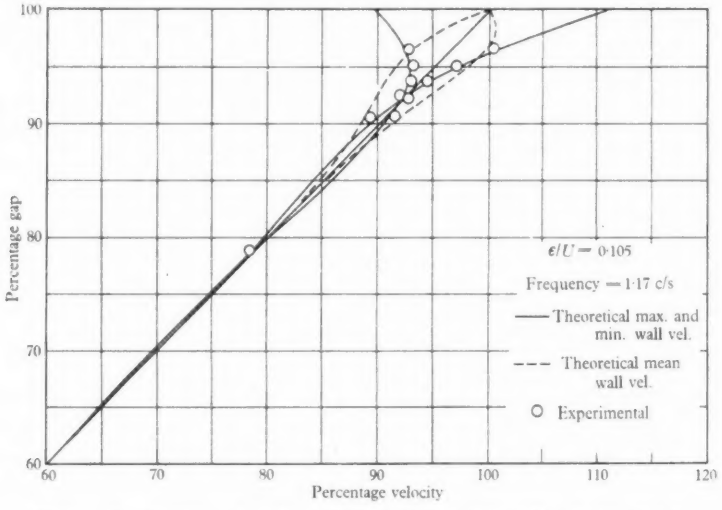

FIGURE 3. Theoretical and experimental velocity profiles for unsteady incompressible Couette flow.

Further evidence of the close check with the incompressible analysis can be seen in figure 4. These were data obtained for a given gap setting and various frequencies, keeping constant the ratio ϵ/U of the perturbation magnitude to the mean wall velocity. The four data points fall about 0·1 % below the theoretical values, corresponding to velocity differences of only 0·007 to 0·010 ft./sec. Within the accuracy of the instrumentation the above results certainly indicate a close check with the incompressible theory. Further, they confirm the initial assumption that any transverse velocity would be small.

When a temperature gradient was formed across the flow, oscillations were noticed. Figure 5 gives the magnitude of these oscillations as a function of gap setting and temperature gradient. The large degree of scatter was primarily caused by difficulties of measurement. Also, the values given in figure 5 were measured peak to peak so the maximum deviation from the mean was about 1·5° F.

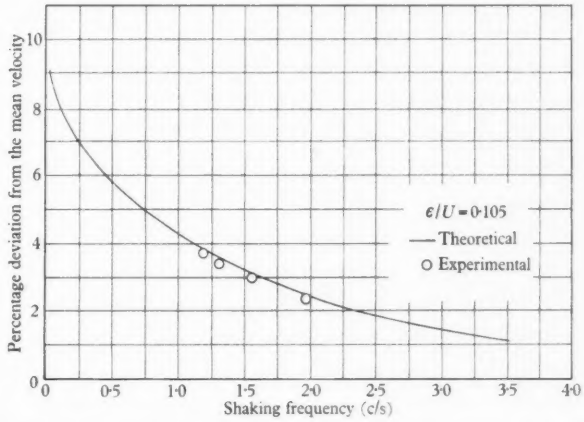

FIGURE 4. Instantaneous velocity fluctuation *vs* shaking frequency at 96·5 % gap.

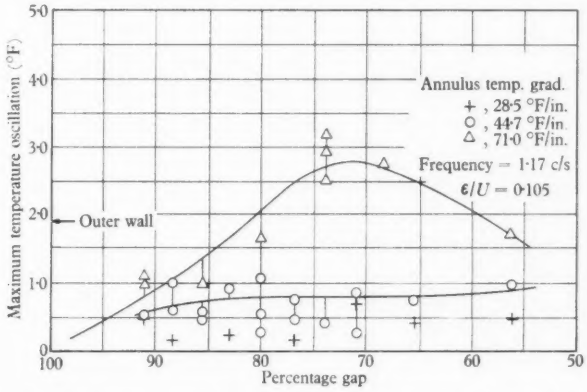

FIGURE 5. Maximum temperature oscillation *vs* percentage gap for various annulus temperature gradients.

The computed values of the transverse velocity are shown in figure 6. Values obtained range from about 0·002 ft./sec to 0·008 ft./sec. Evidently, such small values could not have been measured directly with the hot-wire.

Since numerical values for v are now obtained, a comparison can be made with the tentative theoretical values obtained from the computed displacement thickness and the linearized compressible equation. Previously, the ratio of $(u_t h)/(Uv)$ at $y = 0{\cdot}9h$ had been determined theoretically and found to be 0·5.

If now u_t is computed from the experimental data and v taken to be about 0·003 ft./sec, there results

$$\left[\frac{u_t h}{Uv}\right]_{\text{exp}} = 1{\cdot}5,$$

which indicates at least an order of magnitude agreement. In view of the nature of the experiments, this is really all that could be expected.

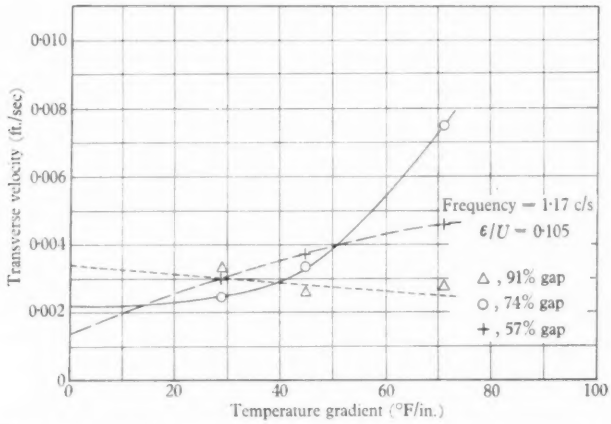

FIGURE 6. Transverse velocity component *vs* annulus temperature gradient.

4. Discussion of results

Temperature fluctuations

From figure 5 it can be seen that the magnitude of the temperature fluctuations increases with the temperature gradient. In fact, it was found to be roughly proportional to the magnitude of the gradient. It would be desirable to check this further, but the instrumentation and free convection set rather definite upper and lower limits on the gradients usable.

The high temperature-gradient readings appeared to have a peak at about the 70 % gap position. Why this occurred is not clear. There could possibly have been some sort of resonance effect present. A careful examination of the other two sets of data shows that the first one or two points tend to be high, so they might also have been drawn with a slight peaking effect close to the outer wall. Without the aid of an analytical solution it would be difficult to suggest anything of a more definite character.

Transverse velocity fluctuations

Since the presence of a transverse component of velocity was detected only with a temperature gradient, a question of prime importance was whether the gradient was a necessary condition for the existence of transverse velocities. Since the gradients used were about the upper and lower limits, the only recourse was to resort to an extrapolation to zero temperature gradient with the data available. This was done and the resulting curves are shown on figure 6. This

procedure was not precise, but it appears from all the data that a non-zero transverse velocity would be obtained at room temperature. The values indicated are of the order of 0·003 ft./sec.

The extrapolation did not change the order of magnitude of the observed velocity, and hence gives a result which still agrees with the analysis. For this reason it was felt the extrapolation was justified. Thus it was concluded that, as indicated to be true by the coupling in the basic equations, a periodic transverse velocity would exist at zero temperature gradient.

Possibility of extraneous effects

Four sources of error which would have affected the results are free convection, centrifugal effects, instability regions in the annulus (even though the outer cylinder was rotated) and viscous dissipation. For the velocities used one would expect viscous dissipation to be very small. Using the results of DeGroff (1956),

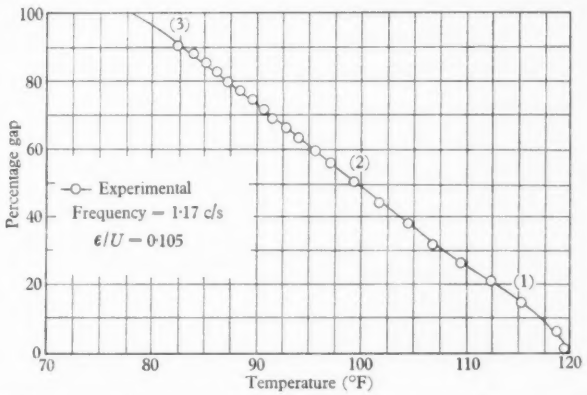

FIGURE 7. Mean temperature profile for unsteady flow (annulus temperature gradient—28·5 °F/in.).

the dissipation was found in this case to raise the fluid temperature a maximum of 0·0007 °F. This is certainly not detectable in the temperature fluctuations. Concerning an instability region, it is felt that the extensive hot-wire measurements which had been made in the previous steady-state investigations would have indicated any that existed.

It was found in the steady-state heat-transfer measurements that free convection had a large effect near the inner cylinder and in a small confined layer along the outer cylinder. These two regions were connected by a linear portion free from convection currents. Figure 7 shows a profile for a particular case chosen to minimize free convection effects. For all gradients used in the present work, the data obtained were restricted to well within the linear regions and hence should be independent of free convection.

Finally, there is the possibility that the transverse velocities noticed could have been caused by centrifugal effects. Continuity considerations require that regardless of whether the motion is cylindrical or plane, the existence of a trans-

verse velocity for the present problem requires some degree of compressibility in the fluid. However, centrifugal force can still contribute to the magnitude of the transverse velocity, and it remains to see how this compares with the effects of the basic coupling as indicated in the equations for plane flow. The coupling for plane compressible Couette flow was indicated by the linearized momentum equation (5). The corresponding equation for unsteady compressible cylindrical Couette flow will now be linearized on the same basis as the plane case, i.e. a small perturbation is superimposed on the steady incompressible motion. The linearization relations are $\bar{\rho} = \rho_0 + \rho$, $\bar{q}_\theta = q_{\theta_0} + q_\theta$ and $\bar{q}_r = q_r$, where the subscript 0 corresponds to the steady incompressible state. The resulting equation for the perturbation velocities is

$$\rho_0\left[\frac{\partial q_\theta}{\partial t} + q_r\left(\frac{\partial q_{\theta_0}}{\partial r} + \frac{q_{\theta_0}}{r}\right)\right] = \mu\left[\frac{\partial^2 q_\theta}{\partial r^2} + \frac{1}{r}\frac{\partial q_\theta}{\partial r} - \frac{q_\theta}{r^2}\right]. \tag{12}$$

The second term on the left-hand side is analogous to the coupling term in (5), and the last term on the left-hand side occurs due to the cylindrical nature of the flow. However, the relative magnitude of these two terms can be readily determined from the relation for the steady incompressible profile

$$q_{\theta_0} = \frac{\omega r_2^2}{r_2^2 - r_1^2}\left[r - \frac{r_1^2}{r}\right]. \tag{13}$$

The ratio between the second and third terms is then

$$\frac{\partial q_{\theta_0}/\partial r}{q_{\theta_0}/r} = \frac{1 + (r_1^2/r^2)}{1 - (r_1^2/r^2)}, \tag{14}$$

which for the present apparatus takes the value 4 at $r = r_2$, and approaches infinity as $r \to r_1$. This indicates that centrifugal forces are felt in the experimental apparatus, but are never predominant, being 25 % of the effect at the outer wall and approaching zero at the inner wall. For the region of the annulus in which the data were obtained, centrifugal force could have caused about 10 to 15 % of the measured effect.

The authors are deeply grateful to Dr P. E. Stanley of Purdue University and Dr S. Goldstein of Harvard University for helpful discussions during the course of the above research. This work was sponsored by the Office of Ordnance Research (Army) under Contract No. DA 33-008 ORD-888.

REFERENCES

DeGroff, H. M. 1955 *Purdue University Rep.* no. A-55-3.
DeGroff, H. M. 1956 *J. Aero. Sci.* **23**, 395.
Howarth, L. 1951 *Quart. J. Mech. Appl. Math.* **4**, 157.
Hromas, L. A. & Kentzer, C. P. 1955 *Proc. 4th Midwest Conf. on Fluid Mech.* p. 23.
Hromas, L. A. & Thompson, T. R. 1956 *Purdue University Rep.* no. A-56-3.
Illingworth, C. R. 1950 *Proc. Camb. Phil. Soc.* **46**, 603.
Stewartson, K. 1955 *Proc. Camb. Phil. Soc.* **51**, 202.
Van Dyke, M. D. 1952 *Z. Angew. Math. Phys.* **3**, 343.

Forced plumes

By B. R. MORTON
Department of Mathematics, University of Manchester

(Received 1 May 1958)

This paper describes an investigation of the turbulent forced plumes generated by steady release of mass, momentum and buoyancy from a source situated in an extensive region of uniform or stably stratified fluid. The treatment, which is an extension of earlier work on buoyant plumes, also brings out the relationship between the *jet* and the *plume* as special cases of forced plumes.

The analysis shows that the behaviour of a forced plume from a source of finite size which delivers buoyancy, mass and momentum can in a uniform environment be related to that from a virtual point source of buoyancy and momentum only, and a treatment is given for the latter type of forced plume. When the environment is weakly stratified it is inferred that forced plumes can be related to point sources in the same way. In a uniform environment the plume fluid rises indefinitely; but when the environment is stably stratified, increasing the release of mass and momentum from a given source of buoyancy has the effect at first of reducing the total height of the plume, and only for very large flux of momentum does the height increase again, without limit. A description is given for the behaviour of vertical jets in a stably stratified environment, and for forced plumes of fluid with negative buoyancy.

Introduction

The plumes generated from steady sources of buoyancy in a uniform or stratified environment have been described by several authors. Laminar thermal plumes in a uniform environment were analysed by Gutman (1949) and Yih (1951, 1952), and Yih has also shown experimentally that such laminar flow is unstable quite close to the source (in terms of a local Rayleigh number) for all but the weakest sources. Thus the flow in most plumes will be effectively turbulent throughout the ascent, and this treatment will be restricted to turbulent flow.

Turbulent plumes in a uniform environment were first investigated by Schmidt (1941) using mixture length theories, and related experiments have been reported since by Yih (1951), Rouse, Yih & Humphreys (1952) and Railston (1954). In these experiments the nearest approximation to a pure source of buoyancy was Schmidt's electrically heated grid set in a circular hole in a table-top; Railston used a similar source near the bottom of a vertical chimney, so that he was actually considering constrained plumes in an induced current; and Rouse *et al.* (1952) carried out a careful set of experiments on free plumes above gas flames. Two treatments have been given for turbulent plumes in an ambient fluid in which the density varies linearly with height: Priestley & Ball (1955) were concerned

specially with plumes rising from heated surfaces, while Morton, Taylor & Turner (1956) investigated the plumes from a virtual source of buoyancy only, and related these to experiments in which a steady stream of light fluid issued from a nozzle.

The purpose of this paper is to find the general effect of variations in the character of the source on the buoyant plumes which are produced. The plume generated from a source of finite size which delivers a flux of buoyancy, momentum and mass will be termed a *forced plume*. It will be shown that there is always an equivalent point (or virtual) source of buoyancy and momentum only which produces the same flow as the extended source, and the plumes from such point sources will also be called forced plumes. It may be noted that there can be no mass flow from a point source when the momentum flow is finite; for the momentum flow is of order (plume radius)$^2 \times$ (plume velocity)^2, so that the plume velocity near such a point source is $O[(\text{plume radius})^{-1}]$, and the mass flow is of order (plume radius)$^2 \times$ (plume velocity) which tends to zero at the source. The forcing considered here is from the source and not from the environment, which is assumed to be at rest except for the influence of the plume. Two limiting cases of the forced plume are the *jet* from a point source of momentum, and the pure *plume* from a source of buoyancy only.

In order that the problem will be mathematically tractable, certain assumptions must be made about the nature of the turbulent flow and its effect on fluid mixture across the mean boundaries of the plume. First, it will be assumed that well-developed turbulent flow in forced plumes is independent of viscosity (i.e. that local values of a Reynolds number are large), and of thermal conductivity (so that behaviour does not depend on the Prandtl number). Then, with the assumption of similarity of profiles at different cross-sections of the plume, it follows that the structure of turbulence within the plume and the rate of entrainment at its mean edge can depend only on the differences in mean density and mean vertical velocity between the plume axis and the ambient fluid. The treatment will be restricted to vertical plumes to eliminate the dependence on Richardson number of turbulent mixing of fluids with different densities across a horizontal interface. And finally it will be assumed that local density variations are everywhere so small in relation to some reference density that the inertia of unit volume of the fluid can be regarded as uniform. This eliminates the effect of density differences on mixing which may be important when large differences in temperature are maintained between the plume and ambient fluid (e.g. in turbulent flames), and is unlikely to introduce serious error for normal plumes, since any large density differences near the source are rapidly reduced as the fluid rises. It is then reasonable to assume that turbulence of similar character will be found in all forced plumes of the kind considered.

The general behaviour of forced plumes will be investigated now by an extension of the methods used by Morton *et al.* (1956) (hereafter referred to as paper I). As in their treatment, the analysis will refer to incompressible fluids, although it can be extended to include convection in the atmosphere by substituting potential temperatures and densities for ordinary temperatures and densities.

The model for forced plumes

The model used is very similar to that of paper I, being based on the assumptions: (i) that the ratio of the mean speed of inflow at the edge of a forced plume to the mean vertical speed on the plume axis is a constant, α, and (ii) that profiles of mean vertical velocity and buoyancy are each of similar form at all heights.

A feature of forced plumes which was ignored in paper I is the greater lateral spread of heat than of vertical momentum. Rouse *et al.* (1952) have illustrated this by experiments with buoyant plumes above isolated gas flames. They plotted their results in non-dimensional form, and chose the Gaussian profile

$$\exp(-96R^2/X^2)$$

as giving the best fit for a wide range of velocity measurements, and

$$\exp(-71R^2/X^2)$$

for the measurements of temperature excess; X is the height above the source and R the radial distance from the plume axis.

The entrainment constant α is clearly associated with the velocity profile rather than the temperature profile, and where the transport of material properties by the plume is of principal importance the temperature profile plays a secondary role even when buoyancy forces give rise to the flow. Thus it will be appropriate to seek a similarity solution for which α measures the rate of flow into a forced plume, with velocity profile characterized by the horizontal length-scale b, and with an associated buoyancy profile of the same shape but with a length-scale λb. λ and α are universal constants for forced plumes in which local density variations are small; they must be evaluated experimentally.

Forced plumes in a uniform environment

Consider an axially symmetrical plume generated from a roughly circular horizontal source in an incompressible environment. The plume will be assumed to have Gaussian profiles of mean vertical velocity $u(X,R) = U(X)\exp(-R^2/b^2)$ and mean buoyancy $g(\rho_e-\rho)(X,R) = \rho_0 P(X)\exp(-R^2/\lambda^2 b^2)$, with characteristic length-scales $b(X)$ and $\lambda b(X)$; $\rho_e(X)$ is the density in the environment and $\rho_0 = \rho_e(0)$ is the reference density. The equations representing conservation of mass, momentum and density deficiency (analogous to equations (6) of paper I) are, for a uniform environment, approximately

$$\left.\begin{aligned} \frac{d}{dX}(b^2U) &= 2\alpha bU, \\ \frac{d}{dX}(b^2U^2) &= 2\lambda^2 b^2 P, \\ \frac{d}{dX}(\lambda^2 b^2 UP) &= 0. \end{aligned}\right\} \tag{1}$$

Under the transformations $V = 2^{-\frac{1}{2}}bU$, $W = b^2U$ and $F = \lambda^2 b^2 UP/(1+\lambda^2)$, these reduce to

$$\frac{dW}{dX} = 2^{\frac{3}{2}}\alpha V, \quad \frac{dV^4}{dX} = (1+\lambda^2)FW, \quad \frac{dF}{dX} = 0. \tag{2}$$

$\pi\rho V^2$ is the momentum flux, $\pi\rho W$ the mass flux and $\pi\rho_0 F$ the buoyancy flux across a plane at position X in the forced plume.

The strength of a source will be defined by specifying the rates of discharge of buoyancy ($\pi\rho_0 F_0$), momentum ($\pi\rho V_0^2$) and mass ($\pi\rho W_0$), and will be labelled (F_0, V_0, W_0).

The forced plume from a source (F_0, V_0, 0)

It will be convenient to find the effect of discharge of momentum from a virtual point source of buoyancy before dealing with real sources of finite size. If there is a finite flux of buoyancy $\propto [b^2UP]_{X=0}$ and of momentum $\propto [b^2U^2]_{X=0}$ from a point source, both U and P are $O(1/b)$ at the source, and hence the corresponding mass flow $\propto [b^2U]_{X=0}$ must be zero. The plume is characterized by the parameters F_0 and V_0, and it may be verified that the transformations

$$\left.\begin{aligned} F = F_0, \quad V = |V_0|v, \quad W = 2^{\frac{3}{2}}\alpha^{\frac{1}{2}}(1+\lambda^2)^{-\frac{1}{2}}\,|V_0|^{\frac{3}{2}}\,|F_0|^{-\frac{1}{2}}\,w, \\ X = 2^{-\frac{3}{2}}\alpha^{-\frac{1}{2}}(1+\lambda^2)^{-\frac{1}{2}}\,|V_0|^{\frac{3}{2}}\,|F_0|^{-\frac{1}{2}}\,x, \end{aligned}\right\} \tag{3}$$

reduce equations (2) to the non-dimensional form

$$\frac{dw}{dx} = v, \quad \frac{dv^4}{dx} = w\,\mathrm{sgn}\,F_0, \tag{4}$$

where $\mathrm{sgn}\,F_0 = \pm 1$ according as $F \gtrless 0$. The reduced boundary conditions are

$$w = 0, \quad v = \mathrm{sgn}\,V_0, \quad \text{at } x = 0;$$

the buoyancy flux remains constant at all heights in a uniform environment.

When x is eliminated from equations (4)

$$w = 2^{\frac{3}{2}}5^{-\frac{1}{2}}\,\mathrm{sgn}\,v\,|v^5 - \mathrm{sgn}\,V_0|^{\frac{1}{2}}; \tag{5}$$

and when w is eliminated from equations (4), after integration

$$x = 2^{\frac{1}{2}}5^{\frac{1}{2}}\,\mathrm{sgn}\,F_0 \int_{\mathrm{sgn}\,V_0}^{v} |v_1^5 - \mathrm{sgn}\,V_0|^{-\frac{1}{2}}\,v_1^3\,dv_1. \tag{6}$$

Equations (5) and (6) provide a parametric solution for the forced plume in a uniform environment from the source (F_0, V_0, 0) in terms of v. The following cases may be of interest:

(i) When the fluid delivered by the source is lighter than its environment and has upward momentum ($F_0 > 0$ and $V_0 > 0$), v increases steadily from its initial value $+1$ and

$$w = 2^{\frac{3}{2}}5^{-\frac{1}{2}}(v^5 - 1)^{\frac{1}{2}}, \quad x = 2^{\frac{1}{2}}5^{\frac{1}{2}} \int_1^v (v_1^5 - 1)^{-\frac{1}{2}}\,v_1^3\,dv_1. \tag{7a}$$

This solution can be written to an accuracy better than 1 % for $v \geqslant 2$

$$w = 2^{\frac{3}{2}}5^{-\frac{1}{2}}v^{\frac{5}{2}}, \quad x = 2^{\frac{3}{2}}5^{\frac{1}{2}}3^{-1}v^{\frac{3}{2}} - 1{\cdot}057; \tag{7b}$$

hence, for $x \geqslant 5$, $v \propto (x + 1{\cdot}057)^{\frac{3}{5}}$ and $w \propto (x + 1{\cdot}057)^{\frac{5}{3}}$, which is precisely the behaviour exhibited by the plume from a source (F_0, 0, 0) of buoyancy only at $x = -1{\cdot}057$, below the given source. Figure 1 shows curves for the non-dimensional horizontal length-scale or effective plume 'radius' w/v ($\propto b$) and the non-

dimensional vertical velocity on the axis v^2/w ($\propto U$). For purposes of comparison the corresponding curves for the 'radii' of plumes from virtual point sources of buoyancy only (marked 'plume') and momentum only (marked 'jet') are also shown by broken lines.

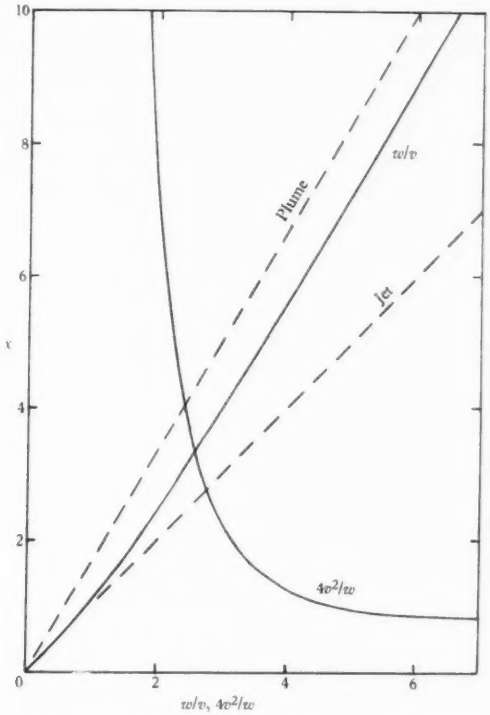

FIGURE 1. The behaviour of a forced plume from a virtual source of buoyancy and momentum, situated in a uniform environment. The non-dimensional quantities w/v, which is proportional to the horizontal length-scale or plume 'radius', and v^2/w, which is proportional to the vertical velocity on the axis, are plotted against x which is proportional to the height above the virtual source; the corresponding 'radii' for simple plumes and jets are shown in broken lines.

(ii) When the fluid from the source is heavier than its environment and has upward momentum ($F_0 < 0, V_0 > 0$), v decreases steadily from its initial value $+1$ to 0, and

$$w = 2^{\frac{3}{2}}5^{-\frac{1}{2}}(1-v^5)^{\frac{1}{5}}, \quad x = 2^{\frac{1}{2}}5^{\frac{1}{2}}\int_v^1 (1-v_1^5)^{-\frac{1}{2}}\, v_1^3\, dv_1.* \tag{8}$$

The fluid in the forced plume will rise to a maximum height

$$x = 2^{\frac{1}{2}}5^{\frac{1}{2}}\int_0^1 (1-v_1^5)^{-\frac{1}{2}}\, v_1^3\, dv_1 = 1{\cdot}454,$$

* Note that x can also be written $2^{\frac{1}{2}}5^{\frac{1}{2}}\{\beta(\frac{4}{5}, \frac{1}{2}) - \beta(\frac{4}{5}, \frac{1}{2}; v^5)\}$, where $\beta(\frac{4}{5}, \frac{1}{2})$ is a β-function and $\beta(\frac{4}{5}, \frac{1}{2}; v^5)$ an incomplete β-function of argument v^5.

and will then spread sideways as it falls back; some plume fluid will remain near the highest point because of entrainment from above (which has been neglected). The present method can provide a solution only for the ascent. The solution curves for $w/v\,(\propto b)$, $v^2/w\,(\propto U)$ and $-1/w\,(\propto P)$ against the dimensionless height x are plotted in figure 2.

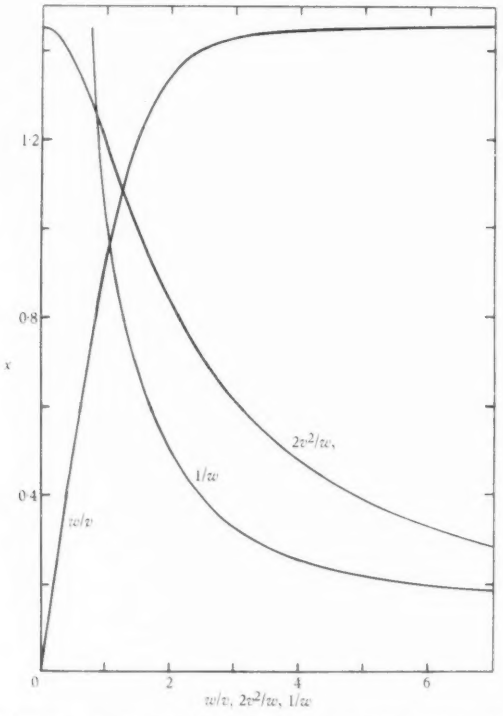

FIGURE 2. The behaviour of a forced plume from a virtual source of momentum and negative buoyancy situated in a uniform environment. w/v is proportional to the plume 'radius', v^2/w to the vertical velocity at the axis, and $1/w$ to the deficiency of temperature at the axis of the plume relative to that of the environment.

(iii) When the fluid from the source is lighter than the environment but has downward momentum ($F_0 > 0$, $V_0 < 0$), v increases steadily from its initial value -1, and

$$w = 2^{\frac{3}{2}}5^{-\frac{1}{2}}\operatorname{sgn} v(1+v^5)^{\frac{1}{2}}, \quad x = 2^{\frac{1}{2}}5^{\frac{1}{2}}\int_{-1}^{v}(1+v_1^5)^{-\frac{1}{2}}v_1^3\,dv_1. \tag{9a}$$

The forced plume descends to a 'singular point' at

$$x = 2^{\frac{1}{2}}5^{\frac{1}{2}}\int_{-1}^{0}(1+v_1^5)^{-\frac{1}{2}}v_1^3\,dv_1 = -1{\cdot}454$$

below the virtual source, and then rises again. The solution for a descending forced plume is valid physically only until the flow spreads sideways, and is just case (ii) inverted. The ascending part of the solution (for $v > 0$) describes a

forced plume from an actual source where the mass flow is too large for case (i) to apply.

Approximate expressions for $v \geqslant 3$ are

$$w = 2^{\frac{3}{2}}5^{-\frac{1}{2}}v^{\frac{5}{2}}, \quad x = 2^{\frac{3}{2}}5^{\frac{1}{2}}3^{-1}v^{\frac{3}{2}} - 3{\cdot}253; \tag{9b}$$

hence for $x \geqslant 8$ the forced plume behaves closely as though it were generated from a virtual source of buoyancy at $x = -3{\cdot}253$, below the given source. There is now an initial region of accelerated flow above the source.

The forced plume from a source (F_0, V_0, W_0)

The effect on a forced plume of independent variation of the mass flux W_0 from the source can be found only by considering the effects due to a source of finite area. The behaviour of the plume is represented again by equations (4). For an extensive source it may be assumed that the flow is directed upwards from the source (i.e. $\operatorname{sgn} V_0 = \operatorname{sgn} W_0 = 1$), so that the boundary conditions at the source (F_0, V_0, W_0) are

$$v = 1, \quad w = 2^{\frac{3}{2}}5^{-\frac{1}{2}}|\Gamma|^{\frac{1}{2}} \quad \text{at } x = 0, \tag{10}$$

where $\Gamma = 2^{\frac{3}{2}}5\alpha^{-1}(1+\lambda^2)F_0V_0^{-5}W_0^2$ is a dimensionless parameter representative of the forced plume in a uniform environment.

A plume which is the same above the level $x = 0$ can be generated from a virtual point source (F_0, γV_0, 0) situated at a certain height $x = -\bar{x}$. (Recall that the flux of buoyancy is constant in a uniform environment.) This equivalent plume must satisfy the same non-dimensional equations as the forced plume from the source (F_0, V_0, W_0), and the modified boundary conditions $v' = \gamma$ and $w' = 0$ at $x' = 0$, where the dashes are used to refer symbols to the equivalent plume from (F_0, γV_0, 0); the corresponding solution is

$$\left.\begin{aligned} v' \geqslant \gamma, \quad w' &= 2^{\frac{3}{2}}5^{-\frac{1}{2}}|v'^5 - \gamma^5|^{\frac{1}{2}}, \\ x' &= 2^{\frac{1}{2}}5^{\frac{1}{2}}\operatorname{sgn} F_0 \int_\gamma^{v'} |v_1'^5 - \gamma^5|^{-\frac{1}{2}} v_1'^3 \, dv_1'. \end{aligned}\right\} \tag{11}$$

The two plumes will be identical above the level of the actual source if at $x' = \bar{x}$, $v' = 1$ and $w' = 2^{\frac{3}{2}}5^{-\frac{1}{2}}|\Gamma|^{\frac{1}{2}}$; these conditions determine γ and $\bar{x}$ as

$$\left.\begin{aligned} \gamma^5 &= 1 - \Gamma, \\ \bar{x} &= 2^{\frac{1}{2}}5^{\frac{1}{2}}\operatorname{sgn} F_0 \int_\gamma^1 |v_1'^5 - \gamma^5|^{-\frac{1}{2}} v_1'^3 \, dv_1' \\ &= 2^{\frac{1}{2}}5^{\frac{1}{2}}|\gamma|^{\frac{3}{2}}\operatorname{sgn} F_0 \int_{\operatorname{sgn}\gamma}^{1/|\gamma|} |t^5 - \operatorname{sgn}\gamma|^{-\frac{1}{2}} t^3 \, dt, \end{aligned}\right\} \tag{12}$$

where $v_1' = |\gamma|\, t$. The significance of these solutions depends on the parameters of the physical system in a complicated way; it will be investigated further in a separate paper on convection by forced plumes in the atmosphere. The following comments may be of interest here:

(*a*) when $0 < \Gamma < 1$, forced plumes behave as though from a virtual source (F_0, $\gamma^{\frac{1}{2}}V_0$, 0) situated at

$$x = -2^{\frac{1}{2}}5^{\frac{1}{2}}\gamma^{\frac{3}{2}} \int_1^{1/\gamma} (t^5 - 1)^{-\frac{1}{2}} t^3 \, dt.$$

The full solution is that of case (i) for the forced plume (F_0, V_0, 0) given above;

(*b*) when $\Gamma = 1$, forced plumes behave as the plume $(F_0, 0, 0)$ from a source of buoyancy only at $x = -2{\cdot}108$;

(*c*) when $\Gamma > 1$, forced plumes behave as though from a virtual source $(F_0, -|\gamma| V_0, 0)$ situated at

$$x = 3{\cdot}162\,|\gamma|^{\frac{3}{2}} \int_{-1}^{1/|\gamma|} (t^5+1)^{-\frac{1}{2}} t^3\,dt;$$

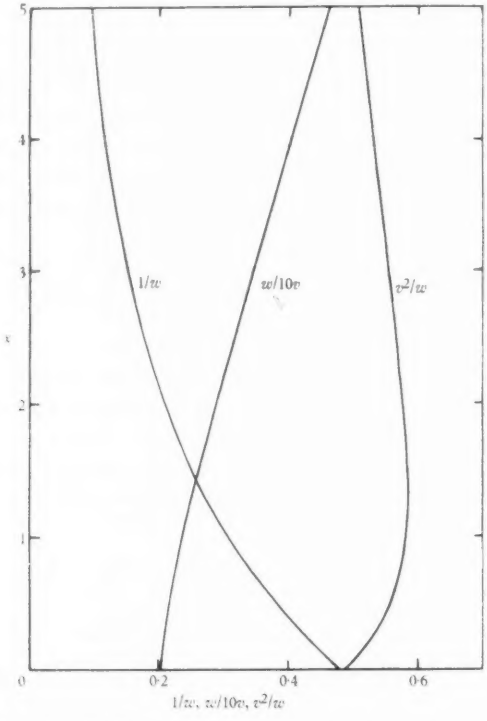

FIGURE 3. The behaviour of a forced plume from an extensive source discharging heated fluid and situated in a uniform environment; for this source $\Gamma = 2{\cdot}69$. w/v is proportional to the plume 'radius', v^2/w to the vertical velocity at the axis, and $1/w$ to the temperature excess at the axis over that in the environment.

this integral can be positive, in which case the virtual source lies *above* the actual source (see case (iii) above). A particular example has been worked for $\Gamma = 2{\cdot}69$ and the results are shown in figure 3. The curves show that when $\Gamma > 1$ the plume fluid is at first accelerated above the source, but that the vertical velocity ultimately decreases steadily with height and the plume becomes straight-sided;

(*d*) when $\Gamma < 0$ the forced plume behaves as though from a virtual source $(F_0, \gamma^{\frac{1}{2}} V_0, 0)$ at

$$x = -3{\cdot}162\gamma^{\frac{3}{2}} \int_{1/\gamma}^{1} (1-t^5)^{-\frac{1}{2}} t^3\,dt$$

(see case (iii) above).

The behaviour of a forced plume in a uniform environment is characterized by the dimensionless parameter Γ, and relative to the straight sided plume from a virtual source of buoyancy the entrainment near the source is increased when $\Gamma < 1$ and decreased when $\Gamma > 1$. Hence the most rapid removal of plume fluid from the neighbourhood of the source is obtained for small V_0^5 and large $W_0^2 F_0$, by releasing the fluid slowly from a large aperture and giving it the maximum buoyancy. The most rapid mixing of the effluent with its environment is obtained in the jet.

Values for the constants λ and α

For *Gaussian* profiles, a value $\lambda = 1{\cdot}16$ can be obtained in the case of thermal diffusion from the profiles recommended by Rouse *et al.* (1952). An improved value $\alpha = 0{\cdot}082$ for the entrainment constant has been found by comparison of the predictions of this analysis with experimental results for jets and plumes (see Morton 1959).

Forced plumes in a stably stratified environment

The foregoing treatment has shown that modifications to the shape of forced plumes caused by changes in the source (i.e. in F_0, V_0 and W_0) are restricted mainly to the lower parts of the plumes. In a weakly stratified environment the effects of stratification will be relatively small near the source, but will dominate the upper regions of plumes. Indeed, the environment can be quite strongly stratified and still produce a negligible effect on the lower part of the forced plume (for example, between the virtual point source and the actual source). This may be demonstrated very clearly by comparing the widths of pure plumes from point sources of buoyancy in uniform and stably stratified environments (see paper I); stratification leads to $< 1\,\%$ increase in width at one-third of the plume height, $3\,\%$ at half the height and $< 8\,\%$ at two-thirds of the height. Similarly, for vertical jets (see below), stable stratification causes $< 2\,\%$ increase in width half-way up the jet, and $5\,\%$ increase at two-thirds of the jet height. Consequently, in a stratified environment the shape of forced plumes in their lower parts will be similar to that which has been predicted for a uniform environment, and in their upper parts will be like that described in paper I. Thus, the calculations of the previous section for the position of virtual point sources in a uniform environment can be carried over directly to the case of a stratified environment with very great saving of labour and without appreciable increase of error; but further analysis is needed to find the dependence on F_0, V_0 and W_0 of the height of the plume top, since this will depend critically on stratification.

For a stratified environment the use of Gaussian profiles is unsatisfactory (Morton 1959) so they will be replaced for this section by 'top hat' profiles, with the mean vertical velocity constant across a section of width $2b(X)$ and zero outside it and the mean buoyancy constant across a symmetrically situated profile of width $2\lambda b(X)$ and zero outside. This change of profile does not affect the height calculated for the plume top, but it does modify the values of the constants; for the plume with 'top hat' profiles, $\alpha = 0{\cdot}116$ and $\lambda = 1{\cdot}108$.

The general forced plume from the source (F_0, V_0, W_0) is in a uniform environment equivalent to a related plume from a virtual source of buoyancy and

momentum, and so it will be sufficient here to consider forced plumes (F_0, V_0, 0) from virtual sources. Only the case of stable stratification with a uniform density gradient will be investigated. The physical conditions of the problem provide the three parameters F_0, V_0 and $G = (g/\rho_0)(d\rho_e/dX)$ (a measure of the stratification); one dimensionless parameter, GV_0^4/F_0^2, can be formed from these, and any two form a basis for a reduction of the system to non-dimensional form.

The equations for plumes with 'top hat' profiles (corresponding with equation (2) for Gaussian profiles) are

$$\frac{dW}{dX} = 2\alpha V, \quad \frac{dV^4}{dX} = 2\lambda^2 FW, \quad \frac{dF}{dX} = -GW, \tag{13}$$

where in this case $V = bU$, $W = b^2U$, $F = b^2UP$ in order to preserve the physical meaning of V, W and F. The transformations

$$F = |F_0|f, \quad V = 2^{\frac{1}{4}}\lambda^{\frac{1}{2}}|F_0|^{\frac{1}{2}}G^{-\frac{1}{4}}v, \quad W = 2^{\frac{5}{8}}\alpha^{\frac{1}{2}}\lambda^{\frac{1}{4}}|F_0|^{\frac{3}{4}}G^{-\frac{3}{8}}w,$$
$$X = 2^{-\frac{3}{8}}\alpha^{-\frac{1}{2}}\lambda^{-\frac{1}{4}}|F_0|^{\frac{1}{4}}G^{-\frac{3}{8}}x,$$

reduce these equations to their simplest non-dimensional form,

$$\frac{dw}{dx} = v, \quad \frac{dv^4}{dx} = fw, \quad \frac{df}{dx} = -w; \tag{14}$$

and the corresponding boundary conditions at $x = 0$ are,

$$w = 0, \quad v = 2^{-\frac{1}{4}}\lambda^{-\frac{1}{2}}|F_0|^{-\frac{1}{2}}G^{\frac{1}{4}}V_0 = v_0 \text{ (say)}, \quad f = \operatorname{sgn} F_0. \tag{15}$$

The following cases include all plumes emitted upwards from sources of finite area.

(i) $F_0 > 0$ and $V_0 > 0$, corresponding with actual sources for which $0 < \Gamma < 1$. From the last two of equations (14)

$$2v^4 + f^2 = 2v_0^4 + 1 = \frac{1}{1-\sigma},$$

where $\sigma = GV_0^4/(\lambda^2F_0^2 + GV_0^4)$ is the most convenient form for the representative parameter. Define the new independent variable $s = 2(1-\sigma)v^4$; then

$$f = \pm\left(\frac{1-s}{1-\sigma}\right)^{\frac{1}{2}}, \tag{16}$$

where the positive sign is taken where the buoyancy force acts upwards and the negative sign where it acts downwards. The value of v increases from $v = v_0$ at the source to a maximum $v = (v_0^4 + \frac{1}{2})^{\frac{1}{4}}$ at the level where f vanishes, and then decreases steadily to zero at the top of the plume ($v^2 \propto$ momentum flux); the corresponding values for s are $s = \sigma\,(< 1)$ at the source, $s = 1$ where $f = 0$, and $s = 0$ at the plume top. f decreases steadily from $f = 1$ at the source to $f = -(1-\sigma)^{-\frac{1}{2}}$ at the plume-top.

From the first two of equations (14), for the lower part of the plume ($\sigma \leqslant s \leqslant 1$),

$$w^2 = 2^{-\frac{1}{4}}(1-\sigma)^{-\frac{3}{2}}\int_\sigma^s t^{\frac{1}{4}}(1-t)^{-\frac{1}{2}}\,dt$$
$$= 2^{-\frac{1}{4}}(1-\sigma)^{-\frac{3}{2}}\{\beta(\tfrac{5}{4}, \tfrac{1}{2}; s) - \beta(\tfrac{5}{4}, \tfrac{1}{2}; \sigma)\}, \tag{17a}$$

and in the upper part of the plume ($1 \geqslant s \geqslant 0$)

$$w^2 = 2^{-\frac{1}{4}}(1-\sigma)^{-\frac{3}{4}}\{2\beta(\tfrac{5}{4},\tfrac{1}{2}) - \beta(\tfrac{5}{4},\tfrac{1}{2};s) - \beta(\tfrac{5}{4},\tfrac{1}{2};\sigma)\}. \tag{17b}$$

The parametric solution is now completed by finding x from equation (14, ii); for the present purpose we need only the height of the plume-top, $x_{\max}$, which is the greatest height to which fluid emitted from the source can penetrate

$$x_{\max} = 2^{-\frac{7}{4}}(1-\sigma)^{-\frac{1}{2}}\left\{\int_\sigma^1 \frac{dt}{\sqrt{(1-t)}\sqrt{\{\beta(\frac{5}{4},\frac{1}{2};t) - \beta(\frac{5}{4},\frac{1}{2};\sigma)\}}} + \int_0^1 \frac{dt}{\sqrt{(1-t)}\sqrt{\{2\beta(\frac{5}{4},\frac{1}{2}) - \beta(\frac{5}{4},\frac{1}{2};t) - \beta(\frac{5}{4},\frac{1}{2};\sigma)\}}}\right\}. \tag{18}$$

A graph of $x_{\max}$ plotted against σ is shown in figure 4; the curve for expression (18) is labelled $0 < \Gamma < 1$. The limiting case $\sigma = 0$ for the plume from a virtual source of buoyancy only has a greatest height $x_{\max} = 2{\cdot}805$, which agrees with the value

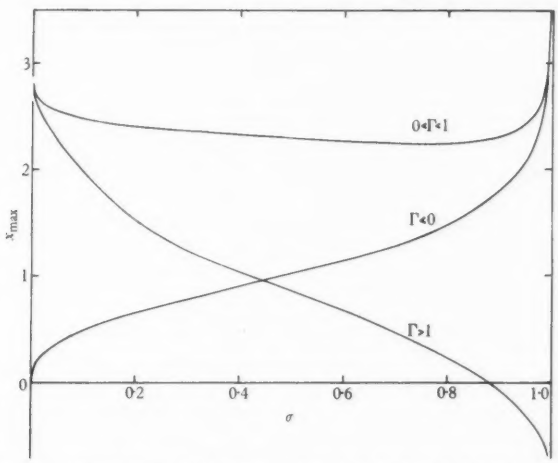

FIGURE 4. The non-dimensional height ($x_{\max}$) of the top of a forced plume in a stably stratified environment, plotted as a function of the dimensionless parameter

$$\sigma = GV_0^4/(\lambda^2 F_0^2 + GV_0^4).$$

The curves drawn are for the following cases: (i) $0 < \Gamma < 1$ represents the plume from a virtual source of positive buoyancy and upward momentum, (ii) $\Gamma < 0$ is that for a source of negative buoyancy and upward momentum, and (iii) $\Gamma > 1$ is that for a source of positive buoyancy and downward momentum.

2·80+, given in paper I; the complete solution for the case $\sigma = 0$ can be found in that paper. As σ is increased the value $x_{\max}$ decreases, at first rapidly owing to the sudden increase in mixing near the source and then more slowly. When σ exceeds 0·8 the buoyancy flux from the source is becoming less important than that of momentum, and forced plumes can be projected to any height by sufficiently increasing the momentum of the fluid as it leaves the sources; the necessary increase may be very large, for example, $GV_0^4/\lambda^2 F_0^2$ must be increased to about 100 before the height of the forced plume is again as great as that of the simple

plume from a virtual point source of buoyancy. (Actual heights are directly proportional to dimensionless heights if V_0 only is varied.)

(ii) $F_0 < 0$ and $V_0 > 0$, corresponding with actual sources for which $\Gamma < 0$. The appropriate boundary conditions at $x = 0$ are

$$f = -1, \quad w = 0, \quad v = v_0 = 2^{-\frac{1}{4}}\sigma^{\frac{1}{4}}(1-\sigma)^{-\frac{1}{4}};$$

and the greatest height to which the heavy plume fluid rises is

$$x_{\max} = 2^{-\frac{1}{4}}(1-\sigma)^{-\frac{1}{8}} \int_0^\sigma \frac{dt}{\sqrt{(1-t)\sqrt{\{\beta(\frac{5}{4}, \frac{1}{2}; \sigma) - \beta(\frac{5}{4}, \frac{1}{2}; t)\}}}}. \tag{19}$$

The variation in height of the plume-top with σ is shown in figure 4 by the curve labelled $\Gamma < 0$. A relatively small flux of momentum is needed to lift the plume top well clear of the source, but thereafter the height increases slowly with increasing V_0. The parts of the curves near $\sigma = 1$ in figure 4 are very similar because here the forced plume is dominated by the momentum flux from the source.

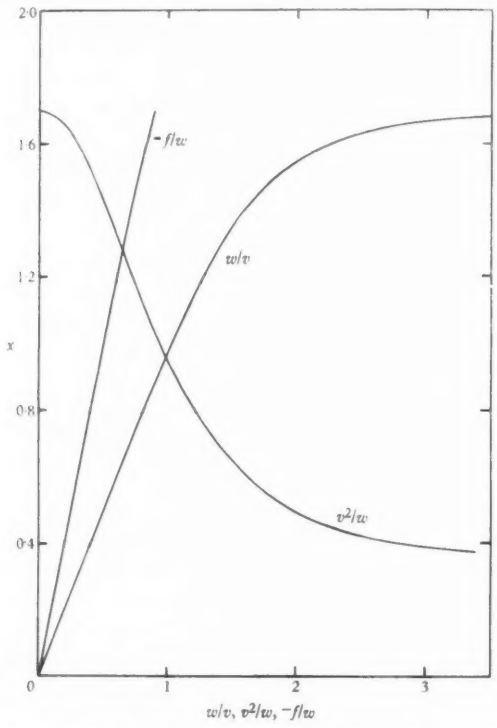

FIGURE 5. The behaviour of the jet from a virtual source of momentum, situated in a stably stratified environment. The non-dimensional quantities plotted are w/v, which is proportional to the horizontal length scale or 'radius' of the jet, v^2/w, proportional to the vertical velocity on the axis, and $-f/w$, proportional to the reduction of temperature at the axis below that of the ambient fluid at that level; x is the non-dimensional height above the virtual source.

(iii) $F_0 > 0$ and $V_0 < 0$, corresponding with actual sources for which $\Gamma > 1$. The initial downwards flow corresponds with case (ii) inverted; the height of the plume-top above the source in the subsequent ascent is

$$x_{\max} = 2^{-\frac{7}{8}}(1-\sigma)^{-\frac{1}{8}}\left\{-\int_0^{\sigma}\frac{dt}{\sqrt{(1-t)}\sqrt{\{\beta(\frac{5}{4},\frac{1}{2};\sigma)-\beta(\frac{5}{4},\frac{1}{2};t)\}}}\right.$$
$$\left.+\int_0^1\left[\frac{1}{\sqrt{\{\beta(\frac{5}{4},\frac{1}{2};\sigma)+\beta(\frac{5}{4},\frac{1}{2};t)\}}}+\frac{1}{\sqrt{\{2\beta(\frac{5}{4},\frac{1}{2})+\beta(\frac{5}{4},\frac{1}{2};\sigma)-\beta(\frac{5}{4},\frac{1}{2};t)\}}}\right]\frac{dt}{\sqrt{(1-t)}}\right\}. \tag{20}$$

The position of the plume top relative to the virtual source is shown by the curve labelled $\Gamma > 1$ in figure 4, and the lowest level to which the plume fluid penetrates can be found from the curve $\Gamma < 0$ in the same figure.

The vertical jet from a source $(0, V_0, 0)$ *in a stratified environment* (G)

In this case the scale of the motion is determined by V_0 and G; the transformations

$$F = 2^{-\frac{1}{2}}\lambda^{-1}V_0^2G^{\frac{1}{2}}f, \quad V = V_0v, \quad W = 2^{\frac{1}{4}}\alpha^{\frac{1}{4}}\lambda^{-\frac{1}{2}}V_0^{\frac{3}{2}}G^{-\frac{1}{4}}w,$$
$$X = 2^{-\frac{3}{4}}\alpha^{-\frac{1}{2}}\lambda^{-\frac{1}{2}}V_0^{\frac{1}{2}}G^{-\frac{1}{4}}x,$$

reduce the equations for the jet to the same form as equations (14), and the boundary conditions at $x = 0$ to $v = 1$, $w = 0$ and $f = 0$. The solution is

$$\left.\begin{aligned} v &= s^{\frac{1}{4}}, \quad w = 2^{\frac{1}{4}}\{\beta(\tfrac{5}{4},\tfrac{1}{2})-\beta(\tfrac{5}{4},\tfrac{1}{2};s)\}^{\frac{1}{4}}, \\ f &= -2^{\frac{1}{2}}(1-s)^{\frac{1}{2}}, \quad x = 2^{-\frac{3}{4}}\int_s^1\frac{dt}{\sqrt{(1-t)}\sqrt{\{\beta(\frac{5}{4},\frac{1}{2})-\beta(\frac{5}{4},\frac{1}{2};t)\}}}; \end{aligned}\right\} \tag{21}$$

the height of the plume top is $x_{\max} = 1{\cdot}70$. Figure 5 shows these results; $v^2/w \propto$ vertical velocity within the plume, $w/v \propto$ radius of the plume, and $f/w \propto$ buoyancy of the plume fluid. These curves may be compared with those for a simple plume shown in figure 1 of paper I; the most obvious and important difference is the more rapid spreading of the jet.

REFERENCES

Gutman, L. N. 1949 *Prik. Mat. i Mech. Leningr.* **13**, 435.

Morton, B. R., Taylor, G. I. & Turner, J. S. 1956 *Proc. Roy. Soc.* A, **234**, 1.

Morton, B. R. 1959 *Intern. J. Air Pollution* (to be published).

Priestley, C. H. B. & Ball, F. K. 1955 *Quart. J. Roy. Met. Soc.* **81**, 144.

Railston, W. 1954 *Proc. Phys. Soc.* B, **67**, 42.

Rouse, H., Yih, C. S. & Humphreys, H. W. 1952 *Tellus*, **4**, 201.

Schmidt, W. 1941 *Z. angew. Math. Mech.* **21**, 265, 351.

Yih, C. S. 1951 *Proc. 1st U.S. Congr. Appl. Mech.* p. 941.

Yih, C. S. 1952 *Trans. Amer. Geophys. Union*, **33**, 669.

The structure of a contact region, with application to the reflexion of a shock from a heat-conducting wall

By F. A. GOLDSWORTHY
Department of Mathematics, University of Manchester

(Received 19 July 1958)

By using methods well known in boundary layer theory, the pressure across a contact region is shown to be approximately constant. A partial differential equation for the temperature is then derived. If the ideal-gas flow external to the contact region is known, the temperature profile can be determined. This can then be used to calculate successively the velocity and a better approximation for the pressure of the gas in the contact region. The theory is illustrated by obtaining the temperature, velocity and pressure distributions for a gas in a contact region moving with uniform velocity. The thermal conductivity of the gas is assumed to vary with the temperature τ like $k = k_n \tau^n$, where $n = 0$, 1 or 2. The results are valid for any temperature ratio across the region.

The general theory is also used to determine the motion of a plane shock which is reflected from a plane-conducting wall. The fluid between the reflected shock and the wall is at a higher temperature than that of the wall and a contact region adjacent to the wall results. Expressions for the temperature, velocity and pressure of the fluid are derived, and it is shown that the effect of heat conduction is to decrease the velocity of the reflected shock by an amount which varies as the inverse square root of the time.

1. Introduction

In ideal-gas theory, a contact region is represented by a discontinuity in the temperature and density but not in the pressure and gas velocity. In this paper the effect of viscosity and heat conduction on the internal structure of a contact region is discussed. By using methods well known in boundary layer theory the pressure across the contact region can be shown to be approximately constant. This enables an approximate equation for the temperature of the gas to be derived and, if the ideal-gas flow external to the contact region is known, the temperature profile to be determined. From this the velocity and a better approximation for the pressure of the gas can be successively calculated. These can then be used to determine a higher-order approximate equation for the temperature. Hall (1954) has considered the case of a contact region moving with uniform speed. He assumed the pressure to be constant across the contact region and checked this assumption by experiment, finding that very little pressure change occurs there. The present paper considers the general problem of an accelerating contact region, where the temperatures at its edges vary with time.

The theory is illustrated by determining the temperature, velocity and pressure distributions in a contact region moving with uniform velocity for gases, whose thermal conductivities vary with the temperature τ like $k = k_n \tau^n$, where $n = 0$, 1 or 2, and the k_n are constants. The results are valid for any temperature ratio across the contact region.

An examination of the distributions suggests that for more complicated problems, in which the replacement of the whole contact region by a discontinuity is no longer a good approximation, the part of the contact region adjacent to the low-temperature side could be regarded as a discontinuity behind which there was finite heat flux. Such discontinuities have been discussed by Fraser (1958) with reference to steady radiation fronts. He finds that two types exist, namely a radiation flame corresponding to a weak deflagration, and a radiation shock corresponding to a strong detonation. Hirschfelder, Curtiss & Bird (1954) have also discussed the structure of a radiation front moving into an opaque material in which the absorption is intense. The expression for the radiation flux uses the Rosseland mean free path for thermal radiation, and the expression is similar in form to that for the heat flux used in this paper with the 'conductivity' proportional to some power, n, of the temperature, where $n \geqslant 3$. Thus in the present paper, the solution for the case $n = 2$ serves as an indication to what happens in radiative heat transfer. For instance, it illustrates that the velocity of such a 'radiation front' relative to the fluid is small compared with the speed of sound and that the discontinuity is rarefactive. We can thus infer that for radiation in an opaque material a radiation flame will result. To find the structure of an unsteady radiation flame requires only a slight modification of the present treatment for a contact region.

The general theory is further illustrated by determining the flow set up when a plane shock hits a plane-conducting wall. The reflected shock is shown to be attenuated by the presence of the conducting wall.

2. General theory

A uniform gas of infinite extent is initially at rest. Heat is then supplied to the gas at a rate depending only on the distance y from some fixed plane $y = 0$ and the time t. If the gas initially in the region $y < 0$ is heated, then the equations governing the subsequent motion are

$$\frac{D\rho}{Dt} + \rho \frac{\partial u}{\partial y} = 0, \tag{1}$$

$$\rho \frac{Du}{Dt} = -\frac{\partial p}{\partial y} + \frac{4}{3} \frac{\partial}{\partial y} \left(\mu \frac{\partial u}{\partial y} \right), \tag{2}$$

$$c_p \frac{D\tau}{Dt} + \frac{\tau}{\rho^2} \left(\frac{\partial \rho}{\partial \tau} \right)_p \frac{Dp}{Dt} = Q(y,t)\, H(y_0 - y) + \frac{4}{3} \frac{\mu}{\rho} \left(\frac{\partial u}{\partial y} \right)^2 + \frac{1}{\rho} \frac{\partial}{\partial y} \left(k \frac{\partial \tau}{\partial y} \right), \tag{3}$$

together with the equation of state

$$\rho = f(p, \tau), \tag{4}$$

where p, ρ, τ and u denote the pressure, density, temperature and gas velocity, respectively, μ and k are the coefficients of viscosity and thermal conductivity and are assumed to be functions of the temperature alone, $y_0(t)$ is the position at time t of the particle initially at the origin, $Q(y,t)$ is the rate at which energy is generated per unit mass of the fluid and $H(y_0-y)$ is the Heaviside unit function, which is zero for $y > y_0(t)$.

If the viscous and heat conduction terms are neglected, then the solution of the problem involves a shock wave which is propagated into the non-heated gas. The shock wave is followed by a contact surface separating the heated gas from the non-heated gas. The motion and conditions at the sides of both these discontinuities can be found given the rate of generation of energy in the fluid. This solution will be referred to as the 'ideal-gas' solution. In reality both the shock and the contact surface are regions of small but finite thickness, where the transition from one state to another takes place rapidly and where viscosity and heat conduction exert a dominating influence. Our attention will be confined to finding the structure of the contact region, assuming that the 'ideal-gas' solution is known.

Since a contact surface moves with the fluid, a Lagrangian frame of reference is convenient. Let x be the initial position of a particle, which is at position y at time t, and let $\bar{\rho}$ denote the initial constant density of the gas. Equation (1), which expresses the law of conservation of mass, can now be replaced by the integral expression

$$\bar{\rho}x = \int_{y_0(t)}^{y} \rho \, dy. \tag{5}$$

Now put $\psi = \bar{\rho}x$, which is by definition a constant for a particular particle, and choose ψ and t as the new independent variables. Equations (2) and (3) transform into

$$\frac{\partial u}{\partial t} = -\frac{\partial p}{\partial \psi} + \frac{4}{3}\frac{\partial}{\partial \psi}\left(\mu\rho\frac{\partial u}{\partial \psi}\right), \tag{6}$$

$$c_p\frac{\partial \tau}{\partial t} + \frac{\tau}{\rho^2}\left(\frac{\partial \rho}{\partial \tau}\right)_p\frac{\partial p}{\partial t} = Q(\psi,t)\,H(-\psi) + \tfrac{4}{3}\mu\rho\left(\frac{\partial u}{\partial \psi}\right)^2 + \frac{\partial}{\partial \psi}\left(k\rho\frac{\partial \tau}{\partial \psi}\right), \tag{7}$$

where $u = (\partial y/\partial t)_\psi$. The reader will note that the above transformation corresponds to the von Mises transformation of the boundary layer equations. If ρ is known as a function of ψ and t, equation (5) can be re-written in the form

$$y - y_0(t) = \int_0^{\psi} (1/\rho)\, d\psi, \tag{8}$$

which, on differentiating with respect to t keeping ψ constant, gives the velocity of a fluid particle

$$u = u_0(t) + \int_0^{\psi} \frac{\partial}{\partial t}\left(\frac{1}{\rho}\right) d\psi, \tag{9}$$

where $u_0(t)$ is the velocity at time t of the particle initially at the origin.

Let P, ω and U denote the 'ideal-gas' solutions for the pressure, density and velocity. Let the actual pressure and gas velocity in the contact region be

$$p = P + p', \quad u = U + u'. \tag{10}$$

Substituting in equations (9) and (6), we obtain

$$u' = u'_0(t) + \int_0^{\psi} \frac{\partial}{\partial t}\left(\frac{1}{\rho} - \frac{1}{\omega}\right) d\psi, \tag{11}$$

$$\frac{\partial u'}{\partial t} = -\frac{\partial p'}{\partial \psi} + \frac{4}{3}\frac{\partial}{\partial \psi}\left[\mu\rho\left(\frac{\partial U}{\partial \psi} + \frac{\partial u'}{\partial \psi}\right)\right]. \tag{12}$$

We now proceed in a manner similar to that used to obtain the boundary layer equations and assume that the effective thickness δ of the contact region is small. Use suffices 1 and 2 to label quantities in the heated and non-heated parts of the gas adjacent to the contact region. Taking t as a quantity having magnitude of standard order, equation (11) shows that u' is $O\{(1-\omega_1/\omega_2)\,\delta\}$. Further, if in the contact region the diffusion terms in equation (7) are to be of the same magnitude as the remaining terms, then $(k\rho)/c_p = O(\delta^2)$, and if also $(\mu c_p)/k$ is at most of order unity, it follows from equation (12) that $\partial p'/\partial\psi$ is $O\{(1-\omega_1/\omega_2)\,\delta\}$. Hence, the total change in p' across the contact region is $O\{(1-\omega_1/\omega_2)\,\delta^2\}$, so that, if terms of this order are negligible, the pressure in equation (7) can be replaced by its 'ideal-gas' value, $P(\psi, t)$, plus an arbitrary function of the time which is $O\{(1-\omega_1/\omega_2)\,\delta\}$. The viscous term in equation (7) can be neglected also. The energy equation then becomes an equation for the temperature alone to be solved subject to the boundary condition at the edges of the contact region. In order to simplify the analysis, terms which are $O\{(1-\omega_1/\omega_2)\,\delta\}$ will be neglected; the pressure in equation (7) can then be replaced by the 'ideal-gas' pressure evaluated at $\psi = 0$, namely $P_0(t)$. Similarly, if the rate of generation of heat in the fluid is not too strongly dependent upon the temperature, $Q(\psi, t)$ can also be replaced by $Q_0(t)$. If this is not the case, then the temperature dependence must be retained and the analysis is more complicated. We also assume that the gas is perfect with constant specific heats. Equation (7) then becomes

$$\frac{\partial \tau}{\partial t} - \frac{\gamma-1}{\gamma P_0}\frac{dP_0}{dt}\tau = \frac{Q_0(t)\,H(-\psi)}{c_p} + \frac{P_0}{c_p R}\frac{\partial}{\partial \psi}\left(\frac{k}{\tau}\frac{\partial \tau}{\partial \psi}\right), \tag{13}$$

which is an equation for the temperature and is solved subject to the boundary conditions $\tau = T_1$ at $\psi = -\infty$, $\tau = T_2$ at $\psi = \infty$, where T_1 and T_2 are the temperatures of the gas on either side of the contact discontinuity. They satisfy the equations

$$\frac{dT_1}{dt} - \frac{(\gamma-1)}{\gamma P_0}\frac{dP_0}{dt}T_1 = \frac{Q_0(t)}{c_p}, \quad \frac{dT_2}{dt} - \frac{(\gamma-1)}{\gamma P_0}\frac{dP_0}{dt}T_2 = 0. \tag{14}$$

Substituting $\tau = T_1\theta(\psi, t)$ in equation (13), and using equations (14), we obtain

$$\frac{\partial}{\partial t}\left[\frac{T_1}{T_2}(\theta - H(-\psi))\right] = \frac{P_0 T_1}{c_p R T_2}\frac{\partial}{\partial \psi}\left(\frac{k}{\tau}\frac{\partial \theta}{\partial \psi}\right). \tag{15}$$

If $k = k_1\tau$, where k_1 is a constant, a slight change in the time variable reduces the equation to the well-known heat conduction equation. When k is some other function of the temperature numerical methods have to be employed. The two cases when k is a constant and when it is proportional to the square of the temperature are dealt with in § 3.

Once the temperature has been found as a function of ψ and t, the position y of a particle can be determined from equation (8), which can be written

$$y - y_0(t) = (R/P_0) \int_0^{\psi} \tau \, d\psi. \tag{16}$$

The temperature distribution in the contact region can then be plotted.

Further, by using equations (13), (11) and (12), the velocity and the pressure can be expressed as

$$u - U = -\frac{1}{\gamma P_0} \frac{dP_0}{dt}(y - Y) + \frac{k}{c_p \tau} \frac{\partial \tau}{\partial \psi} + f(t), \tag{17}$$

$$p - P = (\tfrac{4}{3}\sigma - 1) \frac{k}{c_p \tau} \frac{\partial \tau}{\partial t} + \frac{1}{c_p P_0} \frac{dP_0}{dt} \int^{\tau} \left(\frac{k}{\gamma \tau} - \tfrac{4}{3}\sigma \frac{dk}{d\tau} \right) d\tau$$

$$+ \left[\frac{d}{dt} \left(\frac{1}{\gamma P_0} \frac{dP_0}{dt} \right) - \left(\frac{1}{\gamma P_0} \frac{dP_0}{dt} \right)^2 \right] \int^{\psi} (y - Y) \, d\psi - f'(t) \, \psi + \frac{1}{\gamma P_0} \frac{dP_0}{dt} f(t) \, \psi + g(t), \tag{18}$$

where $\sigma = (\mu c_p)/k$, $f(t)$ and $g(t)$ are arbitrary functions of the time, and Y is the position of a particle at time t given by 'ideal-gas' flow theory, this particle being at position y when the effects of viscosity and heat conduction are considered. Y is related to y by the approximate equation

$$\psi = \int_{y_0}^{y} \rho \, dy = \omega_1 (Y - Y_0) \, H(Y_0 - Y) + \omega_2 (Y - Y_0) \, H(Y - Y_0), \tag{19}$$

where ω_1 and ω_2 are the values of the density on either side of the contact discontinuity where the gas is assumed to be ideal.

The functions $f(t)$ and $g(t)$ are determined by considering the effect the contact region has on the external ideal-gas flow. The obvious question to ask is to what order of approximation can the flow inside the contact region be fitted to the gas flow outside without change from that described by the 'ideal-gas' solution. For this we require that $y \to Y$, $u \to U$ and $p \to P$ at *both* edges of the contact region. Now just outside the contact region $\partial\tau/\partial\psi$ and $\partial\tau/\partial t$ are at most $O(1)$. Equation (17), in which terms of $O(\delta^2)$ are neglected, shows that the first two requirements are satisfied if $f(t)$ is identically zero. Equation (18) shows that to $O(\delta)$, $p = P$ everywhere in the contact region if $g(t)$ is $O(\delta^2)$, so that the third requirement can be satisfied. Hence the external gas flow is unaltered to $O(\delta)$. Equation (18) with $f(t) \equiv 0$ can now be used to determine the path of any particular particle in the contact region. However, to determine the pressure from equation (18), it is necessary to know $g(t)$ to $O(\delta^2)$ and this can only be found by considering the effect of the contact region on the gas flow external to it. In one case only can $g(t)$ be determined easily and this is for the case of a uniformly moving contact surface for which $dP_0/dt = 0$ and $\partial\tau/\partial t \to 0$ at the edges of the contact region. Equation (18) then shows that p can tend to P_0 at both edges of the contact region if $g(t) \equiv 0$. The effect of the contact region on the external flow is then $O(\delta^3)$. Once the pressure and velocity of the gas have been determined from equations (17) and (18), a higher order approximation for the temperature could be worked out.

3. The structure of a contact region moving with constant velocity

In this case the ratio of the temperatures at the edges of the region remains constant. The thermal conductivity of the gas is assumed to vary with the temperature like $k = k_n \tau^n$, $n = 0$, 1 or 2. Hall (1954) has already treated the case $n = 1$ and obtained results for the case $n = 0$ by assuming small temperature changes across the contact region. The same assumption will not be made here, so that the results are applicable for any temperature ratio.

(i) $k = k_0$.

This case is best treated by transforming equation (15) back into the Eulerian system and making use of equation (17). Equation (15) becomes

$$\frac{\partial\theta}{\partial t} + \left[u_0 - \frac{k_0}{c_p\omega_1}\left(\frac{\partial\theta}{\partial y}\right)_0\right]\frac{\partial\theta}{\partial y} = \frac{k_0}{c_p\omega_1}\left[\theta\frac{\partial^2\theta}{\partial y^2} - \left(\frac{\partial\theta}{\partial y}\right)^2\right]. \tag{20}$$

A similarity solution of the above equation depending upon the variable $\eta = \alpha_0[y - y_0(t)]/\sqrt{t}$ is now sought. Choosing $\alpha_0 = \sqrt{\{(\omega_1 c_p)/k_0\}}$, equation (20) becomes

$$-\left[\tfrac{1}{2}\eta + \left(\frac{d\theta}{d\eta}\right)_0\right]\frac{d\theta}{d\eta} = \theta\frac{d^2\theta}{d\eta^2} - \left(\frac{d\theta}{d\eta}\right)^2. \tag{21}$$

Now divide equation (21) by $d\theta/d\eta$ and then differentiate with respect to η. Substituting $\theta = \phi^2$ in the resulting equation and multiplying the equation by ϕ''/ϕ' we obtain on integration,

$$\frac{\phi\phi''}{\phi'} = \pm\sqrt{\{\phi'^2 - \log_e\phi' + \kappa\}}, \tag{22}$$

where κ is a constant and the dash indicates differentiation with respect to η. Equation (22) integrates again to give

$$\log_e\frac{\phi}{\phi_c} = \pm\int_{\phi_c'}^{\phi'}\frac{d\phi'}{\sqrt{\{\phi'^2 - \log_e\phi' + \kappa\}}}, \tag{23}$$

where $\phi' = \phi_c'$ when $\phi = \phi_c$. Substitution of equation (22) into (21) yields the expression for the similarity variable

$$\eta = \mp 2\phi\sqrt{\{\phi'^2 - \log_e\phi' + \kappa\}} + 2\phi\phi' - 4\phi_0\phi_0'. \tag{24}$$

The signs are fixed by considering conditions at infinity where ϕ' becomes zero. This shows that the upper signs in expressions (23) and (24) are taken for $\eta < \eta_c$ and the lower signs for $\eta > \eta_c$, where η_c is the value of η for which

$$\sqrt{\{\phi_c'^2 - \log_e\phi_c' + \kappa\}} = 0, \tag{25}$$

thus determining κ in terms of ϕ_c'.

Now as $\eta \to \infty$, $\phi \to \sqrt{(T_2/T_1)}$, $\phi' \to 0$; hence

$$\log_e\frac{1}{\phi_c}\sqrt{\frac{T_2}{T_1}} = -\int_{\phi_c'}^{0}\frac{d\phi'}{\sqrt{\{\phi'^2 - \phi_c'^2 - \log_e(\phi'/\phi_c')\}}}. \tag{26}$$

Similarly, as $\eta \to -\infty$, $\phi \to 1$, $\phi' \to 0$, so that

$$\log_e\frac{1}{\phi_c} = \int_{\phi_c'}^{0}\frac{d\phi'}{\sqrt{\{\phi'^2 - \phi_c'^2 - \log_e(\phi'/\phi_c')\}}}. \tag{27}$$

Hence it is seen that $\phi_c^2 = \sqrt{(T_2/T_1)}$ or $\tau_c = \sqrt{(T_1 T_2)}$, i.e. at $\eta = \eta_c (\neq 0)$ the temperature is the geometric mean of the temperatures at $\pm\infty$.

Equation (23) can be integrated numerically given ϕ_c', which corresponds to fixing the temperature ratio T_1/T_2; for instance, $\phi_c' = 1/\sqrt{2}$ corresponds to $T_1/T_2 = \infty$. The temperature is then found as a function of ϕ'. Equation (24) can now be used to find η as a function of ϕ', thus enabling the temperature distribution to be plotted (see figures 1 and 2).

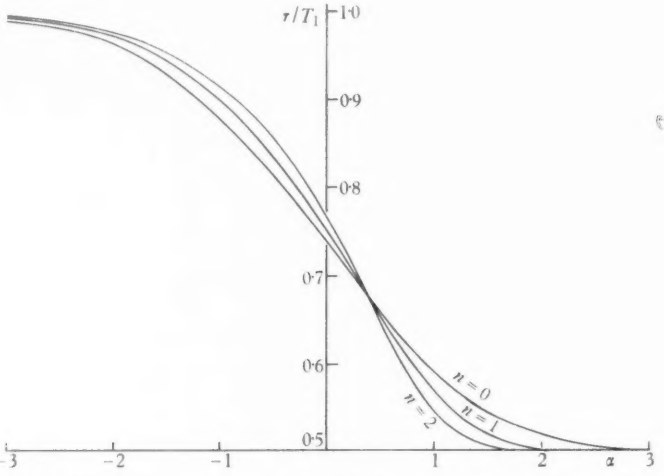

FIGURE 1. The temperature ratio τ/T_1 as a function of the similarity variable $\alpha = \{y - y_0(t)\}\,[(c_p\omega_1)/(k_n T_1^n t)]^{\frac{1}{2}}$ for $n = 0$, 1 and 2, and $T_2/T_1 = \frac{1}{2}$.

(ii) $k = k_1\tau$.

The solution of equation (15) for this case is well known and is

$$\tau = \tfrac{1}{2}(T_1 + T_2) - \tfrac{1}{2}(T_1 - T_2)\,\mathrm{erf}\,\tfrac{1}{2}\eta, \tag{28}$$

where $\eta = \sqrt{[(c_p R)/(P_0 k_1 t)]}\,\psi$. By substituting equation (28) into equation (16), $\sqrt{[(c_p\omega_1)/(k_1 T_1 t)]}\,(y - y_0(t))$ can be determined as a function of η. The temperature distribution can then be plotted (see figures 1 and 2).

(iii) $k = k_2\tau^2$.

Equation (15) becomes

$$\frac{\partial\theta}{\partial t} = \frac{k_2 P_0 T_1}{c_p R}\frac{\partial}{\partial\psi}\left(\theta\frac{\partial\theta}{\partial\psi}\right). \tag{29}$$

The reader will note that this equation is of the same form as that used to determine the velocity distribution in a laminar boundary layer of incompressible fluid. The problem now under consideration is analogous to the laminar mixing of two parallel streams, the velocity in this case being identified with the temperature in our problem.

We look for a similarity solution depending on the variable $\eta = \alpha_2 \psi/\sqrt{t}$. Choosing $\alpha_2 = \sqrt{[(c_p R)/(P_0 k_2 T_1)]}$, equation (29) becomes

$$-\tfrac{1}{2}\eta \frac{d\theta}{d\eta} = \frac{d}{d\eta}\left(\theta \frac{d\theta}{d\eta}\right). \tag{30}$$

Putting $\theta = d\eta/d\zeta$ and taking ζ as the new independent variable, we obtain the Blasius equation

$$2\frac{d^3\eta}{d\zeta^3} + \eta \frac{d^2\eta}{d\zeta^2} = 0. \tag{31}$$

This has been solved numerically by Lock (1951) for the case of laminar mixing of two parallel streams for various ratios of the velocities. These results can be applied directly to obtain the temperature distribution for various values of the ratio T_1/T_2.

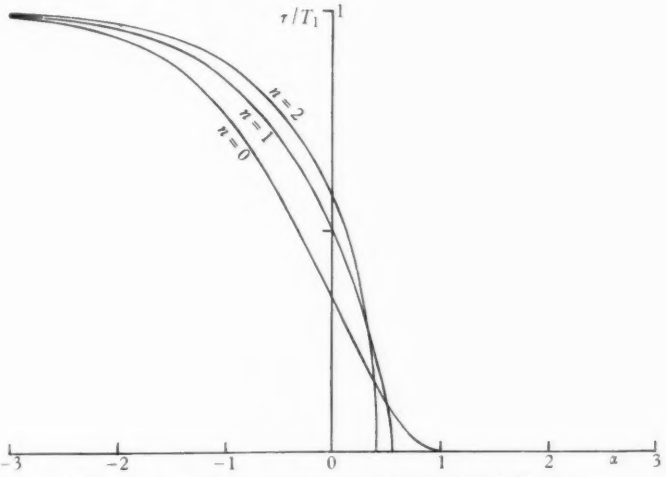

FIGURE 2. The temperature distribution for $T_2/T_1 = 0$ (with the same abscissa as in figure 1).

Results

Solutions have been obtained for the cases $T_2/T_1 = \frac{1}{2}$ and 0. The temperature distributions are plotted in figures 1 and 2 for $n = 0$, 1 and 2. They suggest that for more complicated problems, where the contact region could not be represented by a discontinuity, a theory could be developed in which that part of the contact region adjacent to the low temperature side could be replaced by a discontinuity behind which there was finite heat flux. The velocity of such a discontinuity relative to the fluid would in general be small compared to the speed of sound. The velocity and pressure distributions are shown in figures 3 to 6. They show that if the above approximate replacement was made, then the discontinuity would be rarefactive and would correspond to a weak deflagration.

Figure 2 shows that when $T_2/T_1 = 0$ the temperature gradient is infinite at the low temperature end for $n = 1$ and 2. This is due to assuming zero temperature

there, thus introducing a singularity into equations (13), (17) and (18). In an actual case, where the temperature is small but finite, the profile would be smooth. The same singular behaviour is exhibited in the velocity and pressure

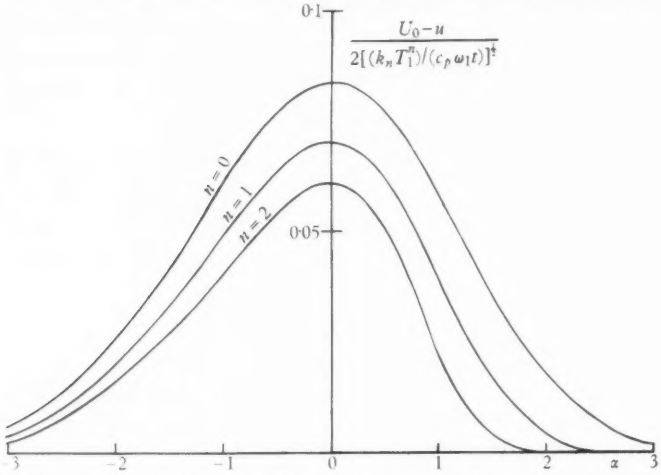

FIGURE 3. The perturbed velocity distribution for $T_2/T_1 = \frac{1}{2}$ (U_0 is the 'ideal-gas' velocity, defined in a similar way to P_0).

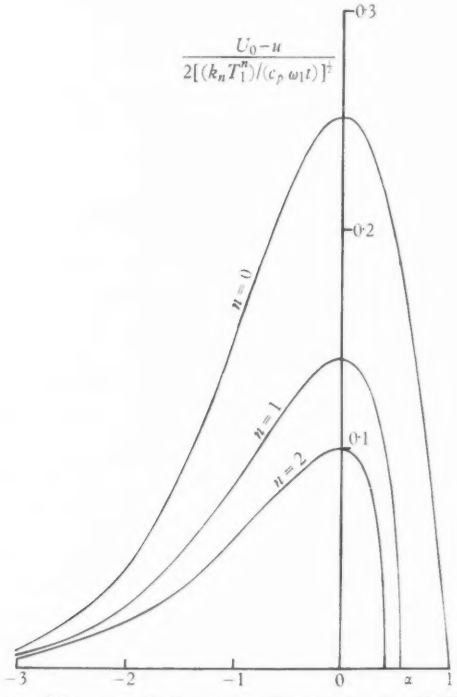

FIGURE 4. The perturbed velocity distribution for $T_2/T_1 = 0$.

diagrams. The pressure distribution for $T_2/T_1 = 0$ and $n = 0$ shows a discontinuity at the low temperature end. This is due to the non-vanishing of the term $(1/\tau)(\partial\tau/\partial t)$ in equation (18) as $\tau \to \tau_c$ $(= 0$ in this case). This discontinuity would not be present if T_2/T_1 was small but finite.

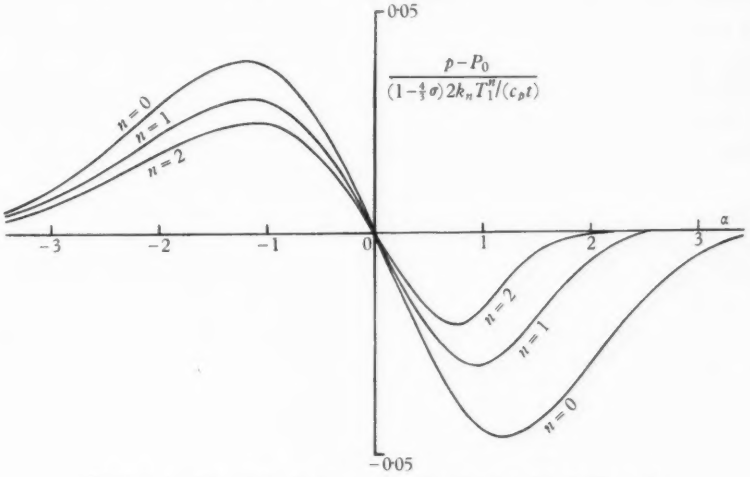

FIGURE 5. The perturbed pressure distribution for $T_2/T_1 = \frac{1}{2}$.

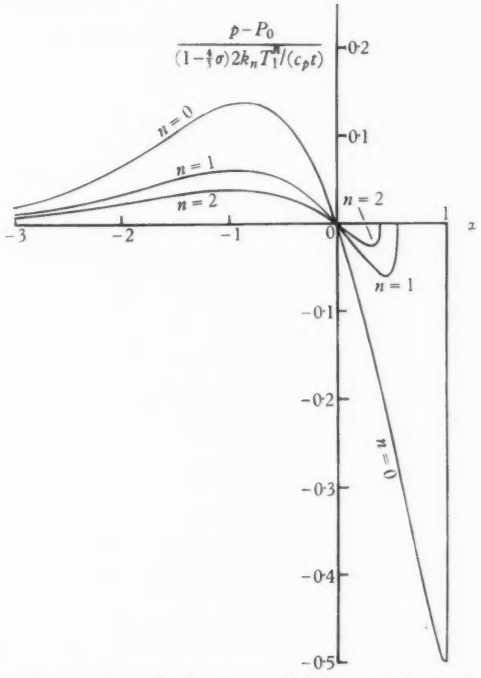

FIGURE 6. The perturbed pressure distribution for $T_2/T_1 = 0$.

4. The normal reflexion of a shock from a plane-conducting wall

At time $t = 0$, a plane shock of given strength is reflected from the face, $y = 0$, of a wall occupying the region $y > 0$. If viscosity and heat conduction are neglected, the velocity of the reflected shock can be determined. Let this velocity be U_s and let subscripts 2 and 3 indicate flow data ahead and behind the reflected shock respectively. The initial temperature of the wall is denoted by T_1. Near the face of the wall there will be a contact region in which heat conduction has an important effect and where we shall determine the temperature distribution.

In the region $y > 0$, the temperature satisfies the equation

$$\frac{\partial \tau}{\partial t} = \frac{k_w}{\rho_w c_w} \frac{\partial^2 \tau}{\partial y^2}, \tag{32}$$

where k_w is the thermal conductivity, ρ_w is the density, and c_w is the specific heat of the wall.

In the gas (in the region $y < 0$) adjacent to the wall, the temperature satisfies the equation [see equation (15)]

$$\frac{\partial \tau}{\partial t} = \frac{\partial}{\partial \psi}\left(\frac{kP_3}{c_p R\tau}\frac{\partial \tau}{\partial \psi}\right). \tag{33}$$

Equations (32) and (33) are now solved subject to the boundary conditions $\tau \to T_1$ at the edge of the contact region in the wall, and $\tau \to T_3$ at the edge of the contact region in the gas. At the wall, the temperature and the flux of heat are continuous; thus

$$\left(k\frac{\partial \tau}{\partial y}\right)_{y=-0} = \left(k_w \frac{\partial \tau}{\partial y}\right)_{y=+0}. \tag{34}$$

To simplify the analysis we assume that $k = k_1\tau$. Equations (32) and (33) can then be solved and yield the solutions

$$\tau - T_1 = A\left[1 - \operatorname{erf}\frac{y}{2\sqrt{\kappa_w t}}\right] \quad (\text{in } y > 0), \tag{35}$$

$$\tau - T_3 = B\left[1 + \operatorname{erf}\frac{\psi}{2\sqrt{\kappa_g t}}\right] \quad (\text{in } y < 0), \tag{36}$$

where $\kappa_w = k_w/(\rho_w c_w)$ and $\kappa_g = (k_1 P_3)/(c_p R)$. Applying the conditions at $y = 0$, we obtain

$$A = \frac{T_3 - T_1}{1 + (1/m)}, \quad B = -\frac{T_3 - T_1}{1 + m}, \tag{37}$$

where $m^2 = (k_1 T_3 c_p \omega_3)/(k_w \rho_w c_w)$. In the gas the Eulerian co-ordinate y is determined by substituting expression (36) in equation (16). This gives

$$(1+m)\frac{\omega_3 y}{2\sqrt{\kappa_g t}} = \left(m + \frac{T_1}{T_3}\right)\frac{\psi}{2\sqrt{\kappa_g t}} - \left(1 - \frac{T_1}{T_3}\right)\left\{\frac{\psi}{2\sqrt{\kappa_g t}}\operatorname{erf}\frac{\psi}{2\sqrt{\kappa_g t}} + \frac{1}{\sqrt{\pi}}\left(e^{-(\psi^2/4\kappa_g t)} - 1\right)\right\}. \tag{38}$$

To find the velocity distribution in the gas, use is made of expression (17). The function $f(t)$ is determined from the condition that the particle velocity must be zero at the wall; hence

$$f(t) = -\left(\frac{k_1}{c_p}\frac{\partial\tau}{\partial\psi}\right)_0, \tag{39}$$

and therefore

$$u = \frac{k_1}{c_p}\frac{\partial\tau}{\partial\psi} - \left(\frac{k_1}{c_p}\frac{\partial\tau}{\partial\psi}\right)_0, \tag{40}$$

where τ is given by expression (36). Outside the contact region $\partial\tau/\partial\psi \to 0$, and the particle velocity there is

$$u_\infty = -\left(\frac{k_1}{c_p}\frac{\partial\tau}{\partial\psi}\right)_0 = -\sqrt{\frac{k_1 T_3}{c_p\omega_3\pi t}}\left(\frac{1-T_1/T_3}{1+m}\right). \tag{41}$$

To determine the pressure of the gas in the contact region, we need to know the function $g(t)$ in expression (18). This function has now to be calculated by perturbing the flow external to the contact region.

5. Solution in the external ideal-gas flow

We assume that the effect on the external flow is small. This is true for $t \gg k_1/(c_p\omega_3 R)$, which is of the order of the time when the shock is at a distance from the wall comparable to the molecular mean free path. We now write

$$u = u', \quad \rho = \omega_3 + \rho', \quad p = P_3 + p', \tag{42}$$

and substitute in the ideal-gas flow equations. By neglecting squares and higher powers of the perturbed quantities we can obtain the wave-equation for u'; thus

$$u' = F(A_3 t + y) + G(A_3 t - y). \tag{43}$$

Also

$$p' = -\omega_3 A_3[F(A_3 t + y) - G(A_3 t - y)]. \tag{44}$$

Linearizing the boundary condition at the edge of the contact region, i.e. applying the condition $u = u_\infty$ at the wall $y = 0$, we obtain

$$F(A_3 t) + G(A_3 t) = -\frac{K}{\sqrt{t}}, \tag{45}$$

where

$$K = \sqrt{\frac{k_1 T_3}{c_p\omega_3\pi}}\left(\frac{1-T_1/T_3}{1+m}\right).$$

In a similar manner we apply the boundary condition at the unperturbed shock position given by $y = -U_s t$. It can be shown that here the velocity and pressure perturbations are related by the equation

$$p' = -\omega_3 A_3 \Phi(M_s)\, u', \tag{46}$$

where $M_s = U_s/A_3$ and

$$\Phi(M_s) = \frac{2M_s[(\gamma-1)M_s^2+2]}{[(3\gamma-1)M_s^2+3-\gamma]}. \tag{47}$$

Substituting expressions (43) and (44) in equation (46), we obtain

$$F(\overline{A_3 - U_s}\,t) = -\left(\frac{1+\Phi(M_s)}{1-\Phi(M_s)}\right) G(\overline{A_3 + U_s}\,t), \tag{48}$$

or

$$F(\xi) = -RG(\lambda\xi), \tag{49}$$

where ξ is a variable, $R = \{1+\Phi(M_s)\}/\{1-\Phi(M_s)\}$ and $\lambda = (1+M_s)/(1-M_s)$. Now put $\xi = A_3 t$ in equation (45) and substitute for $F(\xi)$ from expression (49), the following equation for G is then obtained,

$$-RG(\lambda\xi)+G(\xi) = -K\sqrt{(A_3/\xi)}, \tag{50}$$

which has the solution

$$G(\xi) = \frac{K}{(R/\sqrt{\lambda})-1}\sqrt{\frac{A_3}{\xi}}. \tag{51}$$

Using equation (49) we obtain

$$F(\xi) = -\frac{K(R/\sqrt{\lambda})}{(R/\sqrt{\lambda})-1}\sqrt{\frac{A_3}{\xi}}. \tag{52}$$

Hence
$$u' = -\frac{K}{(R/\sqrt{\lambda})-1}\left[\frac{R/\sqrt{\lambda}}{\sqrt{[t+(y/A_3)]}} - \frac{1}{\sqrt{[t-(y/A_3)]}}\right] \tag{53}$$

and
$$p' = \frac{\omega_3 A_3 K}{(R/\sqrt{\lambda})-1}\left[\frac{R/\sqrt{\lambda}}{\sqrt{[t+(y/A_3)]}} + \frac{1}{\sqrt{[t-(y/A_3)]}}\right]. \tag{54}$$

The function $g(t)$ in expression (18) can now be determined, for it equals the perturbed pressure at the edge of the contact region, namely

$$p'_{y=0} = \omega_3 A_3 K \frac{(R/\sqrt{\lambda})+1}{(R/\sqrt{\lambda})-1}\frac{1}{\sqrt{t}}, \tag{55}$$

which is $O(\delta)$. A higher order approximate equation for the temperature in the contact region could now be obtained by substituting $p = P_3+(p')_{y=0}$ in equation (7) with the viscous term neglected.

From equation (53) and the perturbed shock equations we can determine how the shock is affected by the conducting wall. It can be shown that the perturbed shock speed, U'_s, is given by the equation

$$U'_s = \Psi(M_s)\, u'_s, \tag{56}$$

where
$$\Psi(M_s) = \tfrac{1}{2}(\gamma+1)\frac{[(\gamma-1)M_s^2+2]}{[(3\gamma-1)M_s^2+3-\gamma]} \tag{57}$$

and
$$u'_s = -\frac{K}{\sqrt{(1+M_s)}}\frac{R-1}{(R/\sqrt{\lambda})-1}\frac{1}{\sqrt{t}}. \tag{58}$$

The reflected shock is thus attenuated, the perturbed speed varying inversely as the square root of the time.

REFERENCES

Fraser, A. R. 1958 *Proc. Roy. Soc.* A, **245**, 536.

Hall, J. G. 1954 *Rep. University of Toronto, Inst. of Aerophys.* no. 26.

Hirschfelder, J. O., Curtiss, C. F. & Bird, R. B. 1954 *Molecular Theory of Gases and Liquids.* New York: Wiley.

Lock, R. C. 1951 *Quart. J. Mech. Appl. Math.* **4**, 42.

JOURNAL OF FLUID MECHANICS

Volume 5, Part 1 January 1959

CONTENTS

The prediction of separation of the turbulent boundary layer
by B. S. STRATFORD *page* 1

An experimental flow with zero skin friction throughout its region of pressure rise
by B. S. STRATFORD 17

Two solutions for inviscid rotational flow with corner eddies
by CHIA-SHUN YIH 36

The structure of the jet-stream in a rotating fluid with a horizontal temperature gradient
by RUTH H. ROGERS 41

The effect of wall shape on the degree of reinforcement of a shock wave moving into a converging channel
by G. A. BIRD 60

The structure of a hydromagnetic shock in steady plane motion
by G. S. S. LUDFORD 67

An experimental investigation of the stability of Poiseuille flow
by RICHARD J. LEITE 81

On the stability of fully developed flow in a pipe
by GILLES M. CORCOS and JOHN R. SELLARS 97

Small-scale variation of convected quantities like temperature in turbulent fluid. Part 1. General discussion and the case of small conductivity
by G. K. BATCHELOR 113

Small-scale variation of convected quantities like temperature in turbulent fluid. Part 2. The case of large conductivity
by G. K. BATCHELOR, I. D. HOWELLS and A. A. TOWNSEND 134

Experimental search for the effect of compressibility in unsteady Couette flow
by LESLIE HROMAS and HAROLD DEGROFF 140

Forced plumes
by B. R. MORTON 151

The structure of a contact region, with application to the reflexion of a shock from a heat-conducting wall
by F. A. GOLDSWORTHY 164

Printed in Great Britain at the University Press, Cambridge
(Brooke Crutchley, University Printer)